UNIVERSITÀ DEGLI STUDI DELLA CALABRIA

DOTTORATO DI RICERCA IN

MECCANICA COMPUTAZIONALE

XIX CICLO

SETTORE SCIENTIFICO DISCIPLINARE ICAR 08

POST-BUCKLING BEHAVIOUR OF TRANSVERSELY STIFFENED PLATE GIRDERS

FRANCESCO PRESTA

Dissertazione presentata per il conseguimento del titolo di

Dottore di Ricerca in Meccanica Computazionale

Cosenza, Novembre 2007

UNIVERSITÀ DEGLI STUDI DELLA CALABRIA

Luogo e data	**Cosenza, Novembre 2007**
Autore	**Francesco Presta**
Titolo	**Post-buckling behaviour of transversely stiffened plate girders**
Dipartimento	**Strutture**

Firma dell'autore _____

Firma del tutor _____

Prof. Emilio Turco

Table of Contents

Abstract

Many investigations have been carried out to date into the behaviour of transversely stiffened web panels in bending and shear and many different theories have been proposed. Different code rules have been developed based on these theories. The British steel bridge code, BS 5400 Part 3, based its design rules for transverse stiffeners on the work of Rockey, while early drafts of Eurocode prEN 1993-1-5 were based on the work of Höglund. The former's tension field theory places a much greater demand on stiffener strength than does the latter's rotated stress field theory. Due to a lack of European agreement, EN 1993-1-5 was modified late on its drafting to include a stiffener force criterion more closely aligned to that in BS 5400 Part 3. The rules for stiffener design in EN 1993-1-5 are thus no longer consistent with the rotated stress field theory and lead to a greater axial force acting in the stiffener. The rules for the design of the web panels themselves in shear however remain based on Höglund's rotated stress field theory, creating an inconsistency.

Recent investigations have suggested that the rules in BS 5400 Part 3 and, to a lesser extent, in the current version of EN 1993-1-5 can be unduly pessimistic. This thesis investigates the behaviour of transversely stiffened plate girders in bending and shear using non-linear finite element analyses. It considers slender symmetrical steel girders with and without axial force and also steel-concrete composite plate girders (which are therefore asymmetric). It discusses the observed web post-buckling behaviour, compares it with the predictions of other current theories and recommends modified design rules. It includes investigation into whether a stiffness-only approach to stiffener design can be justified, rather than a combined stiffness and force approach. The shear-moment interaction behaviour of the girders as a whole are also investigated and compared to the codified predictions of BS 5400 Part 3 and EN 1993-1-5.

Acknowledgements

I would like to thank Professor Emilio Turco for being my guide during these years, for his availability in meeting me during the limited time I was in Cosenza and for his general revision of this work.

I also would like to thank Rosamaria Iaccino for helping me in submitting this thesis. She was kind, as always, even though this period was quite frantic for her for the submission of her own thesis.

I am grateful to my wife Tiziana for her patience and understanding in the last three years. I studied over the weekends and during our free time, and she was always supportive and confident I could successfully complete this Doctorate. A huge thank you for your patience and for your love.

Finally, a particular thank you is due to Chris Hendy. He gave me the initial idea for this research, he put at my disposal his knowledge, publications, bibliography search and time in the day-to-day supervision of this work. Any acknowledgements would be inadequate because I share with him the successful completion of this Doctorate.

Rende (Cosenza), Italy — Francesco Presta
November 30, 2007

Introduction

It was known since the 30's that transversely stiffened web panels in bending and shear had a post-critical resistance, but only in the '50s the behaviour was for the first time investigated [2,3]. The experimental and theoretical research undertaken resulted in a deeper knowledge on the nature of stability of plated structures. After that many investigations have been carried out to date, many different theories have been proposed and design rules have been developed based on these theories.

The shear resistance theories behind most codes (e.g. the tension field theory of Rockey in BS 5400 Part 3 and Höglund's rotated stress field theory in EN 1993-1-5) assume that the web operates in pure shear until elastic critical buckling occurs, and bands of tension form to carry further increases in shear. What is not agreed at present across Europe is the force induced in the stiffeners when these tension fields develop.

Rockey's tension field theory places a much greater demand on stiffener strength than does Höglund's rotated stress field theory. In fact, according to the former's theory, after the shear in a plate panel has exceeded the elastic critical shear buckling load of the panel, any additional shear is resisted by diagonal tensile and compression zones in the buckled web. For equilibrium, vertical force components are induced in the stiffeners. On the other hand, Höglund's theory does not require the stiffeners to carry any load other than the part of the tension field anchored by the flanges. In the absence of a stiff flange to contribute, the stiffeners simply contribute to elevating the elastic critical shear stress to the web. Earlier versions of EN 1993-1-5 thus required web stiffeners to be designed and checked for adequate "stiffness-only", an approach believed to be consistent with several other European standards.

These early drafts of EN 1993-1-5 raised concern in the UK as a stiffness-only check was not compatible with the strength based tension field theory approach traditionally used in BS 5400 Part 3. EN 1993-1-5 was then modified late on its drafting to include a stiffener force criterion more closely aligned to that in BS 5400 Part 3, as a result of objection from the UK. The rules for stiffener design in EN 1993-1-5 are thus no longer consistent with the rotated stress field theory and lead to a greater axial force acting in the stiffener. The rules for the design of the web panels themselves in shear however remain based on Höglund's rotated stress field theory, creating an inconsistency.

The use of a stiffness-only approach would give the optimum opportunity for mitigating assessment over-stresses in transverse stiffeners and reducing steel bridge strengthening costs. Nevertheless, the use of a stiffness-only approach is complicated by the absence of sufficient background papers proving the stiffener assessment clauses to be safe.

Another difference between the two codes occurs in the treatment of coexisting axial stresses. Axial stresses in the web, induced by either external axial loads or unsymmetrical sections, are assumed to have no effect on the shear buckling load of the plate panel in EN 1993-1-5. In BS 5400 axial stresses are assumed to reduce the elastic critical shear buckling load of the plate panel. In same cases, BS 5400 predicts that the axial stresses are high enough to render the elastic critical shear buckling resistance of the web as negligible. In those cases, all of the applied shear is then carried on the stiffener, resulting in an assessment overstress or in a conservative design. As EN 1993-1-5 does not require the elastic critical shear buckling load to be reduced in the presence of axial stresses, this results in the stiffeners passing the assessment or in a more sensible design. Given the general feeling in Europe that the force in the stiffeners produced by the BS 5400 approach was already too conservative, any further increase in force due to axial stresses was rejected by the drafters of EN 1993-1-5.

Both the methods appear to be quite conservative when compared with test results indicating that only small forces are developed in transverse stiffeners. Höglund's rotated stress field theory predicts low stiffener forces as observed in earlier non-linear finite element studies, whilst it does not predict a tension-field direction that necessarily aligns with the stiffener ends in contrast with test observations. Rockey's tension field predicts higher stiffener forces but predicts a tension field direction that aligns with the stiffener ends.

This thesis investigates in detail, with the use of a non-linear finite element analysis package, the behaviour of a plate girder arrangement, and seeks to investigate:

1) the adequacy of the "stiffness-only" approach to stiffener design and assessment;
2) the effects of axial stresses in the web on the stiffener;
3) the mechanism for resisting shear if the stiffeners are not picking up tension field forces acting as web members of a truss;
4) the effects of panel aspect ratio on the collapse load;

5) the effects of the ratio M/V of bending moment to shear force on the collapse load and comparison with moment-shear interaction diagrams produced by Eurocode EN 1993-1-5;
6) sensitivity of the collapse load to web and stiffener imperfections.

It is organized as follows:

- in the **1st chapter** a brief review of the most important tension field theories proposed in the literature is reported;

- in the **2nd chapter** a calibration exercise is performed. Tests from [11] are modelled with non-linear finite element analyses in order to gain confidence in the results for subsequent analyses;

- in the **3rd chapter** the finite element modelling is discussed, along with the parameters used and the non-linear analysis strategy adopted;

- in the **4th chapter** the investigation into the behaviour of symmetrical steel girders and steel-concrete composite plate girders is reported and a new proposed approach is discussed.

Chapter 1

Tension field theories

Many investigations have been carried out to date into the behaviour of transversely stiffened web panels in bending and shear and many different theories have been proposed.

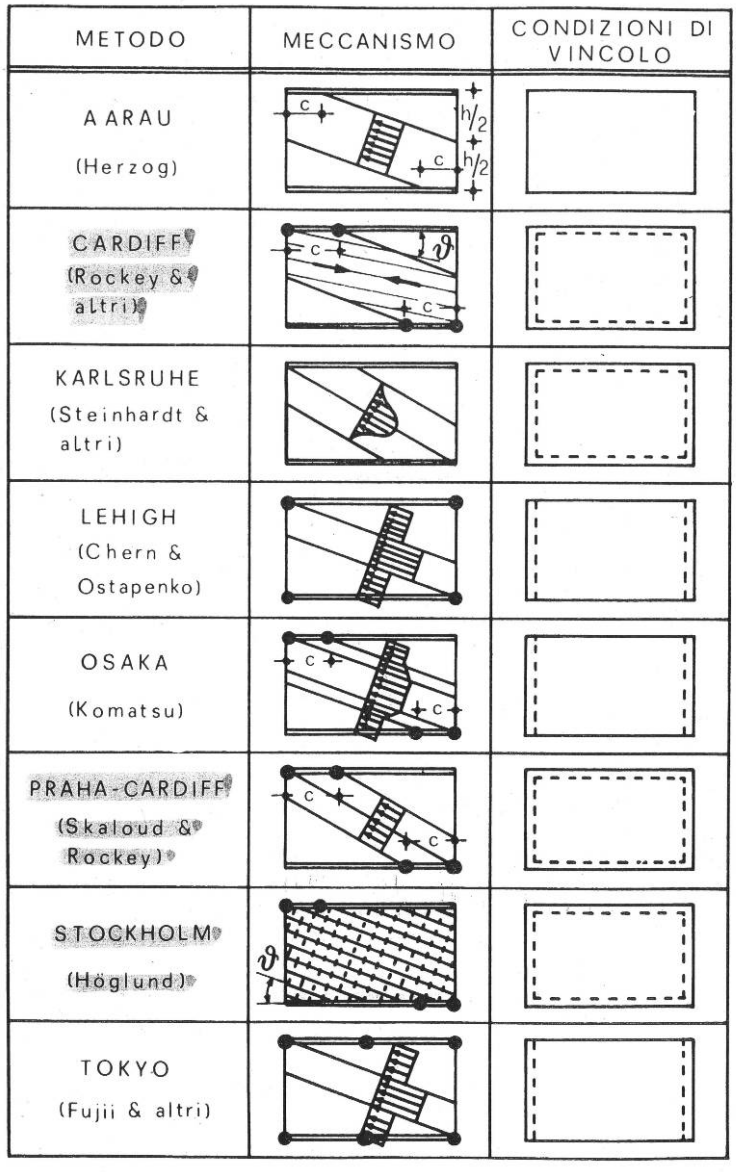

Figure 1.1 – Main failure mechanisms proposed (Extract from [14])

Nevertheless a general and rigorous solution is not possible due to the complexity of the problem, which is non-linear for geometry and material. Generally the theories are based on approximated or empirical procedures or on collapse mechanisms chosen to suit available experimental results. These have indicated that, when a thin walled plate girder is loaded in shear, failure occurs when the web plate yields under the joint action of the post-buckling membrane stress and the initial buckling stress of the web panel, and plastic hinges develop in the flanges, as shown in Figure 1.2.

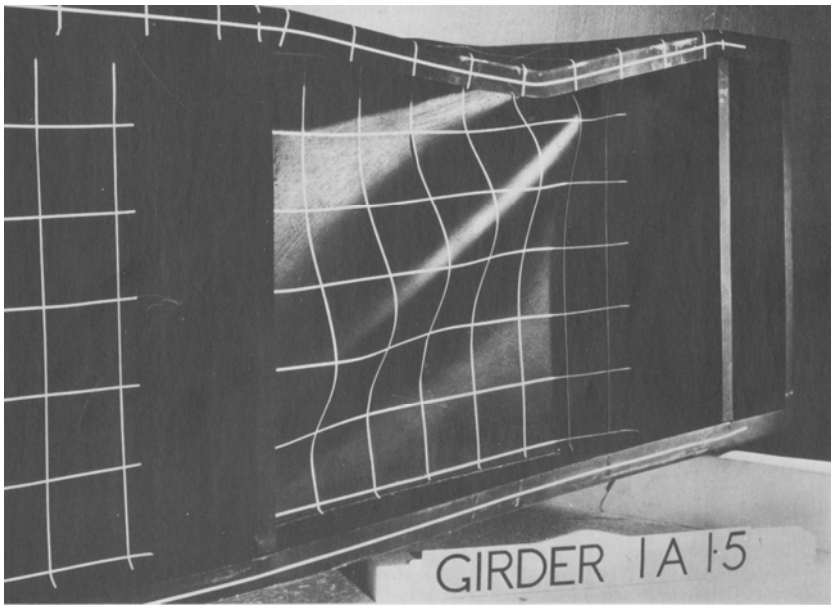

Figure 1.2 – High shear test from (Extract from [21])

Different code rules have been developed based on these theories. The British steel bridge code, BS 5400 Part 3, based its design rules on Rockey's tension field theory [8,9]. Höglund's rotating stress field theory [10] formed the basis of the simple post-critical design procedure for predicting the ultimate shear resistance of stiffened and unstiffened plate girders in ENV 1993-1-5. A second procedure in ENV 1993-1-5 was the tension field method, which could be only applied to girders having intermediate transverse stiffeners and web panel aspect ratios b/d (width of web/depth of web panel) between 1.0 and 3.0. This method was based on the Rockey's tension field theory and was intended to produce more economical designs for a limited range of girder configurations. Theoretical predictions of the ultimate shear resistance of the plate girders based on the simple post-critical design procedure appeared inconsistent and conservative when compared with currently available test data, primarily because it neglected the contribution of flanges to the ultimate shear resistance. Theoretical predictions based on the tension field design procedure, taking into account the limited range of web panel aspect ratios, were less

conservative. Höglund's rotating stress field theory forms the basis of EN 1993-1-5. It contains supplementary rules for planar plated structures without transverse loading, developed together with the EN 1993-2 Steel Bridges. It covers stiffened and unstiffened plates in common steel bridges and similar structures. These rules are not specific for bridges, which is the reason for making them a part of EN 1993-1, which contains general rules. The resistance of slender plates to shear according to EN 1993-1-5 replaces the two methods in ENV 1993-1-1.

1.1 Cardiff tension field theory

The tension field theory developed by Rockey et al. [8,9] is the basis of the post-critical design procedure for predicting the ultimate shear resistance of plate girders in BS 5400 Part 3. According to this theory the loading of the panel can be divided into three phases as shown in Figures 1.3, 1.5 and 1.6.

Stage 1. A uniform shear stress develops throughout the panel prior buckling, with principal tensile and compressive stresses of magnitude τ acting at 45° and 135°.

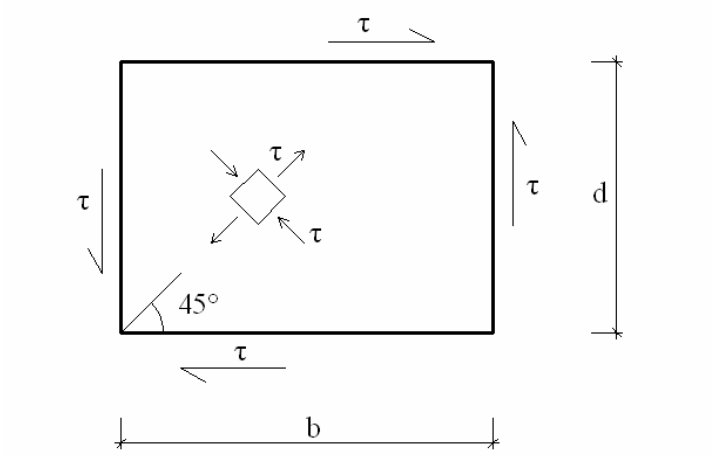

Figure 1.3 – Shear failure mechanism assumed in Cardiff theory (Stage 1)

This stress system exists until the shear stress τ equals the critical shear stress τ_{cr}. The buckling shear stress τ_{cr} for a simply supported rectangular plate is given by:

$$\tau_{cr} = k_b \frac{\pi^2 E}{12(1-\upsilon^2)}\left(\frac{t}{d}\right)^2$$

where k_b is the buckling coefficient for a simply supported plate given by

$$k_b = 5.35 + 4\left(\frac{d}{b}\right)^2 \quad \text{for} \quad b/d \geq 1$$

$$k_b = 5.35\left(\frac{d}{b}\right)^2 + 4 \quad \text{for} \quad b/d < 1$$

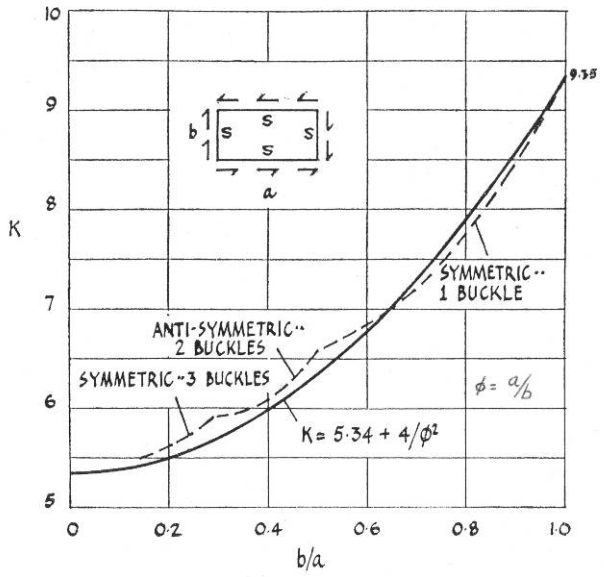

Figure 1.4 – Buckling coefficient for simply supported plates in shear (Extract from [4])

Stage 2. Once the critical shear stress τ_{cr} is reached, the panel cannot sustain any increase in compressive stress and it buckles. The load carrying system changes and any additional load is supported by the tensile membrane stress σ_t. Under the action of this membrane stress, the flanges bend inward and the extend of the inclination of the tensile membrane stress field is influenced by the rigidity of the flanges.

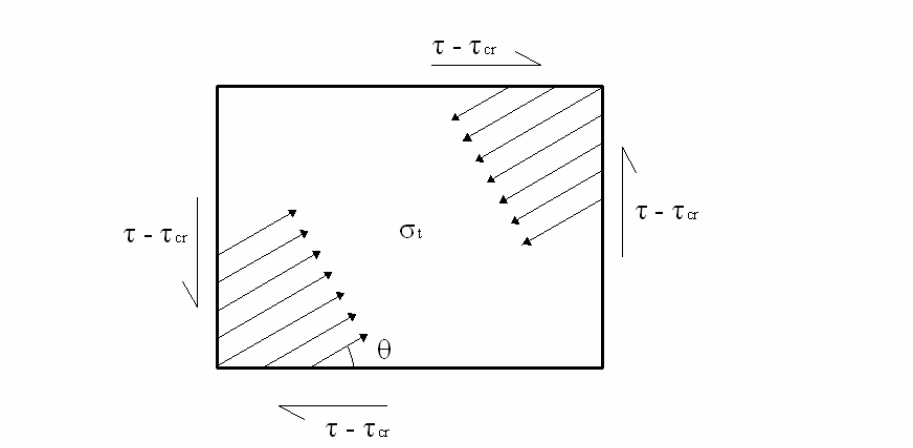

Figure 1.5 – Shear failure mechanism assumed in Cardiff theory (Stage 2)

Stage 3. Additional load can be carried until the tensile membrane stress σ_t plus the buckling stress τ_{cr} produces yielding in the web. The membrane stress at this point is $\sigma_{t,y}$. Failure occurs when hinges have formed in the flanges.

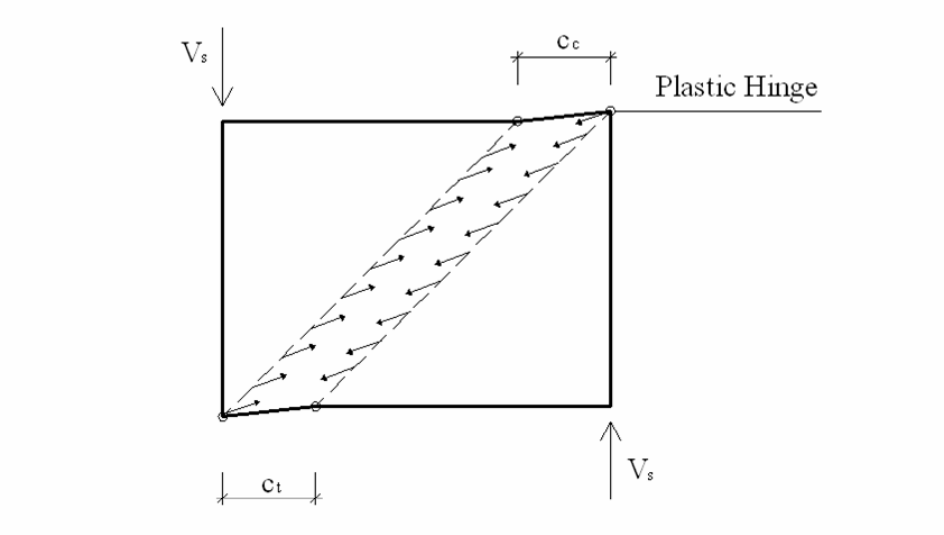

Figure 1.6 – Shear failure mechanism assumed in Cardiff theory (Stage 3)

It is then possible to establish a set of forces and moments which together with the yield zone form an equilibrium solution which does not violate the yield condition.

The ultimate shear resistance V_s of the transversely stiffened girder is expressed as:

$$V_s = \tau_{cr} d\, t + \sigma_{t,y}\, t \sin^2\theta \left(d\cos\theta - b + \frac{c_c}{2} + \frac{c_t}{2} \right) + \frac{2M_{pfc}}{c_c} + \frac{2M_{pft}}{c_t}$$

where:

- M_{pfc} and M_{pft} are the plastic moments of the compression and tension flanges;
- c_c and c_t are the distances at which plastic hinges form in the flanges;
- θ is the angle of inclination of the web tension-field stress $\sigma_{t,y}$.

The position of the internal hinges is obtained by equilibrium considerations:

$$c_c = \frac{2}{\sin\theta}\sqrt{\frac{M_{pfc}}{\sigma_{t,y}\, t}}$$

$$c_t = \frac{2}{\sin\theta}\sqrt{\frac{M_{pft}}{\sigma_{t,y}\, t}}$$

The angle θ can be either determined by iteration to give the maximum value of V_s or approximated as

$$\theta = \frac{2}{3}\tan^{-1}\left(\frac{d}{b}\right)$$

Substituting equations for $\mathbf{c_c}$ and $\mathbf{c_t}$ into equation for $\mathbf{V_s}$ and assuming that $M_{pfc} = M_{pft}$, the ultimate shear resistance can be rewritten as

$$V_s = \tau_{cr} d\, t + 2\sigma_{t,y}\, c\, t \sin^2\theta + \sigma_t^y\, d\, t \sin^2\theta(\cot\theta - \cot\theta_d)$$

where θ_d is the inclination of the web panel diagonal.

Interaction between shear and coexisting bending moment is represented by diagram in Figure 1.7, which defines the coexisting values of shear and bending that will result in failure of the girder.

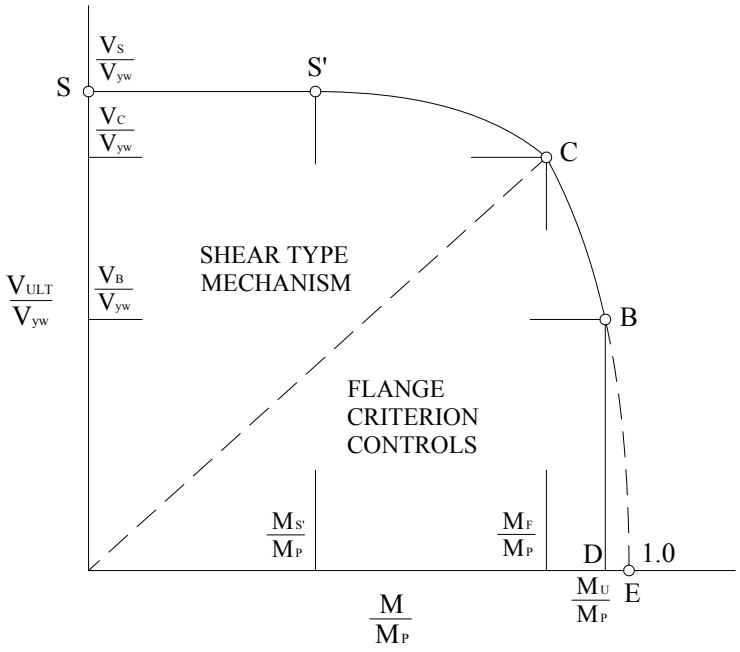

Figure 1.7 – Interaction diagram

Point S represents the collapse load when the panel is subjected to pure shear. Point C represents the position on the interaction diagram at which the mode of failure changes from the shear mechanism mode to the flange failure mode. This change occurs when the applied bending moment M is approximately equal to M_F, which is the contribution of the flanges to the plastic moment of resistance of the girder. When the panel is subjected primarily to bending stresses, inward collapse of the compression flange occurs when the applied moment is close to that which will result in the extreme flange bending stress reaching the yield stress. Where the web plate buckles before collapse, it is not possible for the plate girder to develop the full plastic moment of resistance. Point D corresponds to the bending moment at which this inward collapse of the flange occurs. V_{yw} is the shear yield resistance of the web and M_P is the fully plastic moment of the girder.

Transverse stiffeners have to fulfill two main functions. The first function is to increase the buckling resistance of the web plate. The second is to continue to remain effective when the web plate buckles and develops a tension field. They also have to restrict the tendency of the flanges to approach each other and are therefore subjected to compressive loadings. Prior to buckling, stiffeners are not subjected to any axial loading but after the plate buckles the axial loads applied to the transverse stiffeners steadily increase as the webplate develops a membrane tension field.

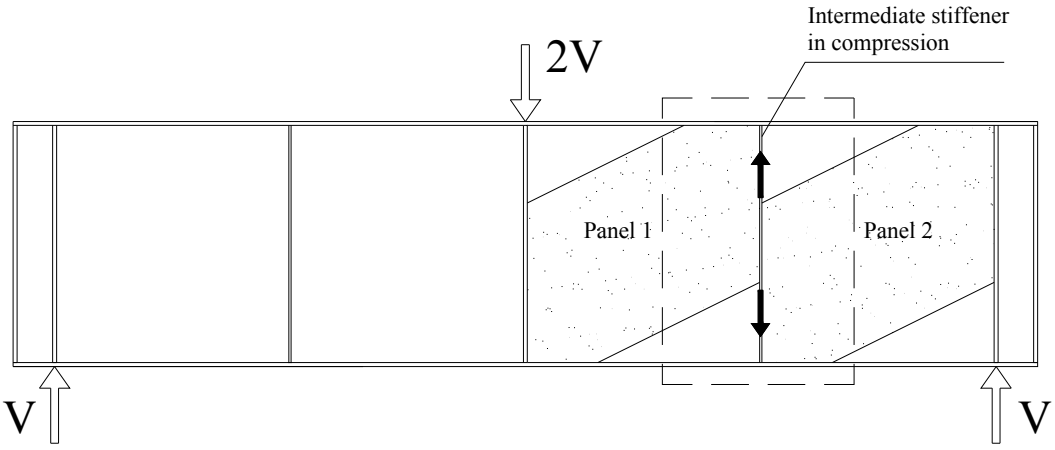

Figure 1.8 – Simply supported plate girder with effective stiffener

The tension field acting in the adjacent web panels applies loading to the flanges and to the transverse stiffeners. As a results the transverse stiffener is subjected to a variable axial loading, as shown in Figure 1.9. This loading acts on the effective cross section area of the stiffener. Research carried out by Mele [6] has shown that a part of the web plate acts with the stiffener even though it is theoretically fully yielded by the tension field action.

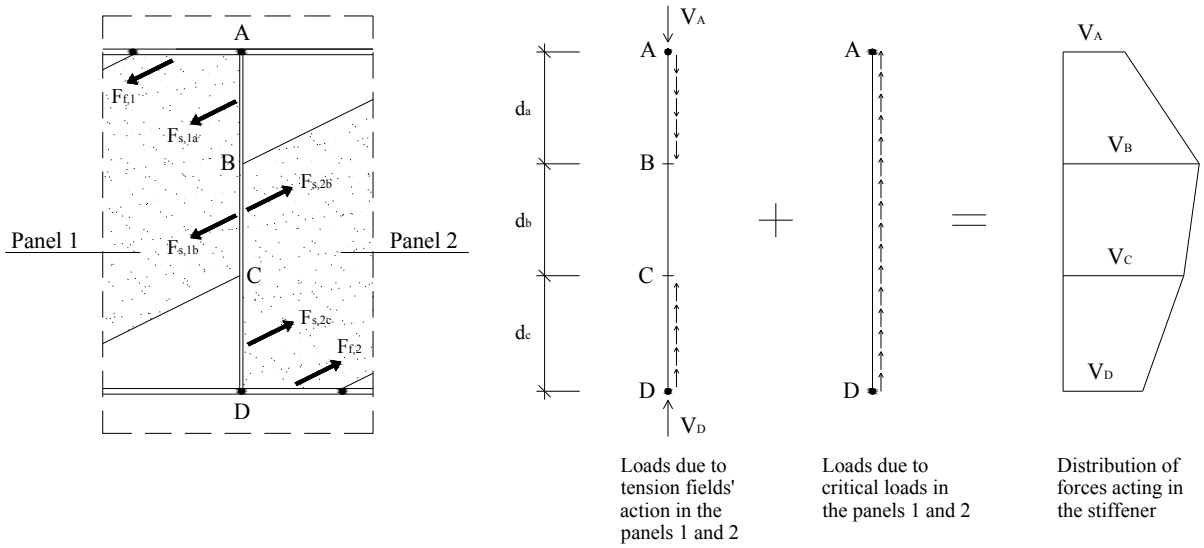

Figure 1.9 – Forces applied by membrane and buckling stress fields to intermediate stiffener AB

1.2 Stockholm rotating stress field theory

The rotating stress field theory developed by Höglund is the basis of the post-critical design procedure for predicting the ultimate shear resistance of plate girders in Eurocode 3.

The ultimate shear resistance V_u can be expressed as

$$V_u = V_{u,w} + V_{u,f}$$

where:

- $V_{u,w}$ is the load carrying resistance of the web due to its membrane behaviour;
- $V_{u,f}$ is the load carrying resistance of the flanges due to their bending stiffness;

In determining $V_{u,w}$ the web panels are represented, in the post-buckling stage, with a system of perpendicular bars in compression and in tension, as shown in Figure 1.10.

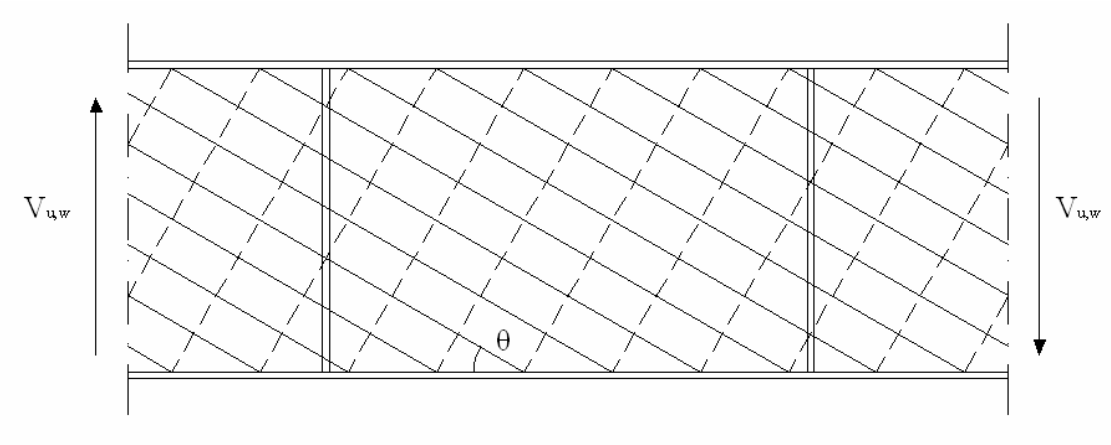

Figure 1.10 – Shear force carried by the web

When the load increases, the compression bars stress is constant and equal to the buckling stress $\sigma_c = \tau_{cr}$ while the tension bars stress σ_t increases when the angle θ decreases. The value $V_{u,w}$ is obtained when plasticity is reached at the intersection between bars, according to Von Mises criteria.

If the stiffeners at the girder ends are rigid, $V_{u,w}$ is expressed as:

$$V_{u,w} = h d \tau_y \qquad \text{when} \quad \alpha \le 0.8$$

$$V_{u,w} = \frac{1.8}{\alpha + 1} h d \tau_y \qquad \text{when} \quad 0.8 \le \alpha \le 2.75$$

$$V_{u,w} = \frac{1.32}{\alpha} h d \tau_y \qquad \text{when} \quad \alpha > 2.75$$

where:

$$\alpha = \sqrt{\frac{\tau_y}{\tau_{cr}}}$$

and τ_{cr} is the buckling shear stress for a simply supported rectangular plate as discussed in section 1.1.

In absence of intermediate stiffeners it would not be possible to imagine a “frame type” mechanism and $V_{u,f}$ would be equal to zero. When web panels are provided with transverse stiffeners, this implies that the web is prevented from deflecting and the flanges are prevented from coming nearer to each other at the stiffeners. If the flanges are non-

rigid then the edges of the web are prevented from approaching each other only locally, at the stiffeners. If the flanges are rigid in bending in the plane of the web, then they also prevent the edges of the web from approaching each other over a length “c” of the web panel. This gives rise to an increase in the shear resistance.

At failure, four hinges form at the top and bottom flange, with a tension stress field developed in the web, between flanges only, as shown in Figure 1.11. The moment at each hinge is assumed to be equal to the plastic moment of the flanges.

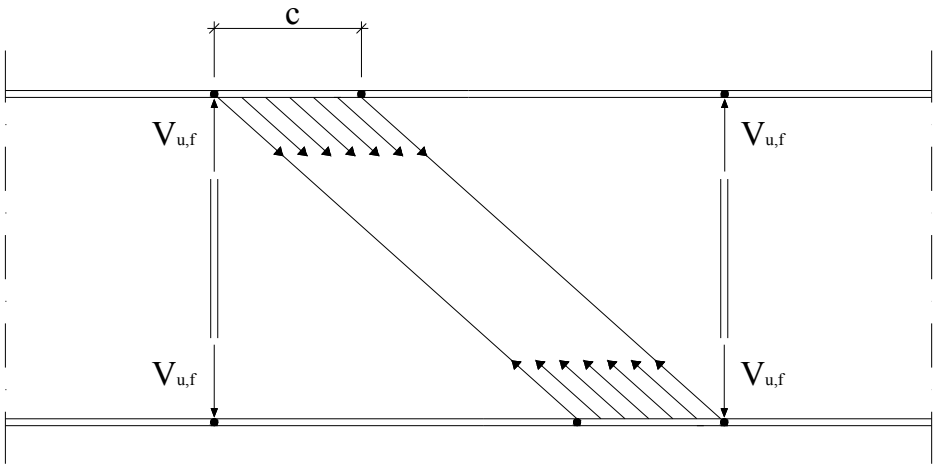

Figure 1.11 – Shear force carried by truss action

The shear force $V_{u,f}$ which is transmitted by the tension stress field is obtained from the equilibrium of the flange portion “c”. This equation gives:

$$V_{u,f} = \frac{4M_{fp}}{c}$$

where c is the distance at which plastic hinges form in the flanges and is given by:

$$c = b\left(0.25 + \frac{b_f\, t_f^2\, \sigma_{yf}}{t\, d^2\, \sigma_{yw}}\right)$$

The stiffener force is equal to $V_{u,f}$.

Interaction between shear and coexisting bending moment is represented by diagram in Figure 1.12.

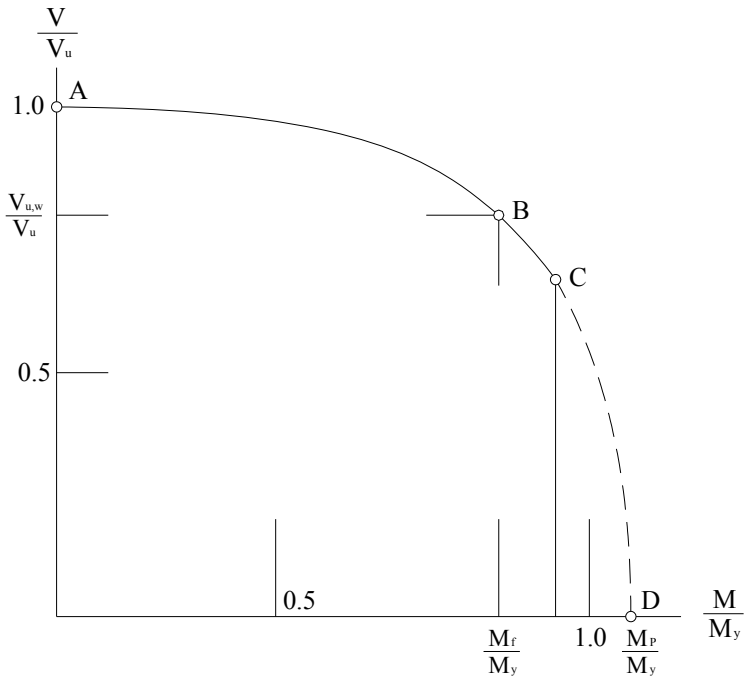

Figure 1.12 – Interaction diagram

When the girder is subjected to a shear force with a small coexisting bending moment, it is assumed that the effect from the latter does not influence the load carrying capacity of the web $V_{u,w}$ but only the load carrying capacity of the flanges $V_{u,f}$.

$$V_u = V_{u,w} + V_{u,f}\left[1-\left(\frac{M}{M_f}\right)^2\right] \quad \text{for} \quad M \le M_f$$

If $M = M_f$ then the flanges are assumed to be completely plastified by the normal force from bending moment. When $M > M_f$ then the flanges cannot contribute to the shear carrying capacity of the girder and the capacity of the web to carry shear forces is reduced.

Chapter 2

Calibration of FE modelling

As an initial exercise, tests TGV7-2 and TVG8-2 from [11] are modelled with non-linear finite element analysis to establish if similar results are obtained. This is intended to gain confidence in the non-linear FE results for subsequent analyses. Both tests have been chosen for validation of the finite element modelling because the load deflection plots of the tested girders under increasing load are included in the paper. These can be directly compared to the load deflection plots generated from the finite element analysis. In addition, test TVG8-2 recorded a failure of the transverse stiffener (which is a rare experimental situation) whereas the stiffener in TGV7-2 remained intact. This work is discussed in the following paragraphs.

2.1 Results of initial FE calibration analysis on test TGV8-2

2.1.1 FE model set-up

As an initial calibration of the finite element analysis, Rockey test TGV8-2 from [11] has been modelled and the results compared to the findings of the original laboratory test. Test TGV8-2 has been chosen for validation because the measured load deflection relationship was published in the original paper and also because it produced a web stiffener ‘failure’ - or at least very large out of plane deflections.

All dimensions, loadings and material properties used in the FE model have been taken from the original paper. Post yield strain hardening has been included via the slope of E/100 in the stress/strain curve as discussed in Chapter 3. An applied load of 180kN has been applied at the midspan point of the girder in the same manner as the original test.

As illustrated in Figure 2.1, the intermediate stiffener dimensions were not equal on both sides of original test girder TGV8. Stiffener SA possessed outstand dimensions of 20.50 x 3.22mm and stiffener SB 15.95 x 5.71mm. Both intermediate stiffeners were single sided. Test TGV8-1 applied a point load to the central stiffener and the girder is recorded to have failed through buckling of stiffener SA when the point load reached 180kN. At this point, the damaged panel was ‘strengthened’ (it is not explained how) and the girder reloaded in

test TGV8-2. Test TGV8-2 was stopped after stiffener SB had buckled at a recorded failure load of 188kN. As test TGV8-2 is the test to be validated in a finite element model, both intermediate stiffeners have been modelled with dimensions equal to stiffener SB.

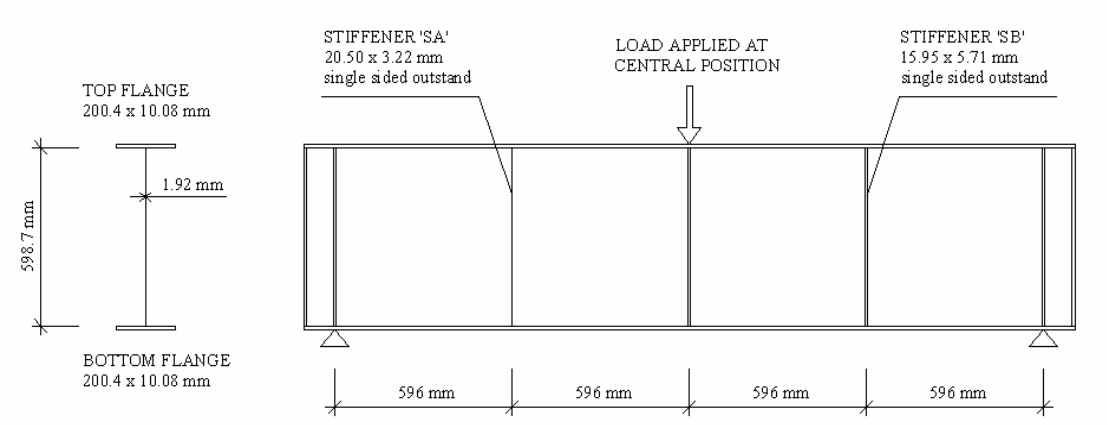

Figure 2.1 – Original Test Girder TGV8

The only necessary data absent from the original paper is the magnitude of geometric imperfection present in the web plate and stiffener prior to loading. Two different initial imperfections have therefore been modelled to investigate the sensitivity of imperfection on the final buckling mode and buckling load.

The first initial imperfection, illustrated in Figure 2.2 is designed to maximise the load on the intermediate stiffener. The 2mm maximum allowable stiffener deflection to BS 5400 Part 6 has been doubled to approximately 4mm to allow for structural imperfections.

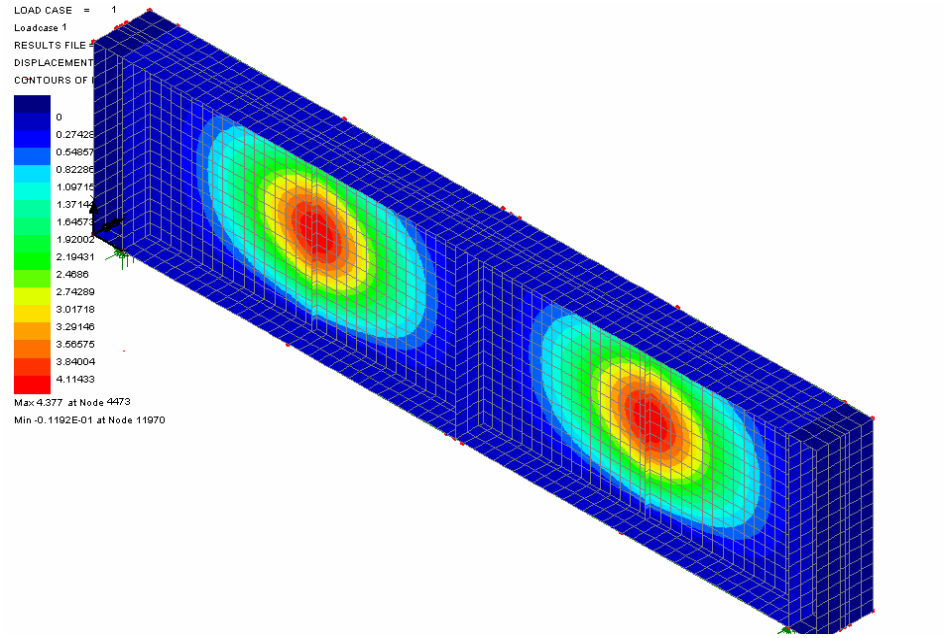

Figure 2.2 – Lateral Displacement Contours (mm) applied as 'Initial Deflection 1' for FE model of Rockey Test TGV8

The second initial imperfection, illustrated in Figure 2.3 below is designed to maximise the loads on the web panels. Each web panel has been bowed out alternately, with the maximum bow dimension calculated at 3mm from EN 1993-1-5 Annex C.

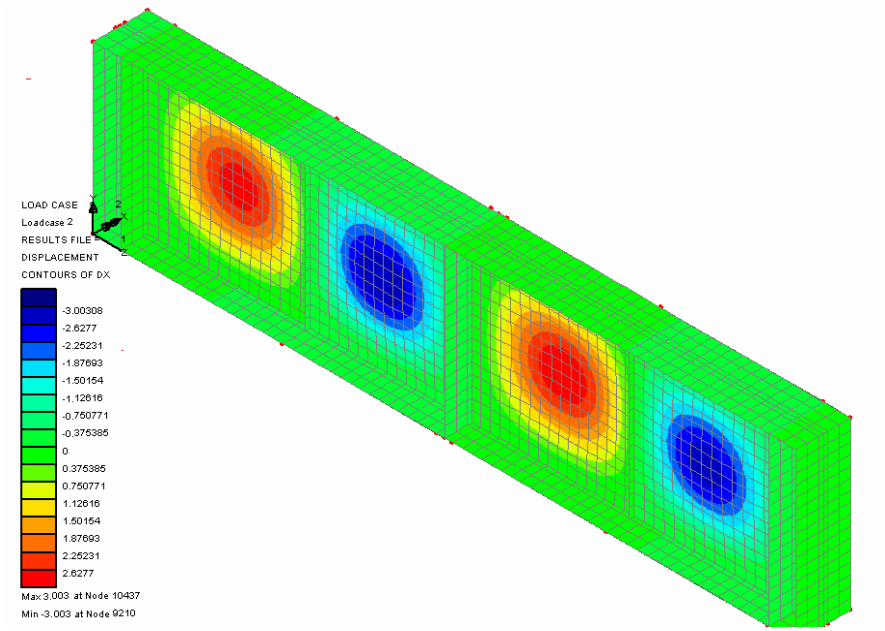

Figure 2.3 – Lateral Displacement Contours (mm) applied as 'Initial Deflection 2' for FE model of Rockey Test TGV8

2.1.2 Results of FE modelling with 'Initial Deflection 1'

The finite element analysis of test TGV8-2 with 'initial deflection 1' stops when the analysis fails to find an equilibrium beyond a load factor of 1.02. The lateral deflections of the web at this point are illustrated in Figure 2.4 below. In Figure 2.4 it can be seen that the girder has failed by the web plate and intermediate stiffener bowing out laterally.

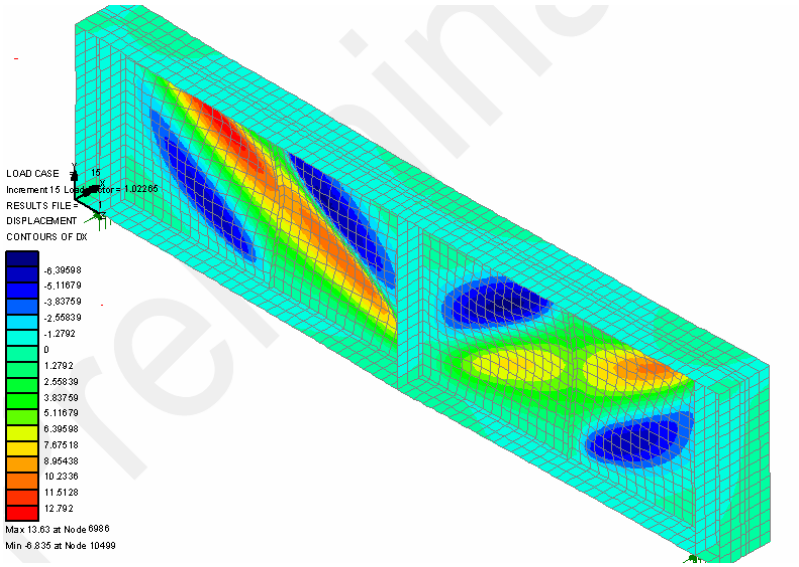

Figure 2.4 – Displacement Contours (mm) showing lateral displacement of webs under an applied load of 180kN x Load Factor of 1.02 = 183.6kN (Contour values do not include original imperfections illustrated in Figure 2.2)

The load-deflection curve obtained from the finite element analysis is illustrated in Figure 2.5. The analysis shows a gradual loss of girder stiffness beyond a load factor of approximately 0.7 culminating in failure at a load factor of 1.02

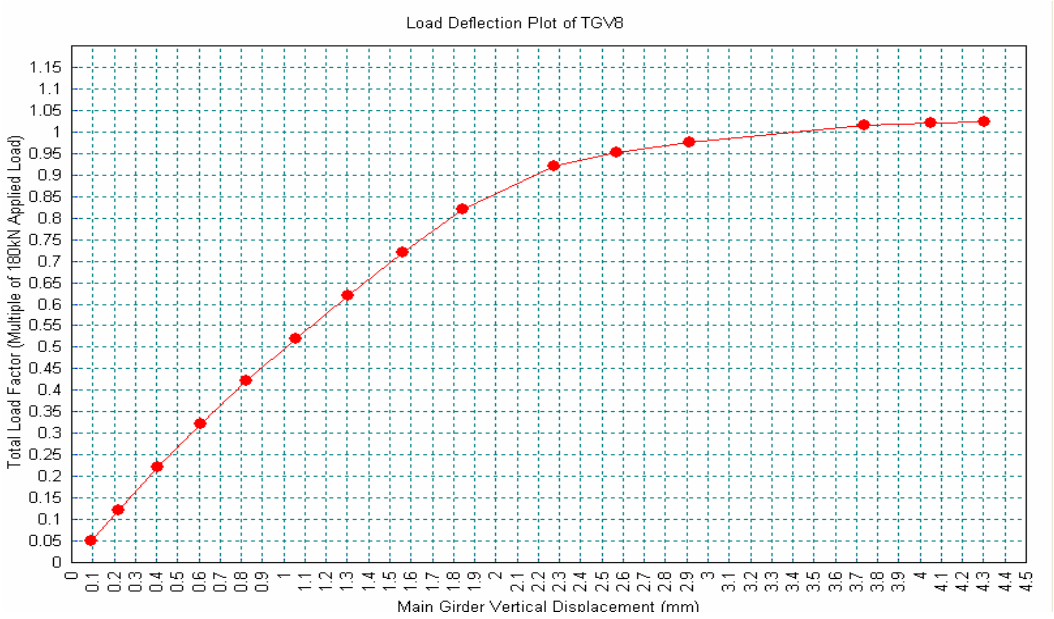

Figure 2.5 – Load-Deflection Curve obtained from FE Analysis of Test TGV8-2 using 'Initial Imperfection 1' in Figure 2.2

2.1.3 Results of FE modelling with 'Initial Deflection 2'

The finite element analysis of test TGV8-2 with 'initial deflection 2' stops when the analysis fails to find an equilibrium beyond a load factor of 1.003. The lateral deflections of the web are at this point are illustrated in Figure 2.6. In Figure 2.6 it can be seen that the girder has again failed by the web plate and intermediate stiffener bowing out laterally, despite a different initial imperfection.

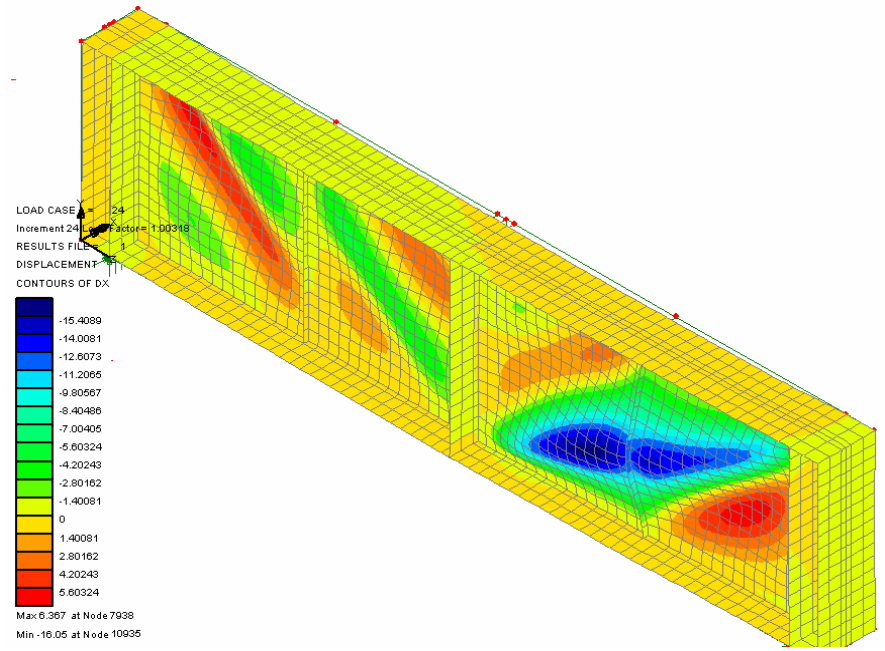

Figure 2.6 – Displacement Contours (mm) showing lateral displacement of webs under an applied load of 180kN x Load Factor of 1.003 = 180.1kN (Contour values do not include original imperfections illustrated in Figure 2.3)

The load-deflection curve obtained from the finite element analysis is illustrated in Figure 2.7. As for 'initial imperfection 1' the analysis shows a gradual loss of girder stiffness beyond a load factor of approximately 0.7 culminating in failure at a load factor of 1.02. In this model, the analysis has been able to establish more equilibriums beyond the failure load. The peak in load and subsequent drop-off is compatible with the lab test results illustrated in Figure 2.9.

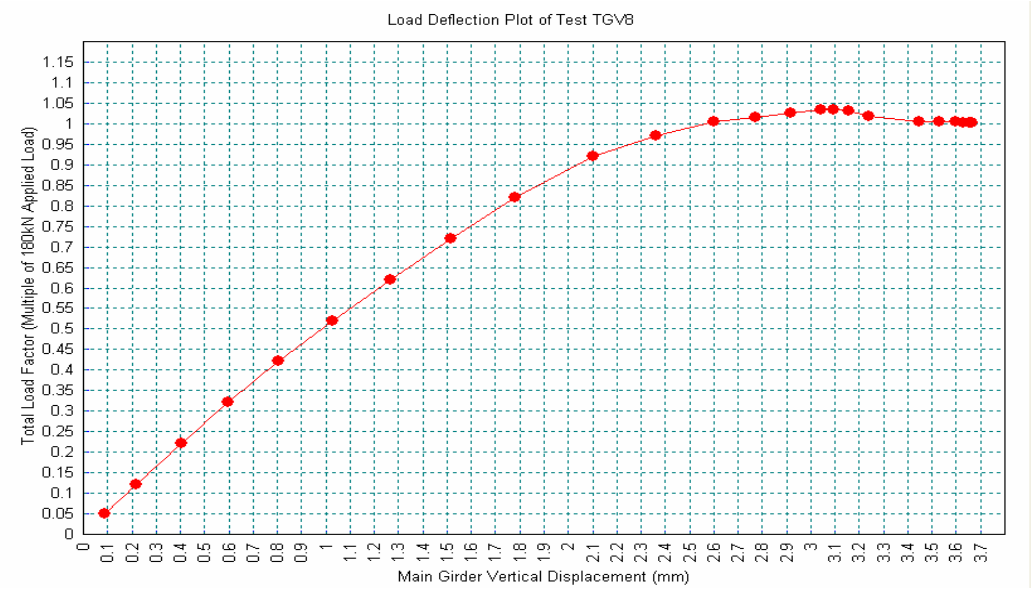

Figure 2.7 – Load-Deflection Curve obtained from FE Analysis of Test TGV8-2 using 'Initial Imperfection 2' in Figure 2.3

2.1.4 Comparison of TGV8-2 FE modelling output with laboratory test results

The photographed failure mode of test TGV8-2 is illustrated in Figure 2.8. The failure modes predicted by the FE generated results in Figures 2.4 and 2.6 compare well with the actual failure mode recorded in testing. Both predicted failure modes involve the lateral bowing out of an intermediate stiffener.

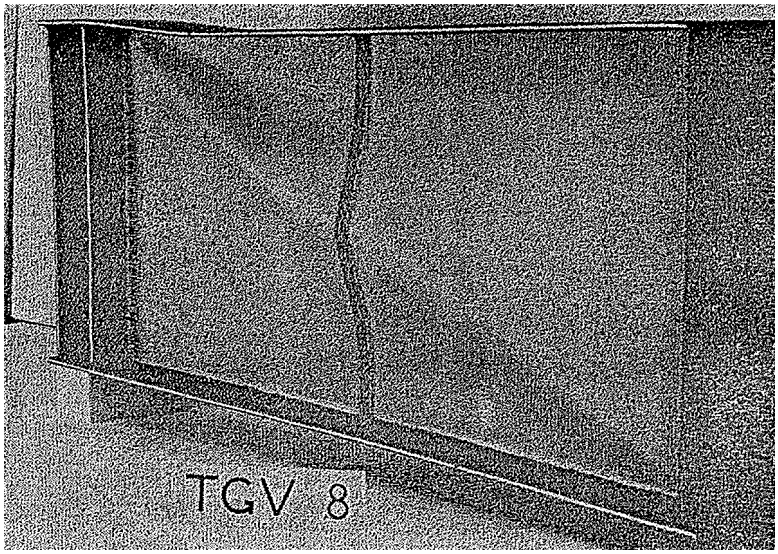

Figure 2.8 – Photograph of failure mode Test TGV8-2 (Extract from [11])

The recorded load-deflection curve for the laboratory test of TGV8 is illustrated in Figure 2.9.

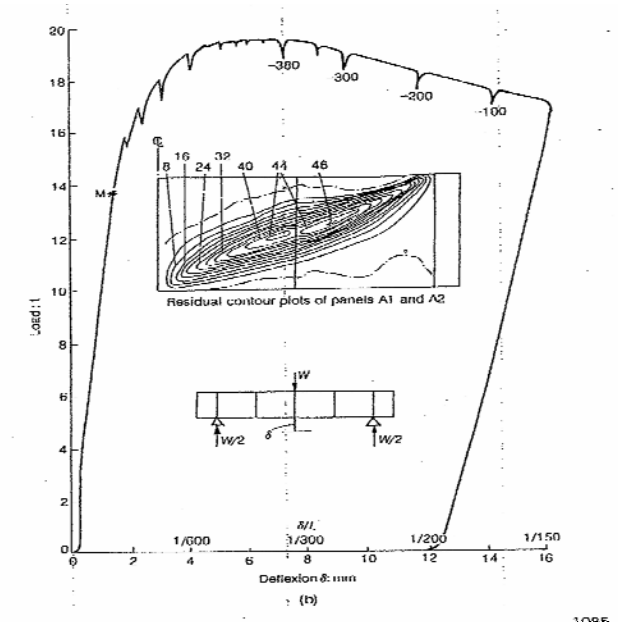

Figure 2.9 – Load-Deflection Plot recorded in laboratory testing of Test TGV8-2 (Extract from [11])

To compare the FE results to the tested results, all load deflection curves have been plotted on Figure 2.10. The results from the laboratory testing have been scaled from Figure 2.9. It is assumed that the units of the Figure 2.9 vertical axis are 'imperial tons.'

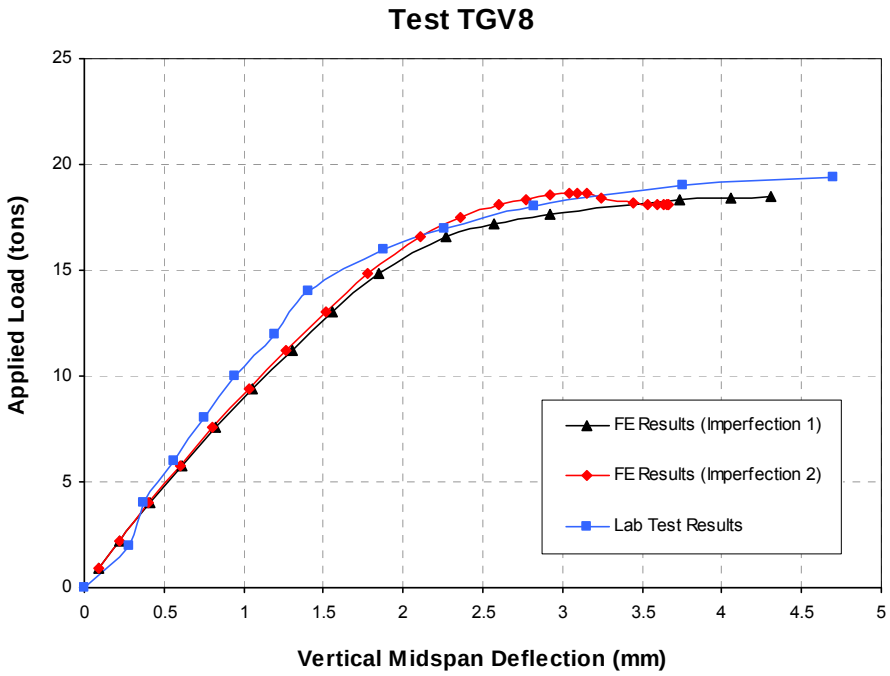

Figure 2.10 – Load-Deflection Plots of FE models and Laboratory Testing

2.1.5 Discussion of results

Figure 2.10 shows that there is a good correlation between the load-deflection relationships calculated by the FE models and that recorded in the test output for TGV8-2. This gives confidence in the accuracy of the output of subsequent FE models. The failure modes illustrated on Figures 2.4 and 2.6 are also similar to the recorded failure mode in Figure 2.8. The fact that a similar failure mode has occurred for 'Initial Deflection 2' also helps to prove that the failure mode developed with 'Initial Deflection 1' has not been 'forced' by the geometry of the initial imperfection.

A check of the TGV8-2 stiffener capacity to EN 1993-1-5 has found that the stiffener has inadequate stiffness when checked against the minimum stiffness requirements of Clause 9.3.3 – although it is only inadequate by 4%. However, when the capacity of the girder is checked against the Eurocode assuming a rigid intermediate stiffener the web shear capacity is critical with a predicted failure shear force of 79.7kN (assumes γ_{M0}=1.0, γ_{M1}=1.0). This shear force would be generated by a central point load of 159.4kN ≅ 16.0 tons. From Figure 2.10, this predicted shear capacity was safely achieved in Girder TGV8 despite the code failure of the intermediate stiffeners.

The check of the transverse stiffener to EN 1993-1-5 Clause 9.3.3 (3) predicts a usage factor of 6.48 where 'Usage factor' = Load / Load Capacity. This failure is largely a consequence of the axial force, applied in the plane of the web plate, predicted by the equation in EN 1993-1-5 Clause 9.3.3 (3) repeated below :

$$\text{Stiffener Force} = V_{Ed} - \frac{1}{\bar{\lambda}^2} \frac{f_{yw} h_w}{\sqrt{3}\ \gamma_{M1}}$$

If this girder was to be designed to the Eurocode a heavier stiffener section would be required to comply with the above equation and the stiffness requirement would be satisfied. However, the results from the testing and FE modelling would show that the combined web-stiffener system used in test TGV8 is adequate for resisting the theoretical shear capacity of 79.7kN – although it is noted from Figure 2.10 that the response is non-linear above a shear force of 69kN (equivalent to a central point load of 138kN ≅ 13.8 tons.)

2.2 Results of initial FE calibration analysis on test TGV7-2

2.2.1 FE model set-up

As discussed previously, Test TGV7-2 has also been modelled with finite element analysis to compare the measured test results with the finite element output. Similarly to girder TGV8, Girder TGV7 possessed two intermediate stiffeners with different dimensions. Stiffener SA consisted of a stiffener outstand 12.40 x 5.75mm and stiffener SB 25.21 x 5.10mm. The test records show that the first test TGV7-1 was stopped at 180kN after stiffener SA had buckled. After strengthening the failed panel and stiffener, the second test TGV7-2 was carried out. This was stopped at 210kN after the web panels adjacent to stiffener SB had failed – even though stiffener SB still remained intact. As the finite element analysis is to repeat test TGV7-2, both intermediate stiffeners have been modelled as having dimensions equal to stiffener SB.

As for the FE modelling on Test TGV8-2, all dimensions and material properties have been taken from the TGV7 girder data in the original paper. Two initial imperfections have been used as starting points. These are identical to the initial imperfections illustrated on Figures 2.2 and 2.3.

2.2.2 Results of FE modelling with 'Initial Deflection 1'

The finite element analysis of test TGV7-2 with 'initial deflection 1' stops when the analysis fails to find an equilibrium beyond a load factor of 1.09. The lateral deflections of the web are illustrated on Figure 2.11. The failure mode is different to the equivalent TGV8 test in Figure 2.4 in that the intermediate stiffeners have remained intact.

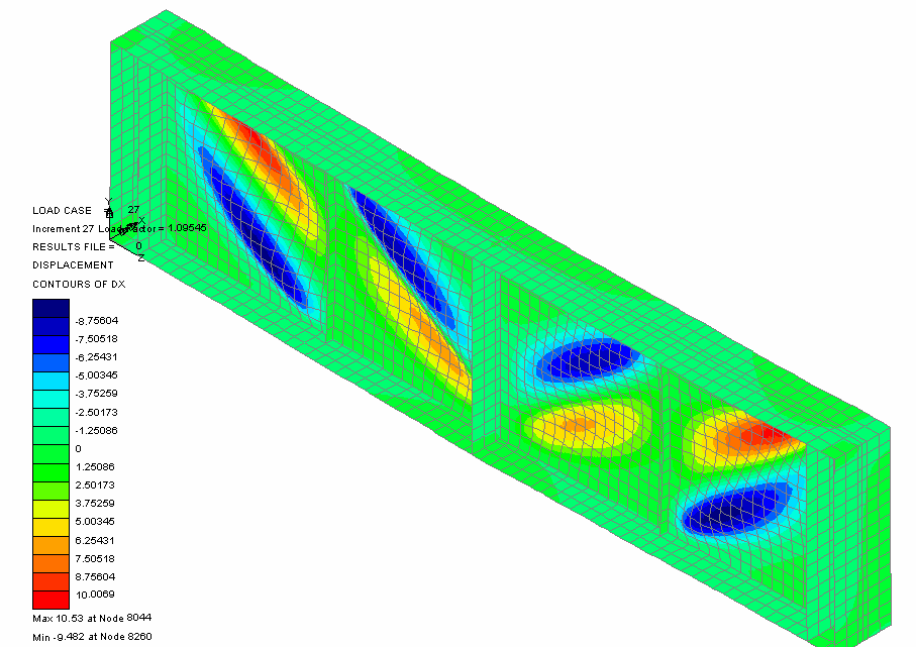

Figure 2.11 – Displacement Contours (mm) showing lateral displacement of webs under an applied load of 180kN x Load Factor of 1.09 = 196.2kN (Contour values do not include original imperfections illustrated in Figure 2.2)

The load-deflection curve obtained from the finite element analysis is illustrated in Figure 2.12.

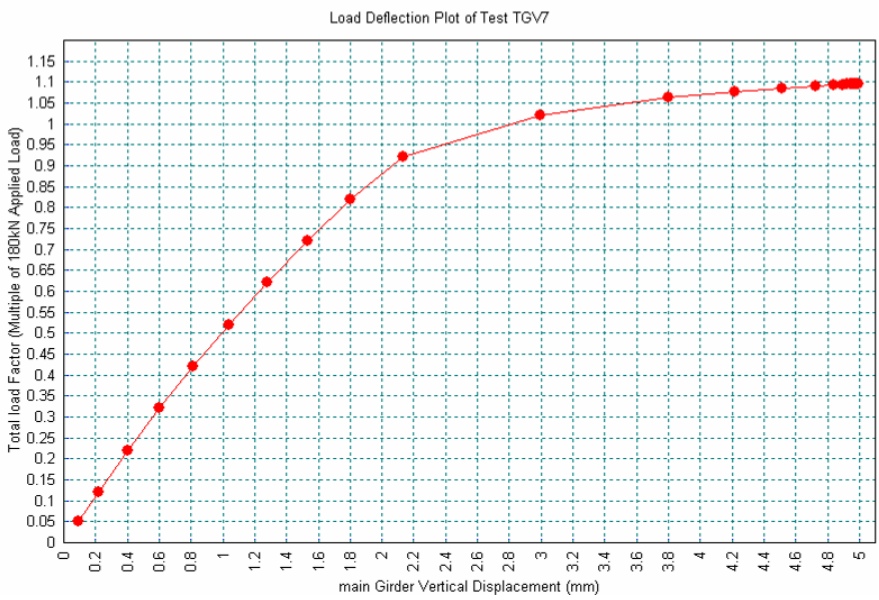

Figure 2.12 – Load-Deflection Curve obtained from FE Analysis of Test TGV7-2 using 'Initial Imperfection 1' in Figure 2.2

2.2.3 Results of FE modelling with 'Initial Deflection 2'

The finite element analysis of test TGV7-2 with 'initial deflection 2' stops when the analysis fails to find an equilibrium beyond a load factor of 1.086. The lateral deflections of the web are illustrated on Figure 2.13. Again, the failure mode is different to the equivalent TGV8 test in Figure 2.6 in that the intermediate stiffeners have remained intact.

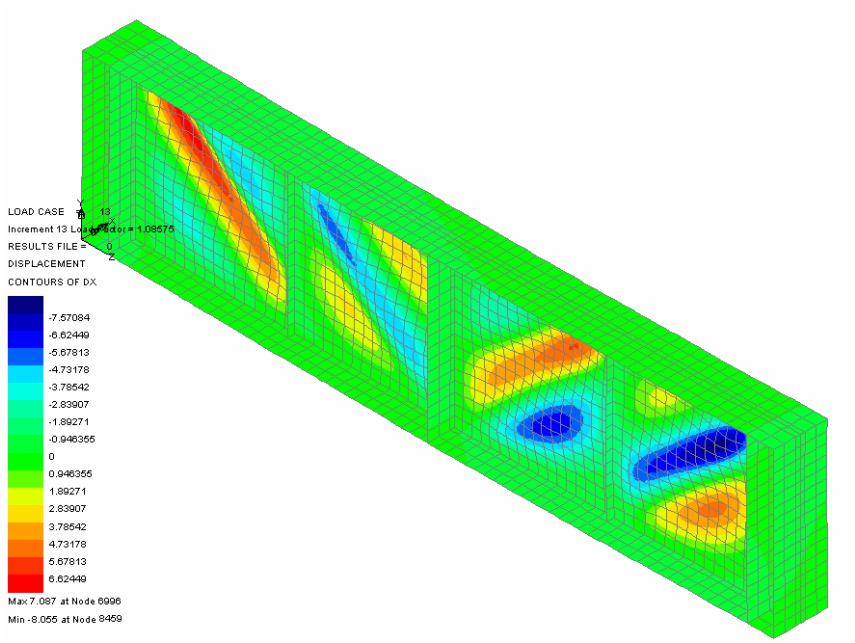

Figure 2.13 – Displacement Contours (mm) showing lateral displacement of webs under an applied load of 180kN x Load Factor of 1.086 = 195.5kN (Contour values do not include original imperfections illustrated in Figure 2.3)

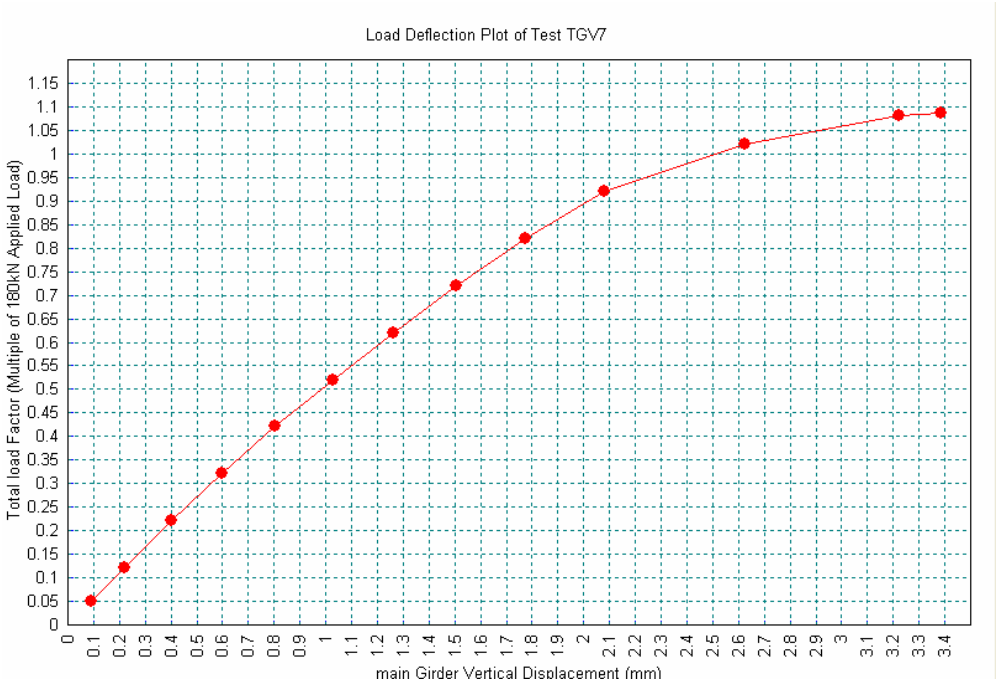

Figure 2.14 – Load-Deflection Curve obtained from FE Analysis of Test TGV7-2 using 'Initial Imperfection 2' in Figure 2.3

2.2.4 Comparison of TGV7-2 FE modelling output with laboratory test results

The photographed failure mode of Test TGV7-2 is illustrated in Figure 2.15. The failure modes predicted by the FE generated results in Figures 2.11 and 2.13 compare well with the actual failure mode recorded during testing. Both predicted failure modes involve buckling of the web plate with the stiffener remaining intact.

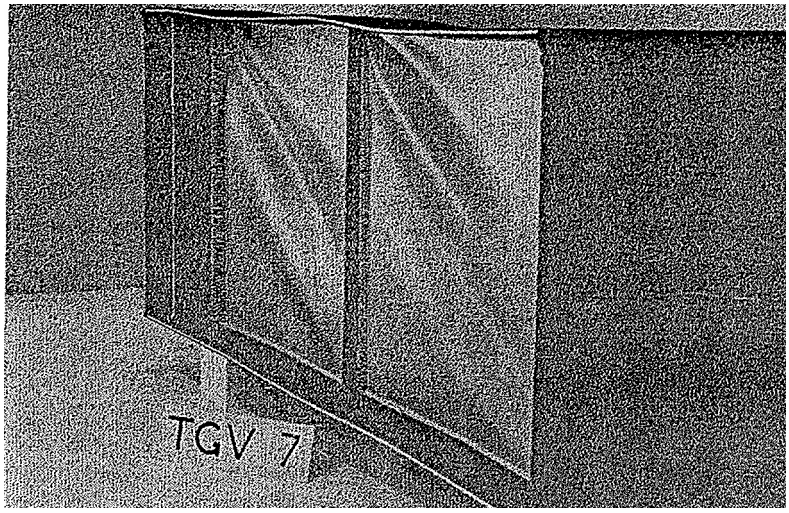

Figure 2.15 – Photograph of failure mode Test TGV7-2 (Extract from [11])

The recorded load-deflection curve for the laboratory test of TGV7-2 is illustrated in Figure 2.16.

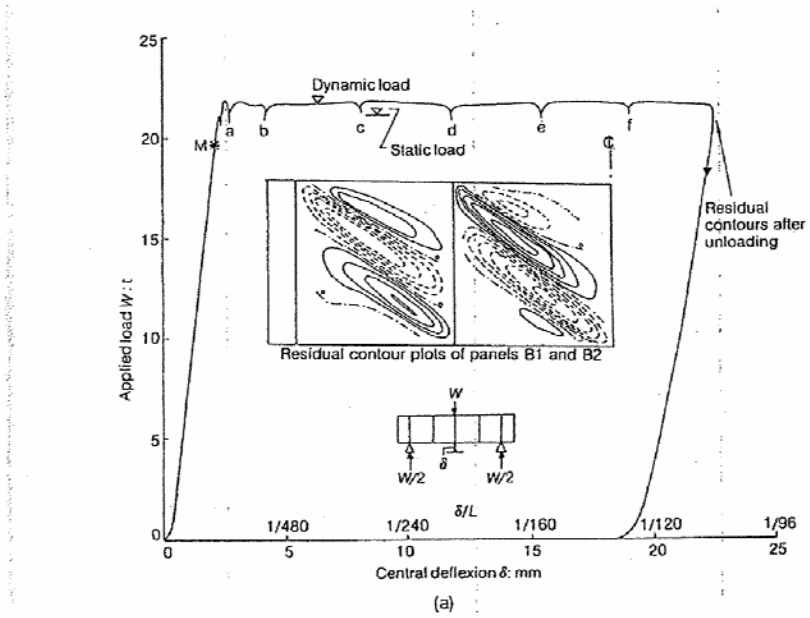

Figure 2.16 – Load-Deflection Plot recorded in laboratory testing of Test TGV7-2 (Extract from [11])

To compare the FE results to the tested results, all load deflection curves have been plotted on Figure 2.17 using the same assumptions explained previously in the TGV8-2 tests in section 2.1.4.

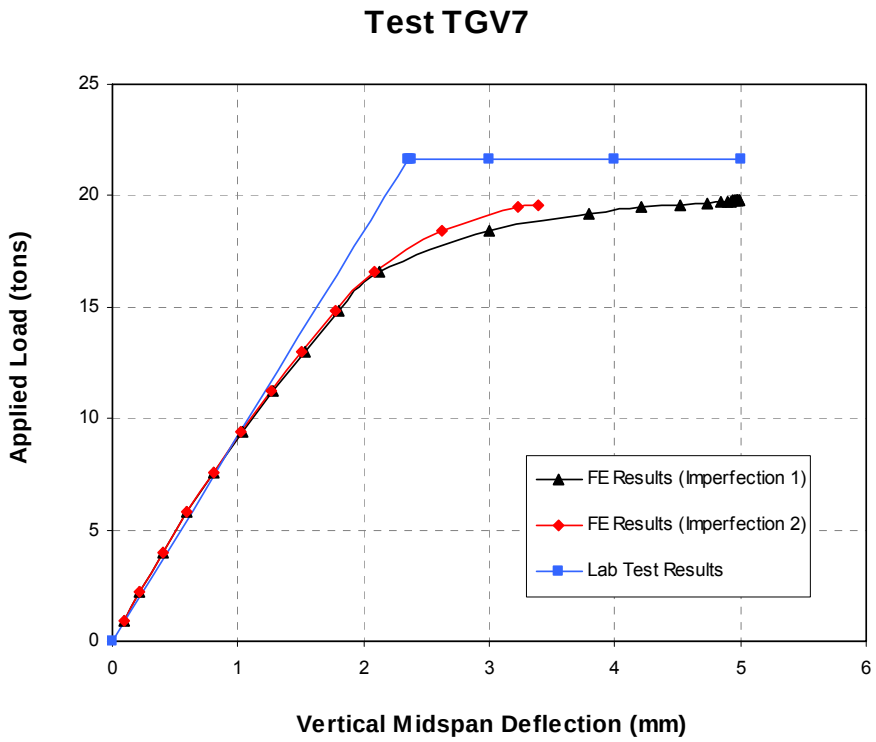

Figure 2.17 – Load-Deflection Plots of FE models and Laboratory Testing

2.2.5 Discussion of results

The graphs in Figure 2.17 do not correlate as closely as those for Test TGV8-2 in Figure 2.10. The principal difference between the two results is that both finite element analyses predict a non-linear response above an applied load of 10 tons whereas the lab test results in Figure 2.17 recorded a linear response until the approximate point of failure at 20 tons. The reasons for the differences are not completely clear, although a larger degree of strain hardening in the finite element models would result in a stiffer response beyond 10 tons which would bring the FE predictions closer to the measured results.

With regard to the theoretical failure load predicted by the Eurocode, as for test TGV8, shear capacity is critical with a predicted shear capacity of 88.8kN (assumes γ_{M0}=1.0, γ_{M1}=1.0). This shear force would be generated by a central point load of 177.6kN $\cong$ 17.8 tons.

A check of the TGV7-2 stiffener capacity to EN 1993-1-5 has found that the stiffener has adequate stiffness (with 2.6 times the required inertia) when checked against the minimum stiffness requirements of Clause 9.3.3. However, the strength of the stiffener is not sufficient, with a calculated usage factor of 3.36. As for test TGV8-2, this high usage factor is largely a consequence of the axial force applied at the centre of the web plate predicted by the equation in EN 1993-1-5 Clause 9.3.3(3). A stockier stiffener section would therefore be required if this girder was to be designed to the Eurocode. However, the results would prove that the Eurocode is conservative in the case of Test TGV7-2 as the intermediate stiffener used still remained intact after failure of the web plate in shear.

2.3 Conclusions from FE calibration exercises

- The FE modelling of lab test TGV8-2 in Figure 2.10 shows a close correlation between predicted results and measured results. This gives confidence in the accuracy of the FE modelling process in this instance.

- Even though the TGV8-2 intermediate stiffener did not possess adequate stiffness, as required by the Eurocode EN 1993-1-5 Clause 9.3.3(3), the combined stiffener-web system was still able to withstand the theoretical panel failure load – as predicted by EN 1993-1-5.

- The 'final failure' mode of test TGV8-2, predicted by the FE modelling, resulted in combined buckling of the web and stiffener (Figures 2.4 and 2.6). This is a similar failure mode to that observed in the tests (Figure 2.8).

- The FE modelling of lab test TGV7-2 in Figure 2.17 does not show as close a correlation between predicted results and measured results when compared to the TGV8-2 results. The FE predicted results show a non-linear response beyond a 10 ton central point load where as the measured results show an approximately linear response up to the point of failure. Although it would be possible to investigate the sensitivity of the results under less pessimistic levels of strain hardening, it can still be concluded that the FE modelling predictions are safe when compared to the measured lab test results in this instance.
- The TGV7-2 FE models predict that the TGV7-2 intermediate stiffeners remain intact after shear failure of the web (Figures 2.11 and 2.13). This was also observed during the lab tests (Figure 2.15). The Eurocode EN 1993-1-5 predicts that although the intermediate stiffener dimensions in TGV7-2 are adequate with regard to stiffness, they are clearly not adequate with regard to strength and a stockier stiffener section would be required.

Chapter 3

FE Modelling

3.1 Layout

The basic layout of girder to be modelled is illustrated in Figure 3.1. This comprises an inverted simply supported beam of length 12 x 2.5m (panel depth “d”) = 30m. By using this beam layout the web panel aspect ratios “a/d” can be set at 1 or 2 easily. Global lateral torsional buckling is restrained in the models by providing adequate lateral restraint to the compression flanges.

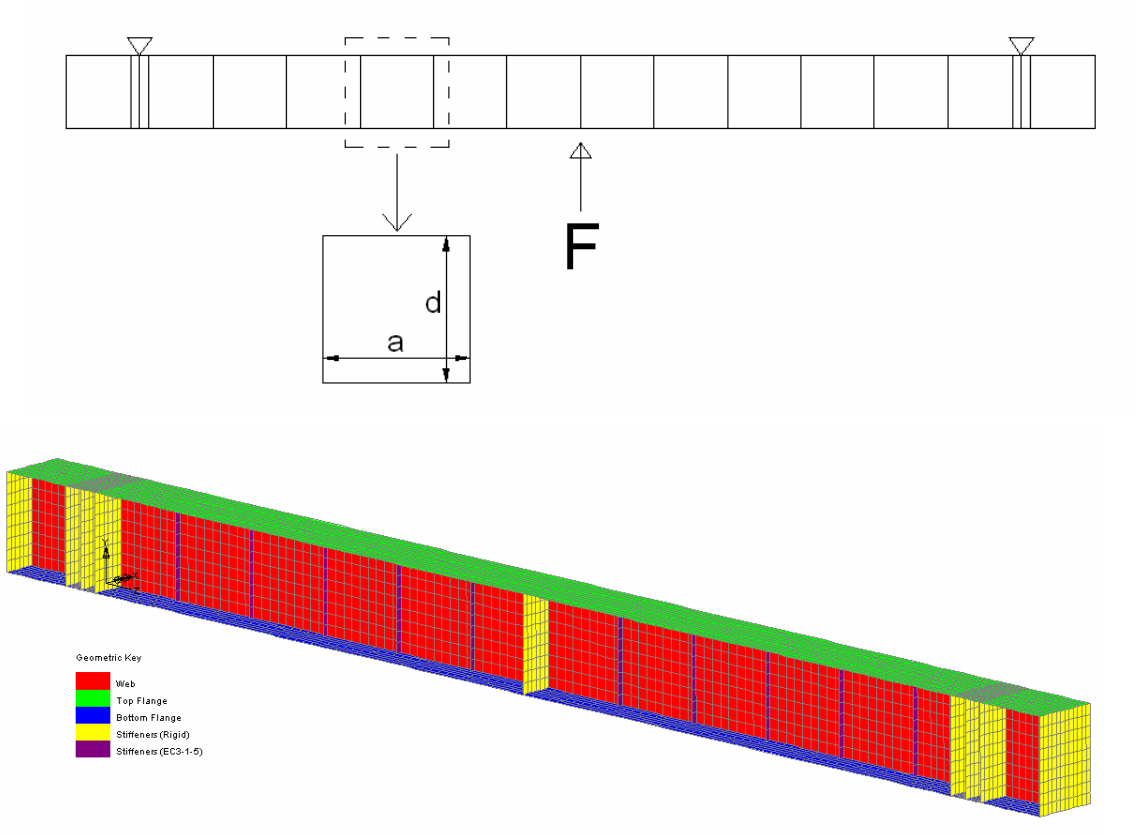

Figure 3.1 – Girder Layout used in FE modelling

Two different models have been considered in this study:

- **Symmetrical steel girder:** a steel plate girder with double sided stiffeners, considered to examine symmetric cases and the influence of axial force (see Section 4.1);

- **Steel-concrete composite girder:** a steel plate girder with a concrete slab on top with single sided stiffeners, considered to examine a real beam case (see Section 4.2). The bending moment also induces a net axial force in the web.

3.2 Stiffeners

The panels are separated by double sided, full height vertical web stiffeners for the steel girder analyses and by single sided, full height vertical stiffeners for the composite beam analyses.

Even though modern designs make greater use of single sided web stiffeners at panel boundaries, double sided stiffeners have been used to reduce the uncertainty in determining stiffener axial forces from finite element stresses, by reducing bending stresses associated with the asymmetry.

Three stiffeners are centred on the end supports to ensure any tension field developed in the end panels is anchored by these stiffeners. The central stiffener has a large area and stiffness to avoid analysis convergence problems caused by local yielding under the point load.

Using the relevant panel failure loads, a minimum allowable stiffener size is calculated using EN 1993-1-5. The EN approach requires that the stiffener conforms to a shape limit to avoid torsional buckling (clause 9.2.1 (8)), has sufficient stiffness to act as a rigid support to web panels (clause 9.3.3) and a sufficient strength under axial force and moment (clause 9.3.3). The minimum stiffener sizes allowed by EN 1993-1-5 based on stiffness have been used in most of the analyses. Several cases have also been run where stiffener sizes were controlled by strength to EN 1993-1-5 (in general the most conservative).

BS 5400 Part 3 requires three checks on the strength of the stiffener under axial force and moment. This includes checking the yielding of web plate (clause 9.13.5.1), the yielding of stiffener (clause 9.13.5.2) and the buckling of stiffener (clause 9.13.5.3). In addition, torsional buckling is taken into account by the specification of minimum outstand shape limits in clause 9.3.4.1.2. Stiffener dimensions calculated according to EN 1993-1-5 have been checked using BS 5400 Part 3 to compare the usage factors of the two codes.

3.3 Imperfections

Three different initial imperfections have been modelled to investigate the sensitivity to imperfection on the final buckling mode and factor.

The first initial imperfection, illustrated in Figure 3.2, is designed to maximise the effect on the web panels. Each web panel has been bowed out laterally, with the maximum bow dimension calculated, according to EN 1993-1-5 Annex C.5, as the minimum of (a/200, d/200), where “a” is panel length and “d” in the panel depth. For a panel aspect ratio of a/d=1 the maximum bow is 2500/200=12.5mm.

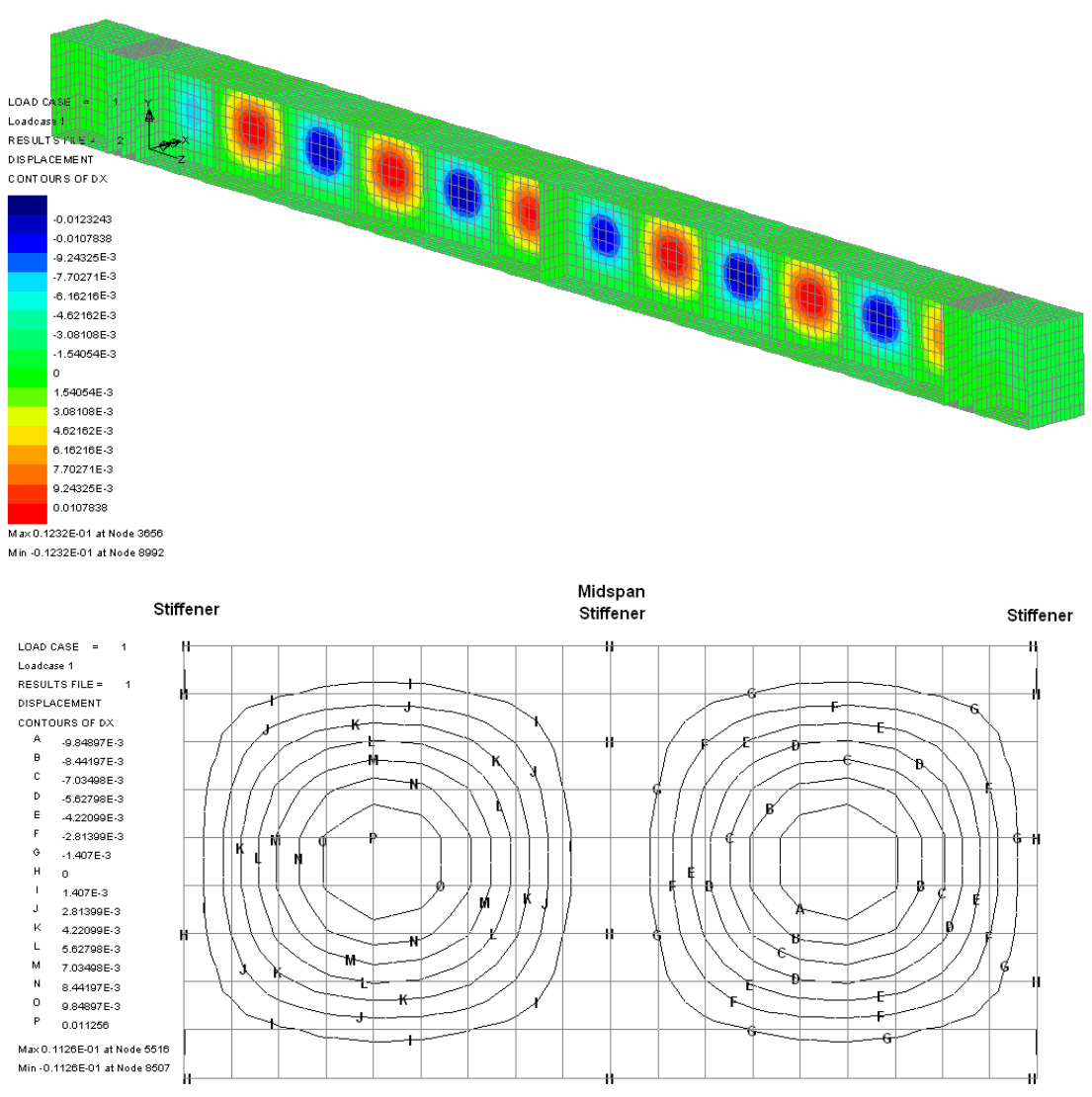

Figure 3.2 – Web Imperfections – Lateral Displacement Contour (m)

The second initial imperfection, illustrated in Figure 3.3, is designed to maximise the effect on the intermediate stiffener. The maximum stiffener deflection is about 2500/200=12.5mm.

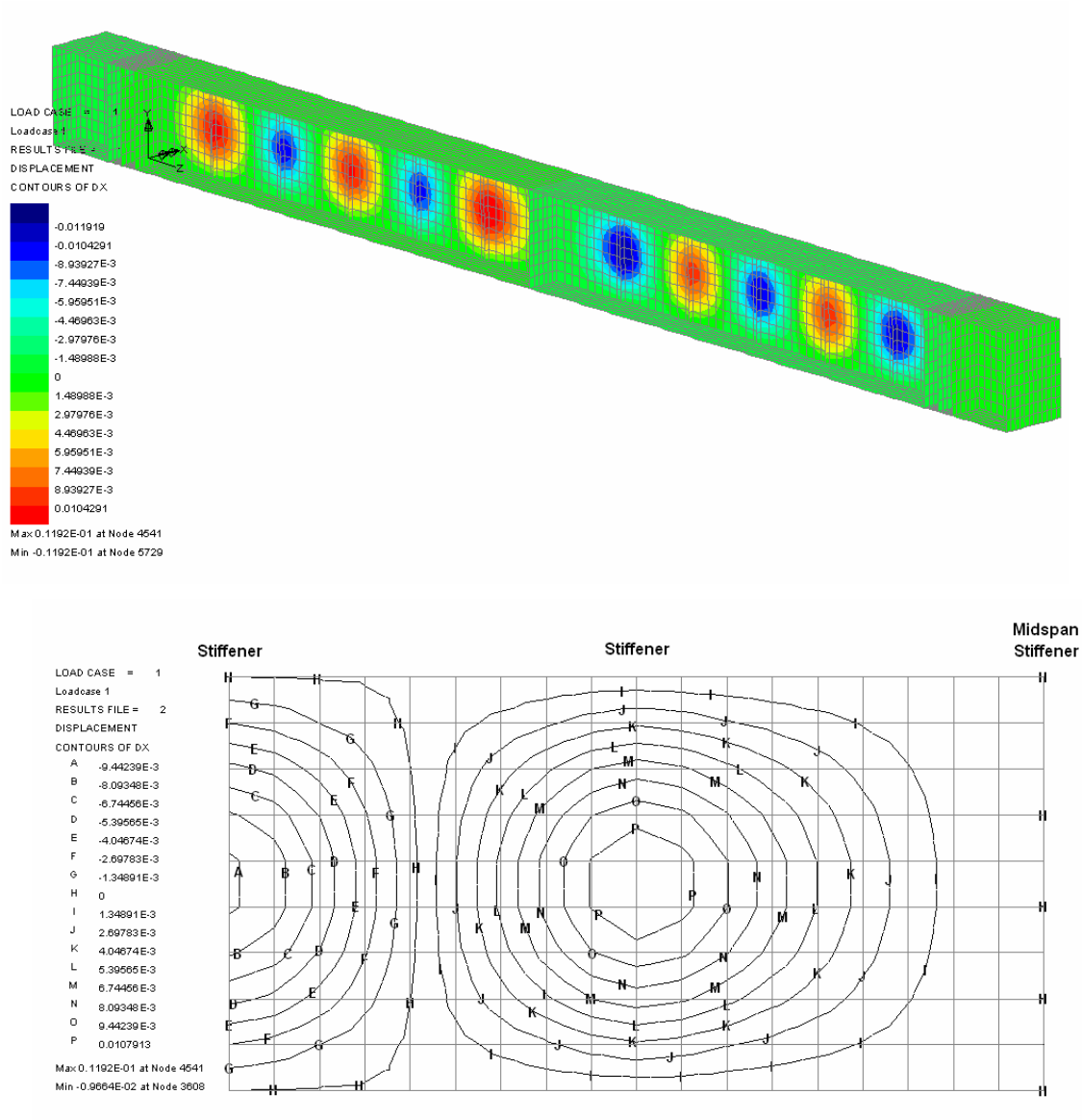

Figure 3.3 – Stiffeners Imperfections – Lateral Displacement Contour (m)

The third initial imperfection considered is based on the relevant elastic critical buckling modes.

3.4 Material properties

The steel yield strength of the plate girder components has been taken to be 355 N/mm^2. The material factor γ_M has been taken as 1.0 for all FE model components, to enable

comparison with code predictions using γ_M =1.0. The models have been analysed with full material non-linearity taken into account. After yield, the steel stress-strain slope has been set at E/100, in accordance with the recommendations in EN1993-1-5 Annex C.6, to model the effect of some strain hardening. Fracture has been assumed to take place at a strain of 5%.

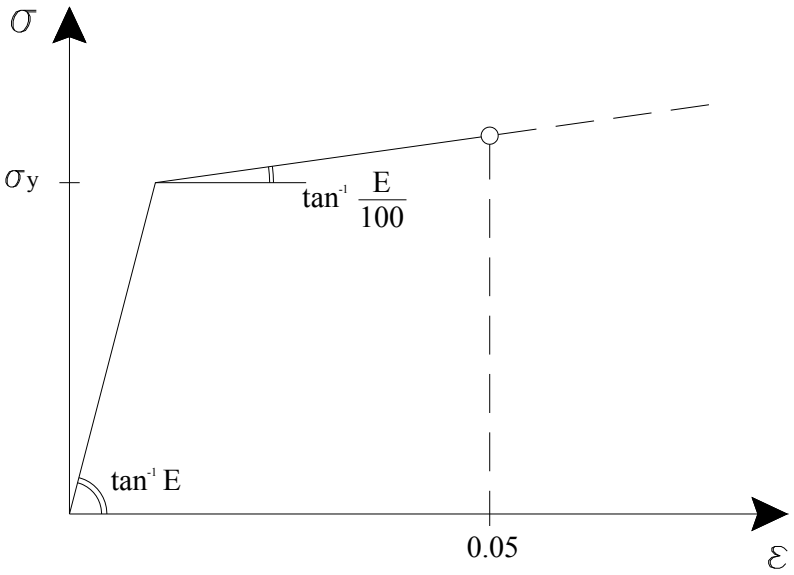

Figure 3.4 – Material behaviour assumed (EN1993-1-5 Annex C.6)

3.5 Meshing

The webs, flanges and stiffeners finite element meshes are formed from quadrilateral 'thick' shell elements. Composite slabs are represented by a non-linear beam element of equivalent area, stiffness and eccentricity, rigidly connected to the tension flange of the girder.

3.6 Loading

Vertical knife edge loadings are applied as distributed per unit length at the mid-span and at the ends of the beam, producing different ratios of bending moment to shear force, while uniform compressive stresses are applied to the beam ends. This simulates the moment and shear loading developed in a girder over a continuous bridge support and the compressive stresses have the same effect as varying the section to be non-symmetric or composite.

3.7 Non-linear analysis control

The models have been analysed with geometric and material non-linearities taken into account. Geometric non-linearities arise from significant changes in the structural configuration during loading when web plates develop membrane behaviour. Material non-linearities arise from a nonlinear constitutive model, when plastic yielding of metal is produced. For non-linear analysis, since it is no longer possible to directly obtain a stress distribution which equilibrates a given set of external loads, a solution procedure is usually adopted in which the total required load is applied in a number of increments. Within each increment a linear prediction of the nonlinear response is made, and subsequent iterative corrections are performed in order to restore equilibrium by the elimination of the residual or 'out of balance' forces. The iterative corrections are referred to some form of convergence criteria which indicates to what extent an equilibrate state has been achieved. Such a solution procedure is therefore commonly referred to as an incremental-iterative (or predictor-corrector) method shown in the Figure 3.5.

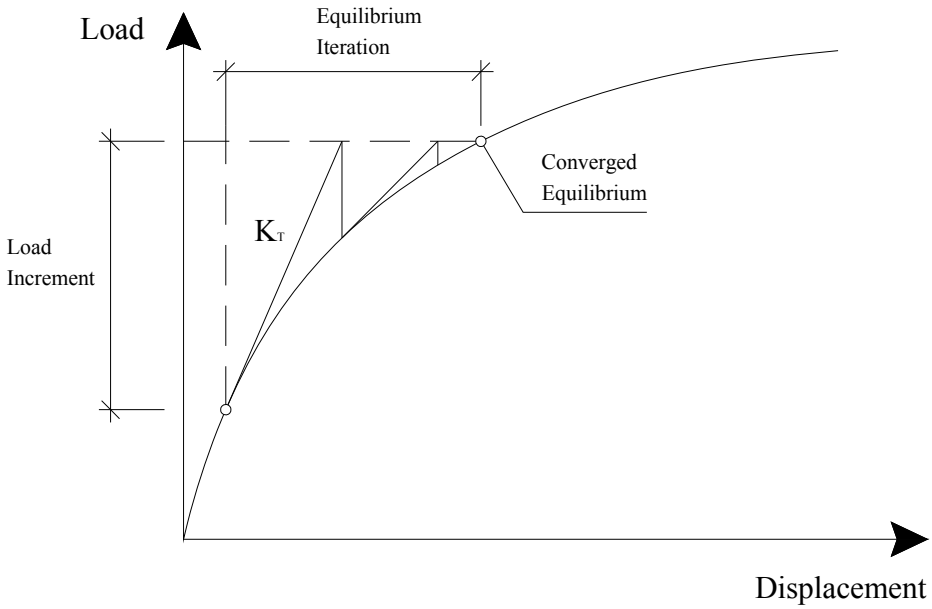

Figure 3.5 – Predictor-Corrector solution procedure

Within the software package used for the analyses, the non-linear solution is based on the Newton-Raphson procedure. In this procedure an initial prediction of the incremental solution is based on the tangent stiffness from which incremental displacements, and their iterative corrections may be derived. It is assumed that a displacement solution may be found for a given load increment and that, within each load increment, the load level

remains constant. Such methods are therefore often referred to as constant load level incrementation procedures. To investigate if limit points in the structural response are encountered, a constrained solution methods has been used. Constrained methods differ from constant level methods in that the load level is not required to be constant within an increment. In fact the load and displacement levels are constrained to follow some pre-defined path. Within the software package used, Crisfield's modified arc-length procedure is used, in which the solution is constrained to lie on a spherical surface defined in displacement space. The use of the arc-length method has advantages over constant load level methods in improving the convergence characteristics and the ability to detect and negotiate limit points.

Figure 3.6 shows a shot of the non-linear control dialog used within the software package used.

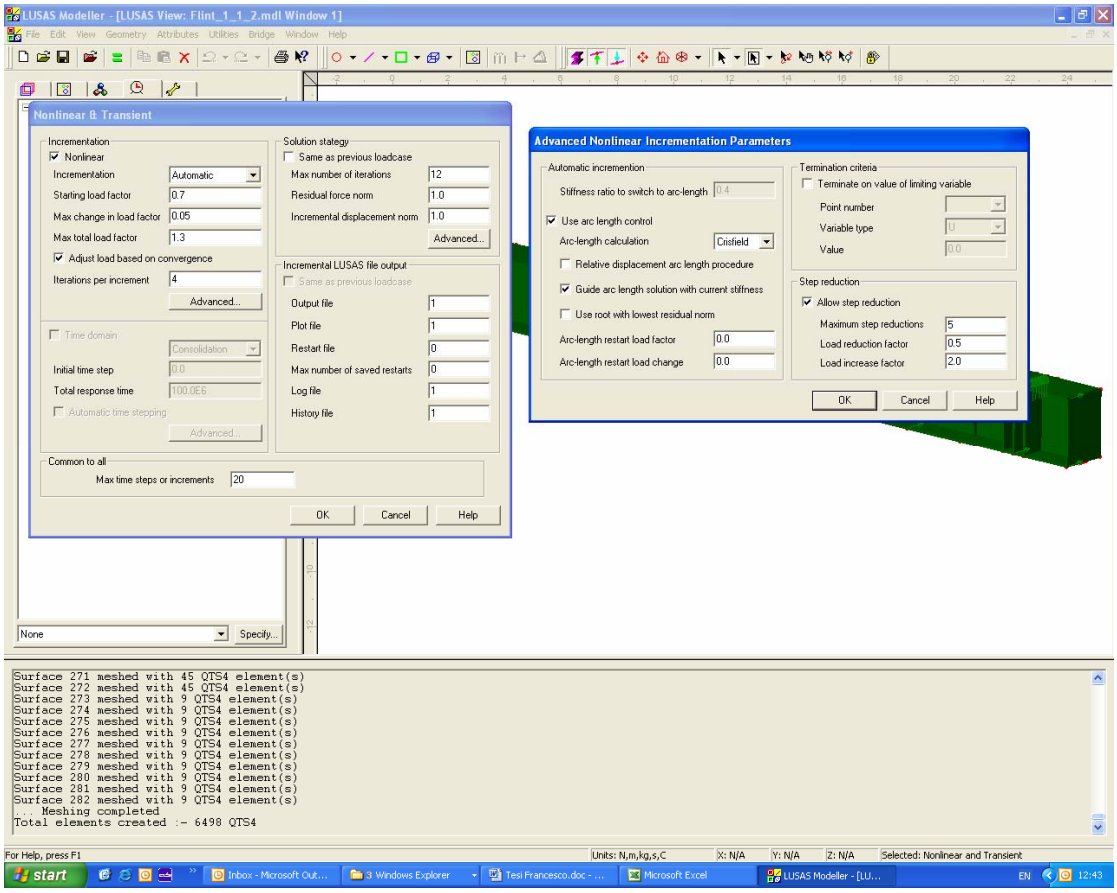

Figure 3.6 – Non-linear analysis control dialog

Chapter 4
Non-linear FE study

4.1 Symmetrical steel girder

A symmetric steel plate girder with double sided stiffeners is modelled. The layout shown in Figure 4.1 produces a high ratio of bending to shear force. Section dimensions are selected in such a way that the web panel adjacent to the middle support reaches its predicted failure load by buckling with tension field action in shear, coincidentally with overall bending yield of the section under the maximum moment at midspan. This leads to thick flanges which in turn gives rise to large boundary restraint. In order to maximise the difference $V_{Ed} - V_{crit}$ the web thickness is chosen to be such that the predicted shear strength by clause 9.9.2.2 in BS 5400 Part 3 is about twice the elastic critical buckling strength. The flange outstand/thickness ratio does not exceed 10 to avoid local buckling of the compression flange.

The iterative procedure to obtain the section dimensions is to assume the ultimate shear strength τ_{ult} as twice the shear critical stress and calculate the flange thickness required to avoid yield. With this thickness then it is possible to calculate the ultimate shear strength τ_{ult} by clause 9.9.2.2 in BS 5400 Part 3. If this does not equal that assumed, adjustment is done to the web thickness until it does.

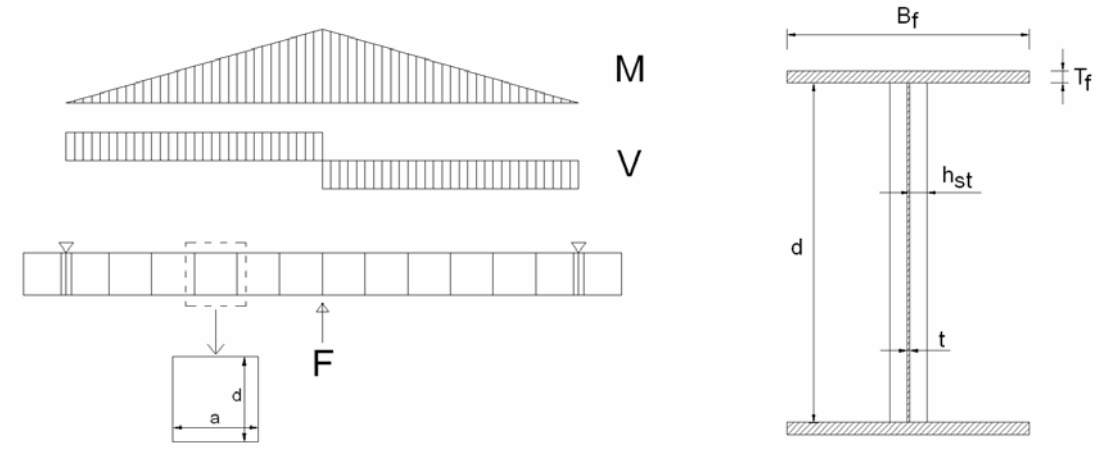

Figure 4.1 – Symmetrical steel beam section and loading

The iterative procedure consists of the following steps:

- a = d = 2500 mm
- t = “assumed”
- Calculate τ_{crit}
- Assume $\tau_{ult} = 2 \times \tau_{crit}$
- $V_{ult} = \tau_{ult} \times t \times d = \frac{F}{2} \rightarrow F = 2 \times V_{ult}$
- $M_{max} = \frac{F \times 12 \times d}{4} = 3\,d\,F = 6\,d\,V_{ult}$

Making the moment of resistance ignoring the web equal to M_{max} and making the flange width B_f equal to 20 times the flange thickness T_f we obtain:

$$T_f = \sqrt{\frac{6 \times \tau_{ult} \times d \times t}{20 \times \sigma_y}}$$

With this thickness, the ultimate shear strength τ_{ult} is calculated from clause 9.9.2.2 in BS5400 Part 3. If this does not equal that assumed, the web thickness is adjusted until it does.

Adjustment of the bending/shear ratios is obtained applying end moments equals to half those due to the point loads at mid-span.

The dimensions of the girders are given in Table 1 with a summary of the results from the non-linear analyses. For each case stiffeners are checked according to EN 1993-1-5 and BS 5400 Part 3.

In the following paragraphs, cases 2-1 and 11 are discussed in more detail.

	Girder							Load applied				stiffener design EN1993-1-5			stiffener design BS 5400 Part 3			Non-linear analysis		
case	a/d	d/t	t	T_f	B_f (= 20xT_f)	h_{st} x t_{st}	τ_{crit} [N/mm^2]	M [KNm]	V [KN]	End Moments [KNm]	σ_1 [N/mm^2]	stiffness ratio	shape limit (<10.5)	strength (U.F.)	web yield (U.F.)	stiffener yield (U.F.)	buckling (U.F.)	imperfections	Load factor	Usage Factor
			web	flange	flange	stiffener	simply supported boundaries					clause 9.3.3 (3)	clause 9.1 (2)	clause 9.4	clause 9.13.5.1	clause 9.13.5.2	clause 9.13.5.3		M_{NL}/M	M/M_{NL}
1-1	1	131.58	19	90	1800	130x40	101.70	148500	9900	0	0	0.35	3.25	0.97	0.84	0.75	1.18	web	0.91	1.10
1-2	1	131.58	19	90	1800	130x14	101.70	148500	9900	0	0	1.00	9.29	1.77	1.04	1.09	2.28	web	0.89	1.12
2-1	1	178.57	14	78	1560	100x12.5	54.87	108000	7200	0	0	1.00	8.00	3.62	1.58	1.79	4.09	web	0.85	1.18
2-2	1	178.57	14	78	1560	90x9	54.87	108000	7200	0	0	1.85	10.00	5.34	1.77	1.99	6.31	web	0.85	1.18
3	2	131.58	19	74	1480	130x14	68.60	148500	9900	0	0	0.50	9.29	1.34	1.14	1.09	2.37	web	0.72	1.39
4	1	131.58	19	64	1280	130x14	101.70	74250	9900	-74250	0	1.00	9.29	1.77	1.04	1.09	2.27	web	0.87	1.15
5-1	1	131.58	19	90	1800	130x40	101.70	148500	9900	0	0	0.35	3.25	0.97	0.84	0.75	1.18	stiffener	0.89	1.12
5-2	1	131.58	19	90	1800	130x14	101.70	148500	9900	0	0	1.00	9.29	1.77	1.04	1.09	2.28	stiffener	0.87	1.15
9	1	131.58	19	68	1360	130x14	52.88	148500	9900	0	25	1.00	9.29	1.77	1.39	1.44	2.94	stiffener	0.60	1.67
10	1	131.58	19	66	1320	130x14	0.00	148500	9900	0	50	1.00	9.29	1.77	1.67	1.84	3.53	stiffener	0.52	1.92
11	1	131.58	19	66	1320	130x14	0.00	148500	9900	0	75	1.00	9.29	1.77	1.69	1.84	3.63	stiffener	0.47	2.13

	Load applied x Load Factor				stiffener design EN1993-1-5		
case	M [KNm]	V [KN]	End Moments [KNm]	σ_1 [N/mm^2]	stiffness ratio	shape limit (<10.5)	strength (U.F.)
					clause 9.3.3 (3)	clause 9.1 (2)	clause 9.4
1-1	135135	9009	0	0	0.32	2.96	0.88
1-2	132165	8811	0	0	0.89	8.27	1.58
2-1	91800	6120	0	0	0.85	6.80	3.08
2-2	91800	6120	0	0	1.57	8.50	4.54
3	106920	7128	0	0	0.36	6.69	0.96
4	64598	8613	-64598	0	0.87	8.07	1.54
5-1	132165	8811	0	0	0.31	2.89	0.86
5-2	129195	8613	0	0	0.87	8.08	1.54
9	89100	5940	0	25	0.60	5.57	1.06
10	77220	5148	0	50	0.52	4.83	0.92
11	69795	4653	0	75	0.47	4.37	0.83

Table 1 – Summary of results and usage factors for M, V and N based on non-linear failure

4.1.1 Case 2-1

The finite element analysis has been run with initial web imperfections as shown in Figure 3.2. The stiffener dimensions are the minimum allowed by the stiffness criteria in EN 1993-1-5.

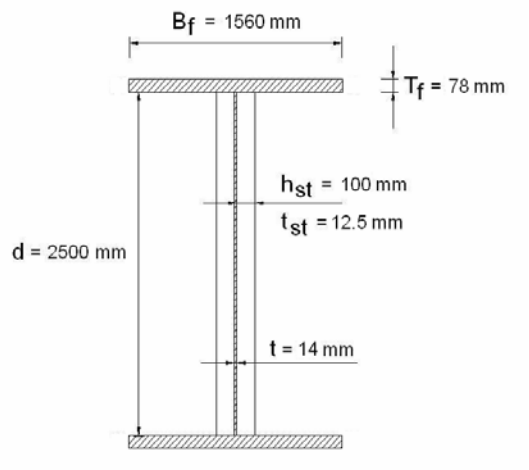

Figure 4.2 – Section dimensions

The panels aspect ratio in this case is a/d = 1, and the critical stress and shear are:

τ_{cr} = 55 N/mm^2 (see Appendix A)

$V_{cr} = \tau_{cr} \times t \times d$ = 1925 KN

Owing to the size of the flanges provided in the model, the web panels are restrained against out-of-plane rotation and their critical stresses are higher than assumed in codified rules. The critical stresses, when calculated from [4] for a plate with built-in edges, become:

τ_{cr} = 86 N/mm^2 (see Appendix A)

$V_{cr} = \tau_{cr} \times t \times d$ = 3010 KN

A force F = 14400 KN ≈ 2 x V_{ult} at midspan, if applied in a linear analysis, would produce the following effects:

M_{max} = F x L / 4 = 14400 x 30 / 4 = 108000 KNm

V = F / 2 = 14400 / 2 = 7200 KN ≈ V_{ult}

The non-linear analysis stops when it fails to find an equilibrium beyond a load factor 0.85.

M_{NL} = 0.85 x 108000 = 91800 KNm $\longrightarrow$ $\overline{\eta}_1$ = 0.771

V_{NL} = 0.85 x 7200 = 6120 KN $\longrightarrow$ $\overline{\eta}_3$ = 1.632

The load-deflection curve obtained from the finite element analysis is illustrated in Figure 4.3. The analysis shows an almost linear behaviour up to a load factor of approximately 0.7, after which it shows a gradual loss of stiffness culminating in a failure at the load factor of 0.85.

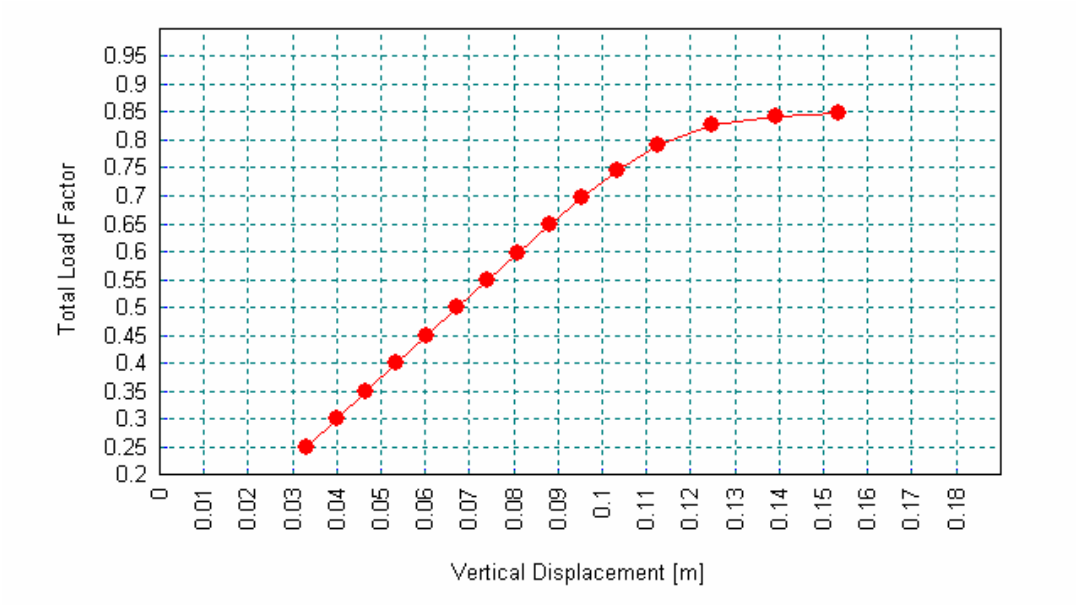

Fig. 4.3 – Vertical Displacement vs Total Load Factor

The lateral deflections of the web at different stages are illustrated in Figures 4.6 to 4.13, where it can be seen that the girder has failed by the web bowing out laterally, while stiffeners twist in sympathy.

The M-V interaction domain from EN 1993-1-5 and the results obtained from the non-linear analysis are illustrated in Figure 4.4. The girder shows an extra capacity of about +20% when compared with Eurocode and the solution point is outside the interaction curve. The interaction curve has been built according to EN 1993-1-5 clause 7.1(1). This domain has been built considering a τ_{crit} value derived for a simply supported plate loaded in shear.

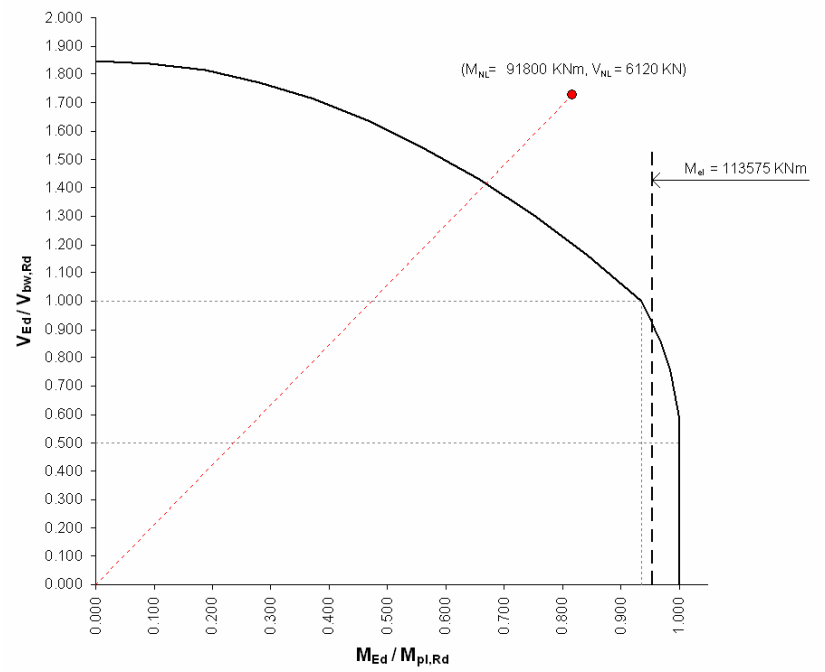

Figure 4.4 – Eurocode M-V interaction domain and result from non-linear analysis (simply supported plates in shear)

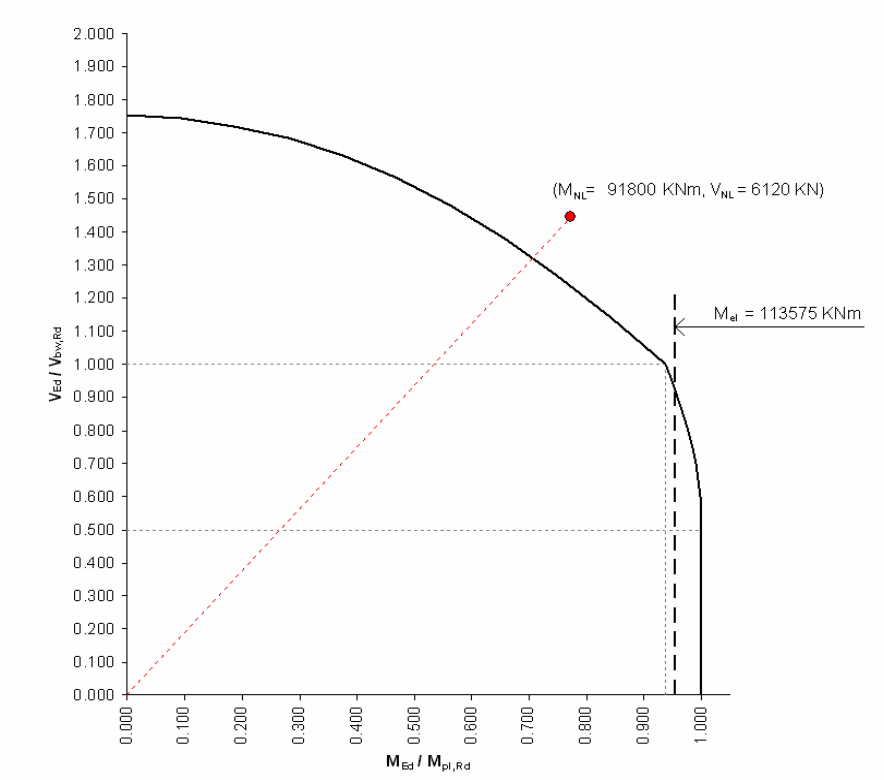

Figure 4.5 – Eurocode M-V interaction domain and result from non-linear analysis (built-in plates in shear)

If more realistically we use the theoretical solutions of a plate with longitudinal edges clamped with transverse stiffeners, the latter having low torsional stiffness, as discussed in [4], the M-V interaction domain becomes bigger with a shift upward due to the increase in value of $V_{bw,Rd}$ and the extra capacity from the non-linear analysis is now reduced to about +10% (Figure 4.5).

The sections through the girder at various stages in the analysis to establish the distribution of internal forces are illustrated in Figures 4.14 to 4.26.

From Figures 4.15, 4.18 and 4.21 it can be seen that for load increments 1 to 3 the longitudinal stresses in the web vary more or less linearly as expected. Tension field effects appear beyond increment 3 at which the mean shear stress is about 72 N/mm^2, compared with a critical stress of 86 N/mm^2 (for fully clamped edges) and 55 N/mm^2 (for simply supported edges), and therefore consistent with theory. Beyond this increment, a membrane tension develops, which modifies the distribution of direct stress in the girder. This gives rise to a net tension in the web, which is balanced by opposing compressive force in the flanges, adding to the flexural compressive stress in one flange and reducing the flexural stress in the other. This behaviour gives an increase in compressive flange force beyond that predicted solely from a cross section bending analysis (see Figures 4.16 and 4.19). There is evidence, from Figures 4.18 and 4.21, that towards the failure load the tension field stresses carry through the first intermediate stiffener, which indicates there to be little transfer of such stresses to the stiffener.

The stiffener forces given in Figure 4.26, at mid-height of the stiffener, are plotted against the load factor. They show a very marked escalation beyond increment 12. It is noted that, at this increment, the shear stress at the bottom of section S3 (Figure 4.20) equals the shear yield stress, whereas at the section S2 (Figure 4.22) the shear stress begins to reduce at the bottom but increase to the yield stress at the top, both of which are compatible with an increase in the force transmitted to the stiffener.

The vertical stresses at mid-height of the stiffeners are plotted against the load factor in Figure 4.25. The maximum vertical force acting on the effective area of the stiffener gives a compressive stress of approximately 100 N/mm^2 while the maximum vertical force acting on the stiffener alone gives a compressive stress of approximately 160 N/mm^2. It is clear that the forces and stresses are dependent on the choice of the effective section for the stiffener. The stresses calculated above ignore significant bending stresses induced in the stiffener due to second order P-Δ moments from initial imperfection. Considering a

pin-ended strut with an initial sinusoidal bow imperfection of maximum displacement 12.5mm (see Section 3.3), the maximum stress in the stiffener outstand is about 225N/mm^2.

The stiffener force, calculated as the difference between the observed ultimate shear force (6120 KN) and the elastic critical shear force with edge fixity (3010 KN), amounts to 3110 KN compared with a value derived from the observed stresses of about 1040 KN for the effective area at mid-height of the stiffener.

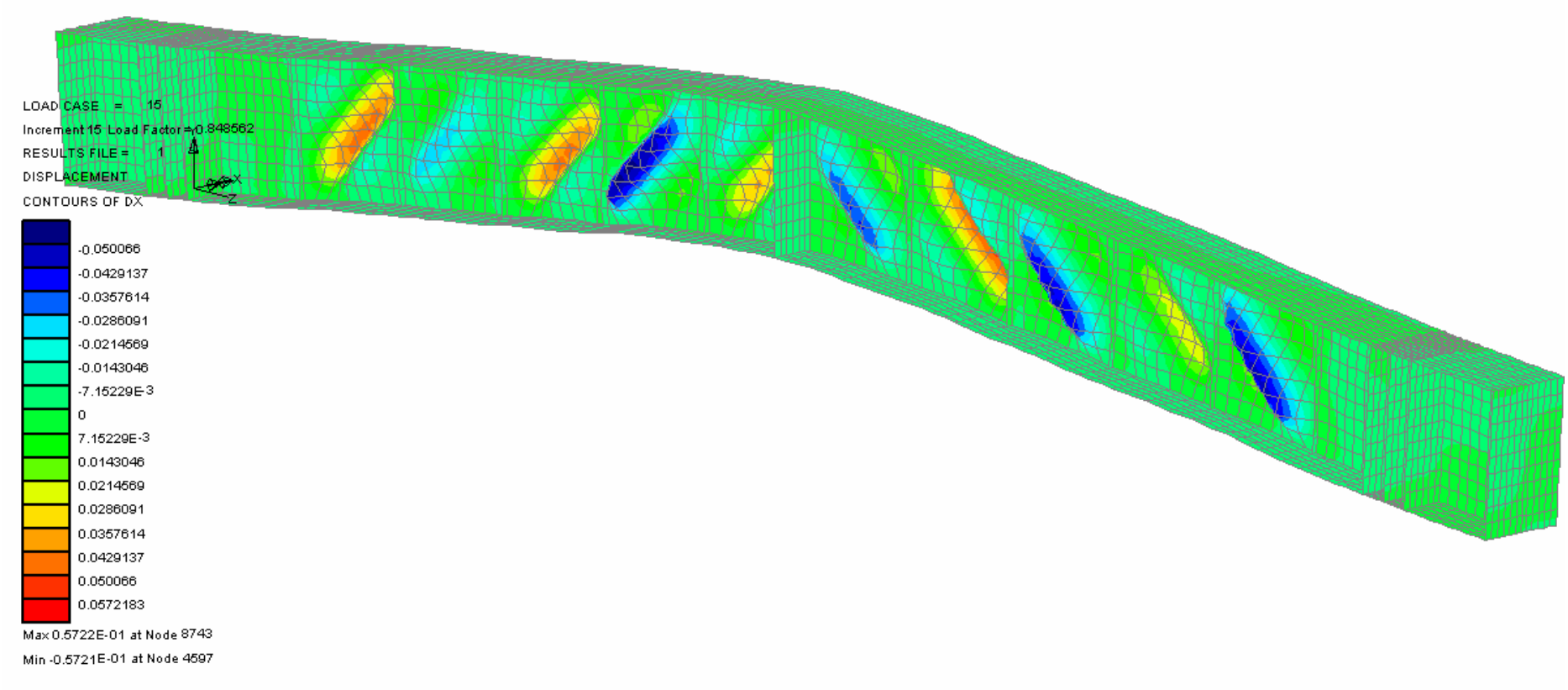

Figure 4.6 – Lateral Displacement Contour (m) at failure

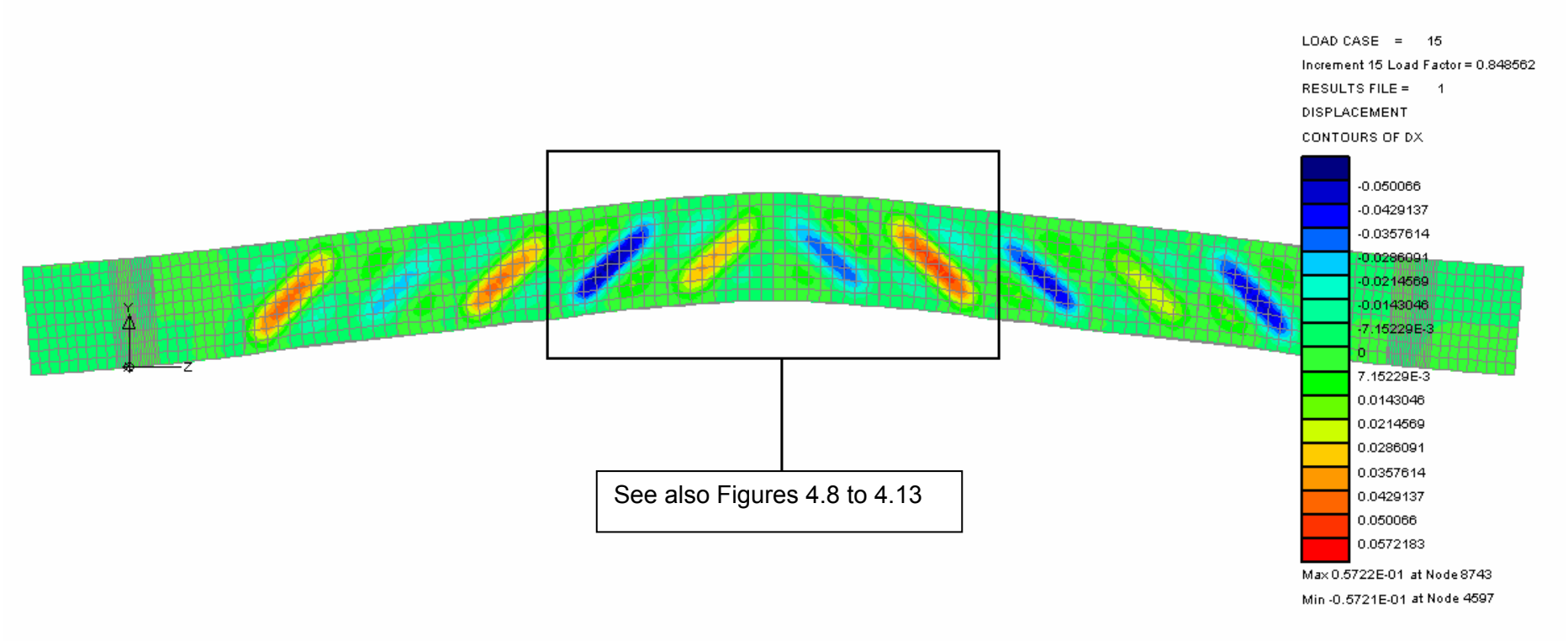

Figure 4.7 – Lateral Displacement Contour (m) at failure

LOAD CASE = 1

Increment 1 Load Factor = 0.249631

RESULTS FILE = 1

DISPLACEMENT

CONTOURS OF DX

A	-3.1822E-3
B	-2.7276E-3
C	-2.273E-3
D	-1.8184E-3
E	-1.3638E-3
F	-0.9092E-3
G	-0.4546E-3
H	0
I	0.4546E-3
J	0.9092E-3
K	1.3638E-3
L	1.8184E-3
M	2.273E-3
N	2.7276E-3
O	3.1822E-3
P	3.6368E-3

Max 0.3637E-02 at Node 5531

Min -0.3637E-02 at Node 8501

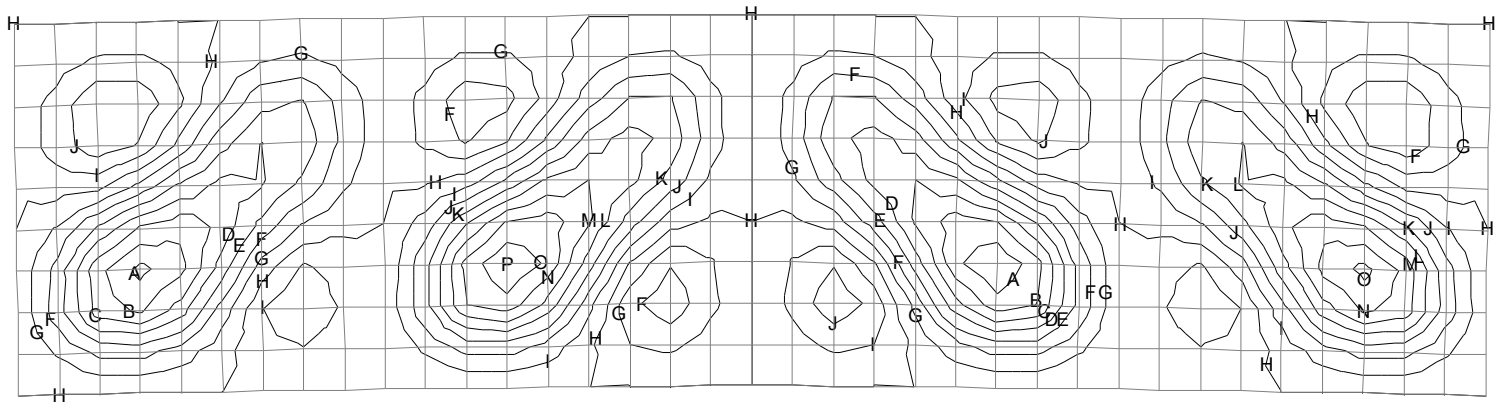

Figure 4.8 – Lateral Displacement Contour (m) at load increment 1

LOAD CASE = 1

Increment 1 Load Factor = 0.249631

RESULTS FILE = 1

DISPLACEMENT

CONTOURS OF DX

A	-3.1822E-3
B	-2.7276E-3
C	-2.273E-3
D	-1.8184E-3
E	-1.3638E-3
F	-0.9092E-3
G	-0.4546E-3
H	0
I	0.4546E-3
J	0.9092E-3
K	1.3638E-3
L	1.8184E-3
M	2.273E-3
N	2.7276E-3
O	3.1822E-3
P	3.6368E-3

Max 0.3637E-02 at Node 5531

Min -0.3637E-02 at Node 8501

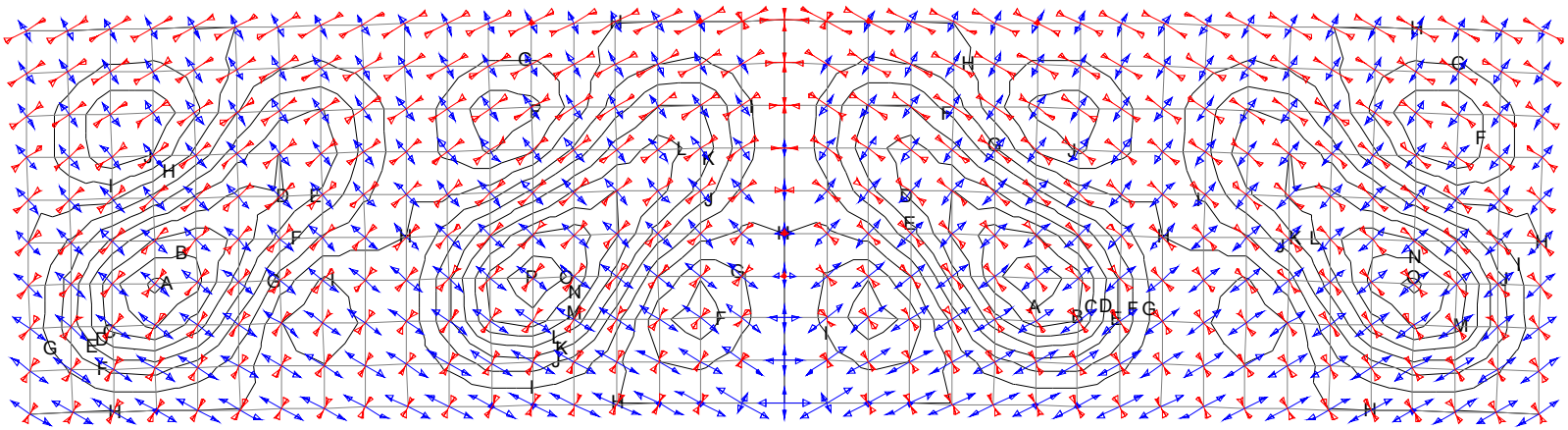

Figure 4.9 – Lateral Displacement Contour (m) and Principal Vector at load increment 1

LOAD CASE = 9

Increment 9 Load Factor = 0.648017

RESULTS FILE = 1

DISPLACEMENT

CONTOURS OF DX

A	-0.0163138
B	-0.0139832
C	-0.0116527
D	-9.32216E-3
E	-6.99162E-3
F	-4.66108E-3
G	-2.33054E-3
H	0
I	2.33054E-3
J	4.66108E-3
K	6.99162E-3
L	9.32216E-3
M	0.0116527
N	0.0139832
O	0.0163138
P	0.0186443

Max 0.1864E-01 at Node 5531

Min -0.1864E-01 at Node 8501

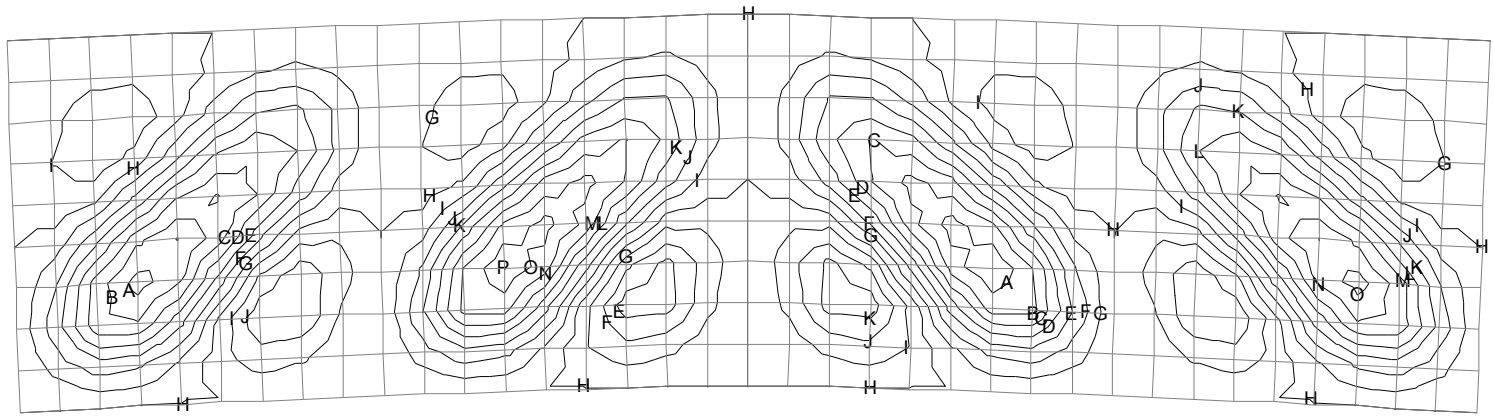

Figure 4.10 – Lateral Displacement Contour (m) at load increment 9

LOAD CASE = 9

Increment 9 Load Factor = 0.648017

RESULTS FILE = 1

DISPLACEMENT

CONTOURS OF DX

A	-0.0163138
B	-0.0139832
C	-0.0116527
D	-9.32216E-3
E	-6.99162E-3
F	-4.66108E-3
G	-2.33054E-3
H	0
I	2.33054E-3
J	4.66108E-3
K	6.99162E-3
L	9.32216E-3
M	0.0116527
N	0.0139832
O	0.0163138
P	0.0186443

Max 0.1864E-01 at Node 5531

Min -0.1864E-01 at Node 8501

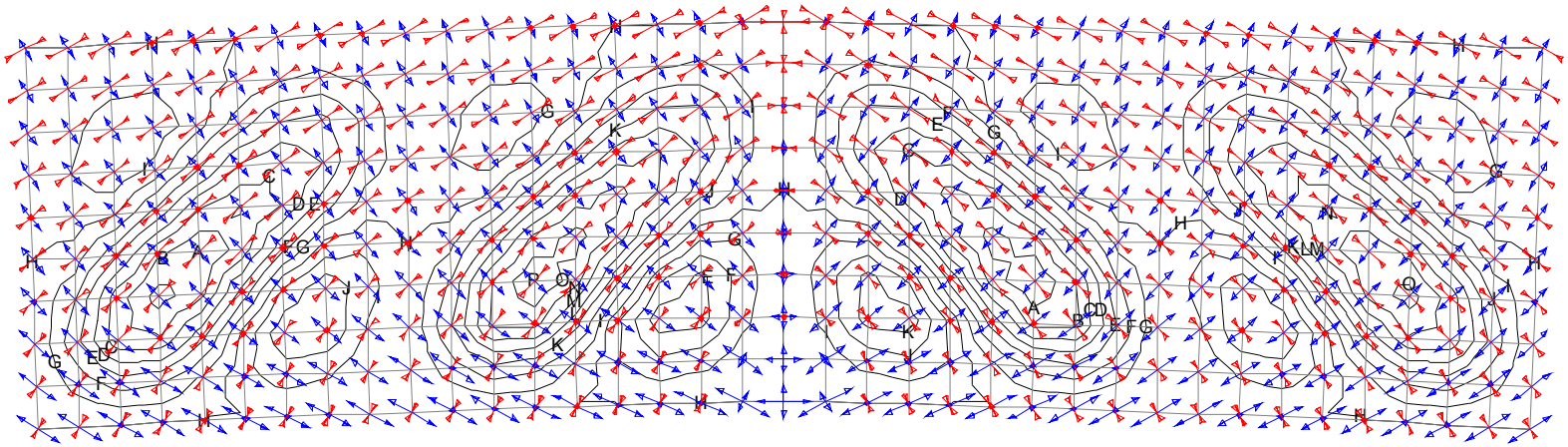

Figure 4.11 – Lateral Displacement Contour (m) and Principal Vector at load increment 9

LOAD CASE = 15

Increment 15 Load Factor = 0.848562

RESULTS FILE = 1

DISPLACEMENT

CONTOURS OF DX

A	-0.050066
B	-0.0429137
C	-0.0357614
D	-0.0286091
E	-0.0214569
F	-0.0143046
G	-7.15229E-3
H	0
I	7.15229E-3
J	0.0143046
K	0.0214569
L	0.0286091
M	0.0357614
N	0.0429137
O	0.050066
P	0.0572183

Max 0.5722E-01 at Node 8743

Min -0.5721E-01 at Node 4597

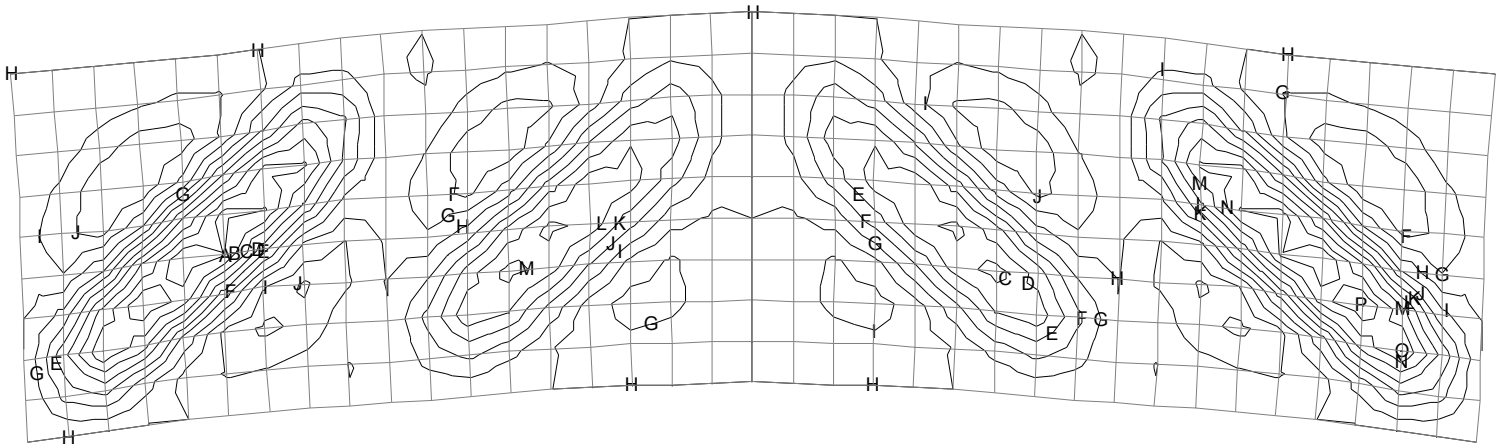

Figure 4.12 – Lateral Displacement Contour (m) at load increment 15 (failure)

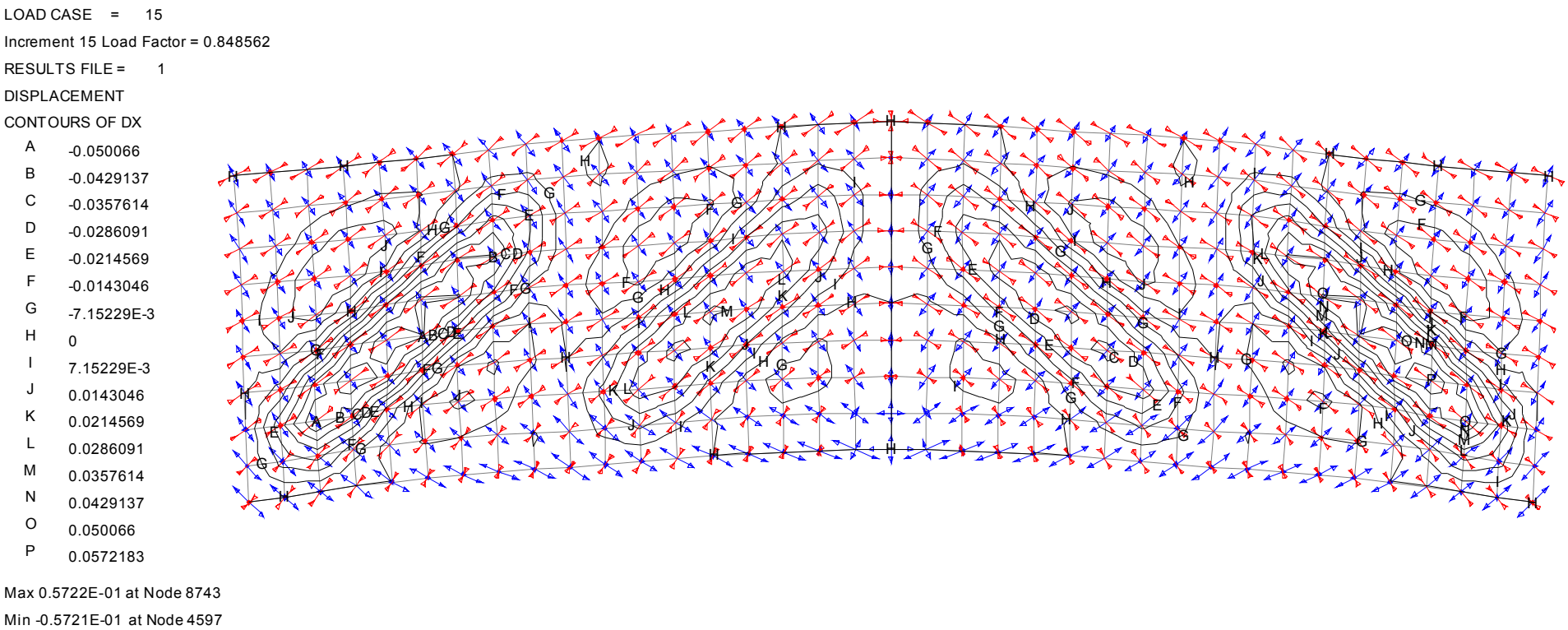

Figure 4.13 – Lateral Displacement Contour (m) and Principal Vector at load increment 15 (failure)

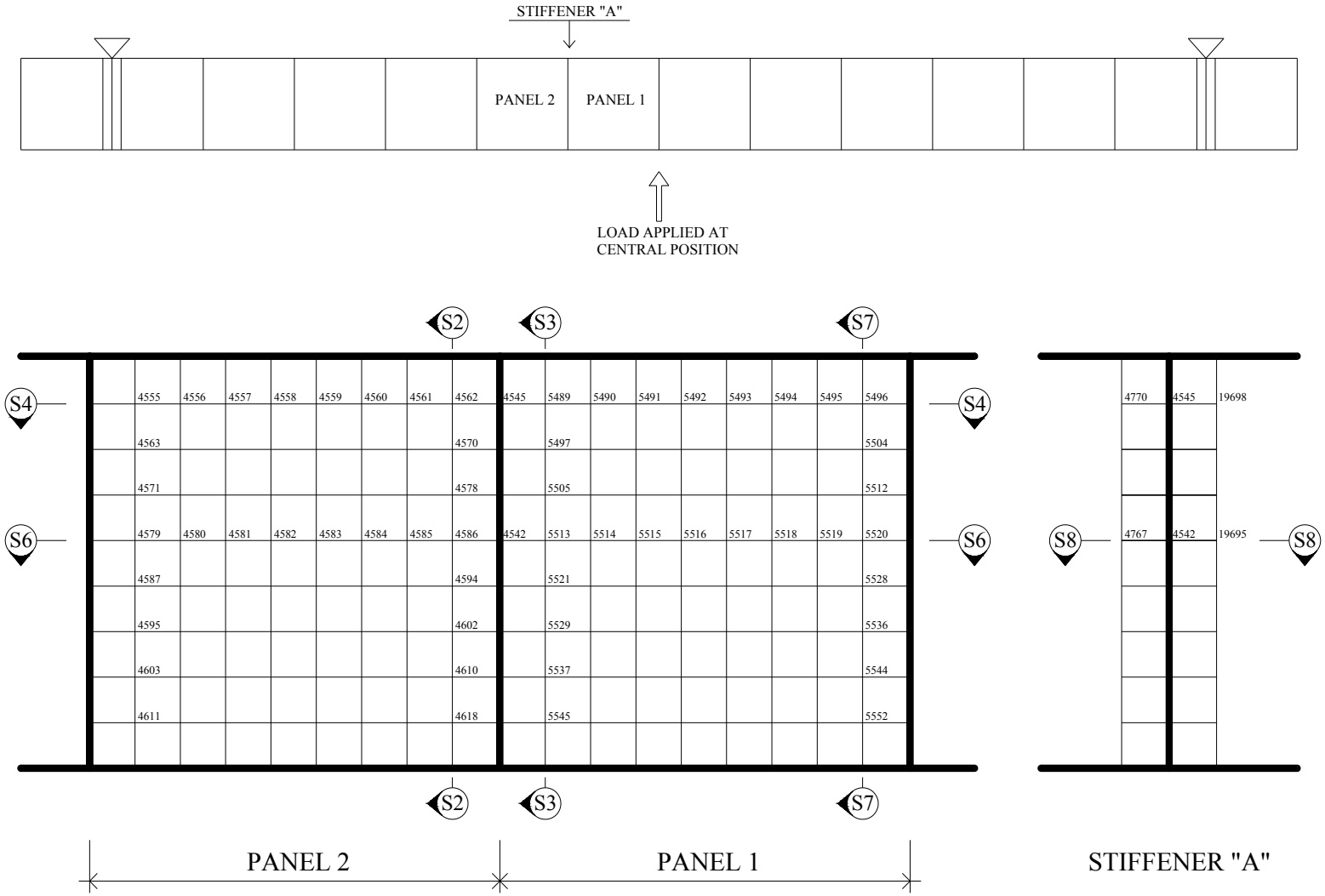

Fig. 4.14 – Investigated area and location of sections

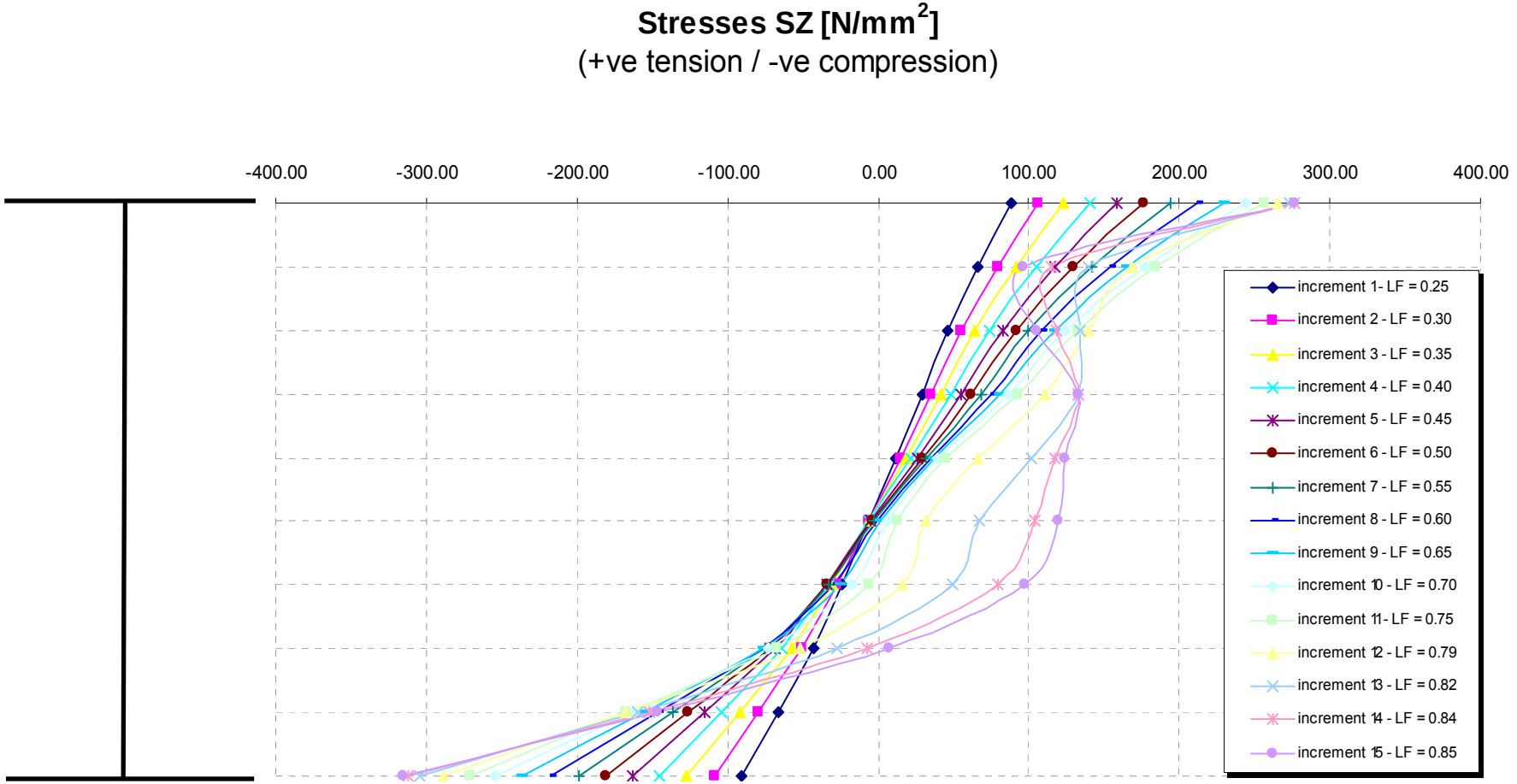

Fig. 4.15 – Section S7 – Longitudinal stresses in web (refer to Figure 4.14)

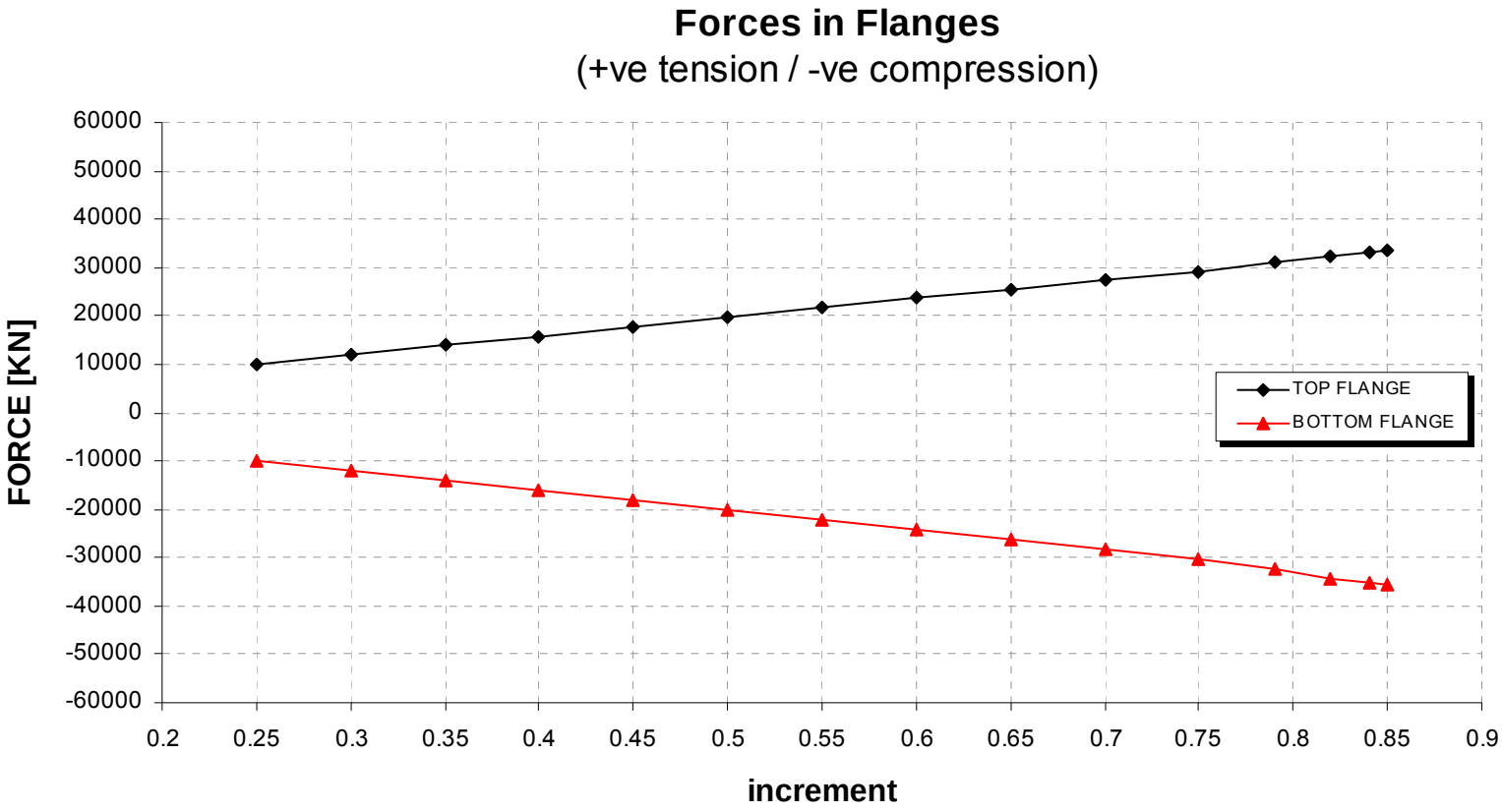

Fig. 4.16 – Section S7 – Longitudinal forces in flanges (refer to Figure 4.14)

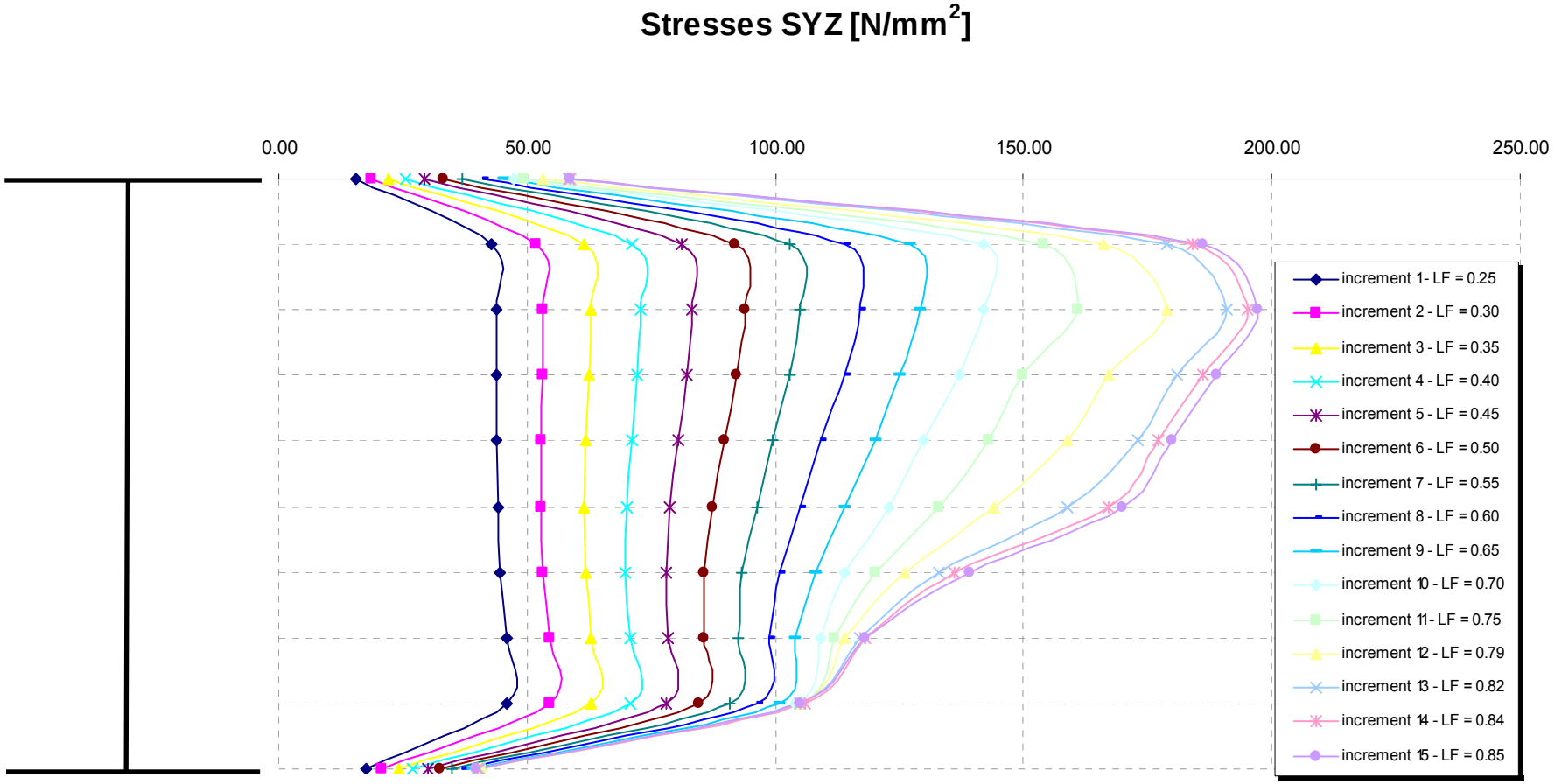

Fig. 4.17 – Section S7 – Shear stresses in web (refer to Figure 4.14)

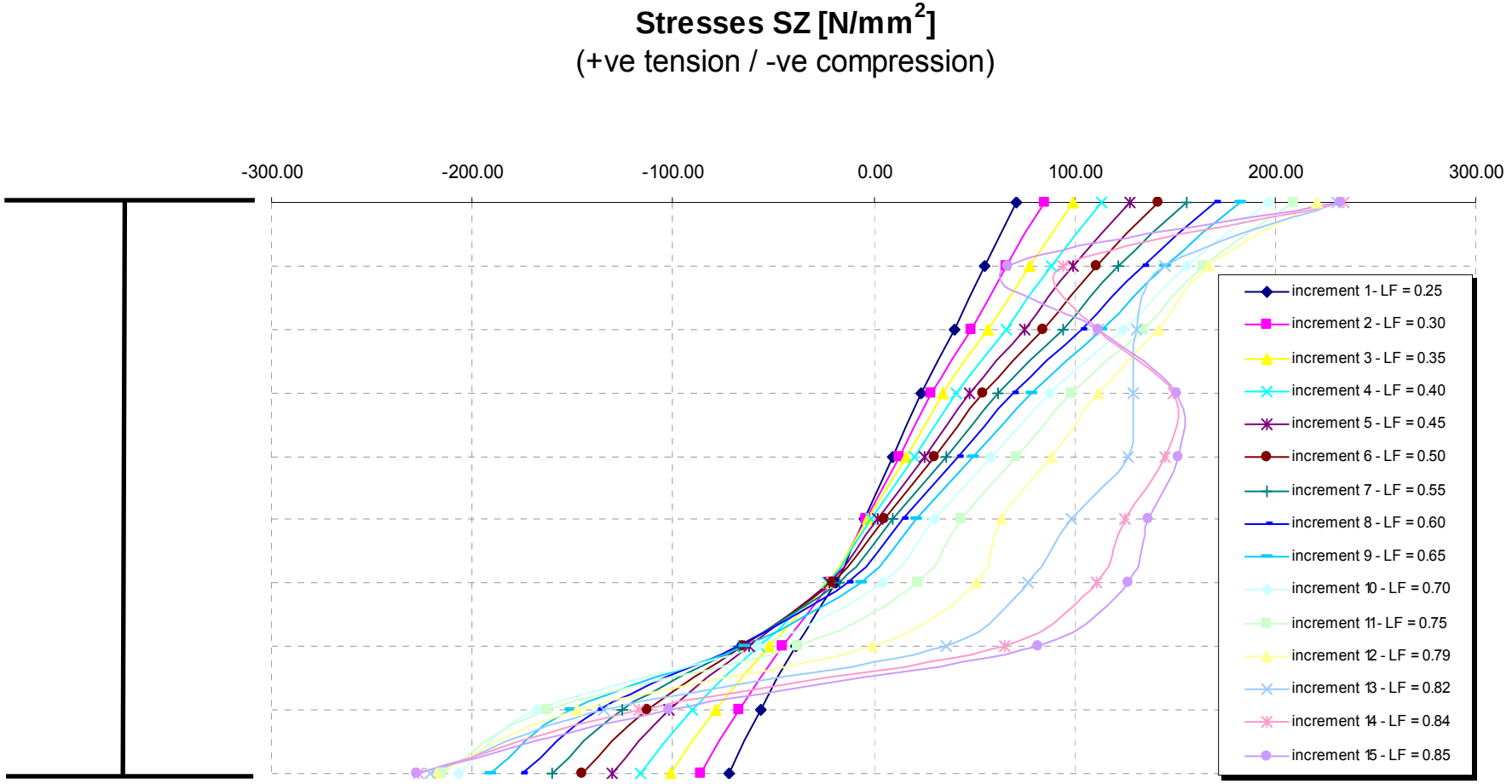

Fig. 4.18 – Section S3 – Longitudinal stresses in web (refer to Figure 4.14)

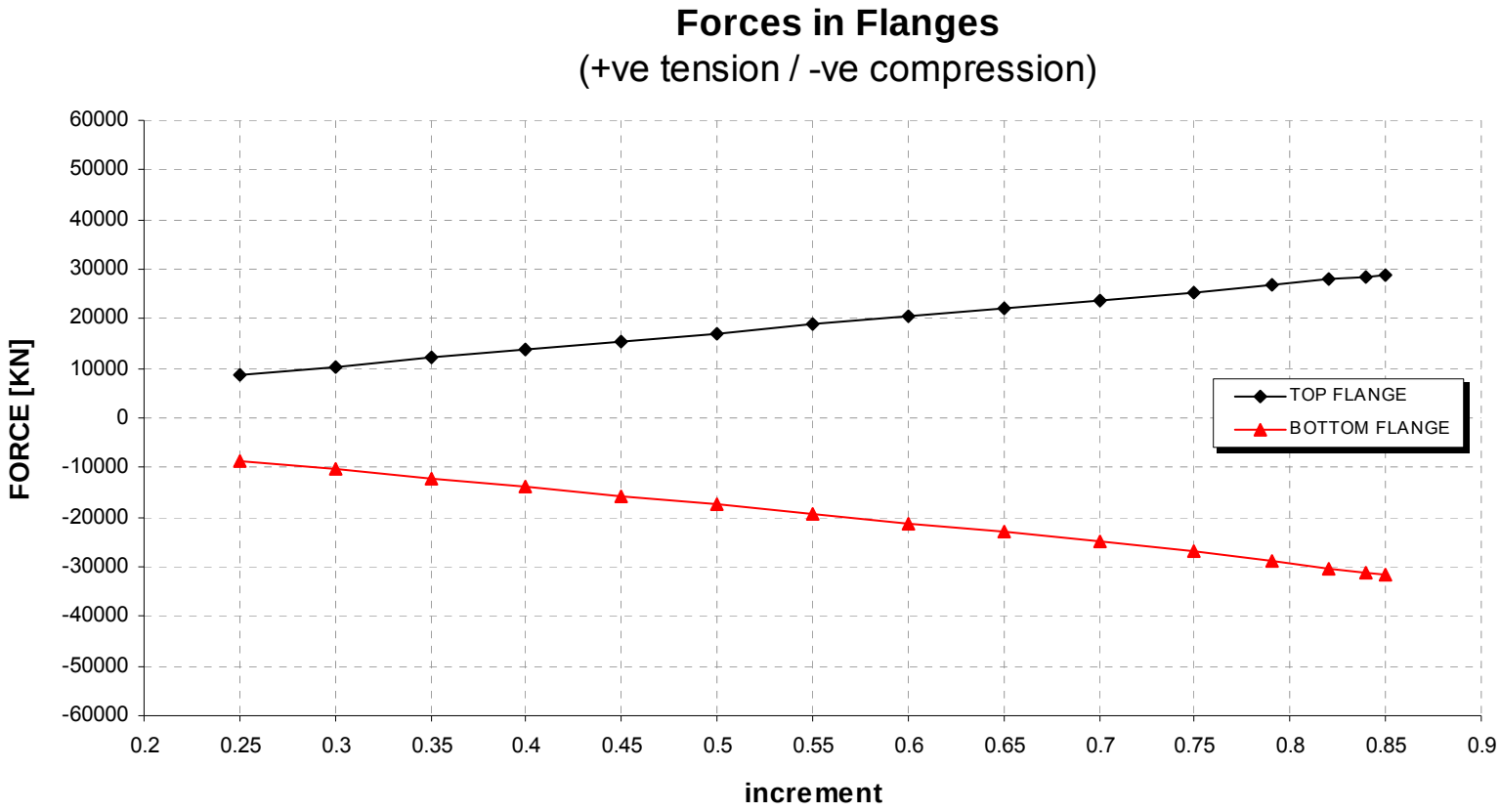

Fig. 4.19 – Section S3 – Longitudinal forces in flanges (refer to Figure 4.14)

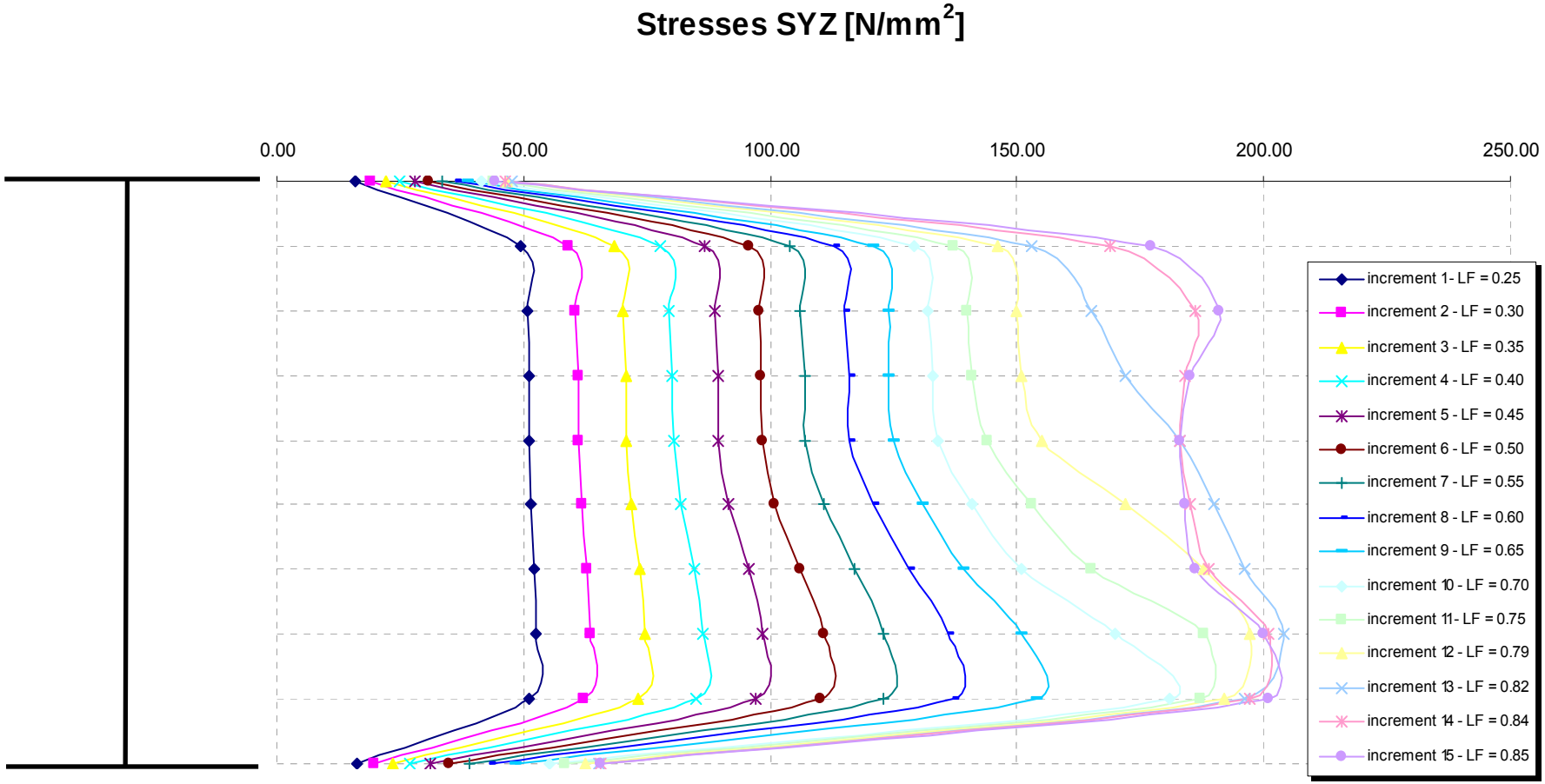

Fig. 4.20 – Section S3 – Shear stresses in web (refer to Figure 4.14)

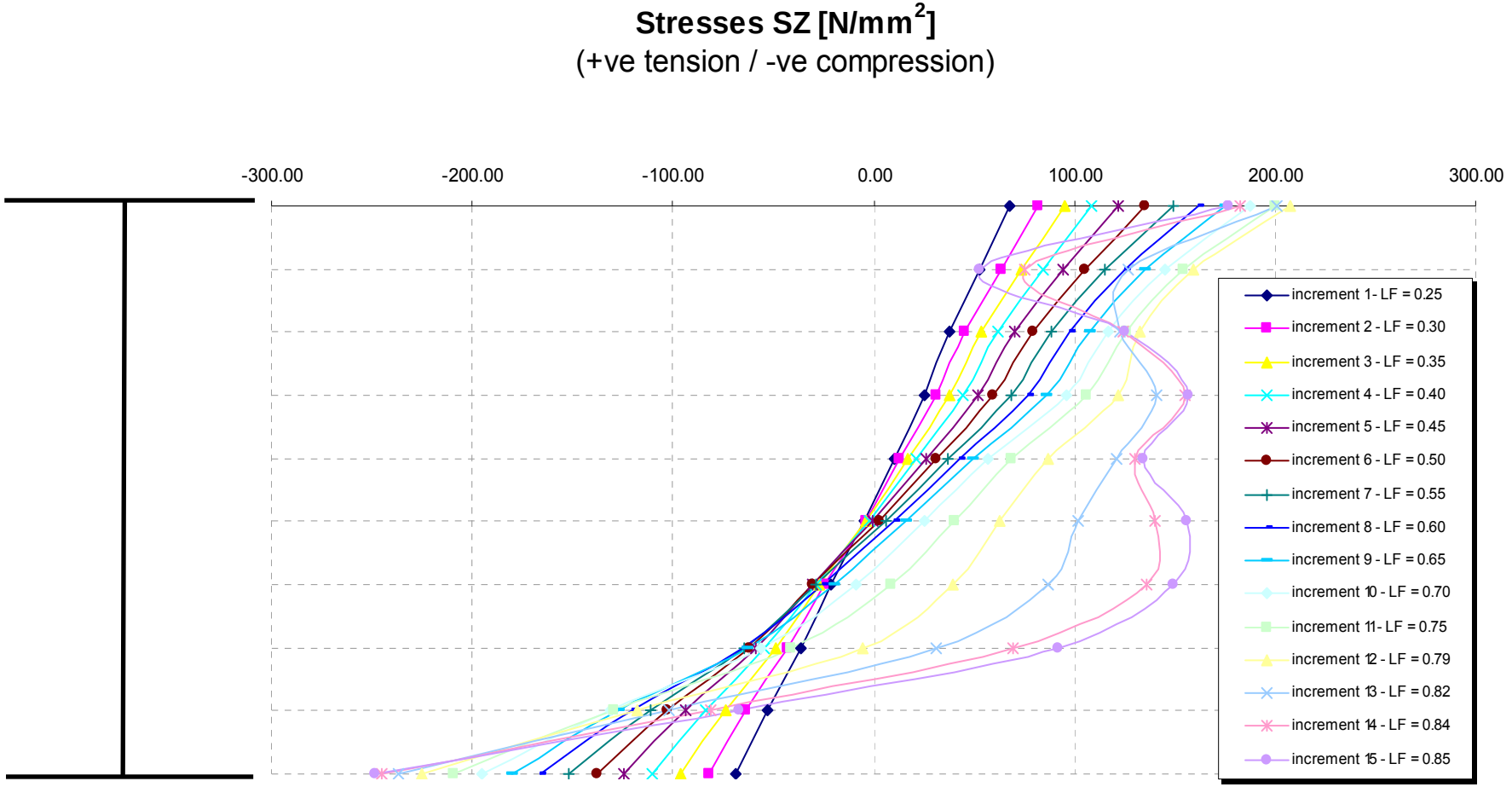

Fig. 4.21 – Section S2 – Longitudinal stresses in web (refer to Figure 4.14)

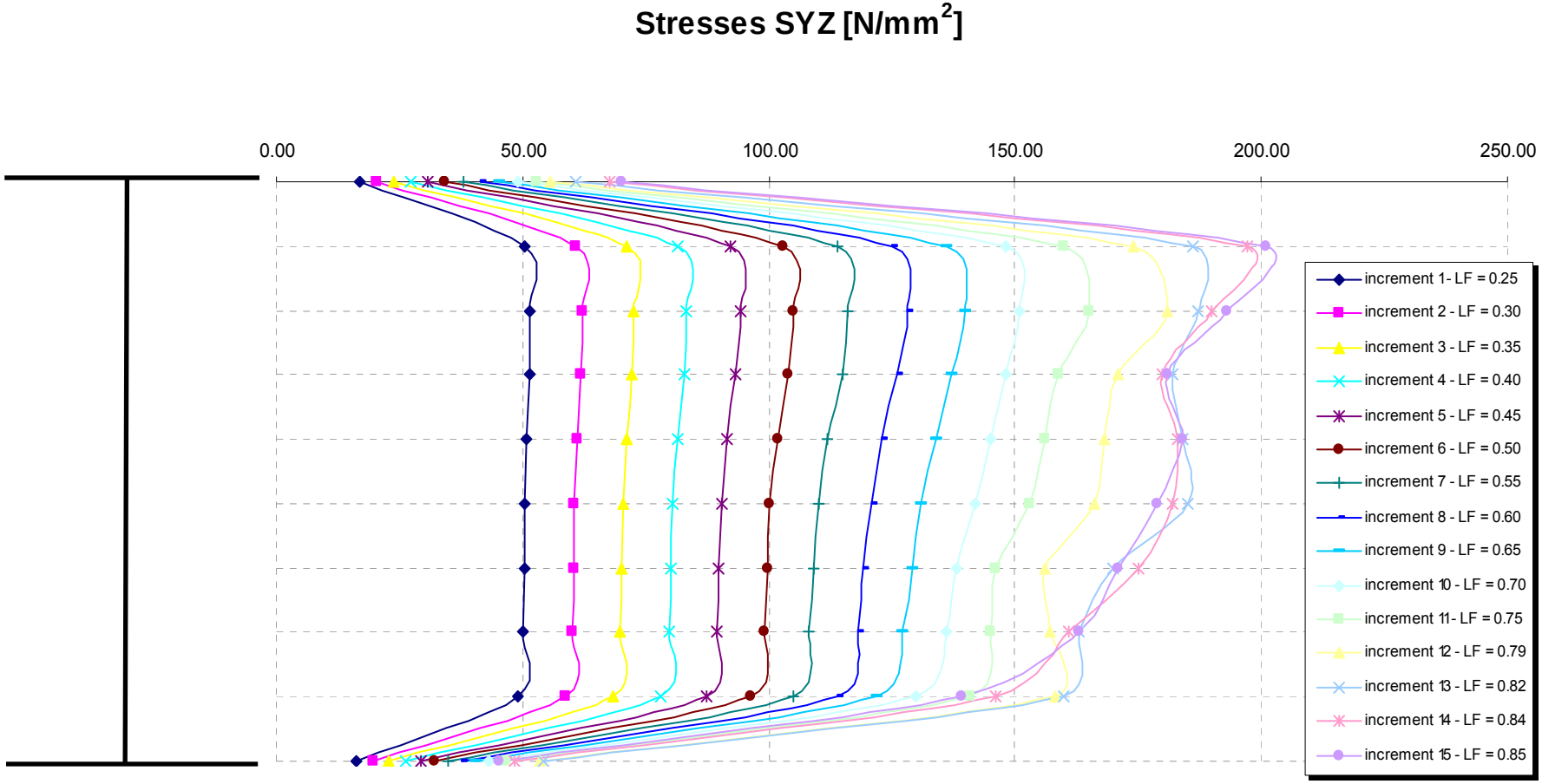

Fig. 4.22 – Section S2 – Shear stresses in web (refer to Figure 4.14)

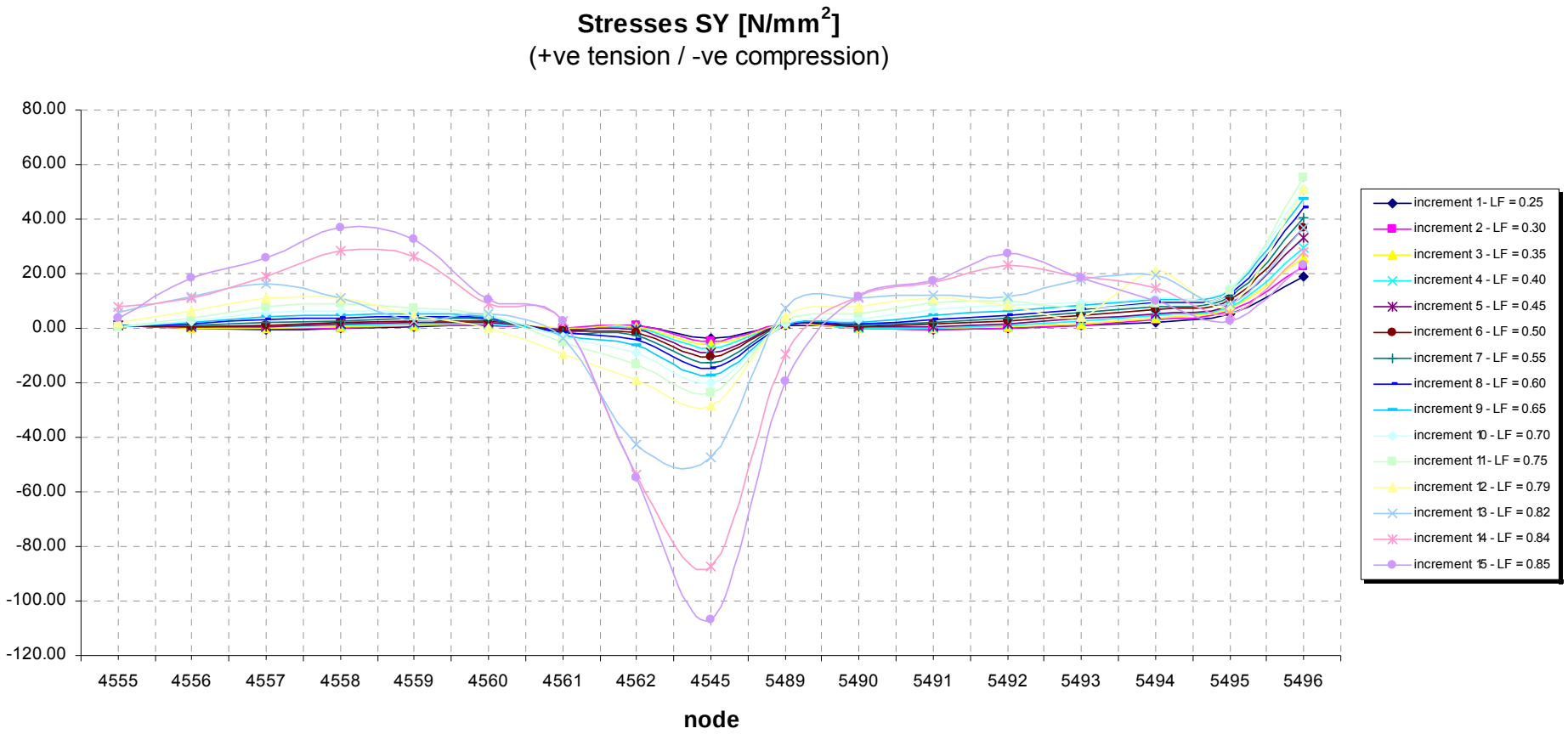

Fig. 4.23 – Section S4 – Vertical stresses in web (refer to Figure 4.14)

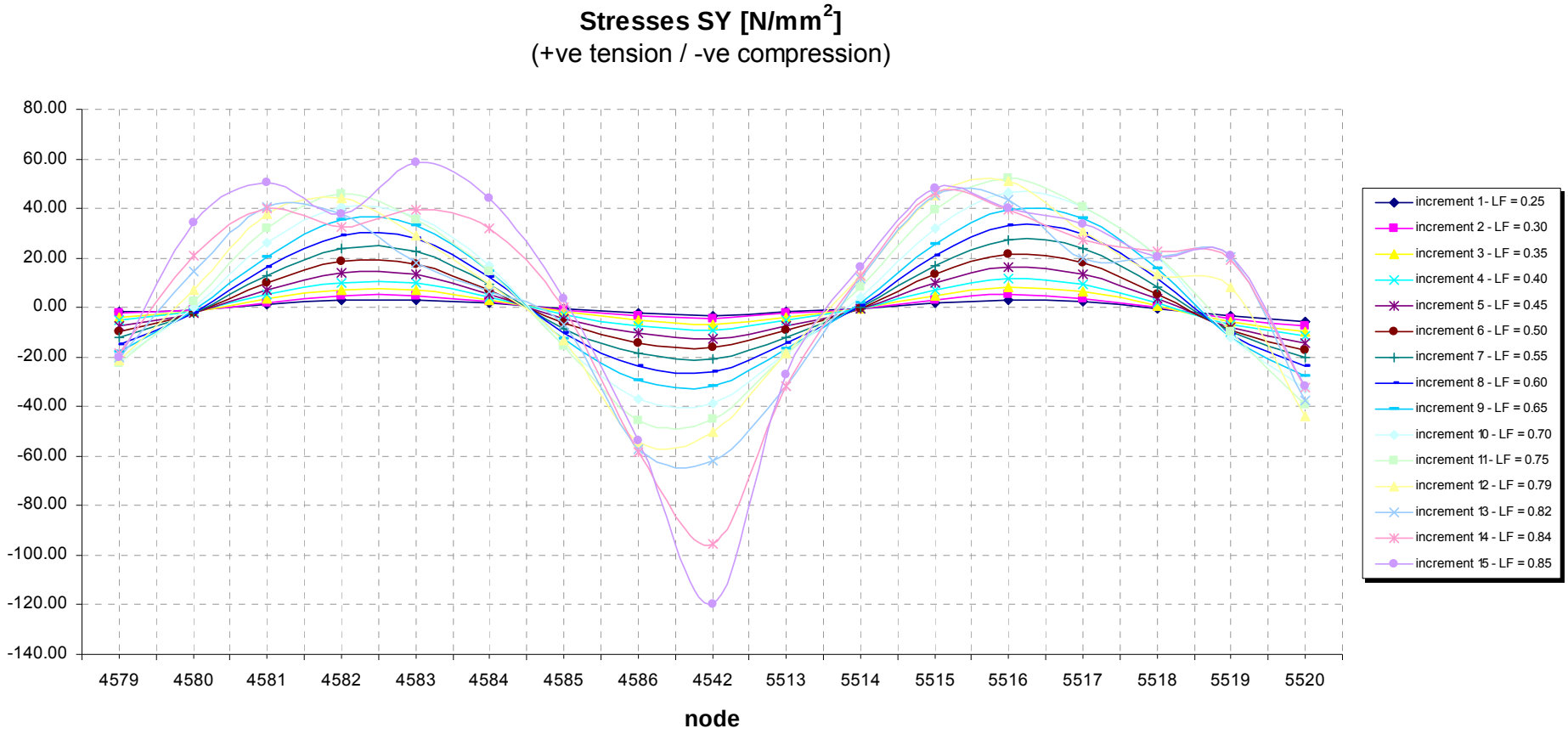

Fig. 4.24 – Section S6 – Vertical stresses in web (refer to Figure 4.14)

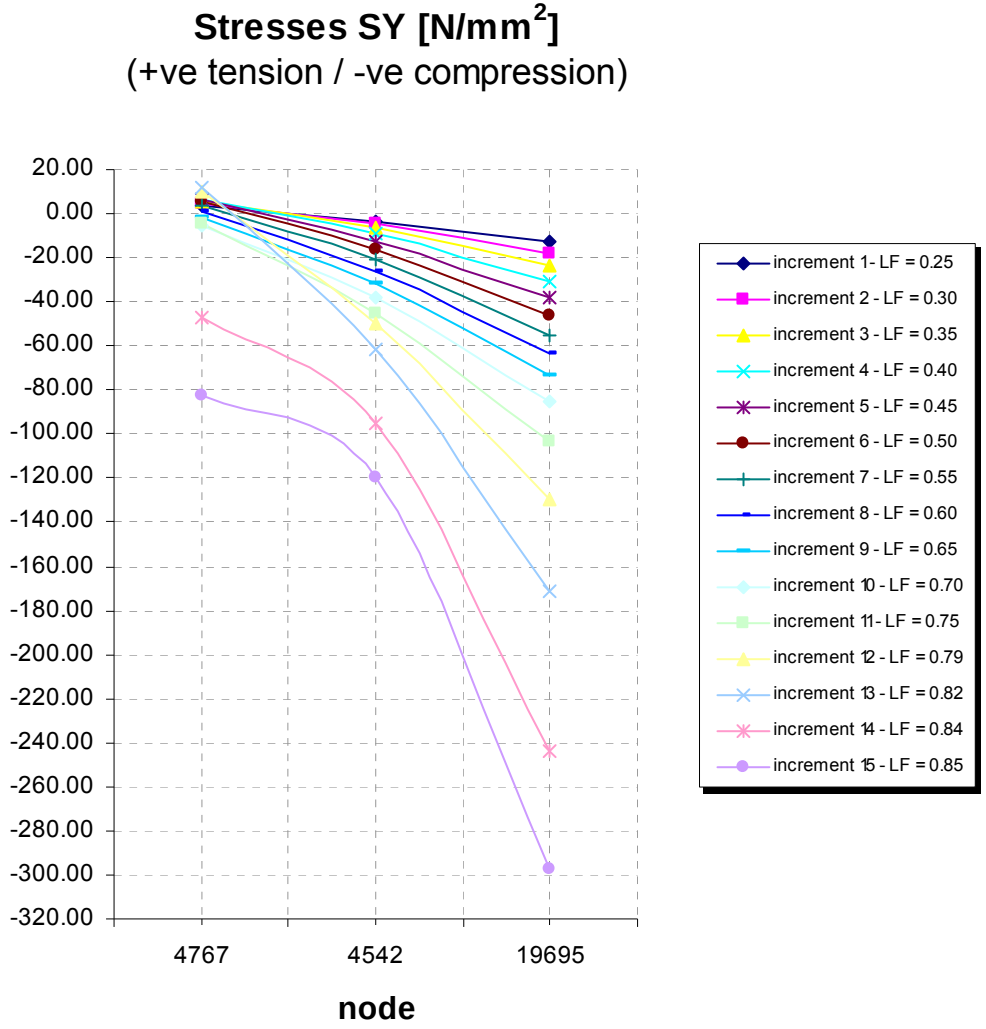

Fig. 4.25 – Section S8 – Vertical stresses in stiffener (refer to Figure 4.14)

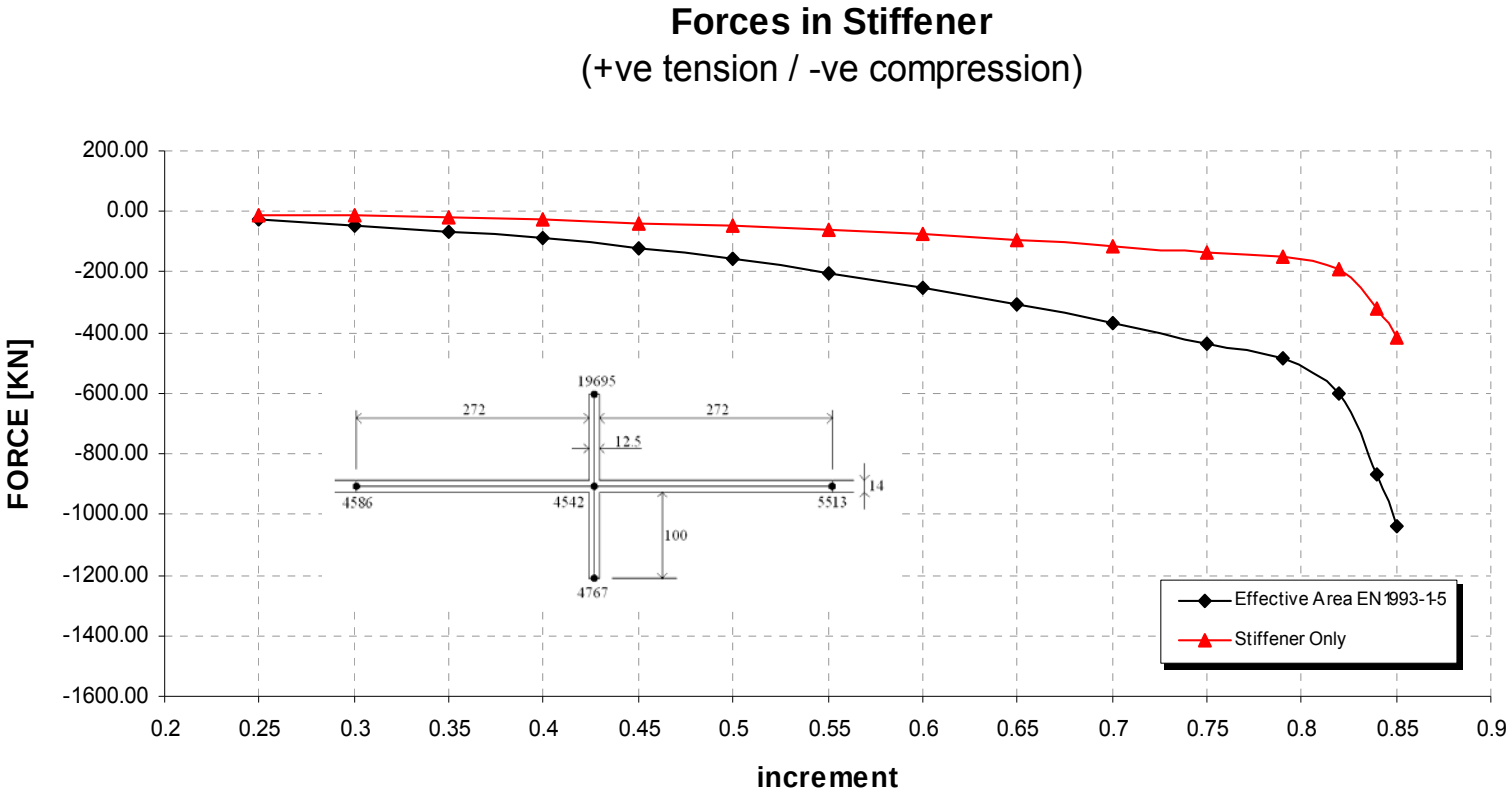

Fig. 4.26 – Section S8 – Vertical forces in stiffener (refer to Figure 4.14)

4.1.2 Case 11

The finite element analysis has been run with initial stiffeners imperfections as shown in Figure 3.3. The stiffeners dimensions are the minimum allowed by the stiffness criteria in EN 1993-1-5. This analysis has been run to investigate the influence of an axial force on stiffeners behaviour. In particular an axial stress of about 75 MPa has been applied.

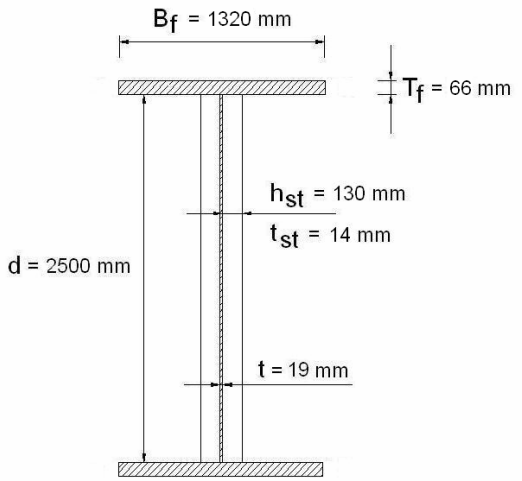

Fig. 4.27 – Section dimensions

A vertical force F = 19800 KN ≈ 2 x V_{ult} at midspan, if applied in a linear analysis, would produce the following effects:

M_{max} = F x L / 4 = 19800 x 30 / 4 = 148500 KNm

V = F / 2 = 19800 / 2 = 9900 KN ≈ V_{ult}

The non-linear analysis stops when it fails to find an equilibrium beyond a load factor 0.47.

M_{NL} = 0.47 x 148500 = 69795 KNm $\longrightarrow$ $\overline{\eta}_1$ = 0.876

V_{NL} = 0.47 x 9900 = 4653 KN $\longrightarrow$ $\overline{\eta}_3$ = 0.738

The load-deflection curve obtained from the finite element analysis is illustrated in Figure 4.28. The analysis shows an almost linear behaviour up to a load factor of approximately 0.45, after which it shows a gradual loss of stiffness culminating in a failure at the load factor of 0.47.

The lateral deflections of the web at this point are illustrated in Figures 4.30 to 4.40. It can be seen that the girder has failed by the web bowing out laterally, while stiffeners are affected by twist in sympathy.

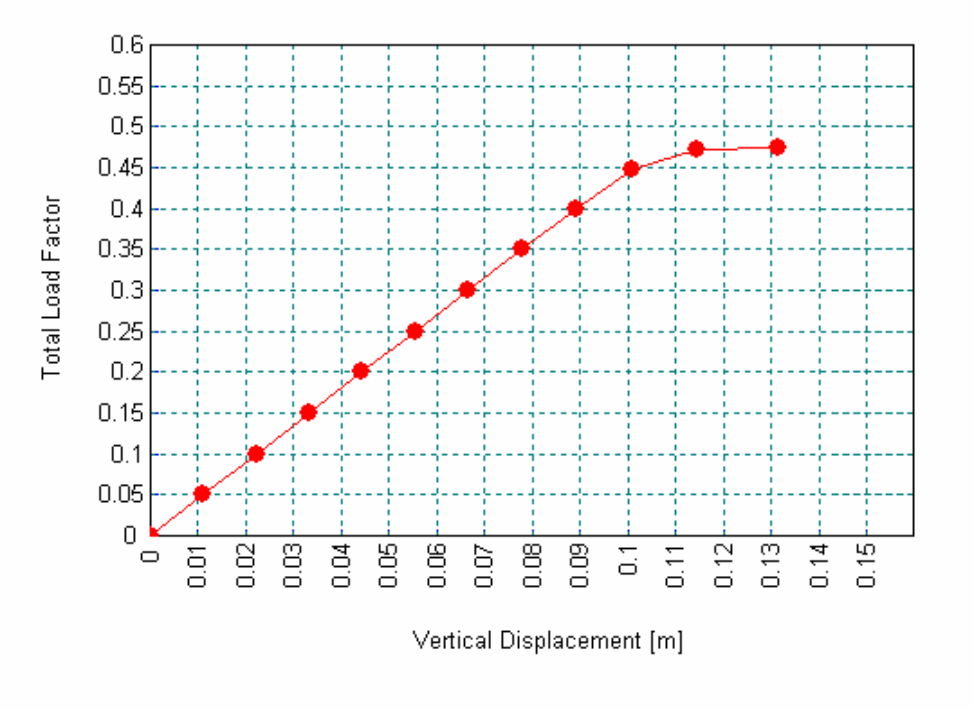

Fig. 4.28 – Vertical Displacement vs Total Load Factor

The M-V interaction domain from EN 1993-1-5 and the results obtained from the non-linear analysis are illustrated in Figure 4.29. The interaction curve has been built according to EN 1993-1-5 clause 7.1(1). Possible benefits considering clause 7.1(2), regarding performing the interaction at "0.5 h_w" from support or checking at support using $V_{pl,Rd}$, have not been considered.

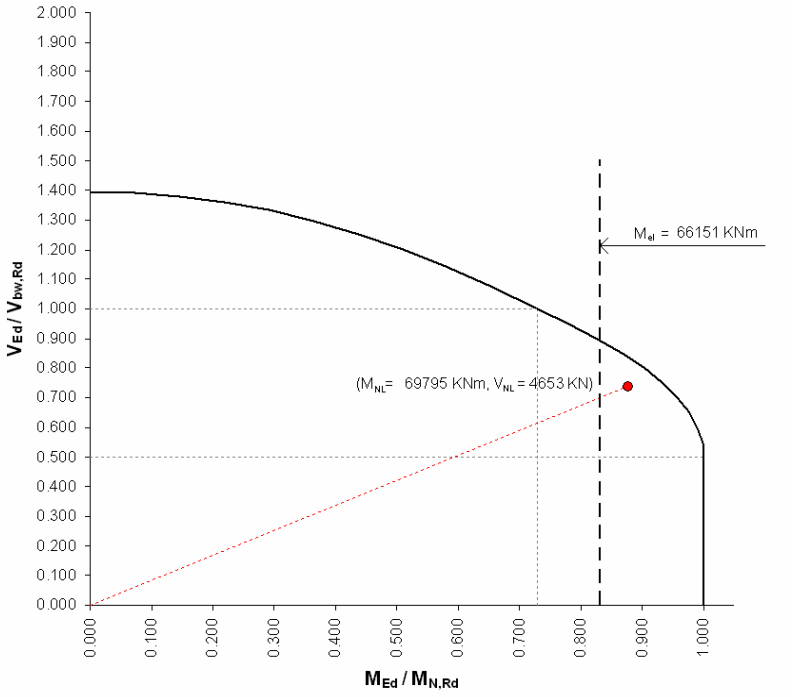

Figure 4.29 – Eurocode M-V interaction domain and result from non-linear analysis

The sections through the girder at various stages in the analysis to establish the distribution of internal forces are illustrated in Figures 4.41 to 4.53.

Figure 4.45 shows non-linearity of the longitudinal stress distribution only beyond increment 5 despite the fact that the applied compressive stress considerably exceeded the elastic critical value for panels with boundaries unrestrained. However owing to the relatively large flanges the longitudinal edges of the web will approach the fully restrained condition calculated from reference [4], for which the critical compressive stress in the absence of shear is calculated as 99 N/mm^2 and the critical shear stress in the absence of compression as 135 N/mm^2. From Figure 4.47, at increment 6, the mean shear stress is about 56 N/mm^2. The critical compressive stress calculated, using the interaction formula for shear and uniform compression for a plate with restrained edges from [4], would then be about the applied stress of 75 N/mm^2.

Figure 4.53 shows the force in the intermediate stiffener, which at increment 12 appears to be of about 130KN. This is very small compared to a predicted force based on the ultimate shear force without deduction of critical shear force of more than 4000KN. This discrepancy may be accounted for by the enhanced critical shear stress discussed.

Figure 4.53 shows tensile forces in the stiffener for the first increment which could be expected to arise due to the restraint provided by the stiffener to Poisson expansion of the web causing a tensile stress of about 0.3 times the longitudinal compressive stress. These forces, which reduce the bending caused by the longitudinal web stresses, decrease with increment due to the ‘softening’ of the web due to out-of plane bowing and, at high load increments, due to the development of tension field forces.

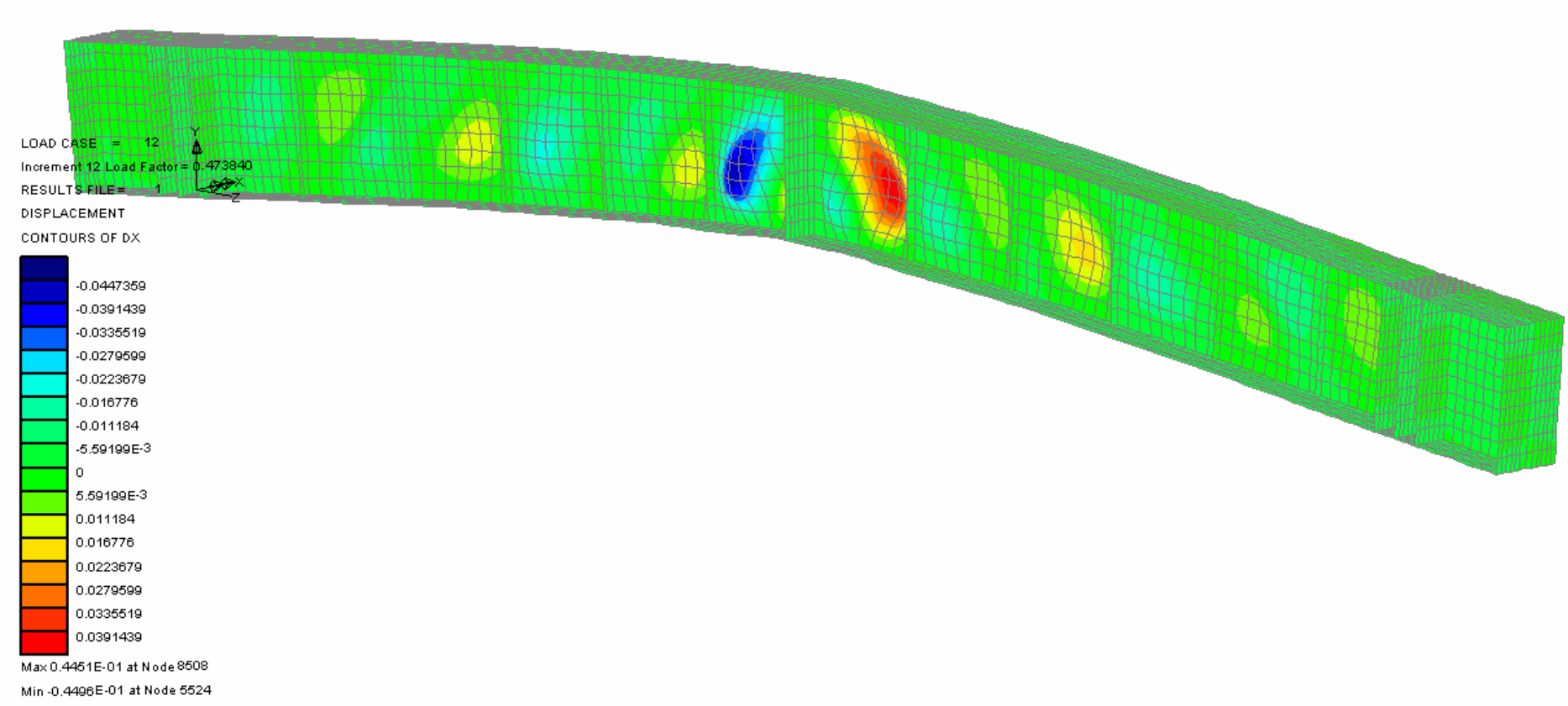

Figure 4.30 – Lateral Displacement Contour (m) at failure

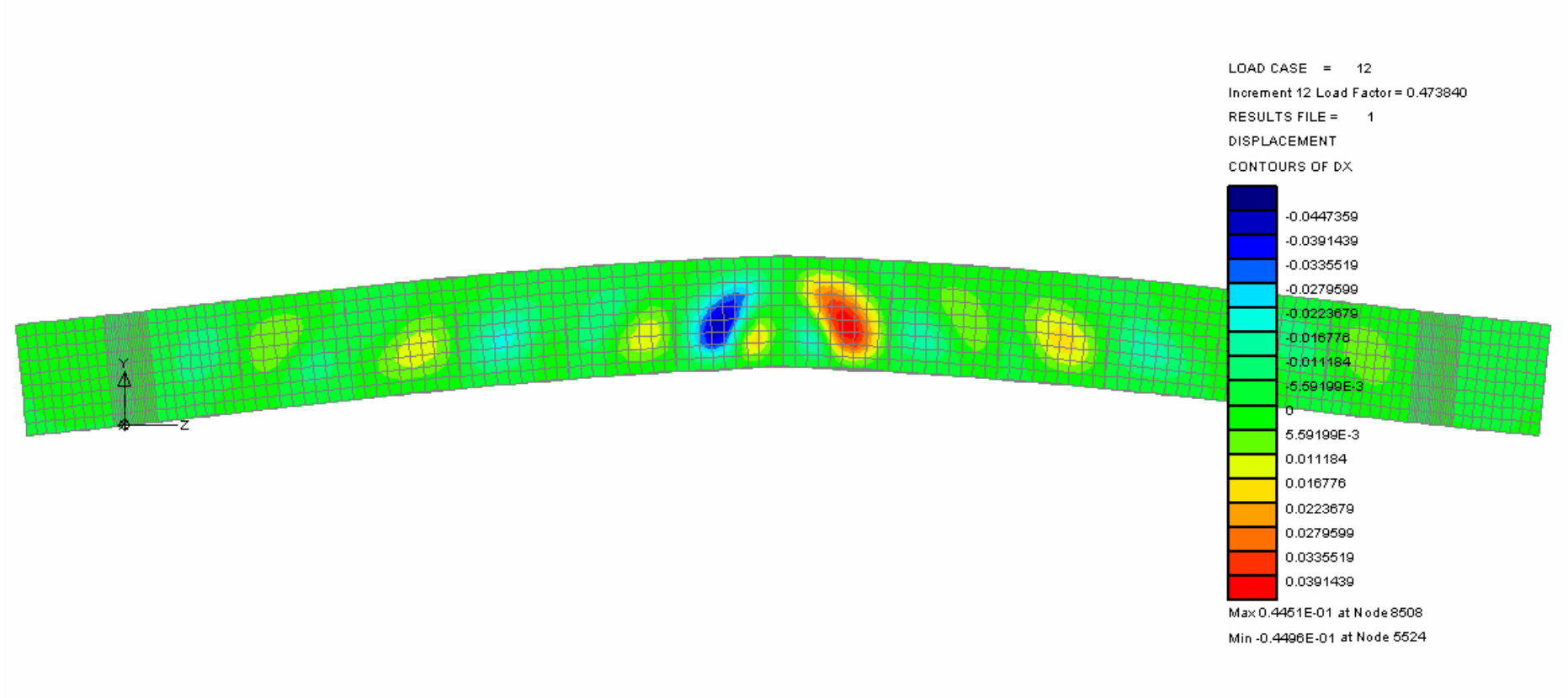

Figure 4.31 – Lateral Displacement Contour (m) at failure

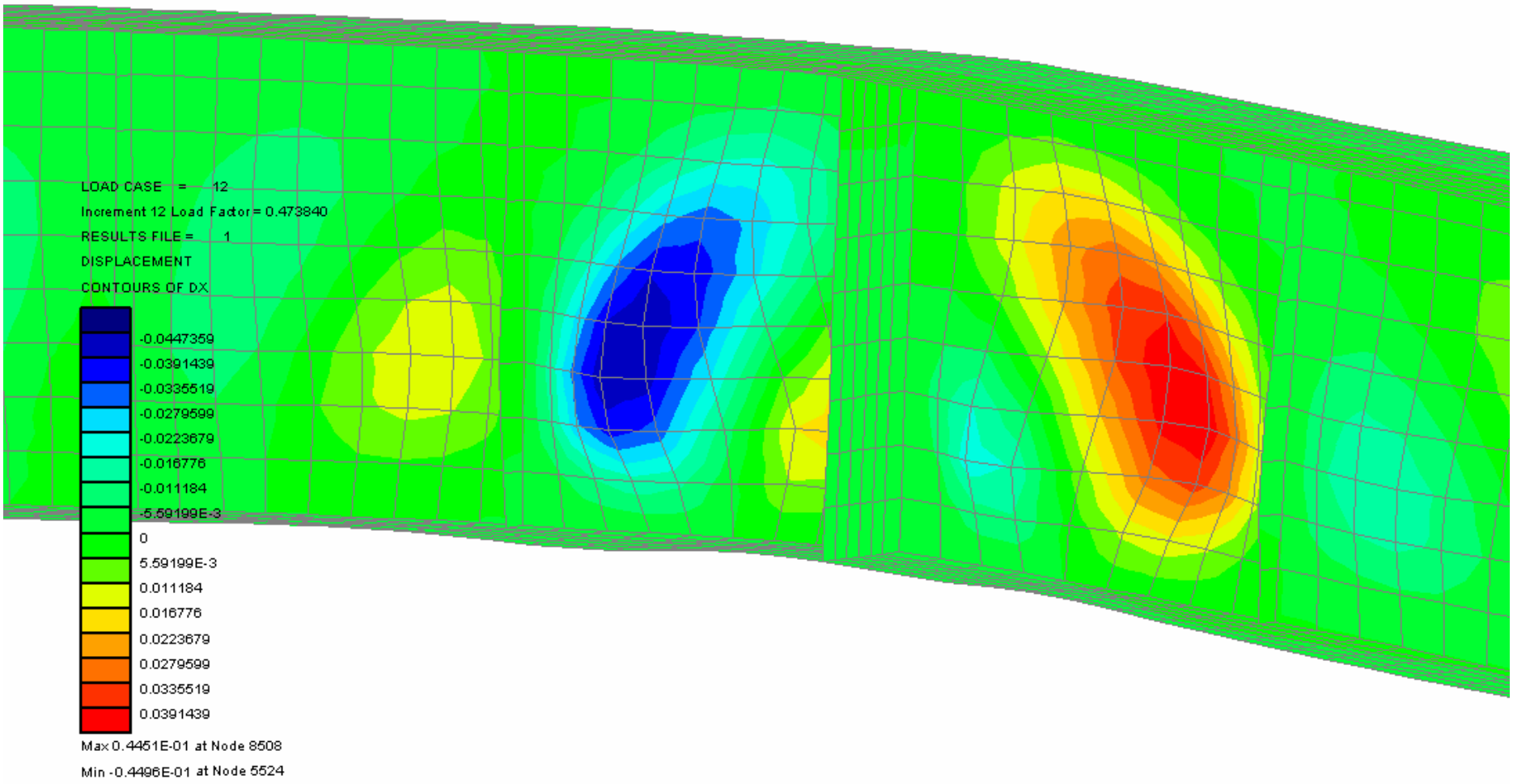

Figure 4.32 – Lateral Displacement Contour (m) at failure

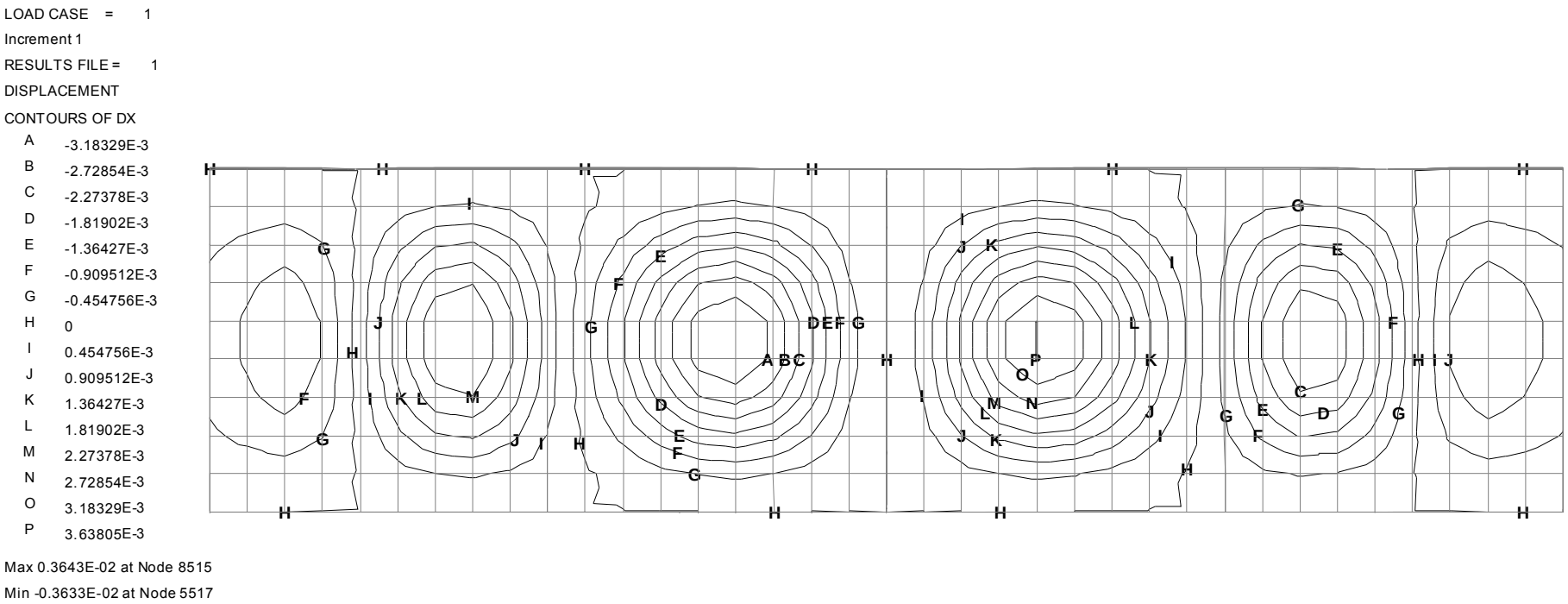

Figure 4.33 – Lateral Displacement Contour (m) at load increment 1

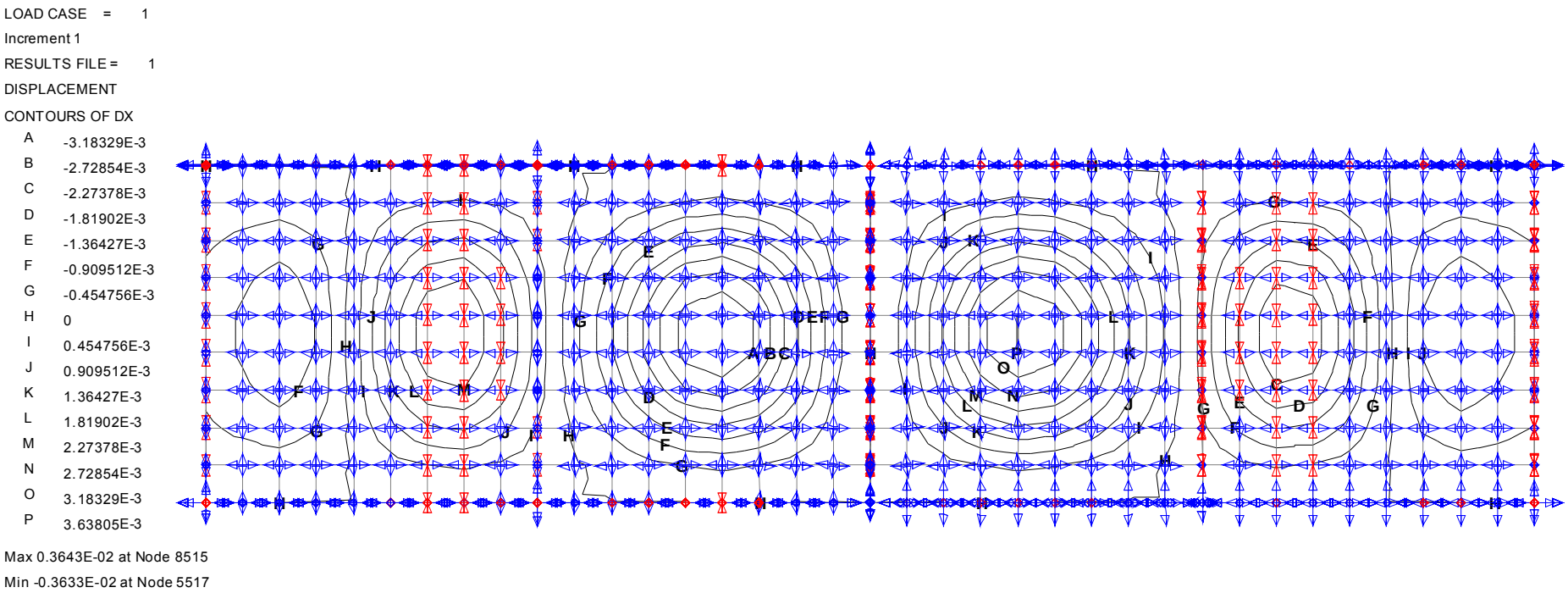

Figure 4.34 – Lateral Displacement Contour (m) and Principal Vectors at load increment 1

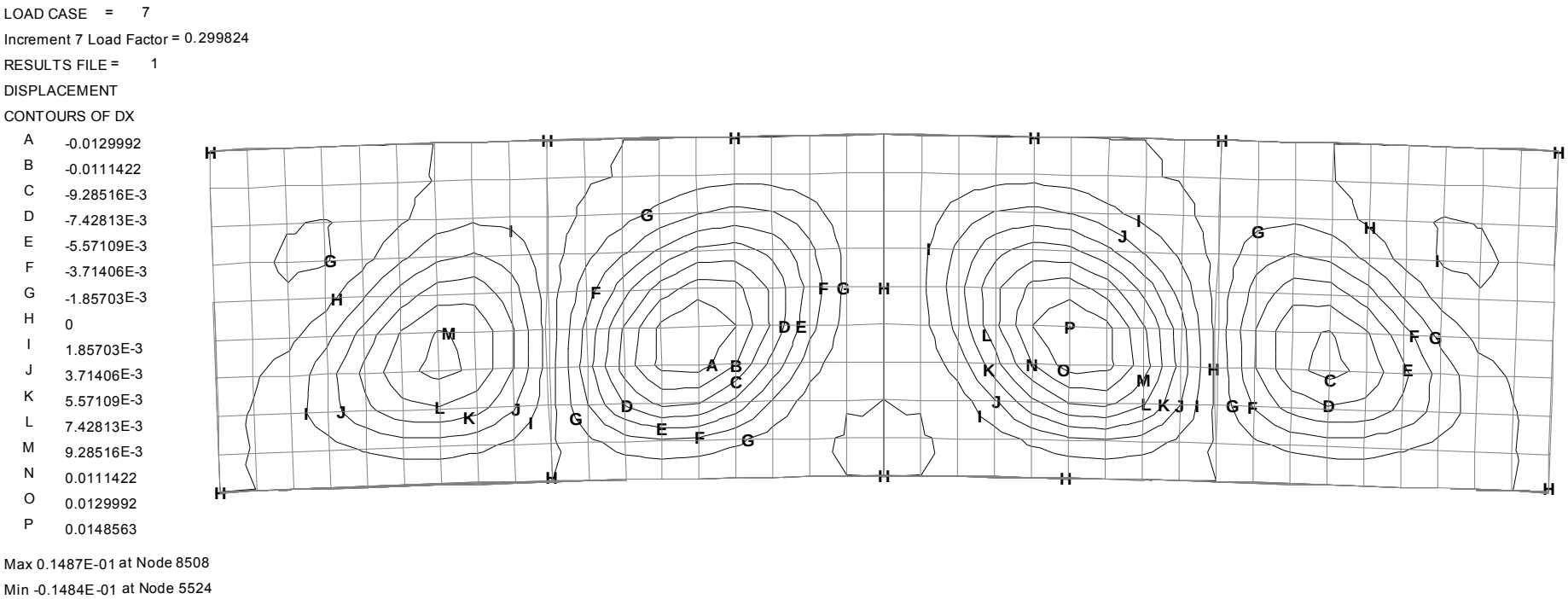

Figure 4.35 – Lateral Displacement Contour (m) at load increment 7

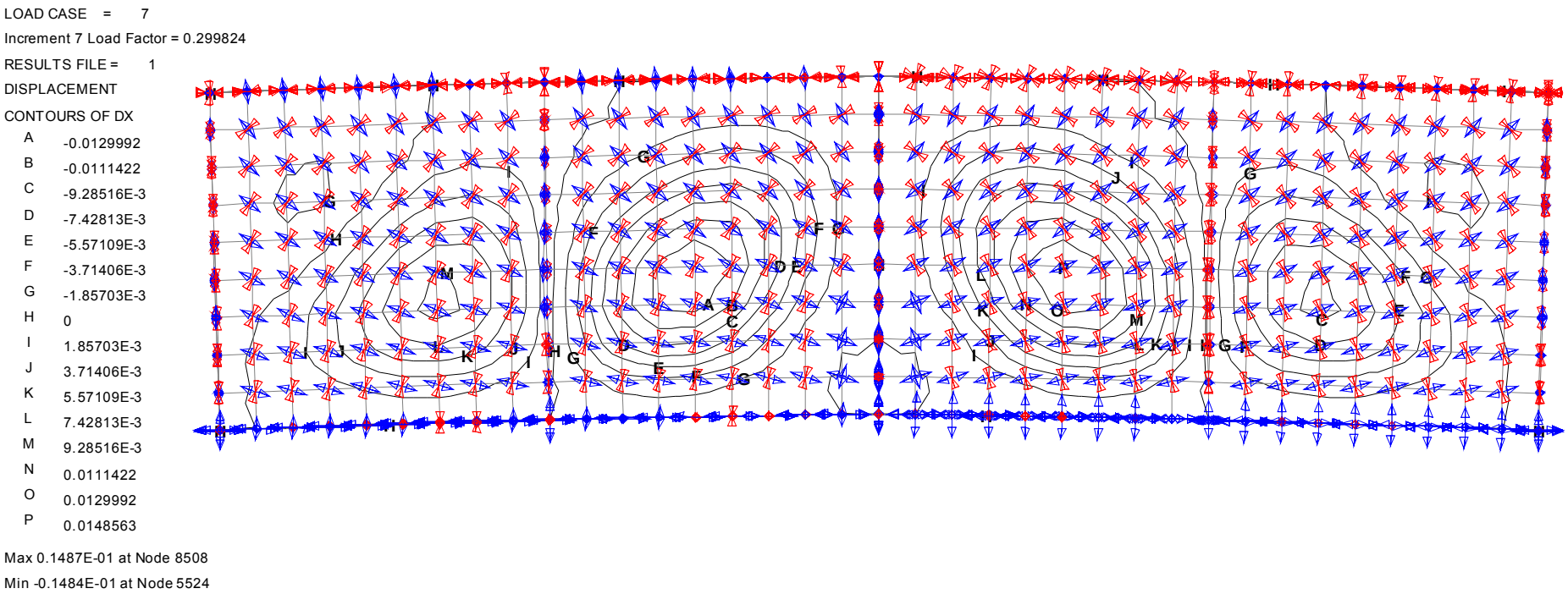

Figure 4.36 – Lateral Displacement Contour (m) and Principal Vectors at load increment 7

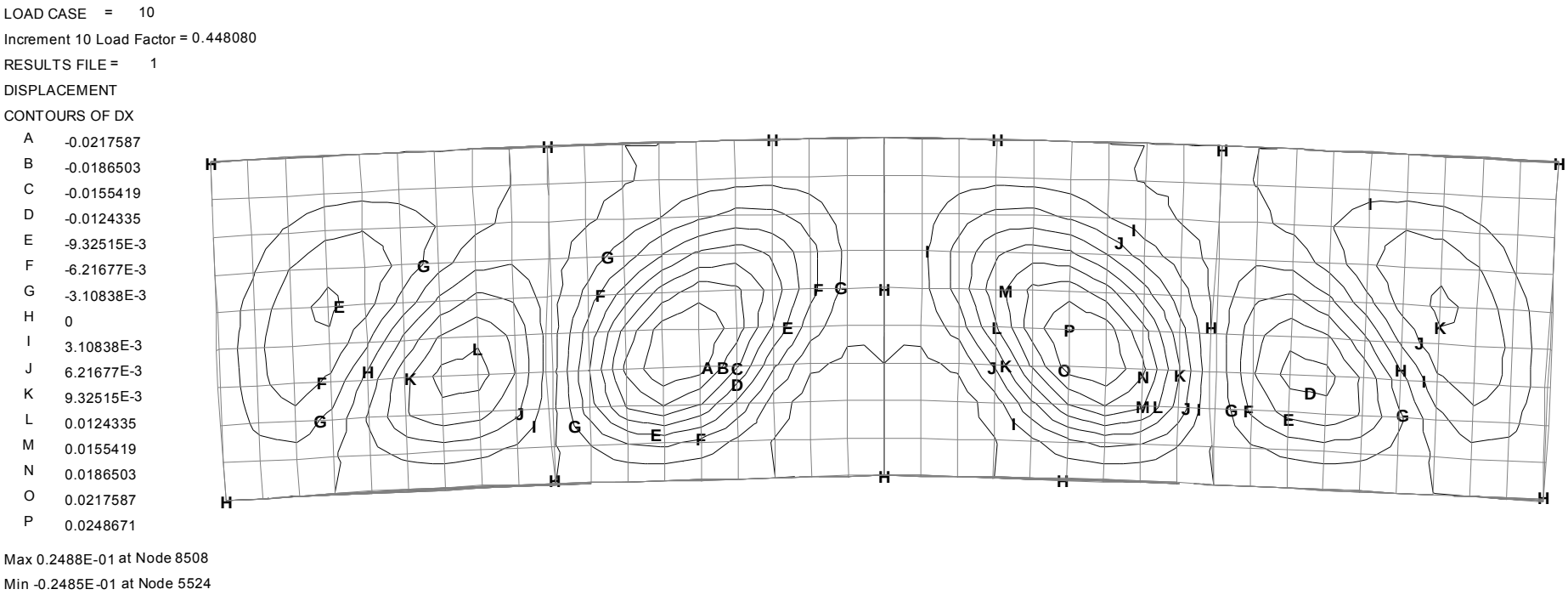

Figure 4.37 – Lateral Displacement Contour (m) at load increment 10

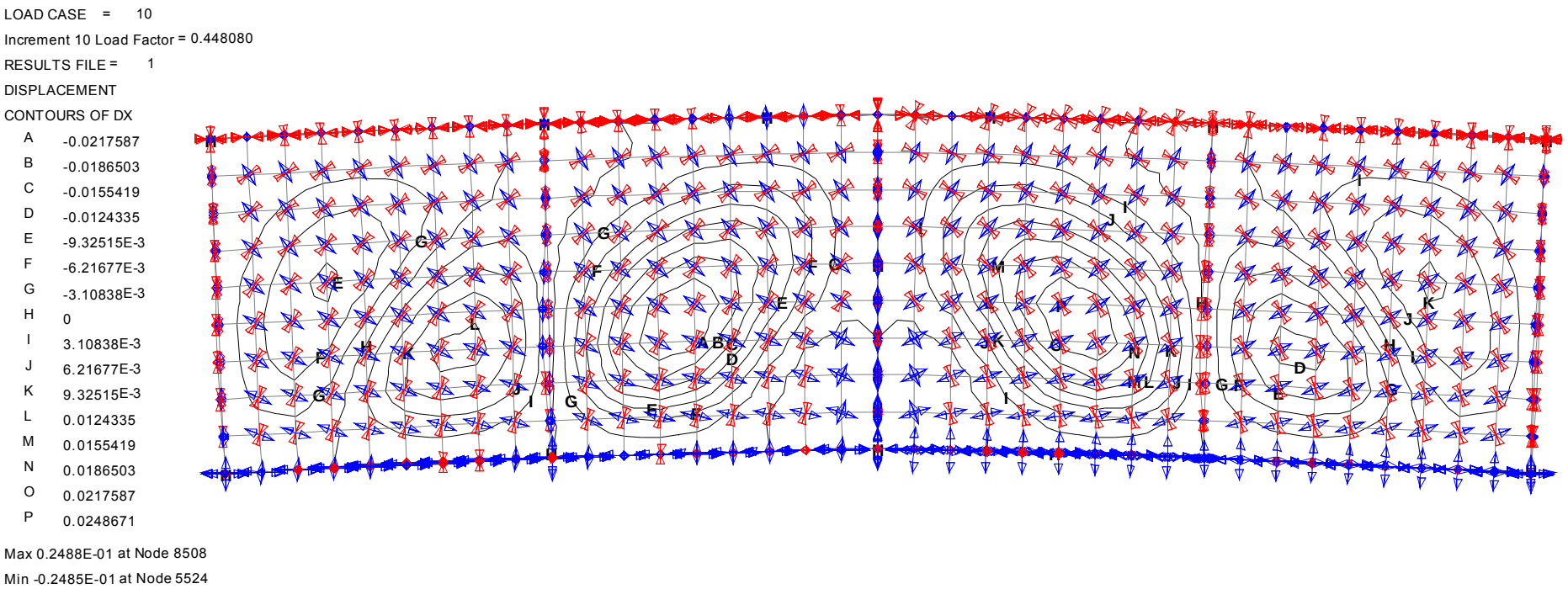

Figure 4.38 – Lateral Displacement Contour (m) and Principal Vectors at load increment 10

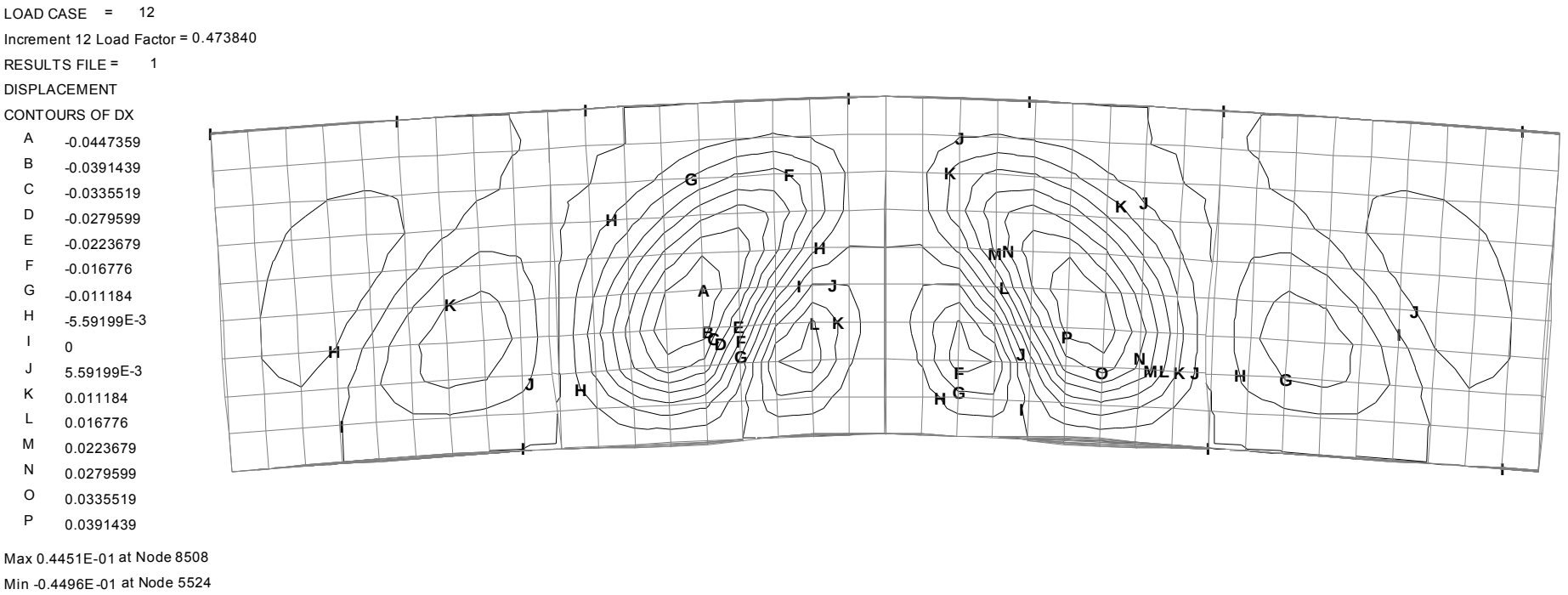

Figure 4.39 – Lateral Displacement Contour (m) at load increment 12

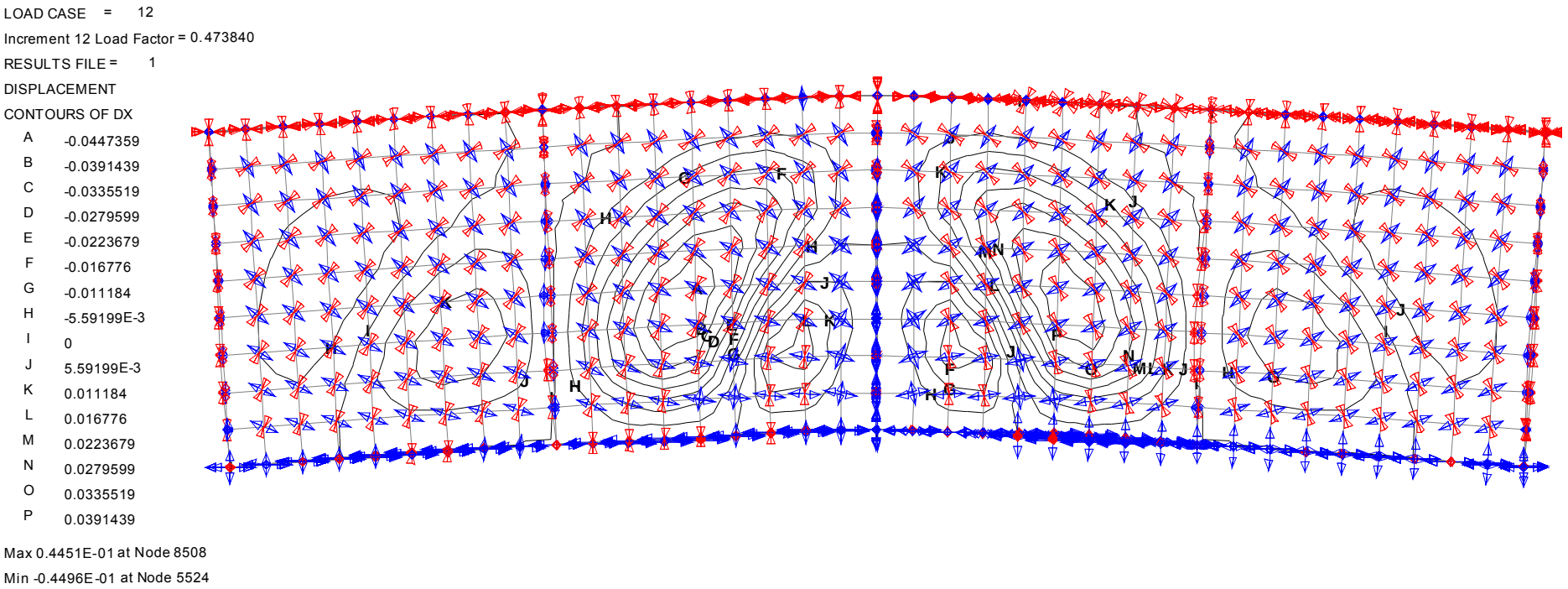

Figure 4.40 – Lateral Displacement Contour (m) and Principal Vectors at load increment 12

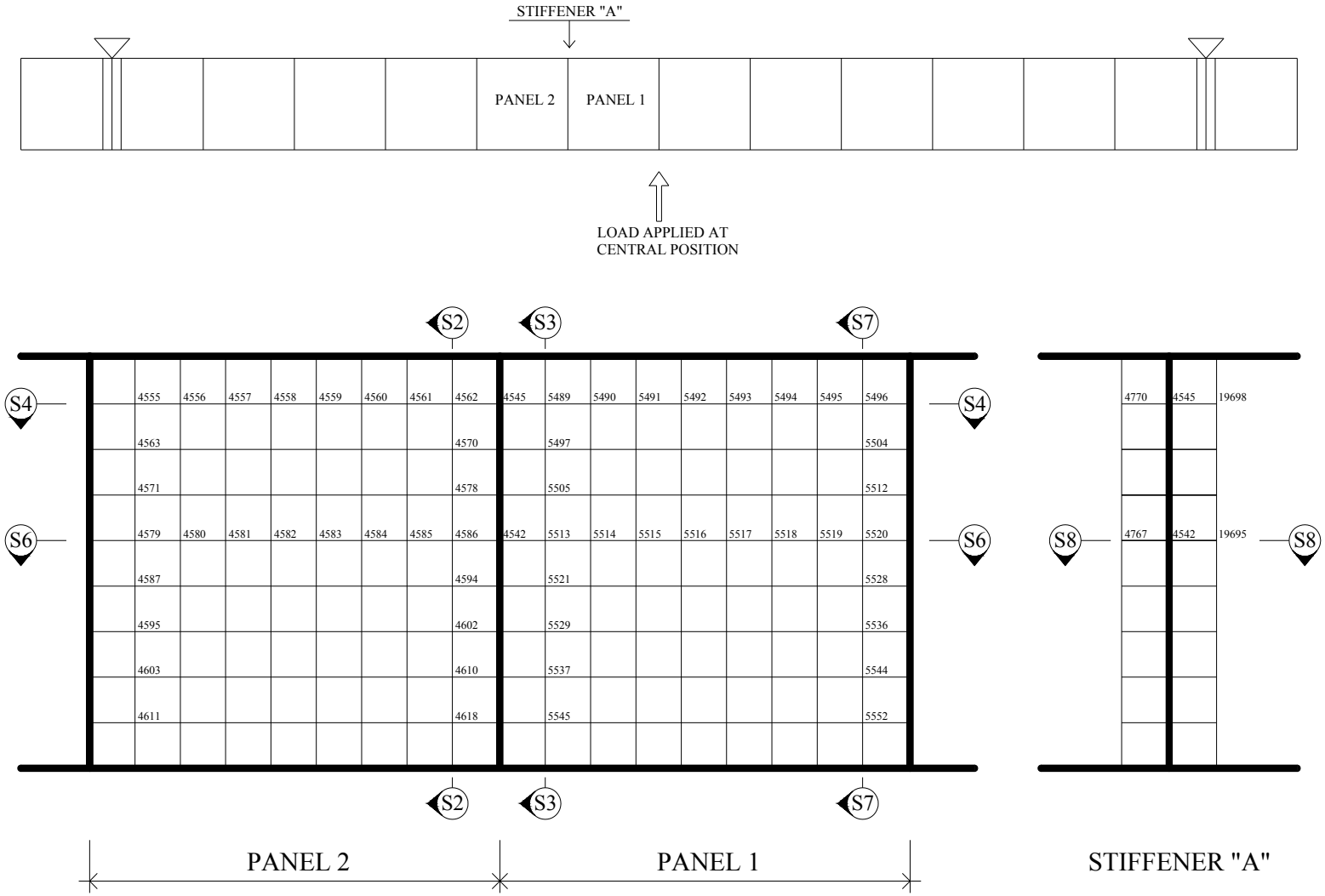

Fig. 4.41 – Investigated area and location of sections

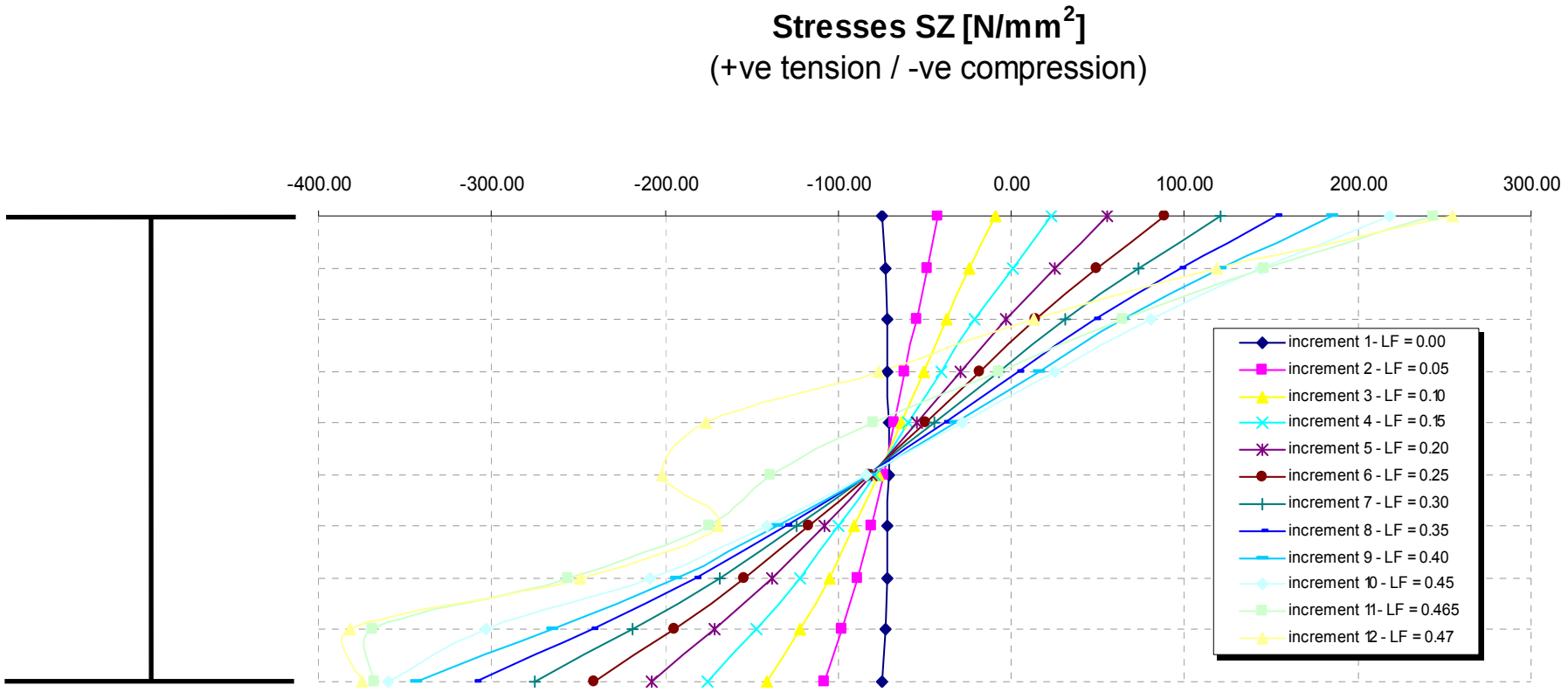

Fig. 4.42 – Section S7 – Longitudinal stresses in web (refer to Figure 4.41)

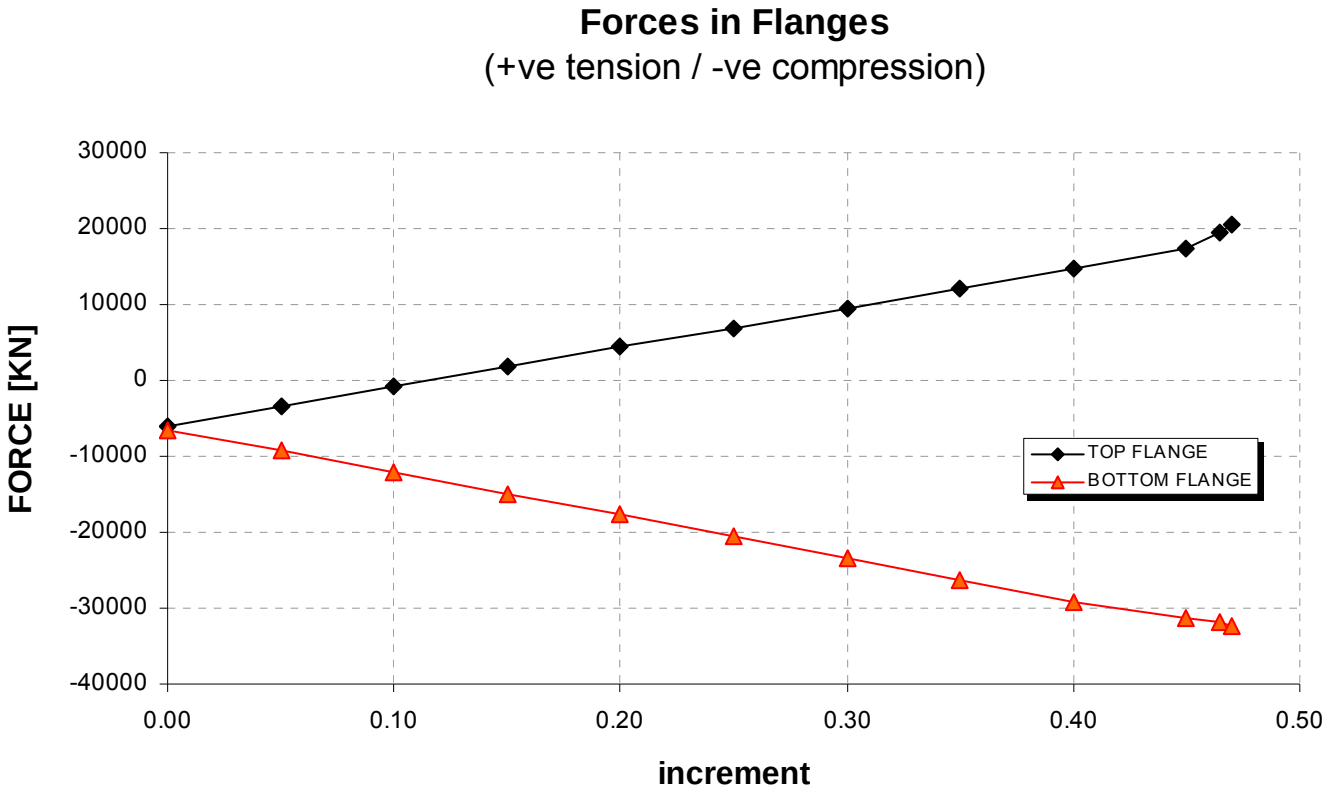

Fig. 4.43 – Section S7 – Longitudinal forces in flanges (refer to Figure 4.41)

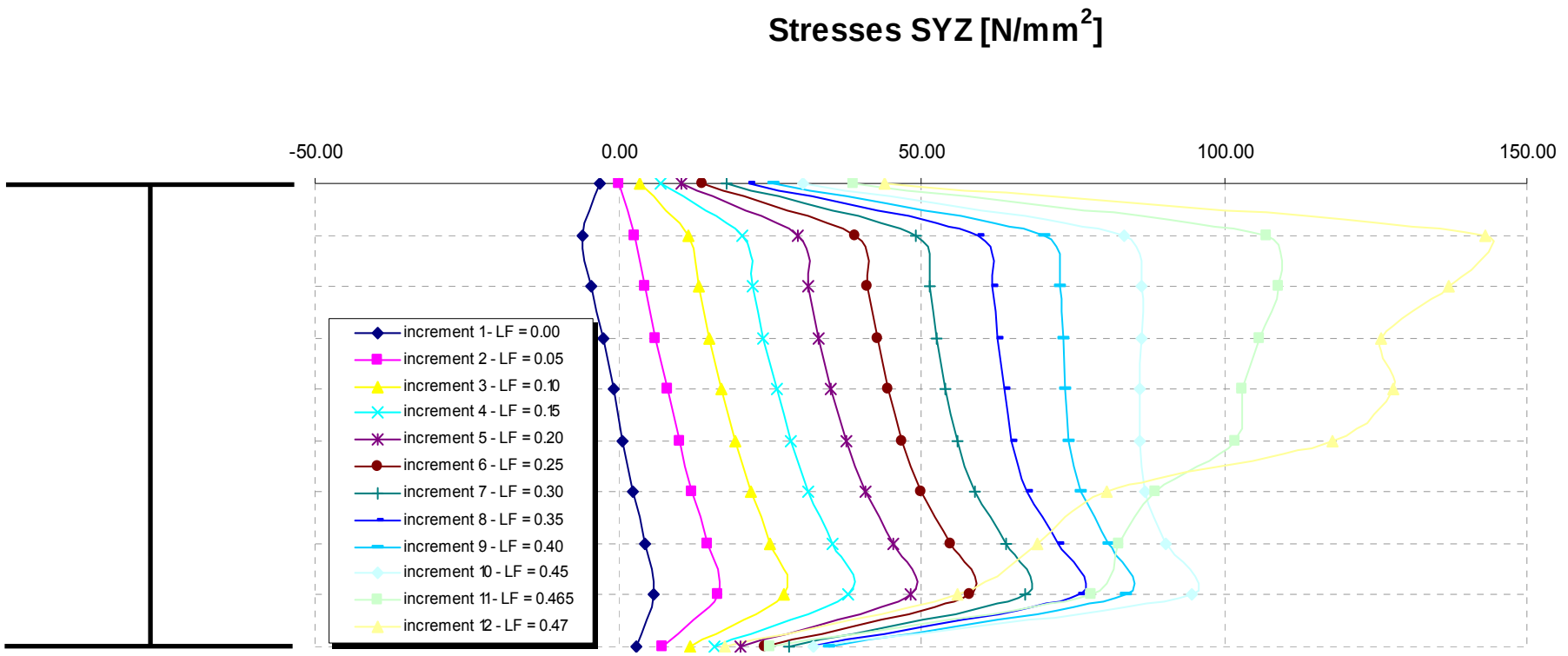

Fig. 4.44 – Section S7 – Shear stresses in web (refer to Figure 4.41)

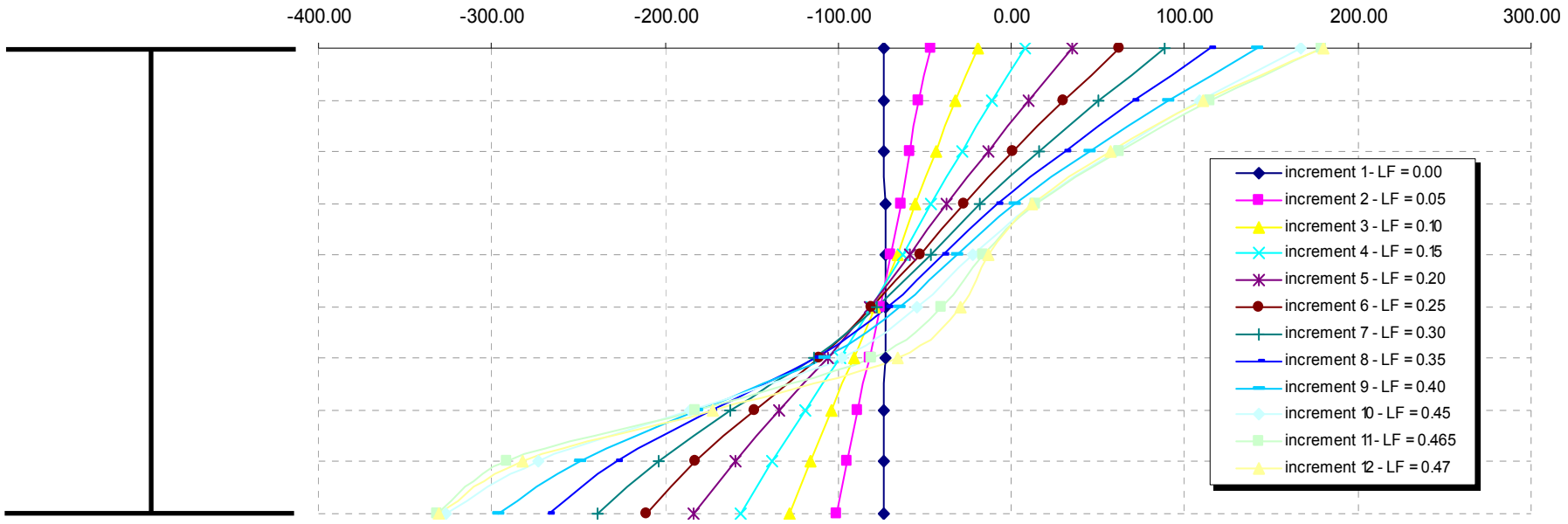

Fig. 4.45 – Section S3 – Longitudinal stresses in web (refer to Figure 4.41)

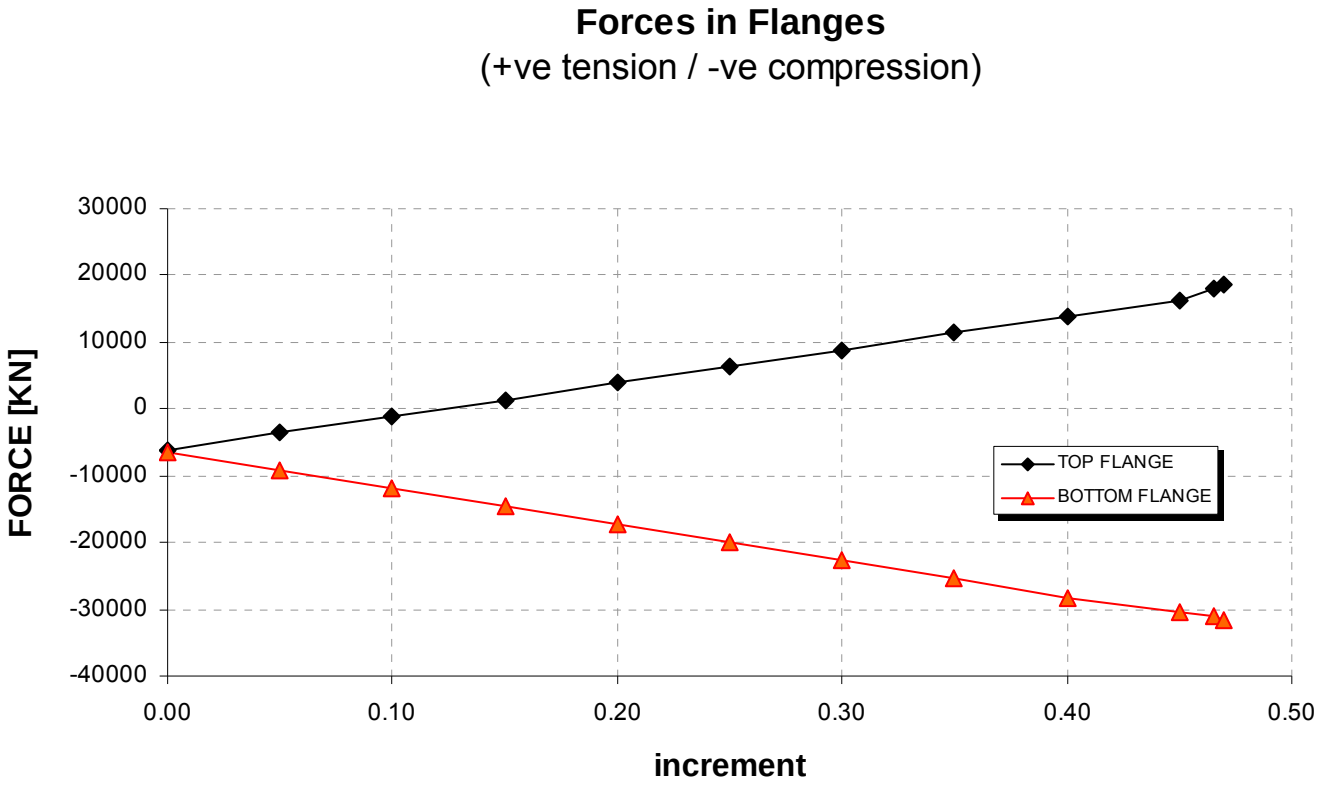

Fig. 4.46 – Section S3 – Longitudinal forces in flanges (refer to Figure 4.41)

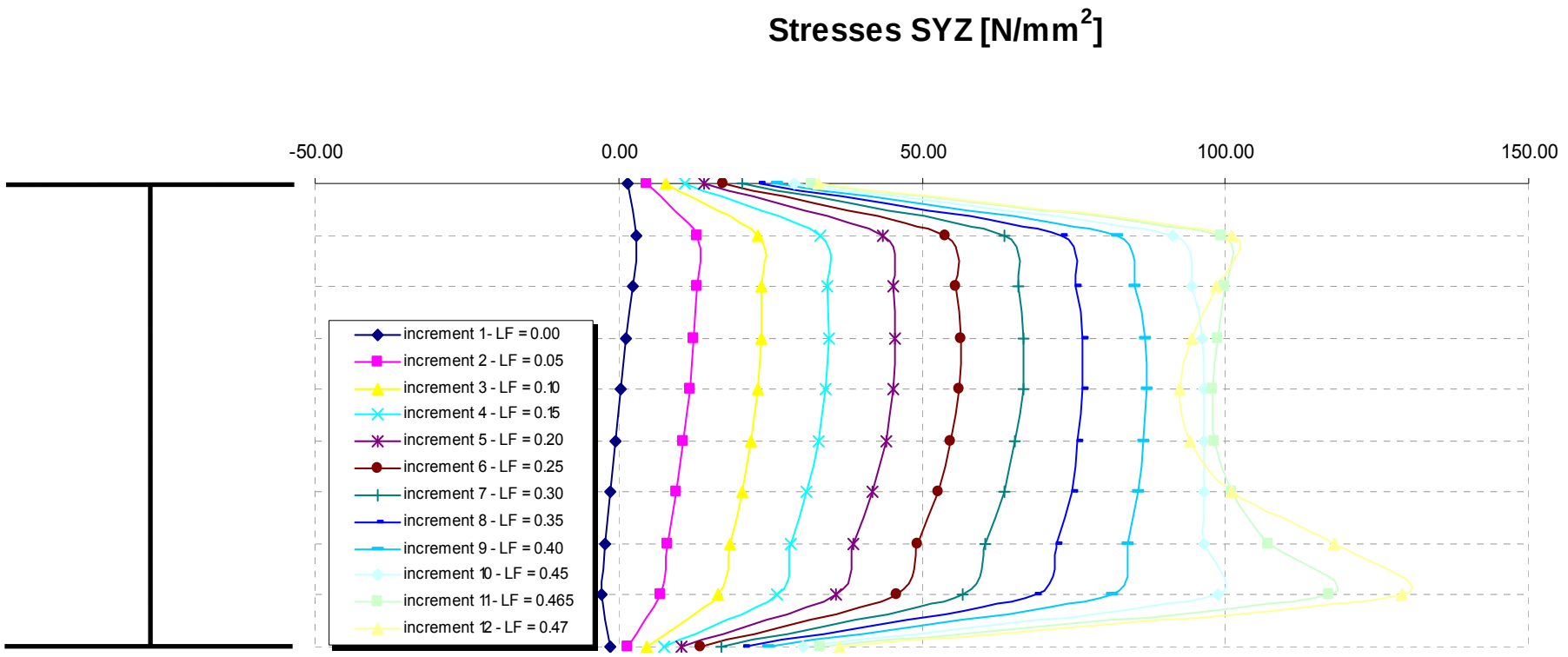

Fig. 4.47 – Section S3 – Shear stresses in web (refer to Figure 4.41)

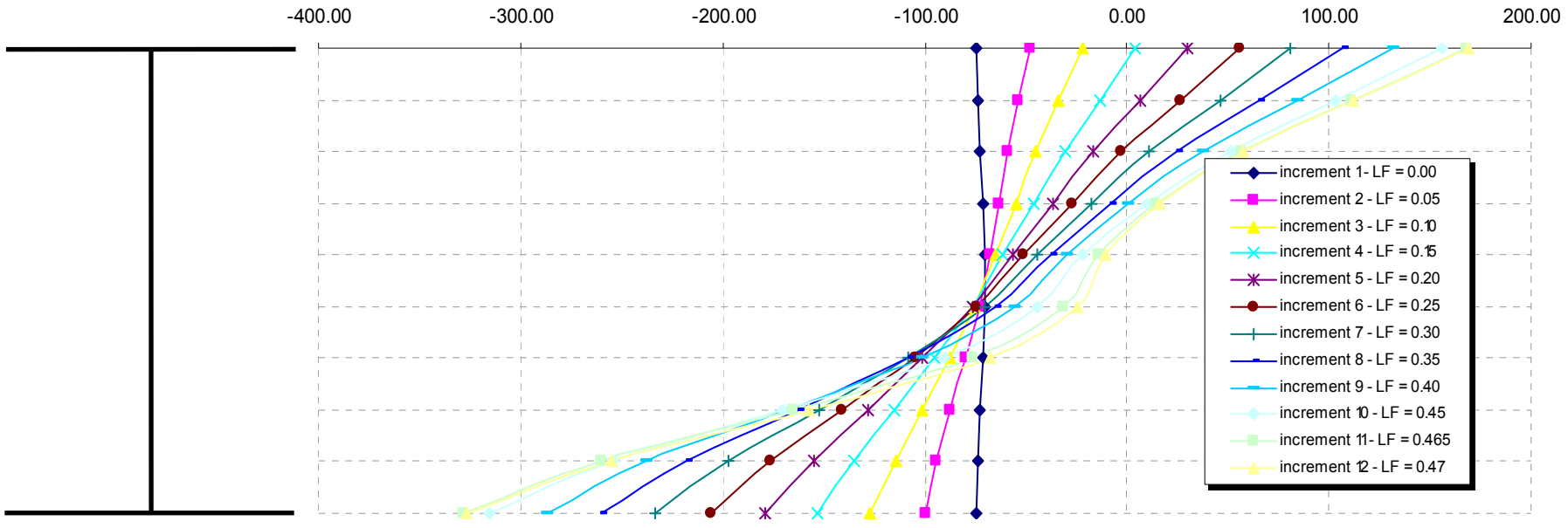

Fig. 4.48 – Section S2 – Longitudinal stresses in web (refer to Figure 4.41)

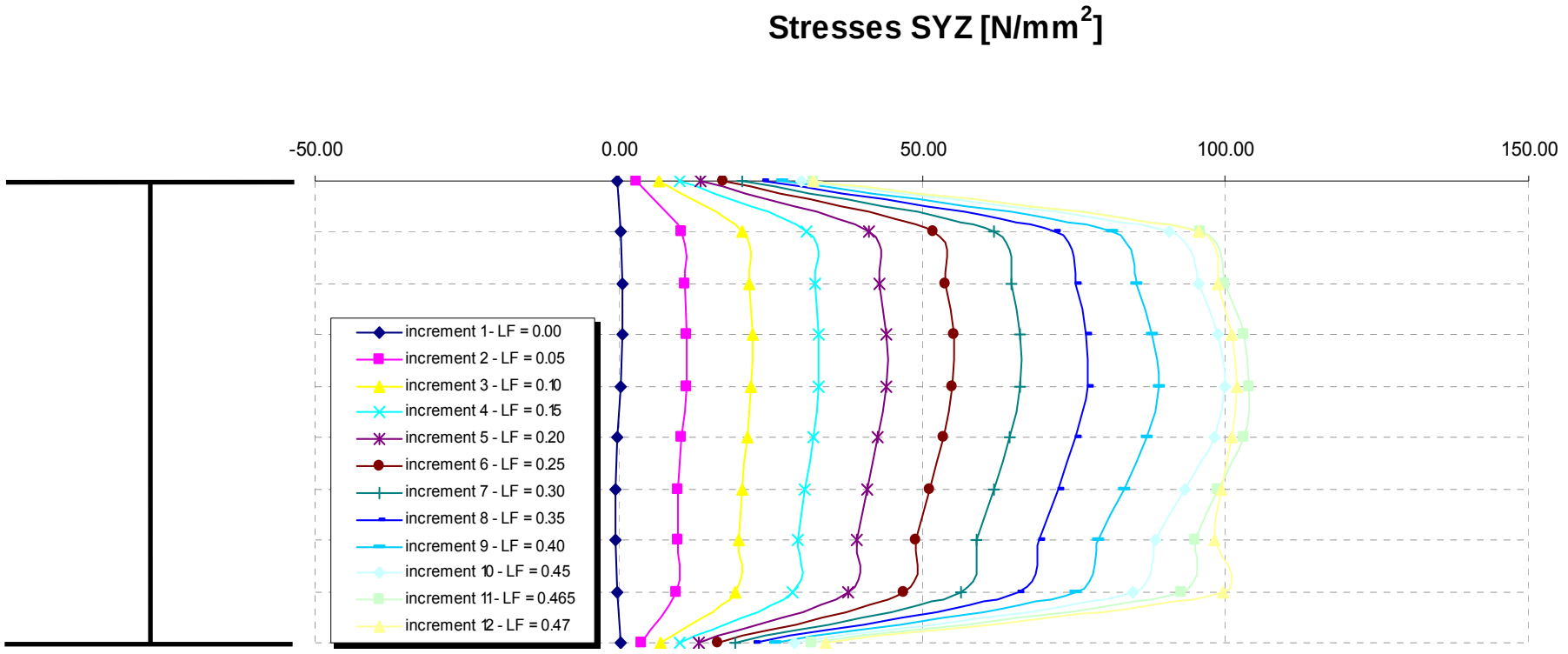

Fig. 4.49 – Section S2 – Shear stresses in web (refer to Figure 4.41)

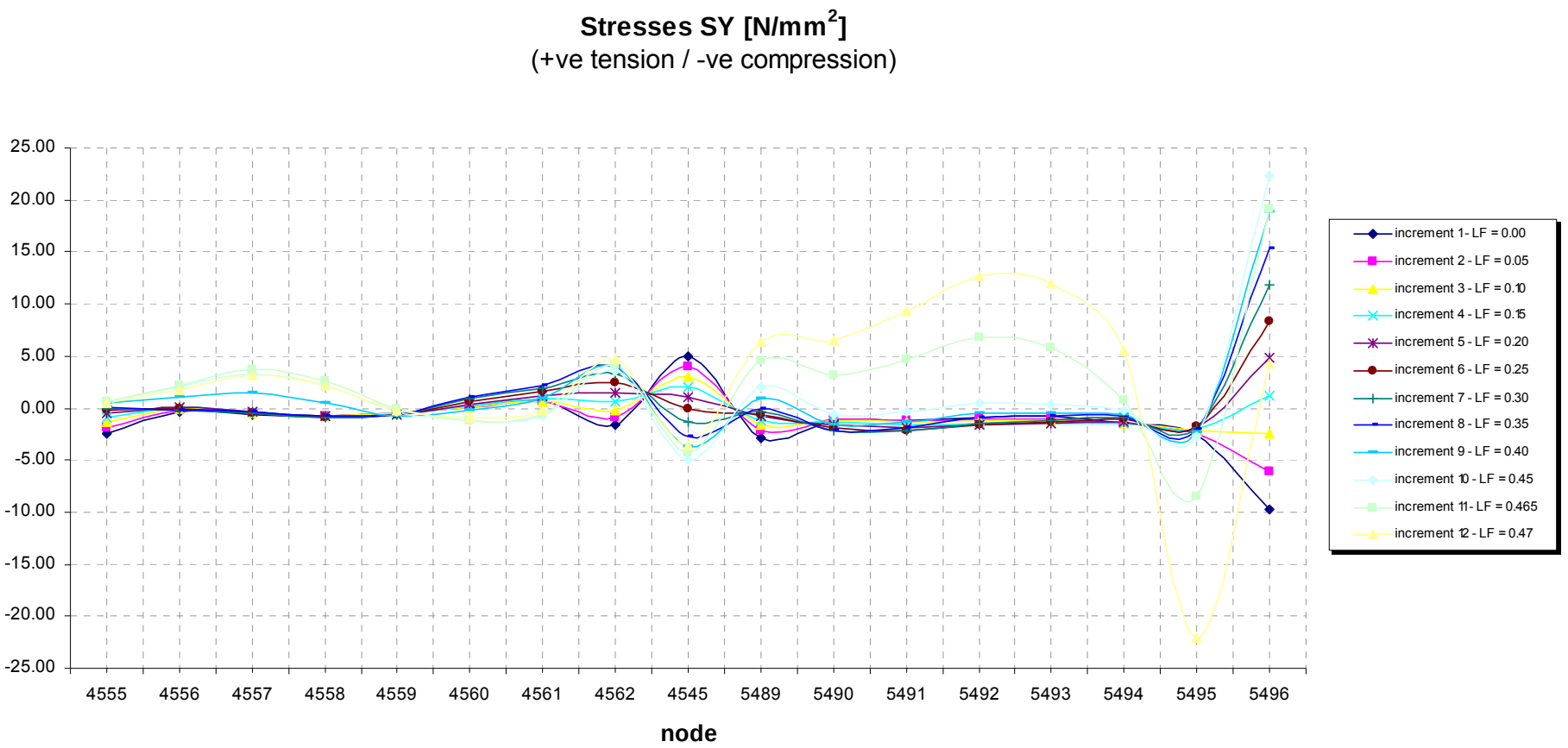

Fig. 4.50 – Section S4 – Vertical stresses in web (refer to Figure 4.41)

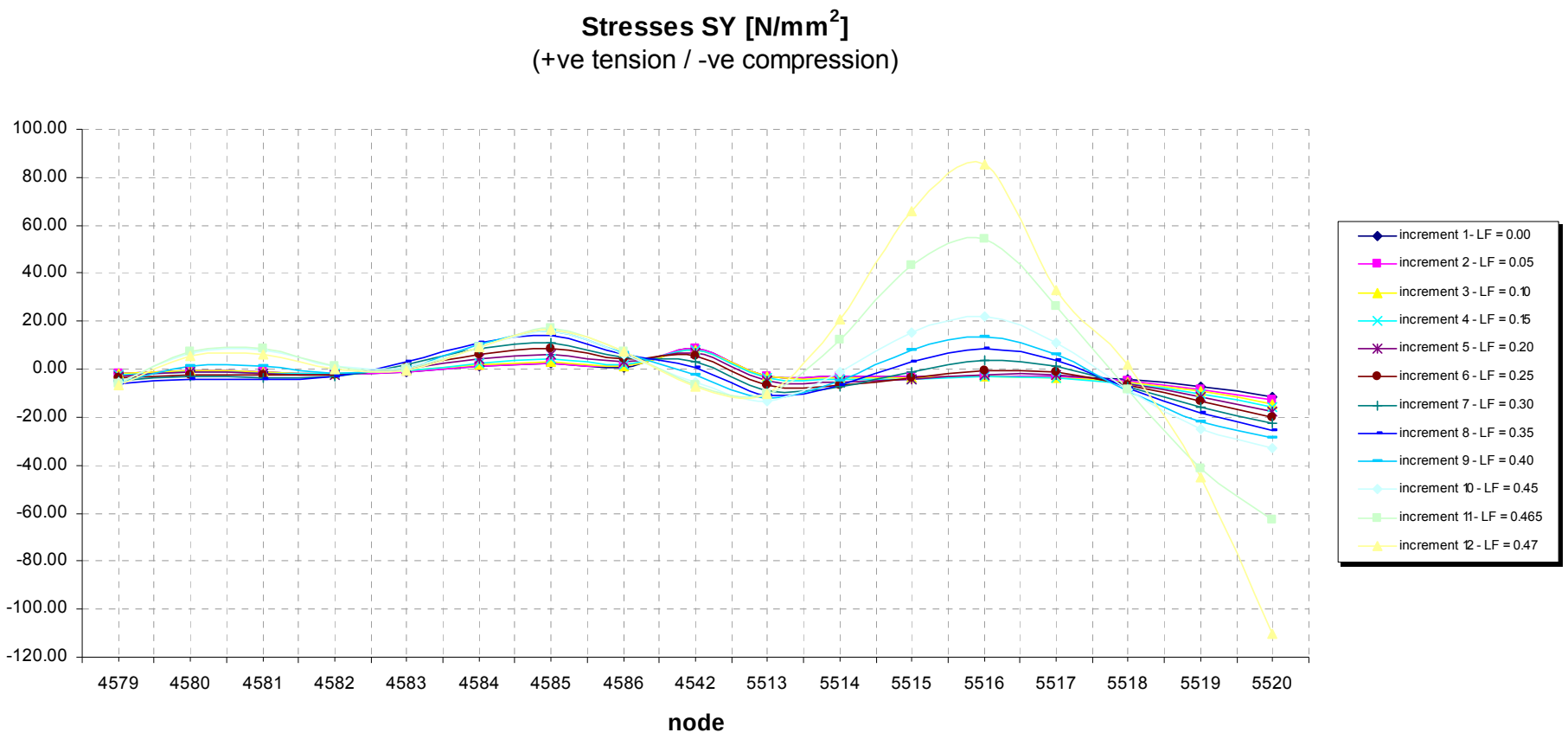

Fig. 4.51 – Section S6 – Vertical stresses in web (refer to Figure 4.41)

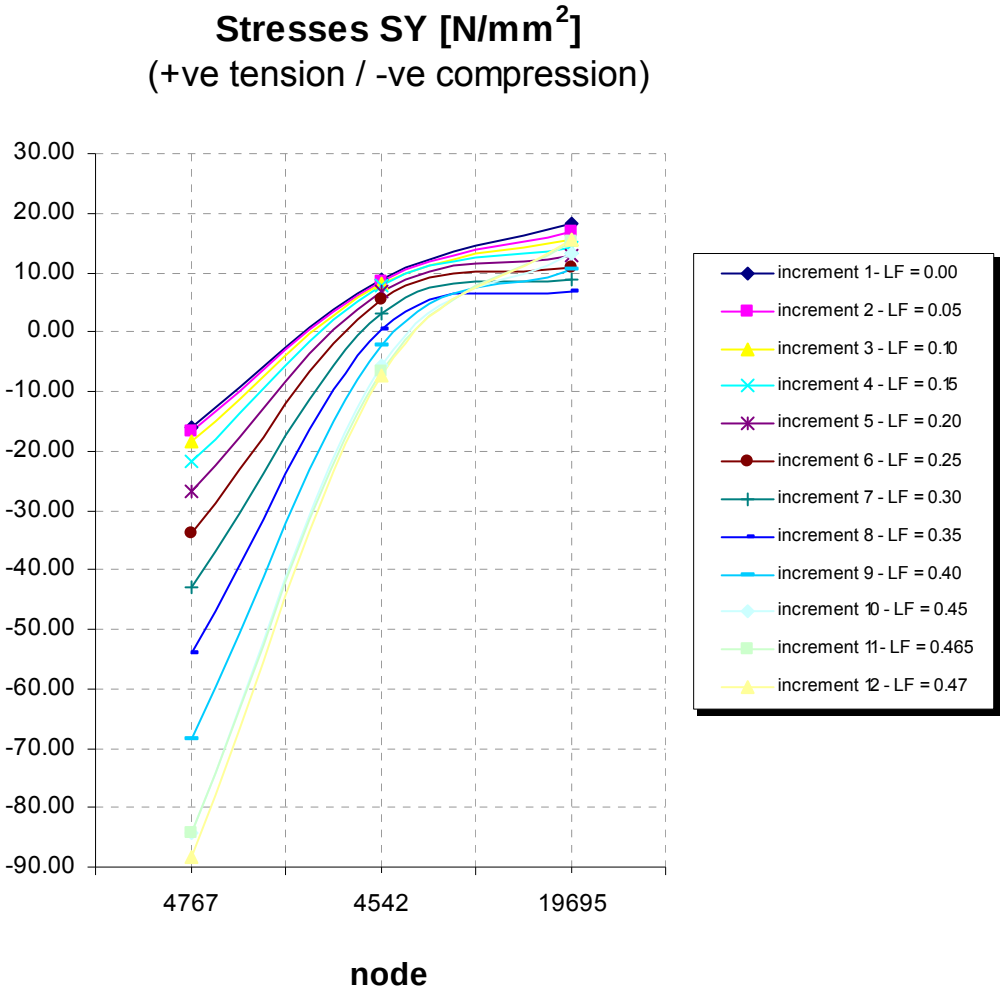

Fig. 4.52 – Section S8 – Vertical stresses in stiffener (refer to Figure 4.41)

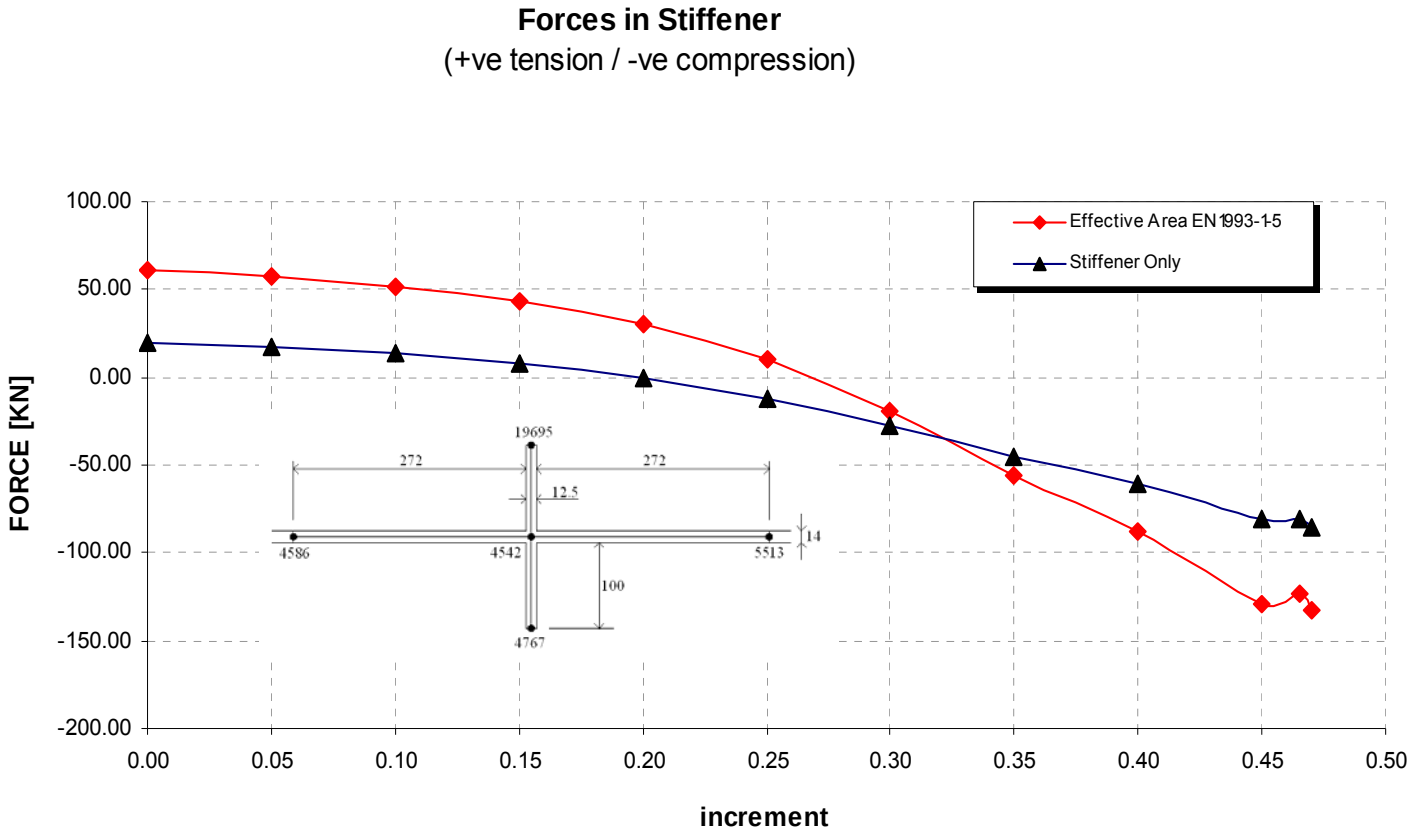

Fig. 4.53 – Section S8 – Vertical forces in stiffener (refer to Figure 4.41)

4.2 Steel-concrete composite girder

A symmetric steel plate girder with a concrete slab on top with single sided stiffeners is modelled. A typical section from existing UK bridge has been used (see Figure 4.54). The concrete is assumed to be cracked due to the hogging moment over the continuous bridge support, and the rebar only is modelled.

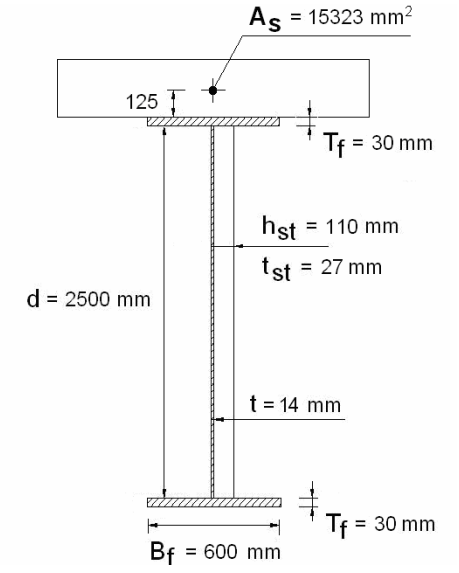

Fig. 4.54 – Old Thelwall Viaduct and section dimensions

Panels aspect ratio = a/d = 1

τ_{cr} = 55 N/mm^2 (see Appendix A)

$V_{cr} = \tau_{cr}$ x t x d = 1925 KN

$M_{f,Rd}$ = 17201 KNm

M_{el} = 19845 KNm

$M_{pl,Rd}$ = 31336 KNm

$V_{bw,Rd}$ = 3750 KN

$V_{pl,Rd}$ = 8610 KN

To investigate different ratios of bending moment to shear force, ends moments are applied. In particular, to obtain low ratios M/V the ends moments are generally bigger than the moment at midspan. To avoid a premature failure away from the midspan, which is the

area investigated, flanges and web are strengthened as shown in Figure 4.55, where ‘x 4’ means that the thicknesses of web panels and flanges have been locally increased with a factor 4 where required.

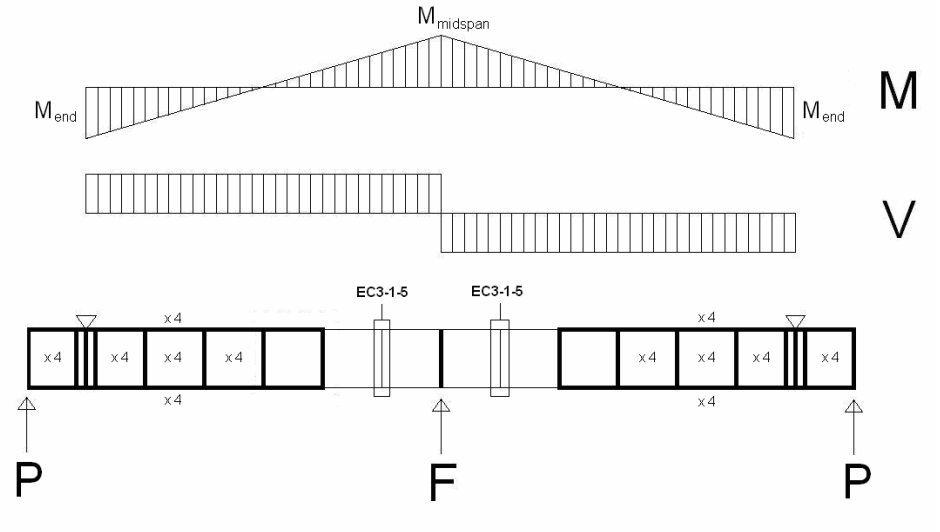

Figure 4.55 – Girder layout used in FE modelling

Several cases have been studied and a graphical summary is reported in Figure 4.56.

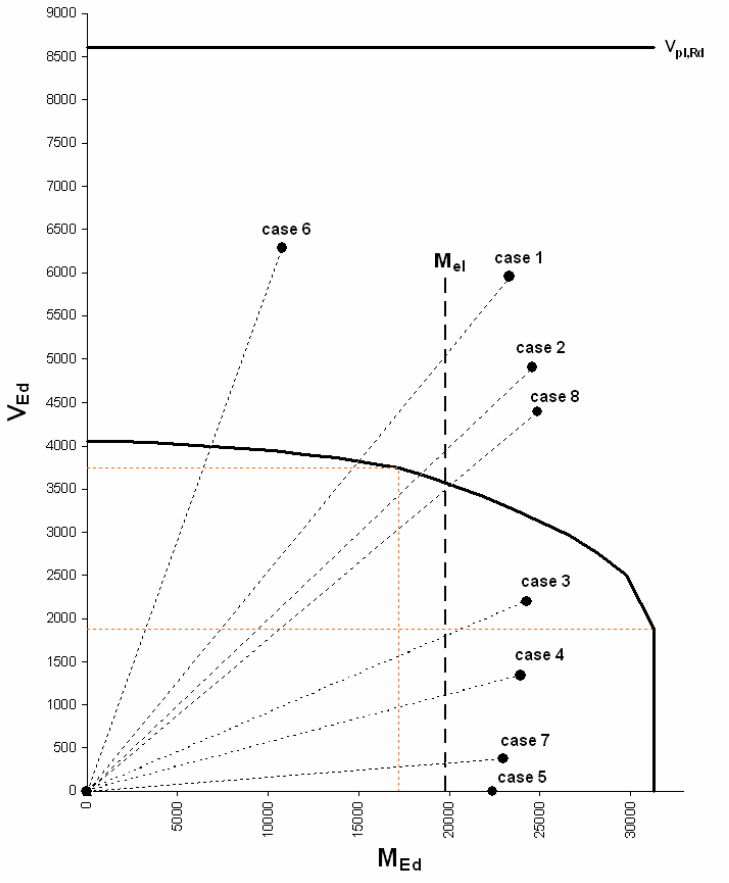

Figure 4.56 – Eurocode M-V interaction domain and result from non-linear analyses

Aspect Ratio	case	Load applied			Stiffener Design EN 1993-1-5			Non-linear analysis	
		N_{Ed} [KN]	M_{Ed} [KNm]	V_{Ed} [KN]	stiffness ratio	shape limit (<10.5)	strength (U.F.)	Imperfections	M_{NL}/ M_{Ed}
1:1	1*	-	13740	3500	1.00	4.07	2.17	no	1.700
	1	-	13740	3500	1.00	4.07	2.17	yes	1.680
	1	3550	13740	3500	1.00	4.07	2.17	no	1.492
	1	7100	13740	3500	1.00	4.07	2.17	no	1.354
	1	14200	13740	3500	1.00	4.07	2.17	no	0.888
	2*	-	17072	3410	1.00	4.07	2.05	no	1.440
	2	-	17072	3410	1.00	4.07	2.05	yes	1.432
	2	3550	17072	3410	1.00	4.07	2.05	no	1.228
	2	7100	17072	3410	1.00	4.07	2.05	no	1.064
	2	14200	17072	3410	1.00	4.07	2.05	no	0.684
	3*	-	27641	2500	1.00	4.07	0.80	no	0.880
	3	-	27641	2500	1.00	4.07	0.80	yes	0.850
	3	3550	27641	2500	1.00	4.07	0.80	no	0.717
	3	7100	27641	2500	1.00	4.07	0.80	no	0.600
	3	14200	27641	2500	1.00	4.07	0.80	no	0.382
	4*	-	30691	1705	1.00	4.07	0.07	no	0.780
	4	-	30691	1705	1.00	4.07	0.07	yes	0.749
	4	3550	30691	1705	1.00	4.07	0.07	no	-
	4	7100	30691	1705	1.00	4.07	0.07	no	-
	4	14200	30691	1705	1.00	4.07	0.07	no	-
	5*	-	30691	0	1.00	4.07	0.07	no	0.730
	5	-	30691	0	1.00	4.07	0.07	yes	0.708
	5	3550	30691	0	1.00	4.07	0.07	no	-
	5	7100	30691	0	1.00	4.07	0.07	no	-
	5	14200	30691	0	1.00	4.07	0.07	no	-
	6*	-	6240	3635	1.00	4.07	2.35	no	1.730
	6	-	6240	3635	1.00	4.07	2.35	yes	-
	6	3550	6240	3635	1.00	4.07	2.35	no	-
	6	7100	6240	3635	1.00	4.07	2.35	no	-
	6	14200	6240	3635	1.00	4.07	2.35	no	-
	7*	-	30691	500	1.00	4.07	0.07	no	0.759
	7	-	30691	500	1.00	4.07	0.07	yes	0.721
	7	3550	30691	500	1.00	4.07	0.07	no	0.622
	7	7100	30691	500	1.00	4.07	0.07	no	0.486
	7	14200	30691	500	1.00	4.07	0.07	no	0.275
	8*	-	18741	3300	1.00	4.07	1.89	no	1.363
	8	-	18741	3300	1.00	4.07	1.89	yes	1.303
	8	3550	18741	3300	1.00	4.07	1.89	no	1.115
	8	7100	18741	3300	1.00	4.07	1.89	no	0.960
	8	14200	18741	3300	1.00	4.07	1.89	no	0.606
2:1	1	-	13740	3500	1.00	4.07	3.06	no	1.600

* Results shown in Figure 4.56

Table 2 – Summary of results from non-linear analyses for composite girder

4.2.1 Case 1

A force F = 7000 KN ≈ 2 x V_{ult} at midspan if applied alone would produce the following effects:

M_{max} = F x L / 4 = 7000 x 30 / 4 = 52500 KNm

V = F / 2 = 7000 / 2 = 3500 KN

In order to obtain the required M/V ratio, as shown in figure 4.56, ends moments M_{end} of 38760 KNm have to be applied. The midspan moment is equal to:

$M_{midspan} = M_{max} - M_{end}$ = 52500 – 38760 = 13740 KNm

The non-linear analysis stops when it fails to find an equilibrium beyond a load factor 1.70.

M_{NL} = 1.70 x 13740 = 23358 KNm $\longrightarrow$ $\overline{\eta}_1$ = 0.745

V_{NL} = 1.70 x 3500 = 5950 KN $\longrightarrow$ $\overline{\eta}_3$ = 1.587

The load-deflection curve obtained from the finite element analysis is illustrated in Figure 4.57. The analysis shows an almost linear behaviour up to a load factor of approximately 1.10, after which it shows a gradual loss of stiffness culminating in a failure at the load factor of 1.70.

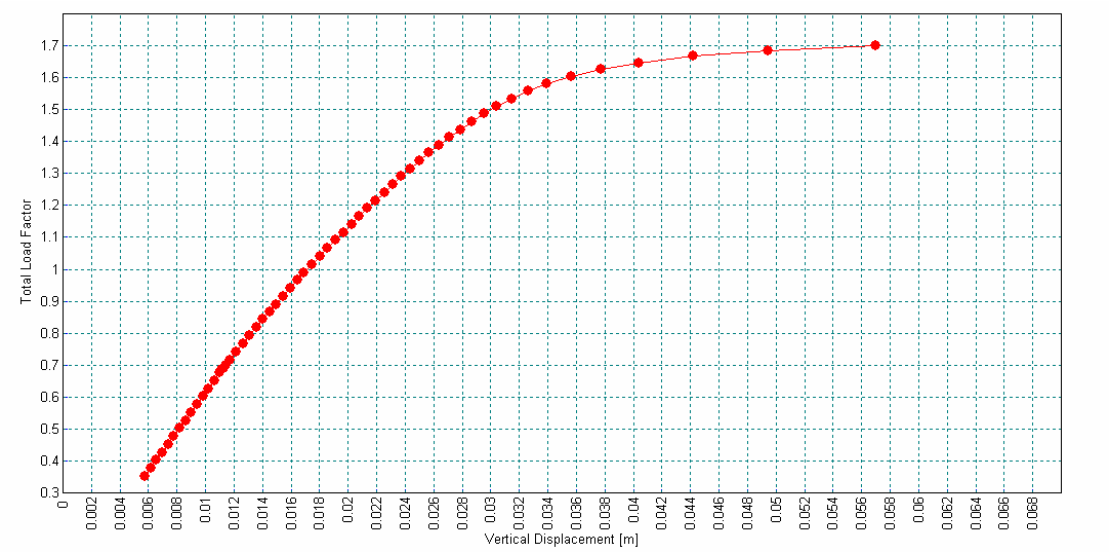

Figure 4.57 – Vertical Displacement vs Total Load Factor

The lateral deflection of the web at this point is illustrated in Figures 4.60 to 4.62. It can be seen that the girder has failed by the web bowing out laterally, while stiffeners remain almost straight.

The M-V interaction domain from EN 1993-1-5 and the results obtained from the non-linear analysis are illustrated in Figure 4.58. The interaction curve has been built according to EN 1993-1-5 clause 7.1(1). Possible benefits considering clause 7.1(2), regarding performing the interaction at "0.5 h_w" from support or checking at support using $V_{pl,Rd}$, have not been considered.

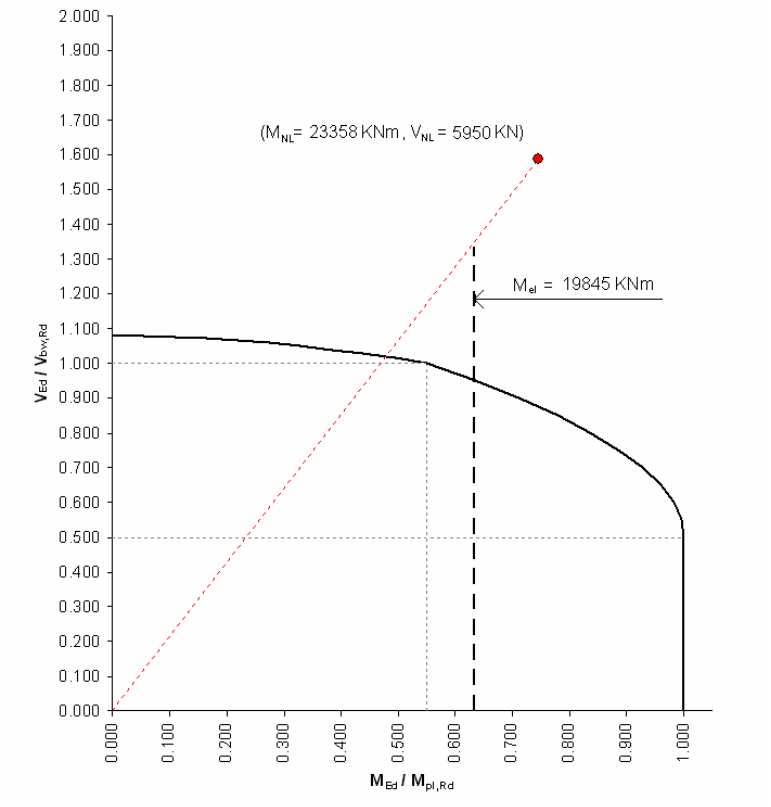

Figure 4.58 – Eurocode M-V interaction domain and result from non-linear analysis

The sections through the girder at various stages in the analysis to establish the distribution of internal forces are illustrated in Figures 4.63 to 4.76.

For this case, several analyses have been run in order to investigate the influence of changing the stiffness of the stiffener, imperfections, axial force applied or not and the influence of the panel aspect ratio on the bearing capacity of the girder. In Table 3 it can be seen that different stiffener dimensions have been used. The stiffness ratio is defined as the ratio of the minimum stiffness required and the actual stiffness of the stiffener in accordance with clause 9.3.3 (3) of EN 1993-1-5. Three different stiffeners have been used:

- Rigid → stiffness ratio = 0.75
- EC3-1-5 → stiffness ratio = 1.00
- 0.5 x EC3-1-5 → stiffness ratio = 2.00

Aspect Ratio	Case	Load Applied			Stiffener Design EN1993-1-5					Non-linear analysis	
		N_{Ed} [KN]	M_{Ed} [KNm]	V_{Ed} [KN]	$h_{st} \times t_{st}$ [mm]	stiffness ratio	shape limit (<10.5)	strength (U.F.)	type	Imperfections	M_{NL}/M_{Ed}
1:1	1	-	13740	3500	110x40	0.75	2.75	1.96	RIGID	No	1.731
1:1	1	-	13740	3500	110x27	1.00	4.07	2.17	EC3-1-5	no	1.700
1:1	1	-	13740	3500	110x27	1.00	4.07	2.17	EC3-1-5	yes	1.680
1:1	1	3550	13740	3500	110x27	1.00	4.07	2.17	EC3-1-5	no	1.492
1:1	1	7100	13740	3500	110x27	1.00	4.07	2.17	EC3-1-5	no	1.354
1:1	1	14200	13740	3500	110x27	1.00	4.07	2.17	EC3-1-5	no	0.888
1:1	1	-	13740	3500	110x11.3	2.00	9.73	3.57	0.5 x EC3-1-5	no	1.603
1:2	1	-	13740	3500	-	-	-	-	-	no	1.460

Table 3 – Results from non-linear analyses shown in Figure 4.59

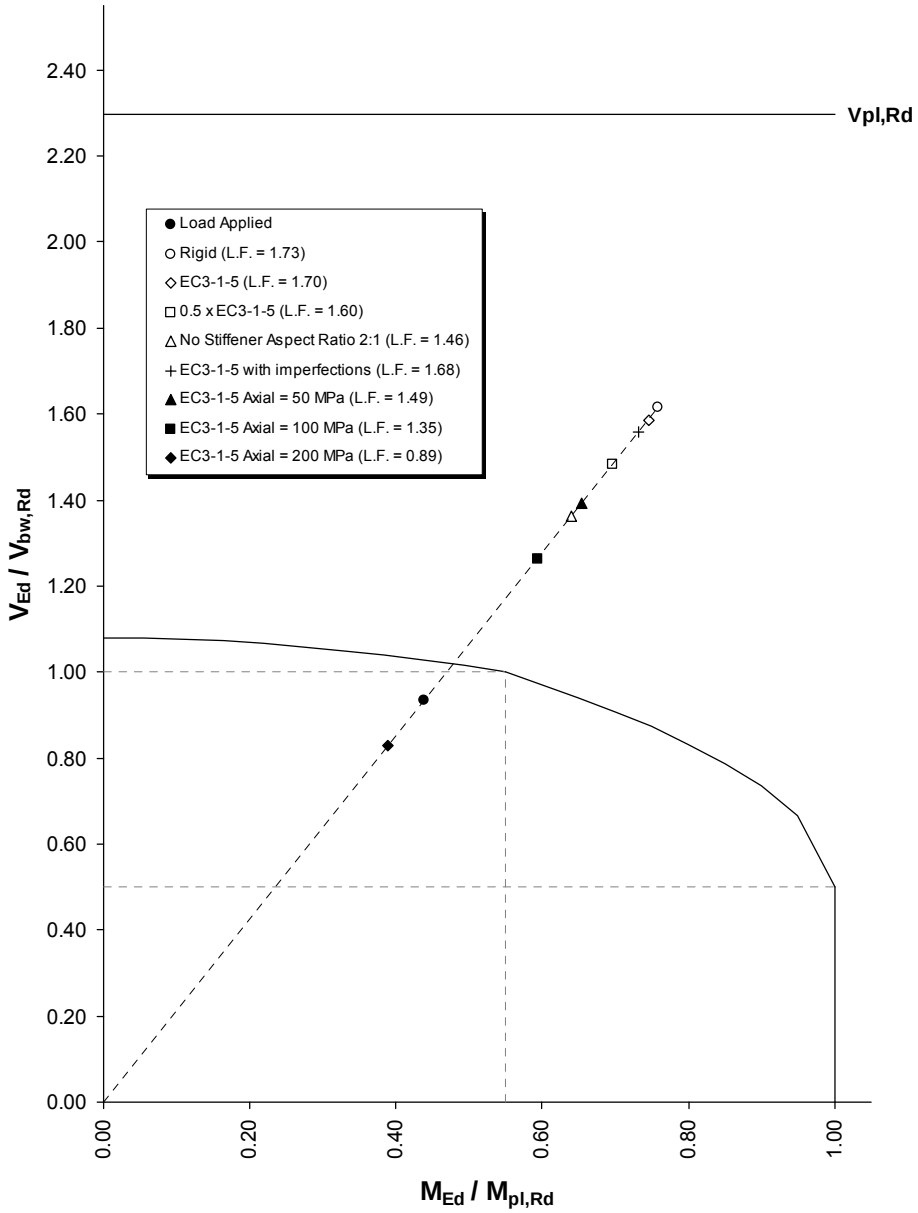

Figure 4.59 – Eurocode M-V interaction domain and results from NL analyses (Table 3)

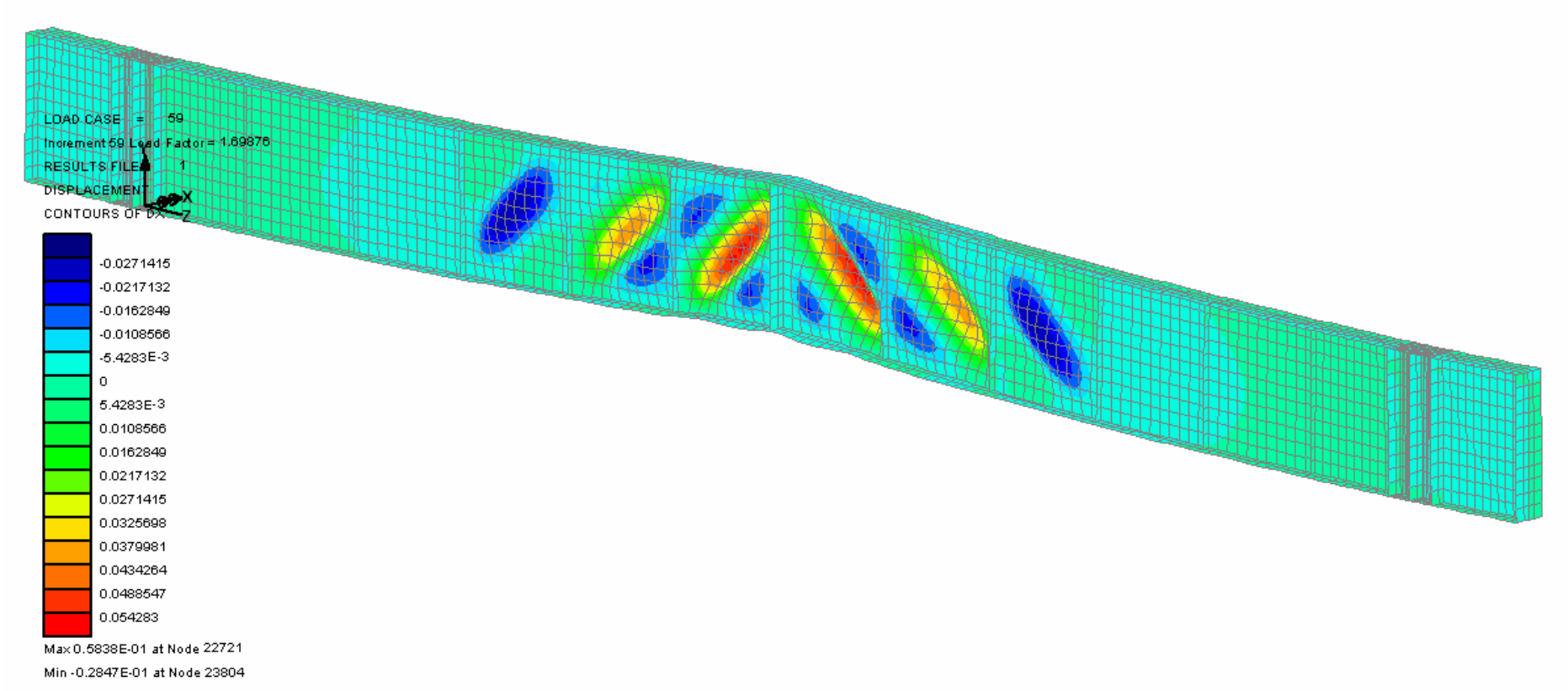

Figure 4.60 – Lateral Displacement Contour (m) at failure

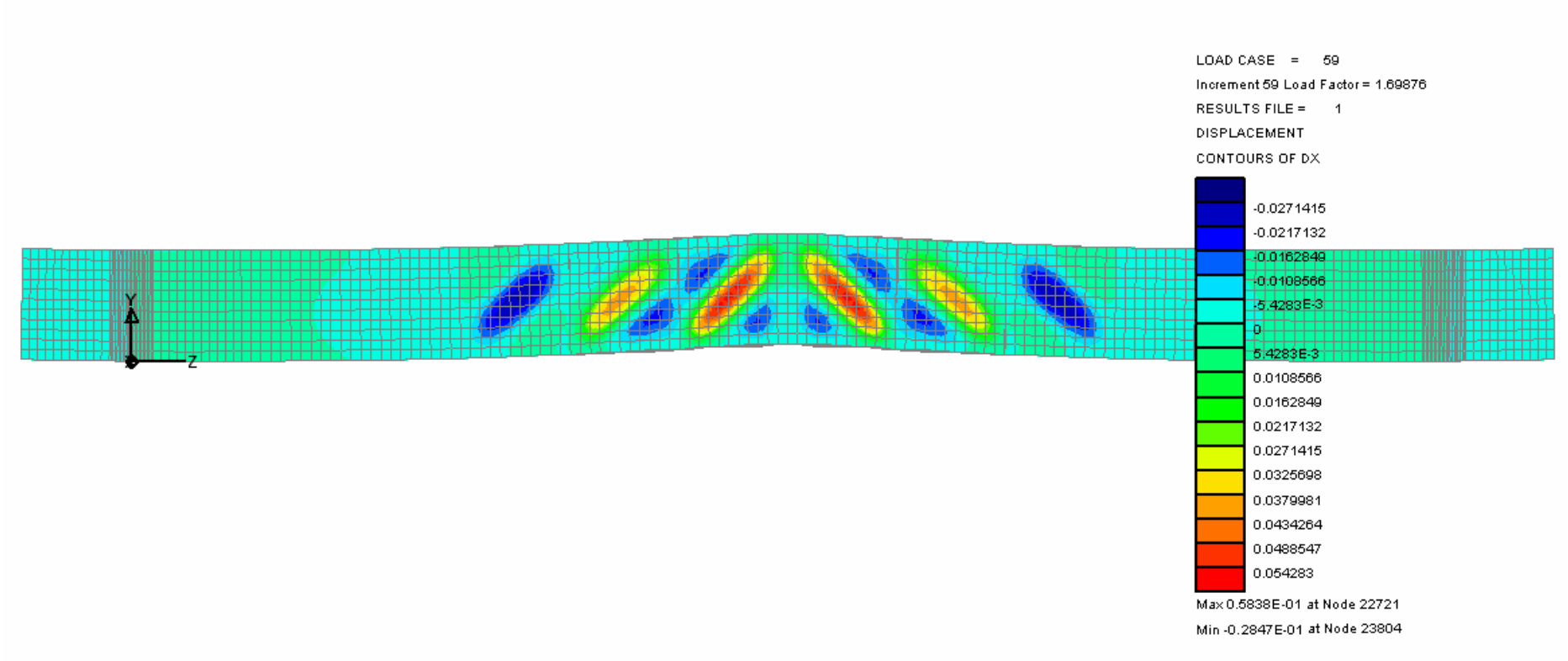

Figure 4.61 – Lateral Displacement Contour (m) at failure

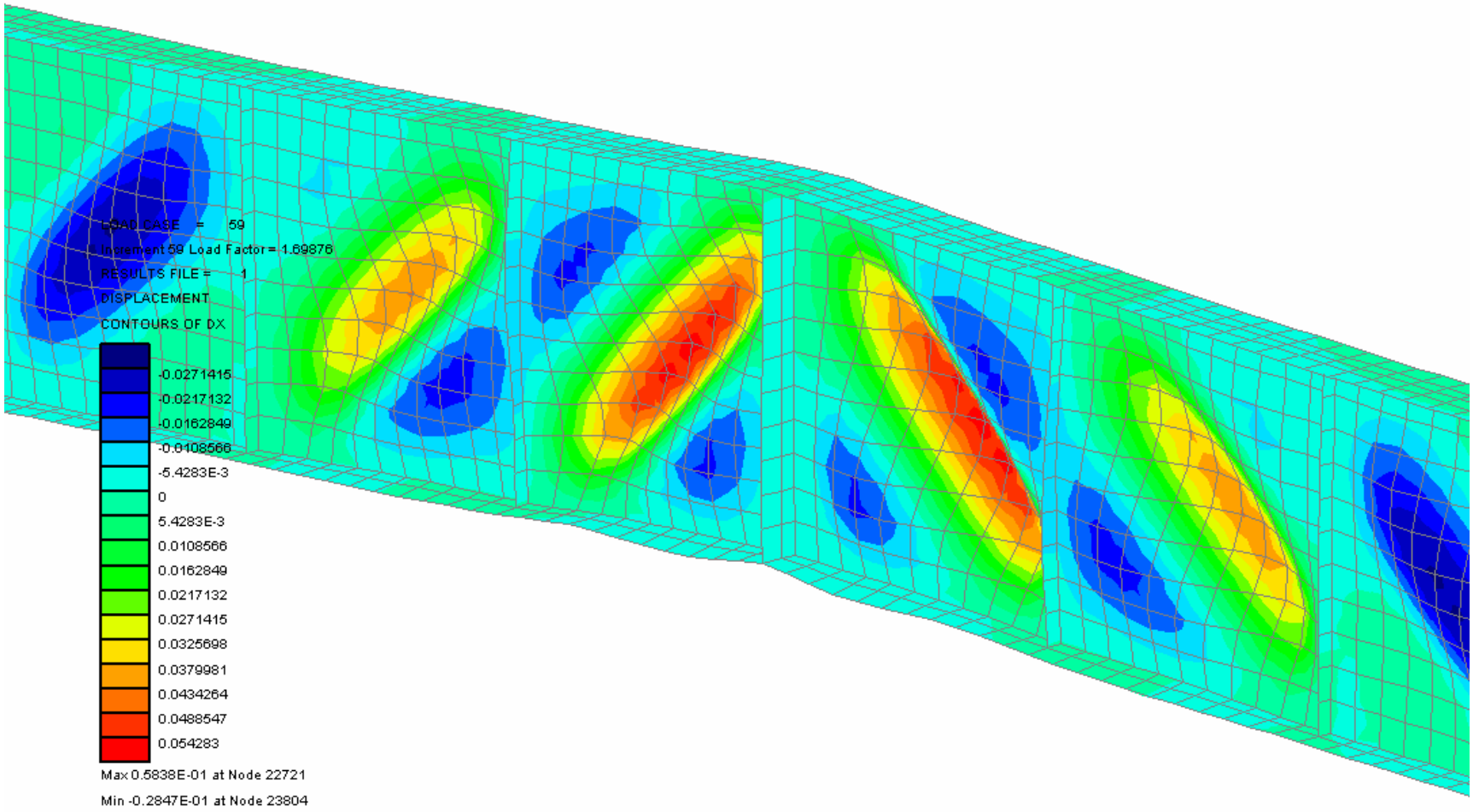

Figure 4.62 – Lateral Displacement Contour (m) at failure

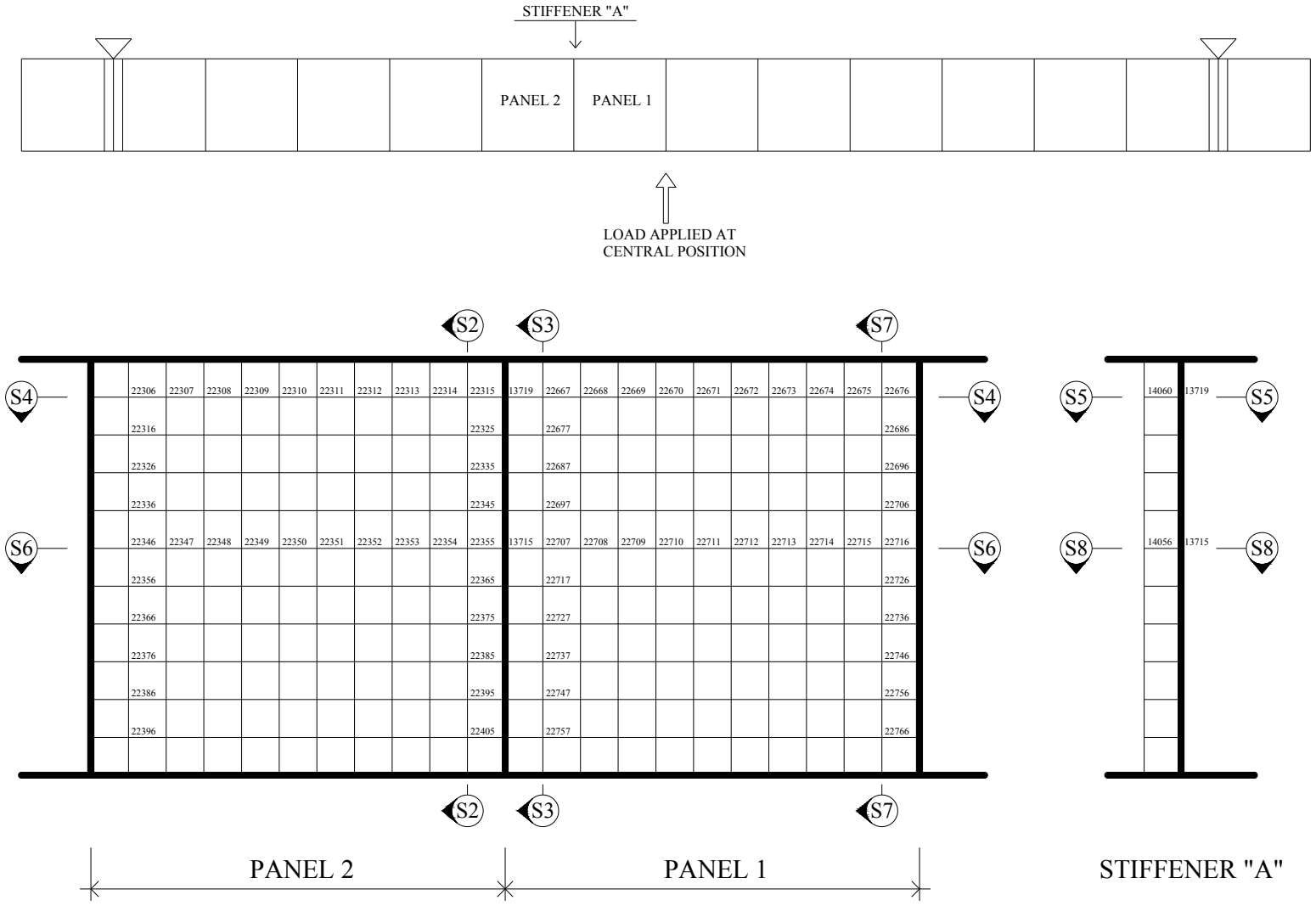

Fig. 4.63 – Investigated area and location of sections

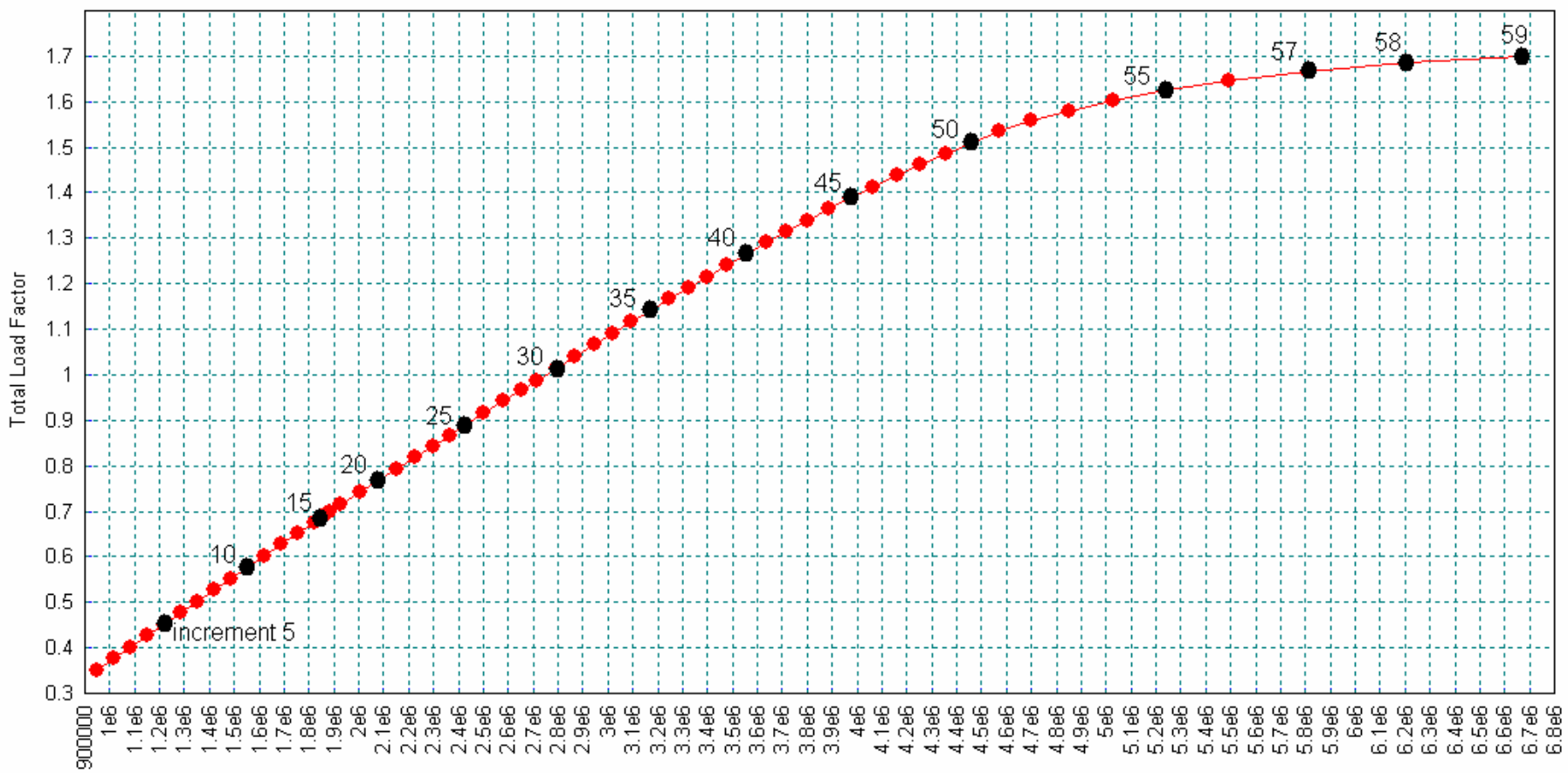

Fig. 4.64 – Section S7 – Force in Rebar [N] (refer to Figure 4.63)

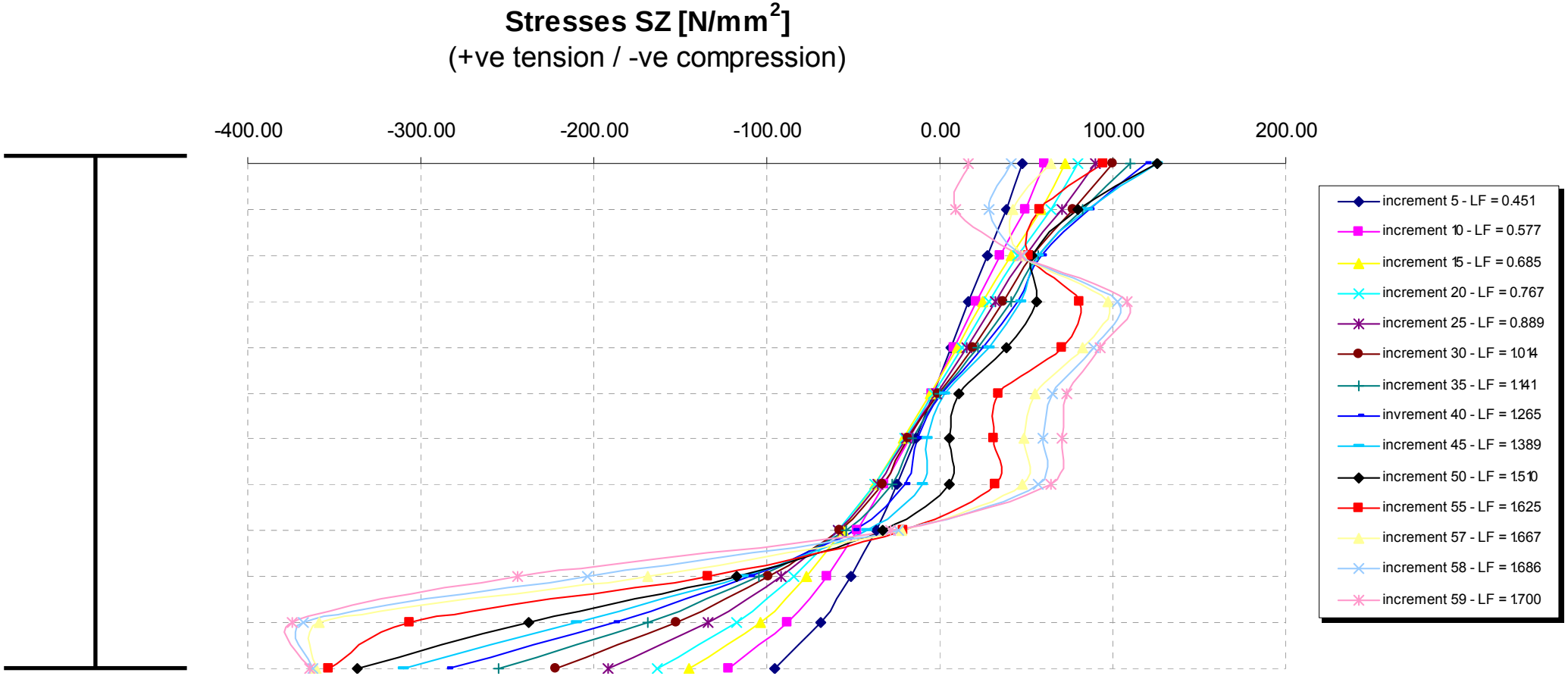

Fig. 4.65 – Section S7 – Longitudinal stresses in web (refer to Figure 4.63)

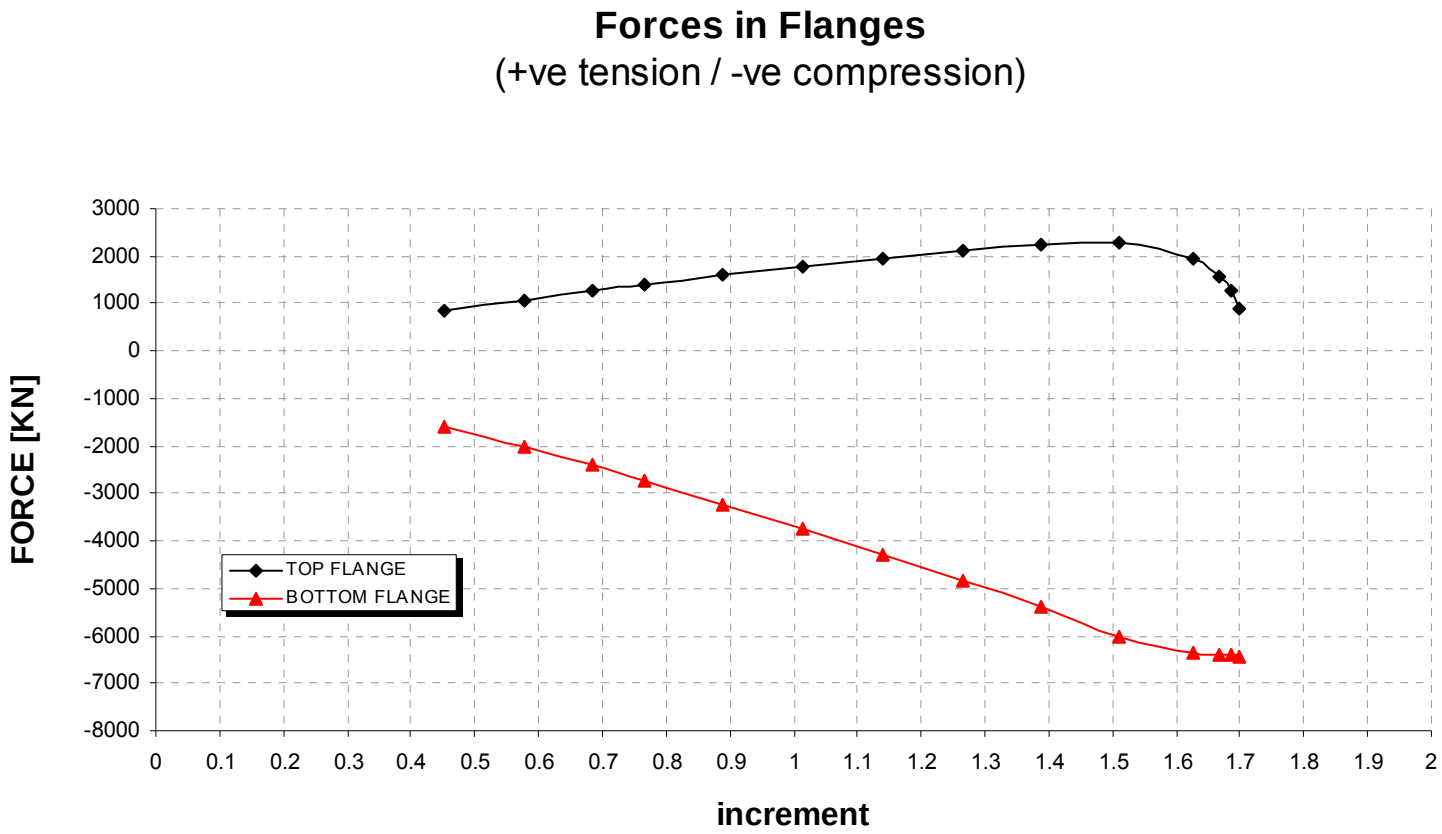

Fig. 4.66 – Section S7 – Longitudinal forces in flanges (refer to Figure 4.63)

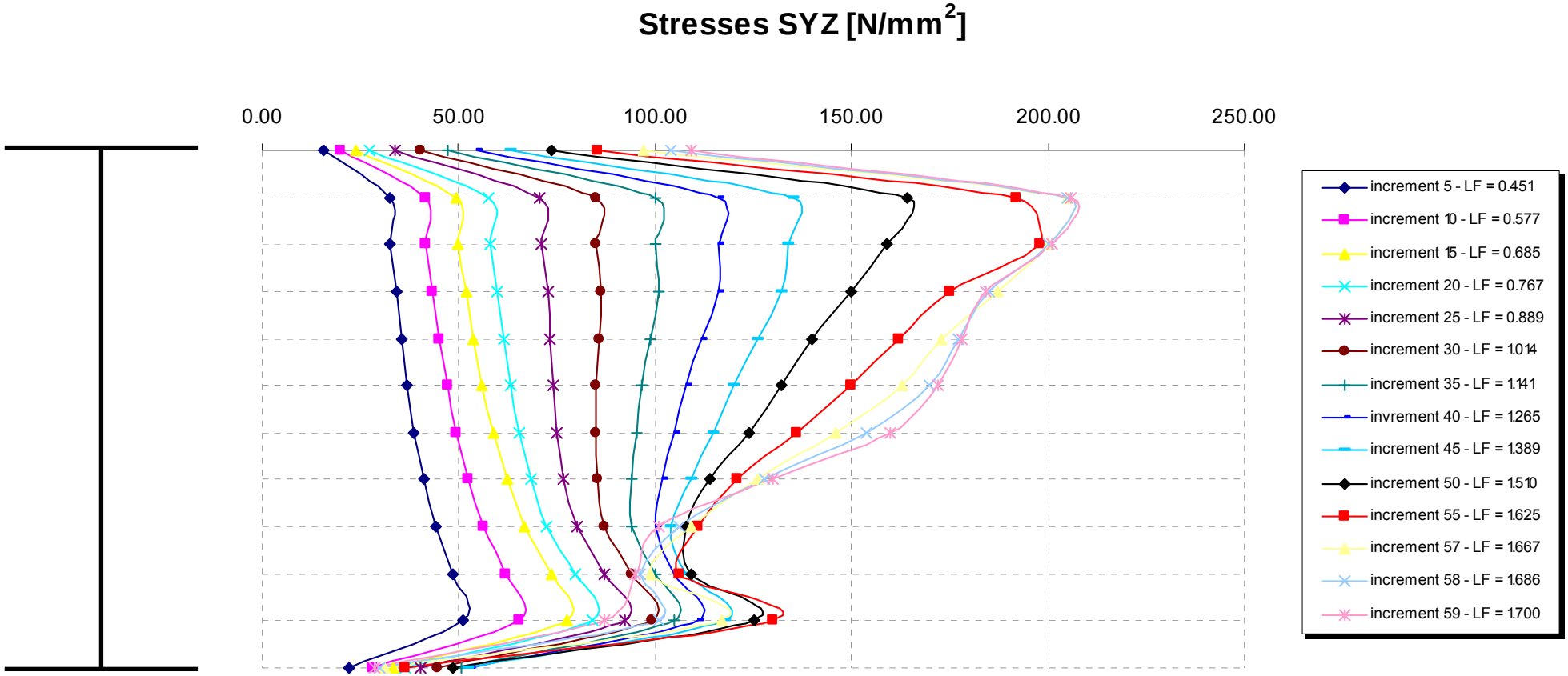

Fig. 4.67 – Section S7 – Shear stresses in web (refer to Figure 4.63)

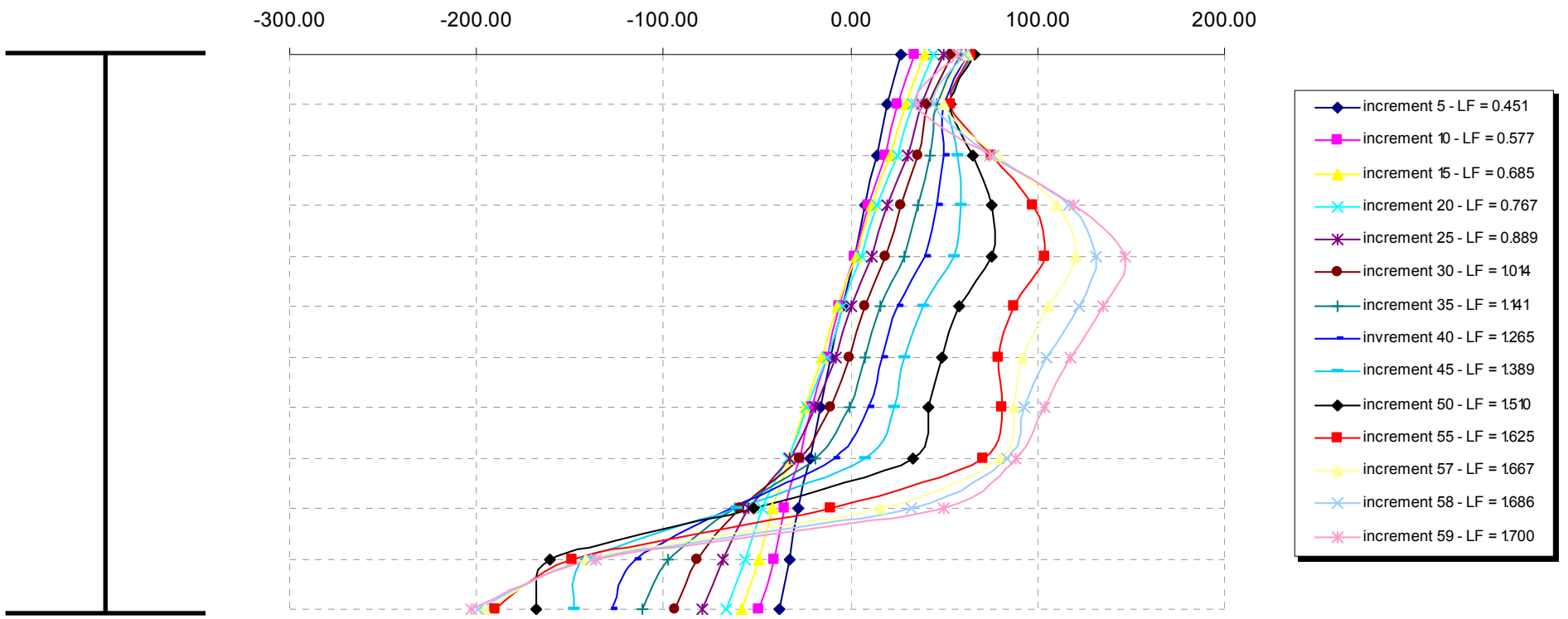

Fig. 4.68 – Section S3 – Longitudinal stresses in web (refer to Figure 4.63)

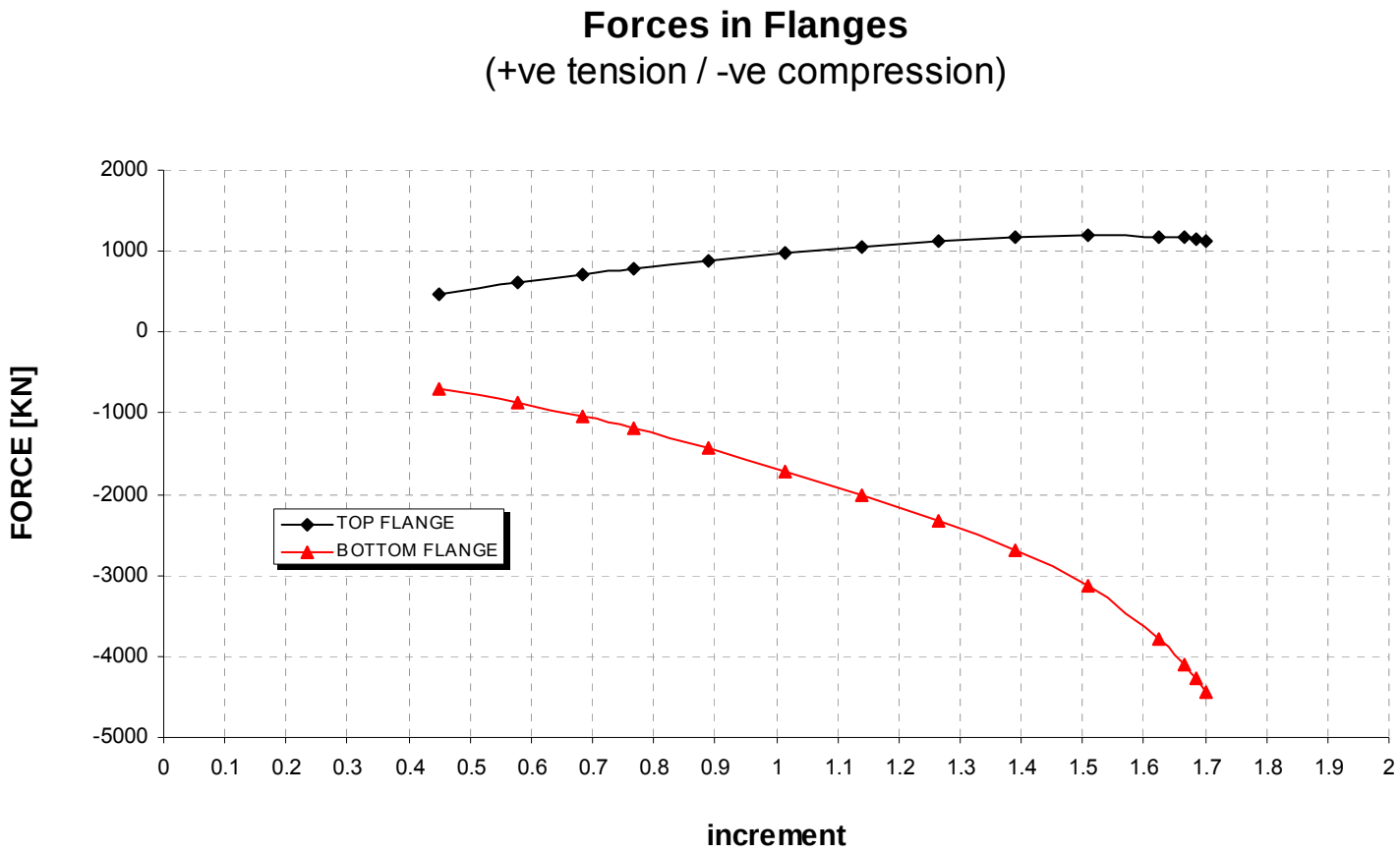

Fig. 4.69 – Section S3 – Longitudinal forces in flanges (refer to Figure 4.63)

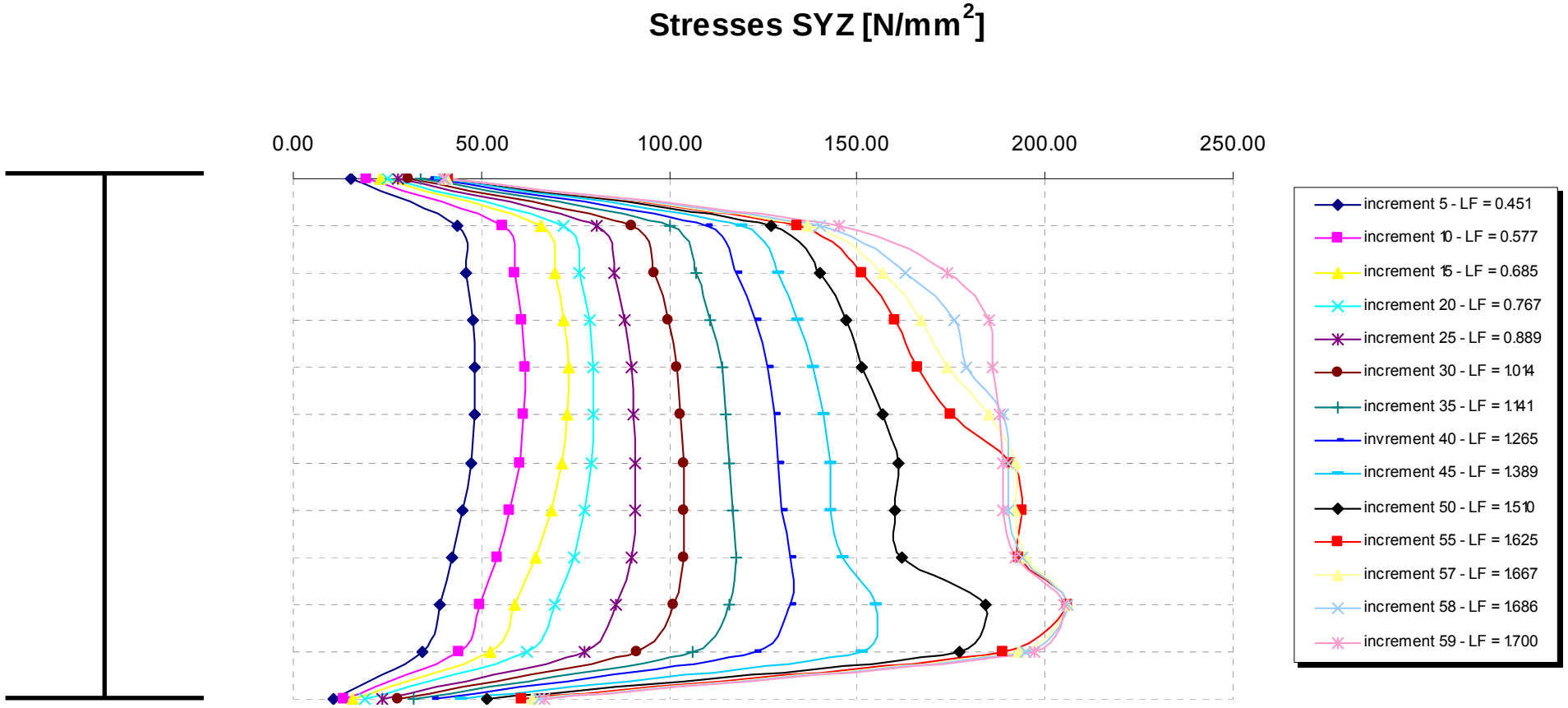

Fig. 4.70 – Section S3 – Shear stresses in web (refer to Figure 4.63)

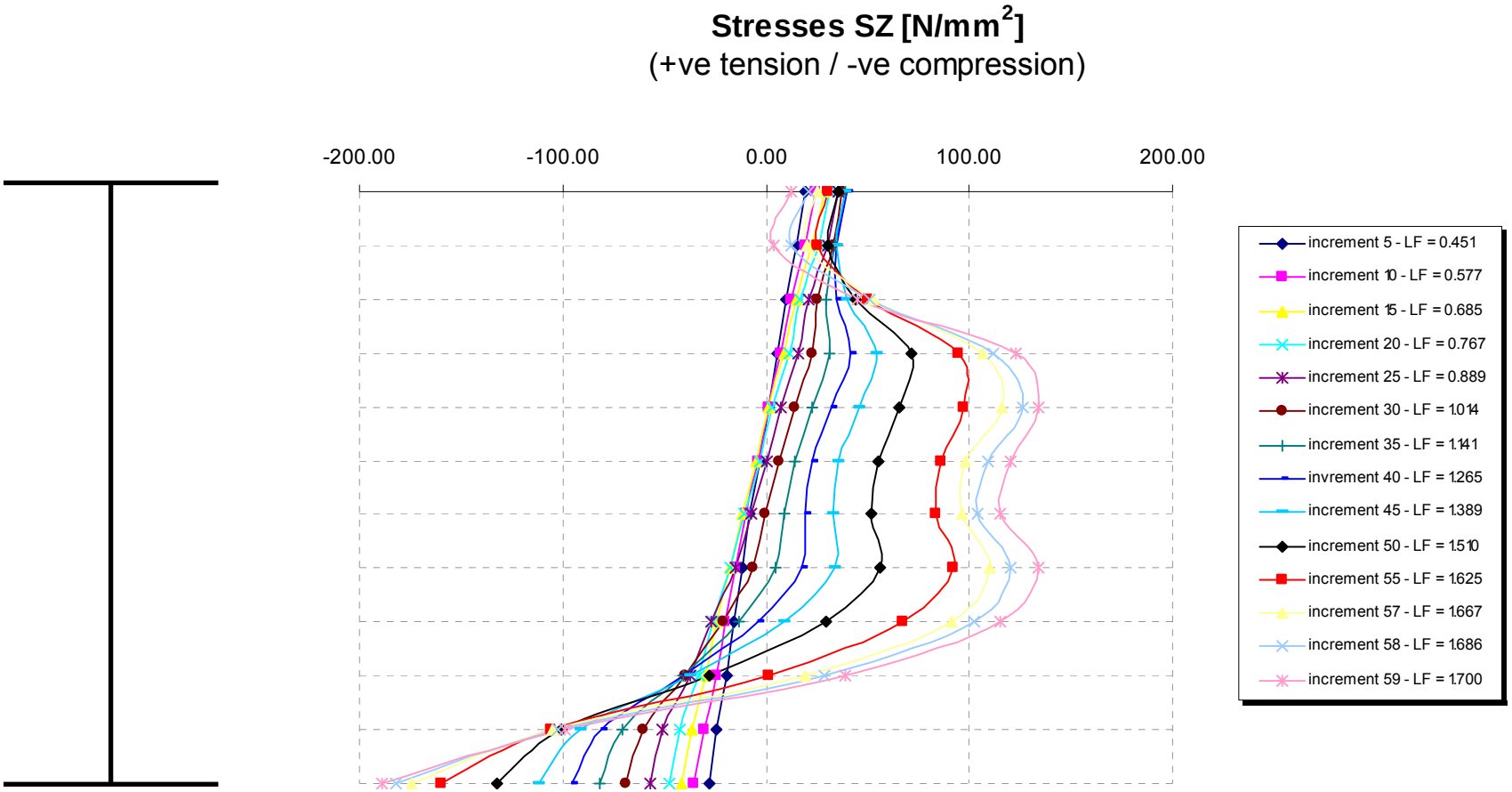

Fig. 4.71 – Section S2 – Longitudinal stresses in web (refer to Figure 4.63)

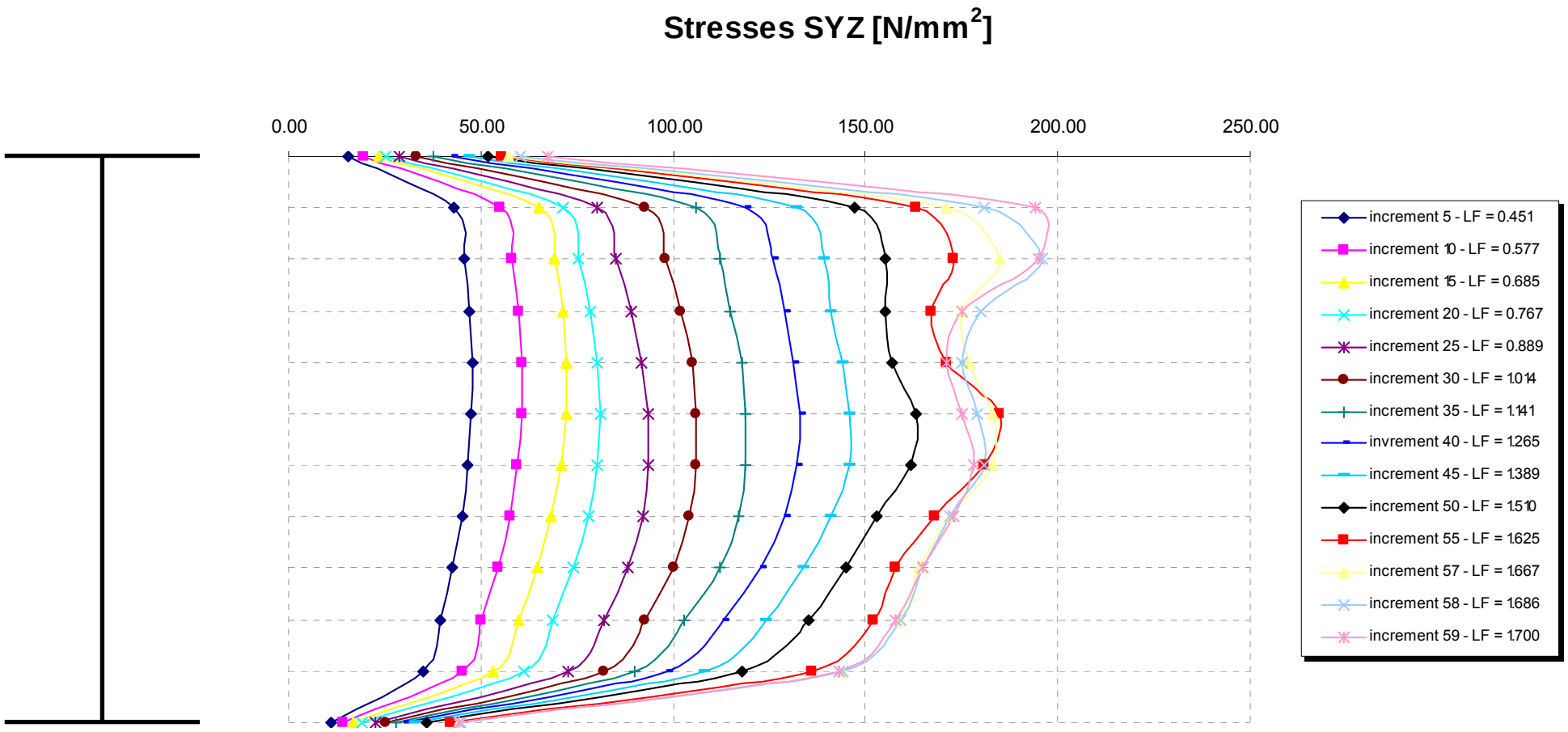

Fig. 4.72 – Section S2 – Shear stresses in web (refer to Figure 4.63)

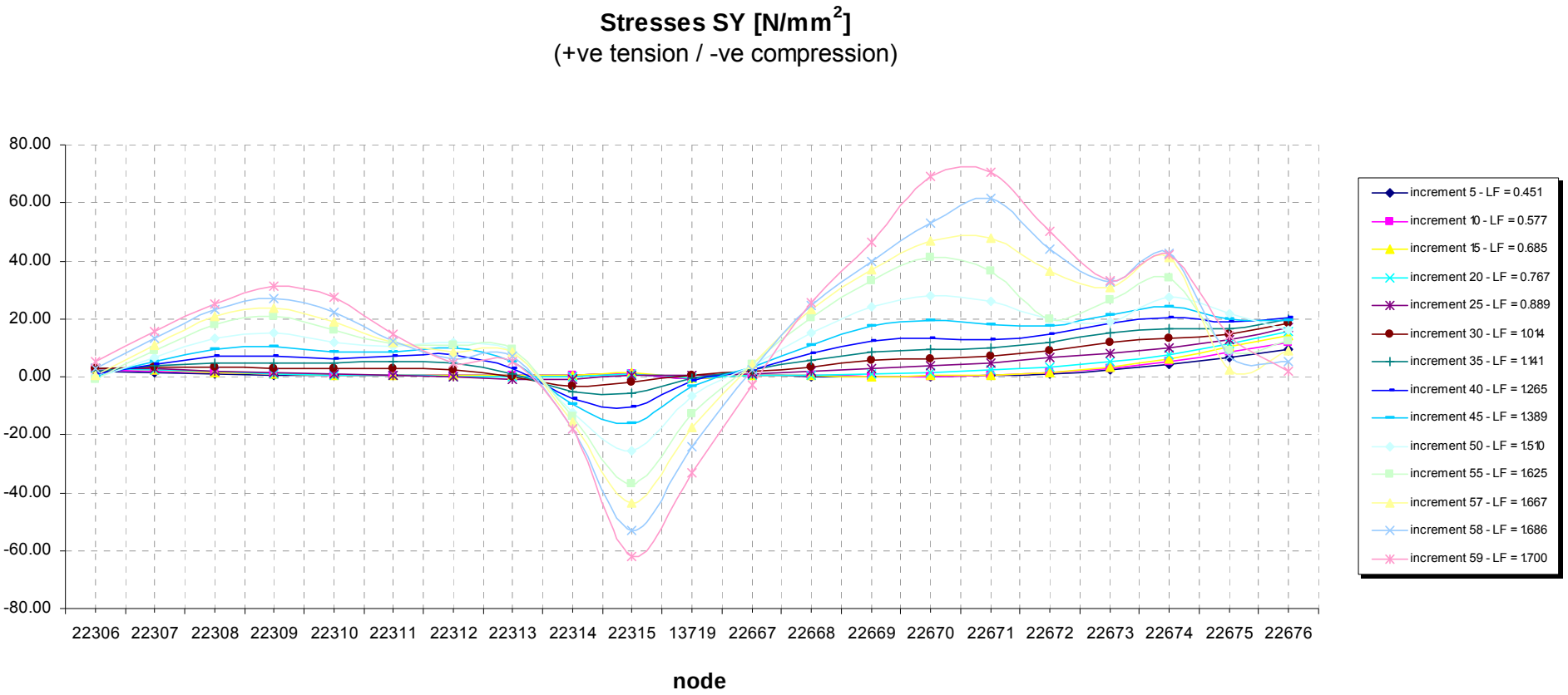

Fig. 4.73 – Section S4 – Vertical stresses in web (refer to Figure 4.63)

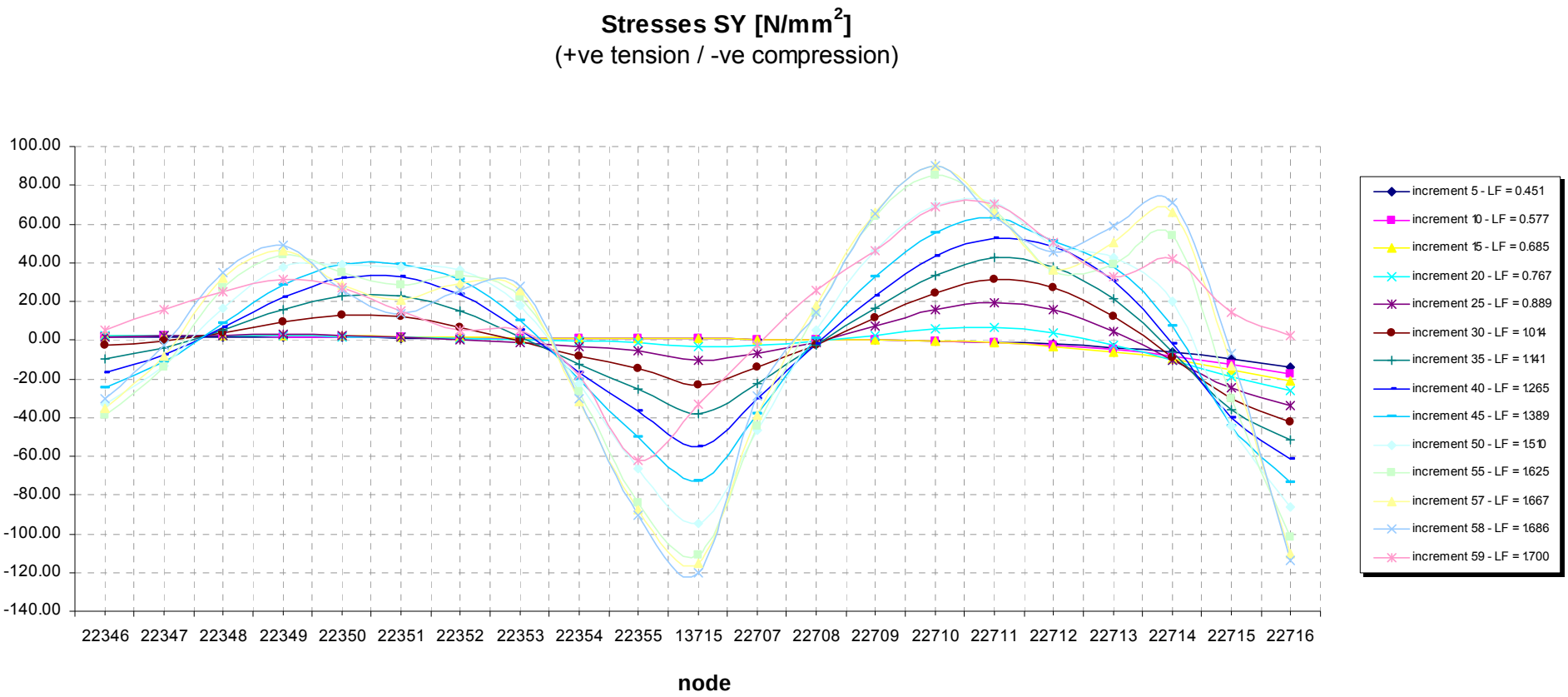

Fig. 4.74 – Section S6 – Vertical stresses in web (refer to Figure 4.63)

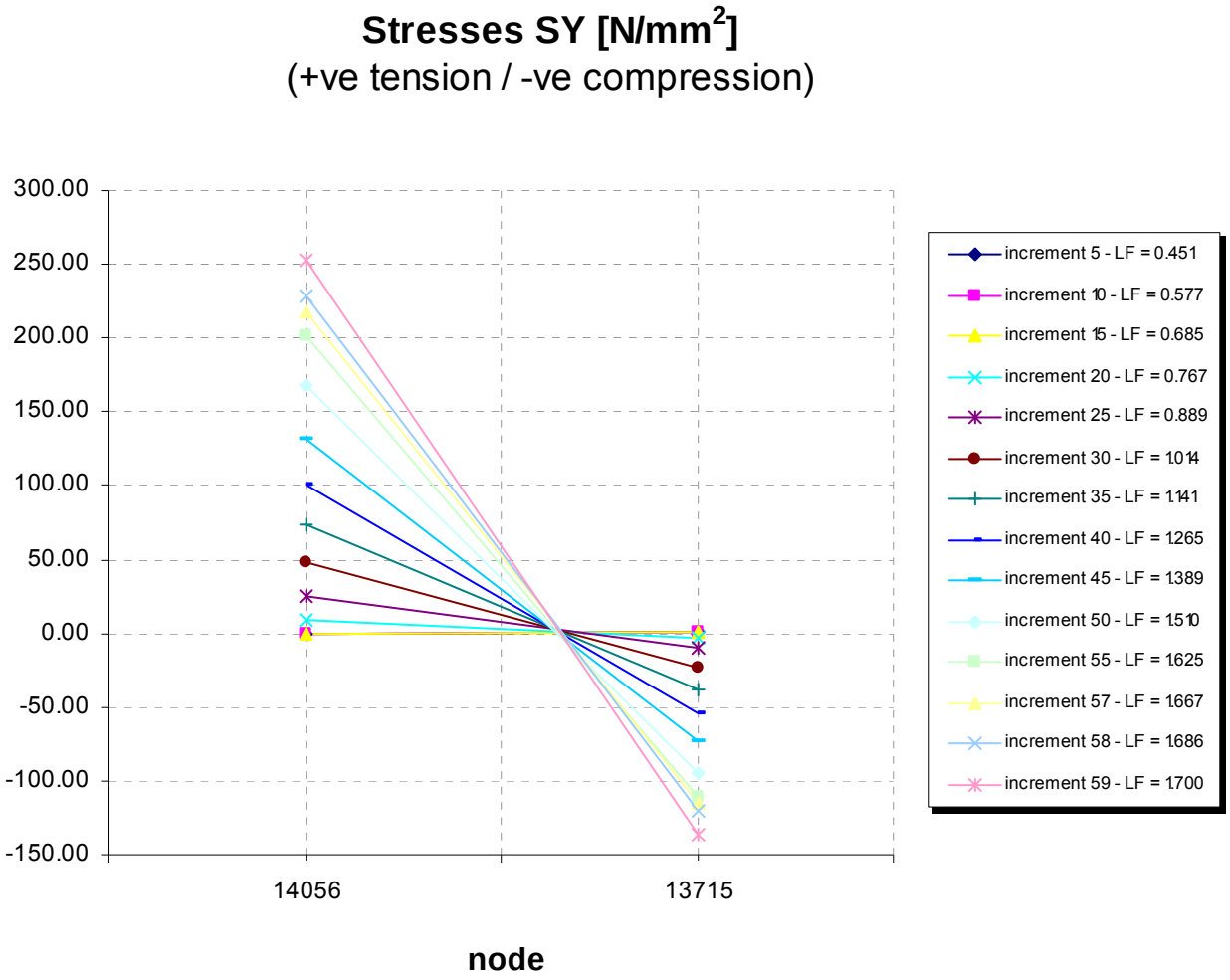

Fig. 4.75 – Section S8 – Vertical stresses in stiffener (refer to Figure 4.63)

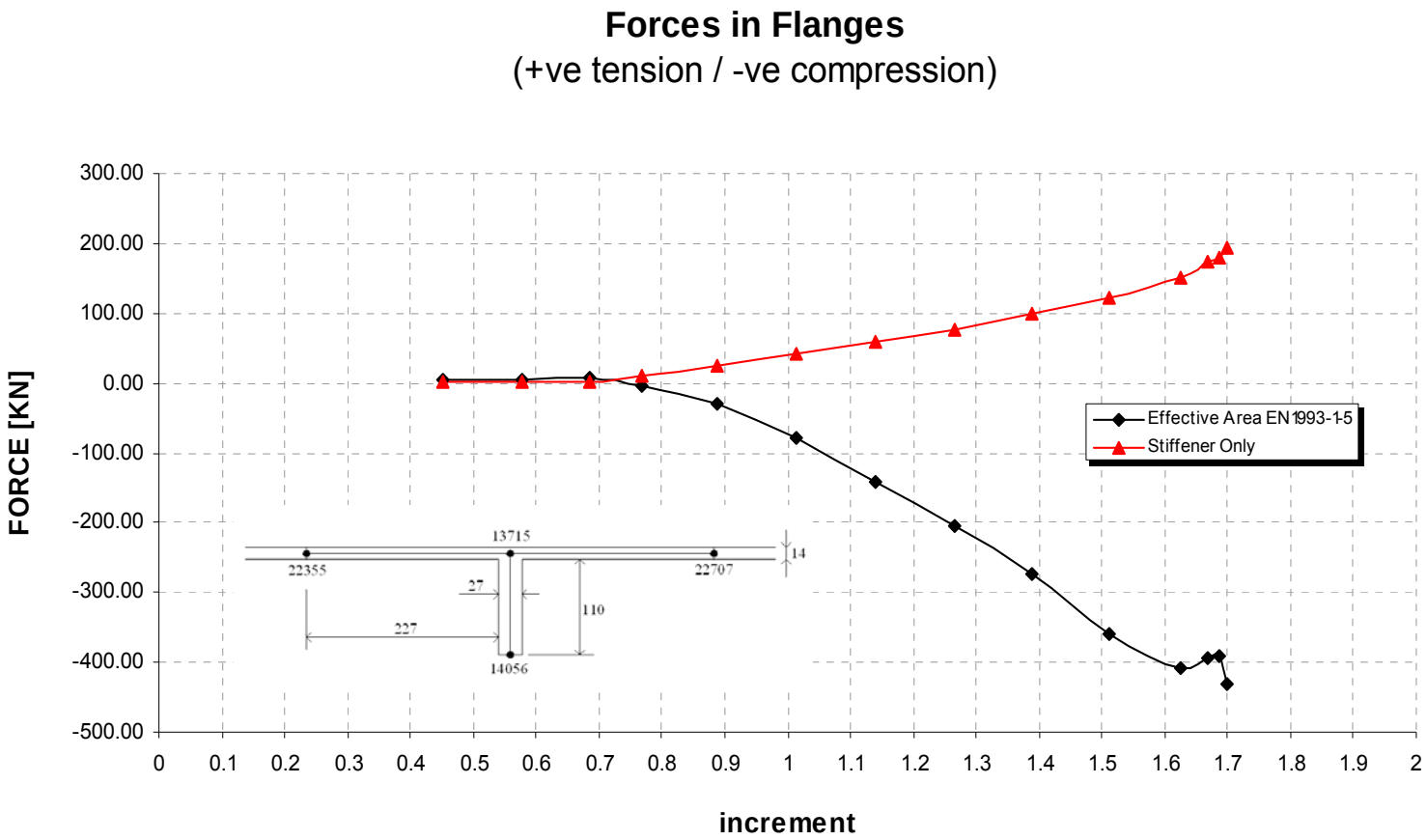

Fig. 4.76 – Section S8 – Vertical forces in stiffener (refer to Figure 4.63)

4.2.2 Case 3

A force F = 5000 KN at midspan, if applied alone would produce the following effects:

M_{max} = F x L / 4 = 5000 x 30 / 4 = 37500 KNm

V = F / 2 = 5000 / 2 = 2500 KN

In order to obtain the required M/V ratio, as shown in figure 4.56, ends moments M_{end} of 9860 KNm have to be applied. The midspan moment is equal to:

$M_{midspan} = M_{max} - M_{end}$ = 37500 – 9860 = 27640 KNm

The non-linear analysis stops when it fails to find an equilibrium beyond a load factor 0.88.

M_{NL} = 0.88 x 27640 = 24323 KNm $\longrightarrow$ $\overline{\eta}_1$ = 0.776

V_{NL} = 0.88 x 2500 = 2200 KN $\longrightarrow$ $\overline{\eta}_3$ = 0.587

The load-deflection curve obtained from the finite element analysis is illustrated in Figure 4.77. The analysis shows an almost linear behaviour up to a load factor of approximately 0.85, after which it shows a gradual loss of stiffness culminating in a failure at the load factor of 0.88.

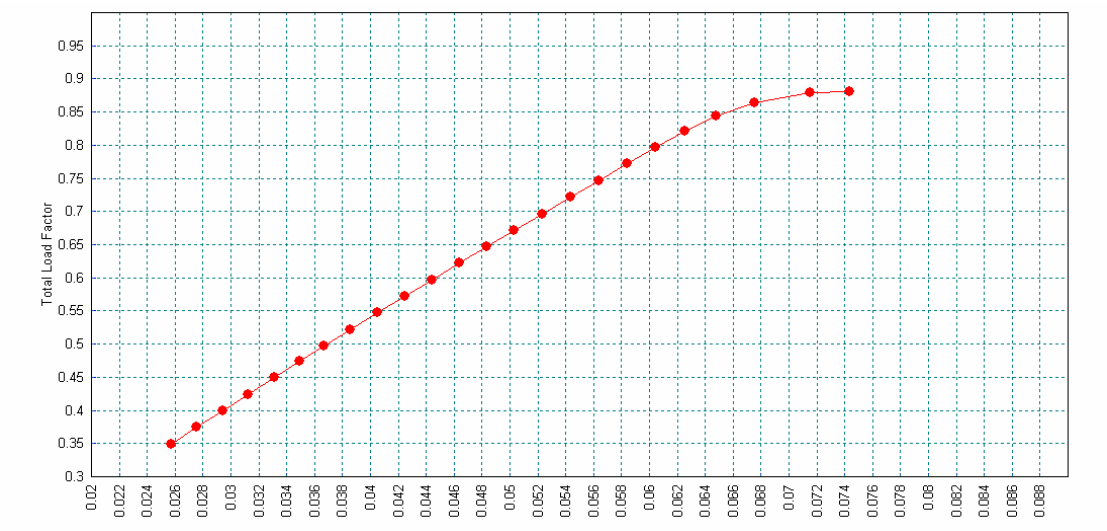

Figure 4.77 – Vertical Displacement vs Total Load Factor

The lateral deflections of the web at this point are illustrated in Figures 4.79 to 4.81. It can be seen that the girder has failed by the web bowing out laterally, while stiffeners remain almost straight.

The M-V interaction domain from EN 1993-1-5 and the results obtained from the non-linear analysis are illustrated in Figure 4.77. The interaction curve has been built according to EN 1993-1-5 clause 7.1(1). Possible benefits considering clause 7.1(2),

regarding performing the interaction at “0.5 h_w“ from support or checking at support using $V_{pl,Rd}$, have not been considered.

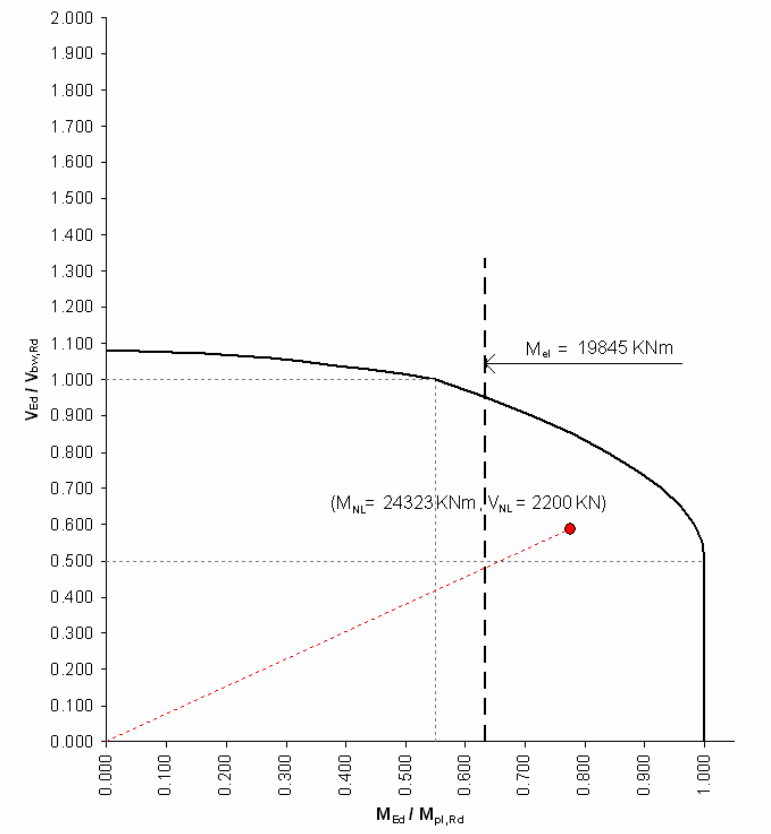

Figure 4.78 – Eurocode M-V interaction domain and result from NL analysis

The sections through the girder at various stages in the analysis to establish the distribution of internal forces are illustrated in Figures 4.82 to 4.95.

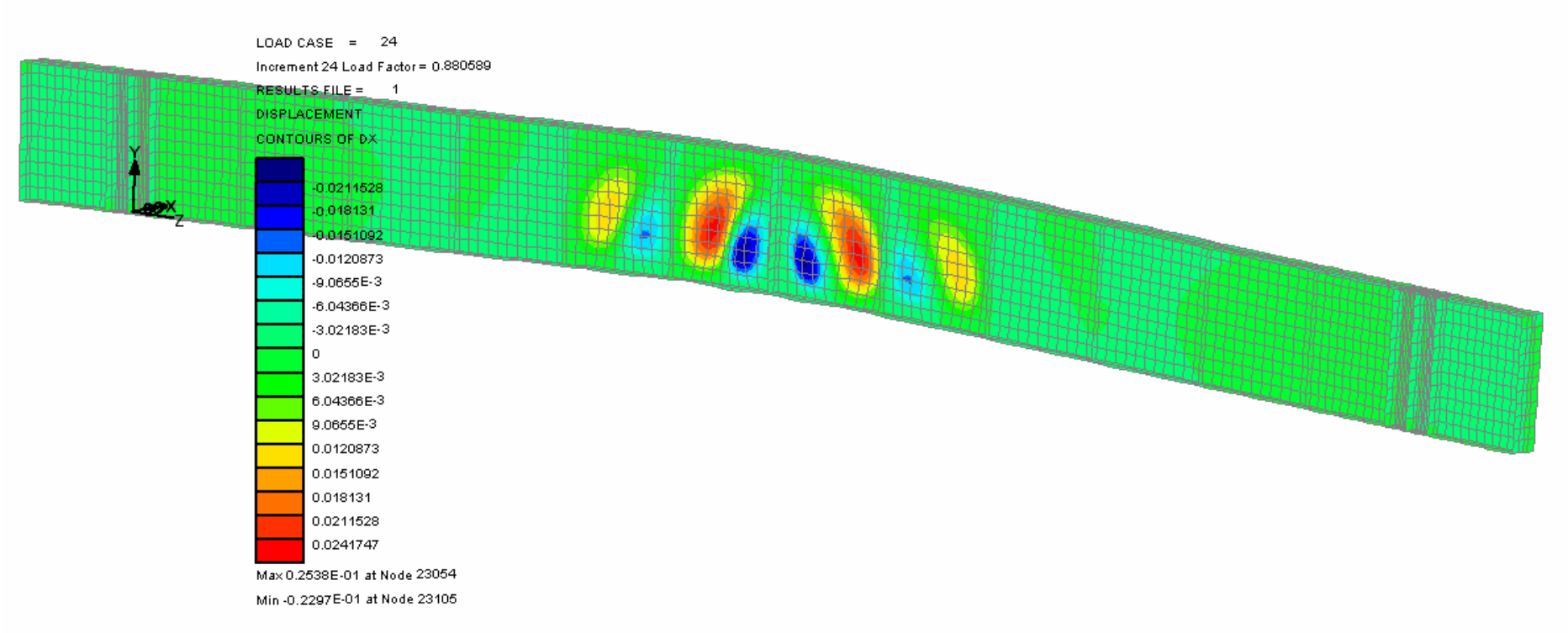

Figure 4.79 – Lateral Displacement Contour (m) at failure

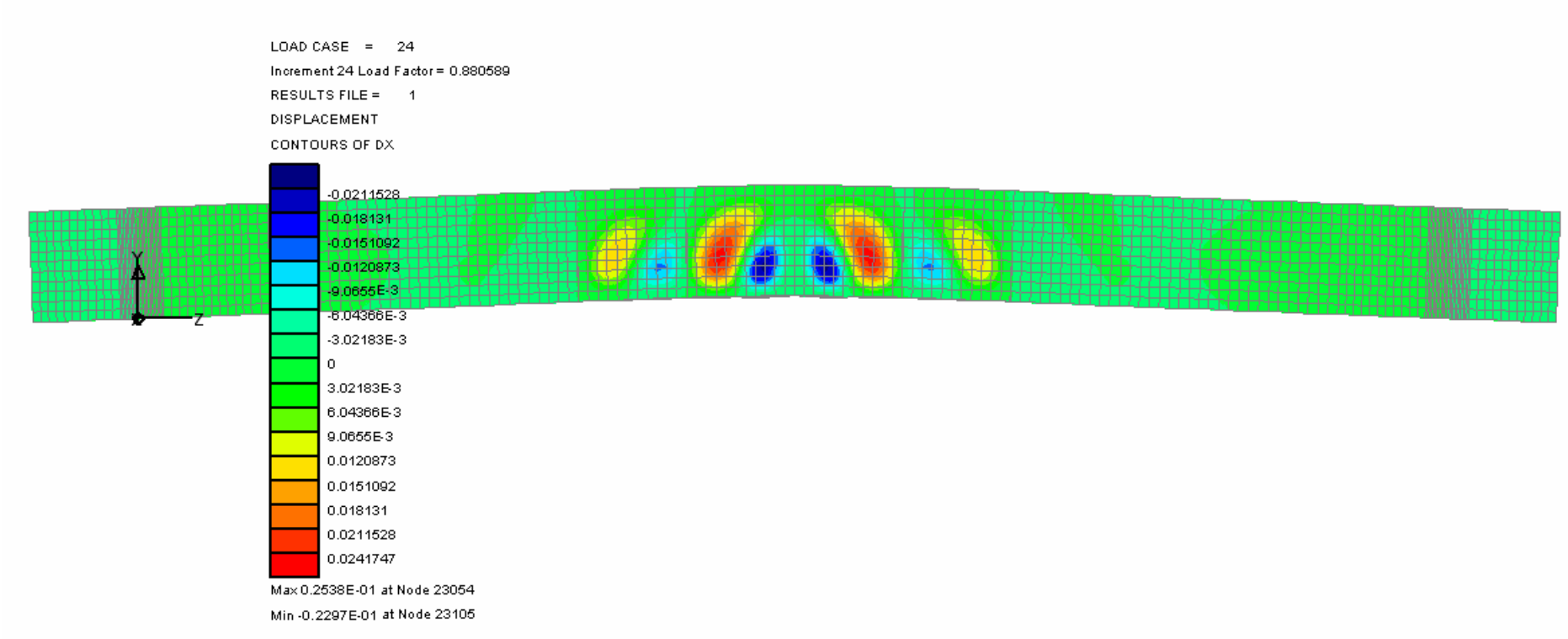

Figure 4.80 – Lateral Displacement Contour (m) at failure

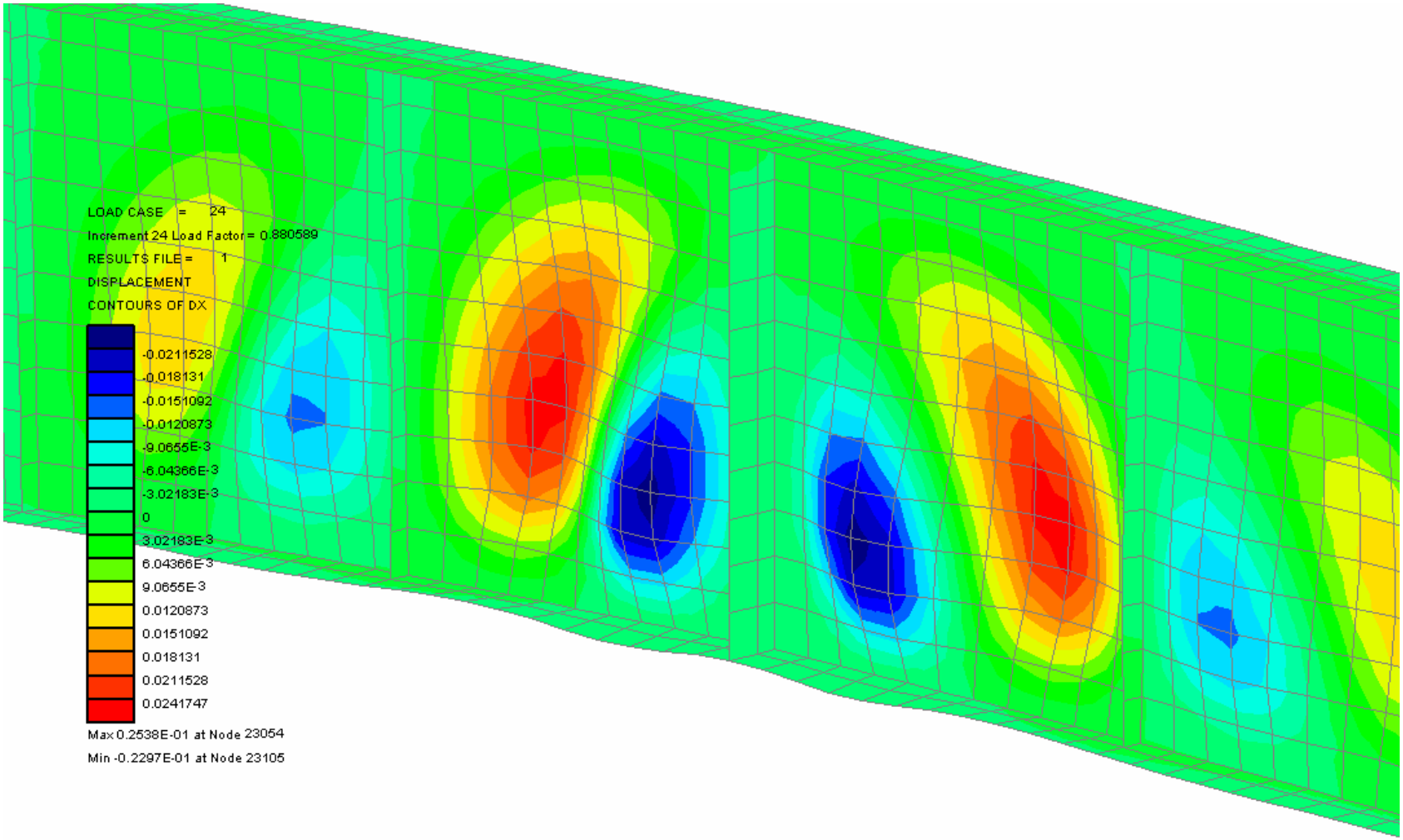

Figure 4.81 – Lateral Displacement Contour (m) at failure

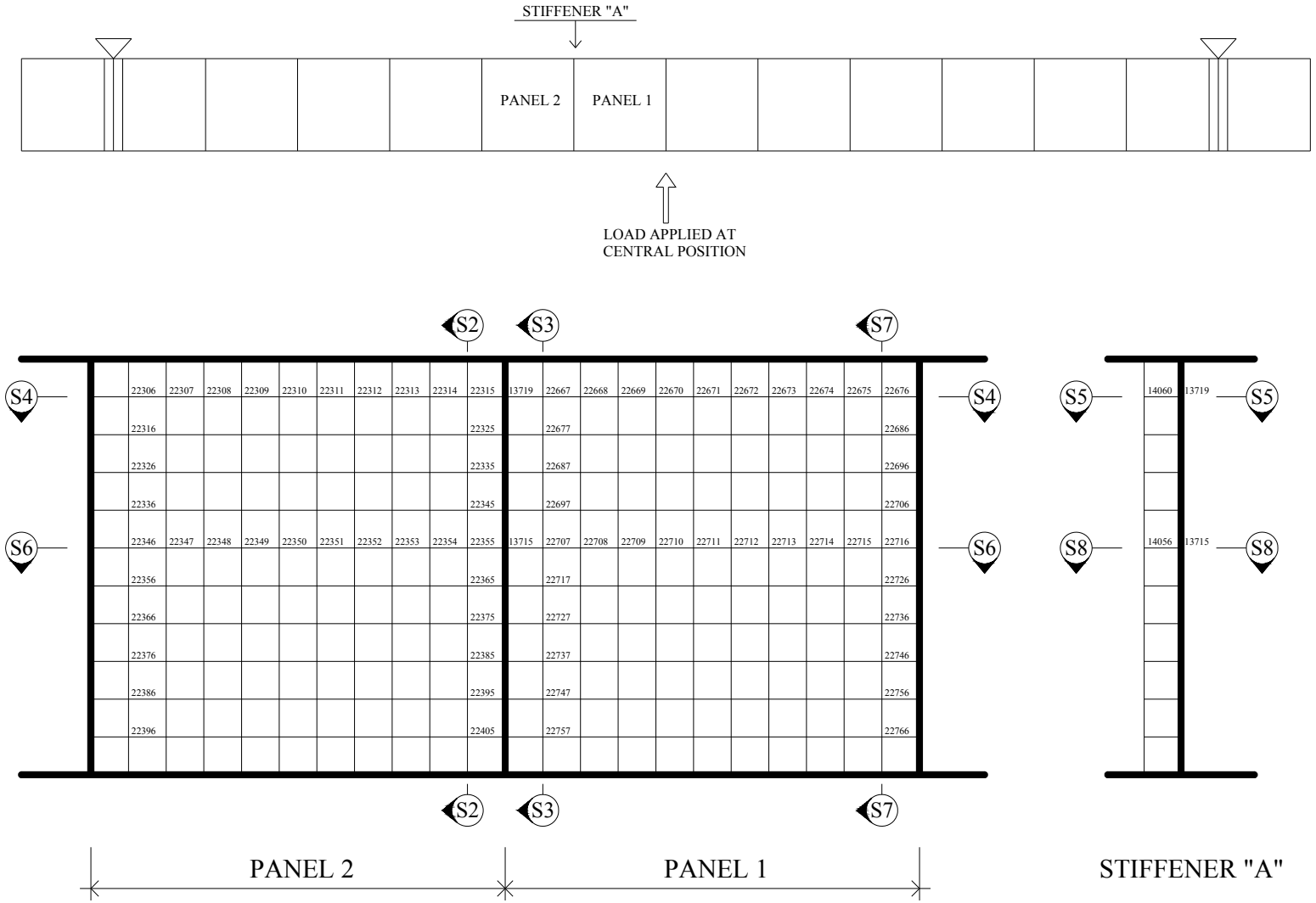

Fig. 4.82 – Investigated area and location of sections

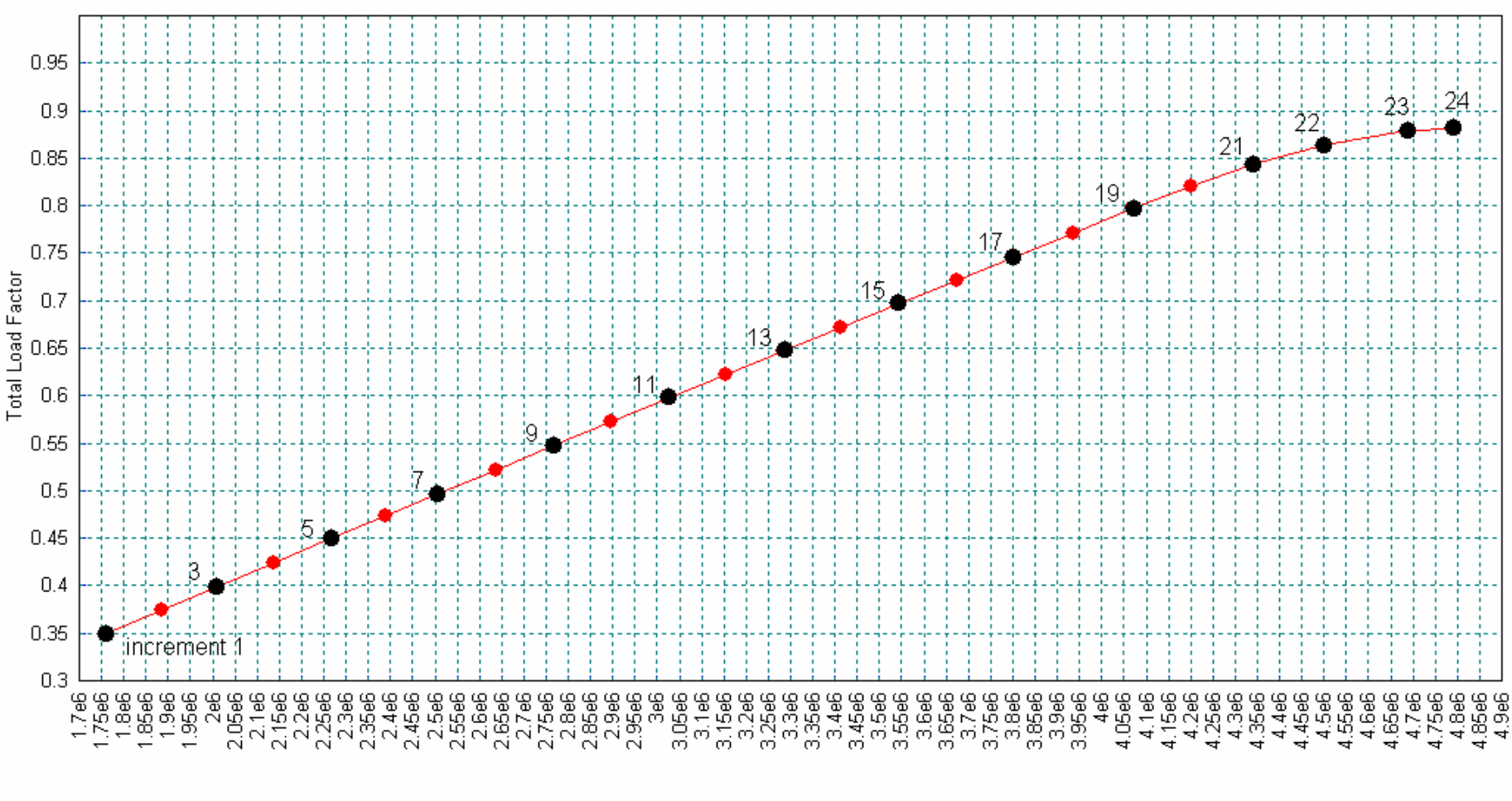

Fig. 4.83 – Section S7 – Force in Rebar [N] (refer to Figure 4.82)

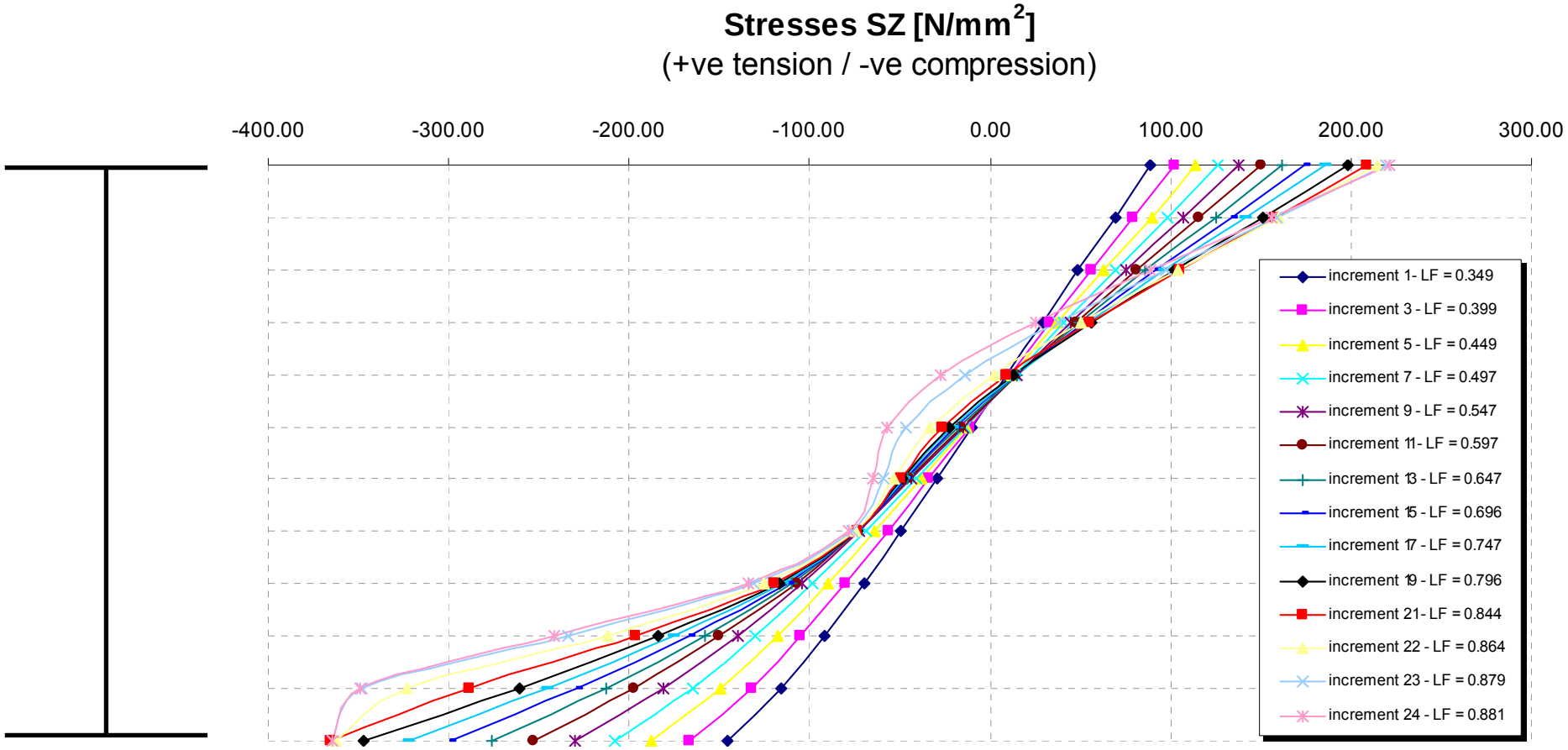

Fig. 4.84 – Section S7 – Longitudinal stresses in web (refer to Figure 4.82)

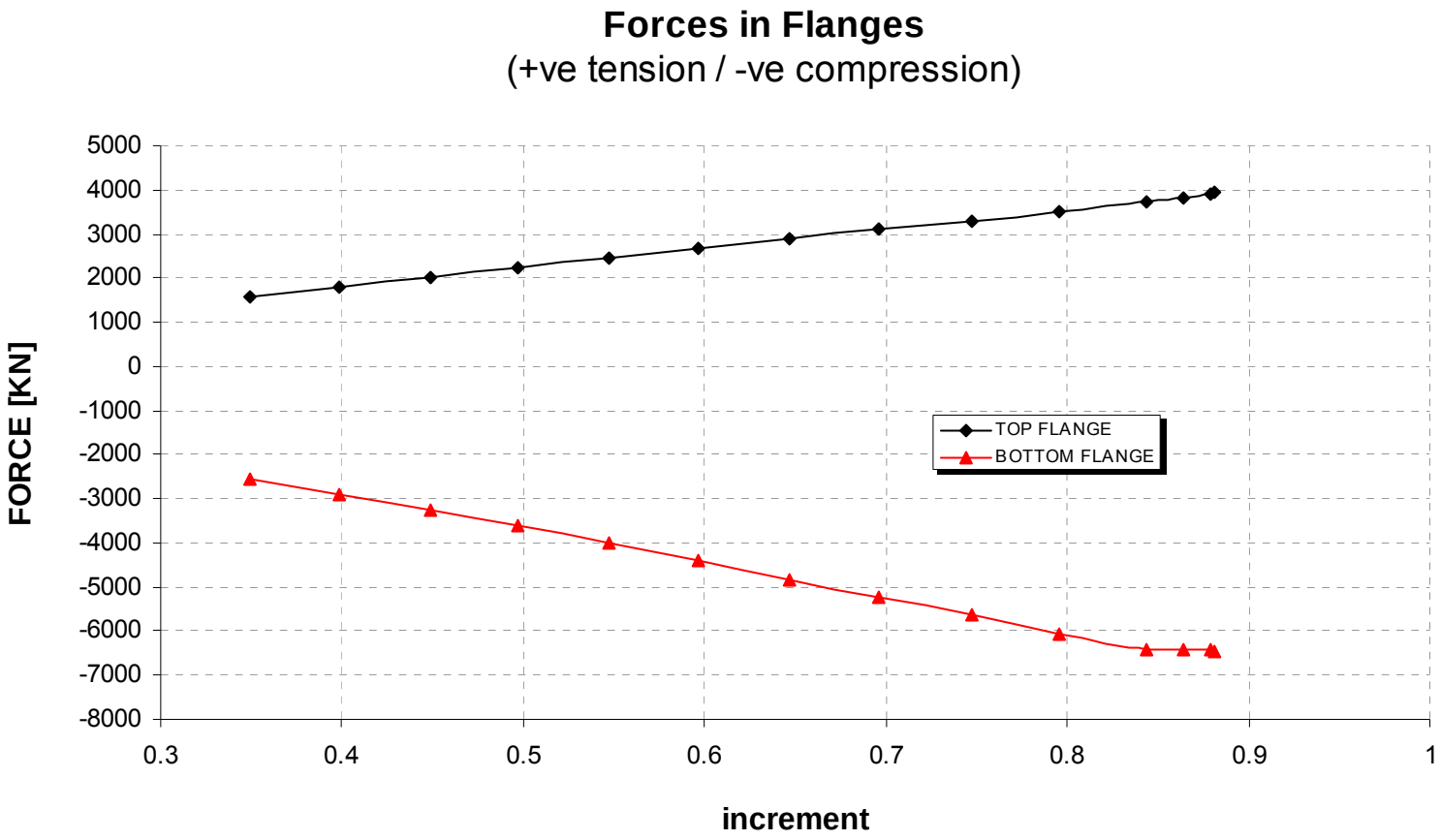

Fig. 4.85 – Section S7 – Longitudinal forces in flanges (refer to Figure 4.82)

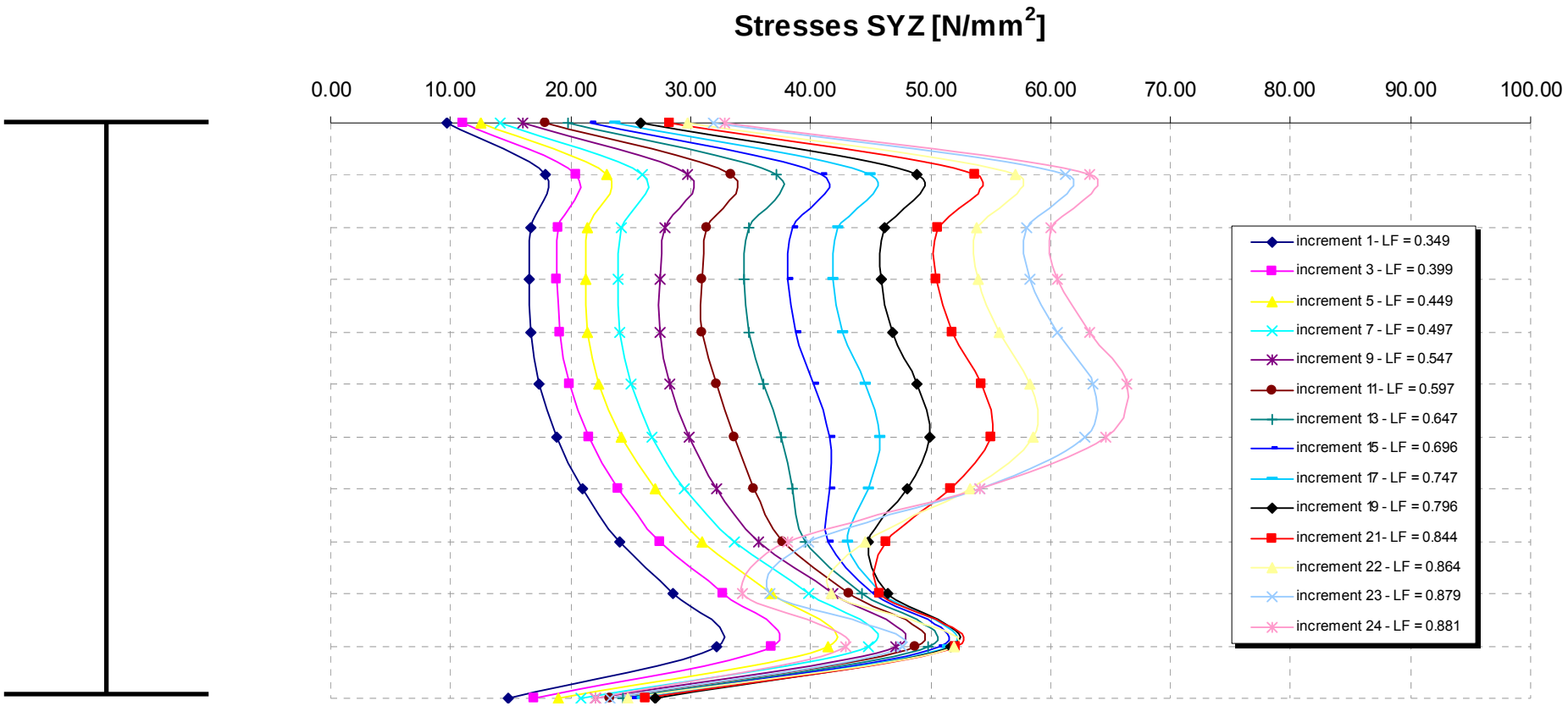

Fig. 4.86 – Section S7 – Shear stresses in web (refer to Figure 4.82)

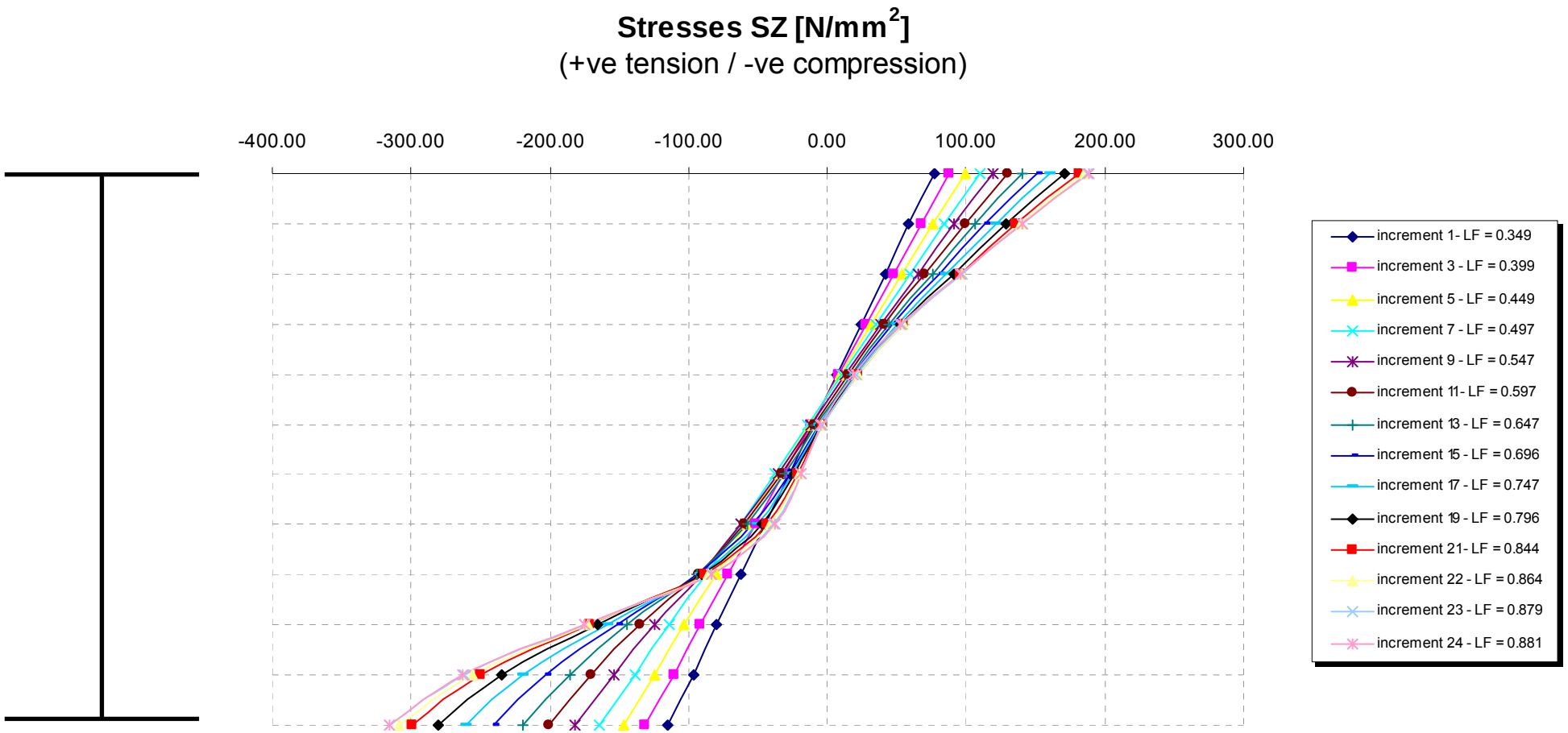

Fig. 4.87 – Section S3 – Longitudinal stresses in web (refer to Figure 4.82)

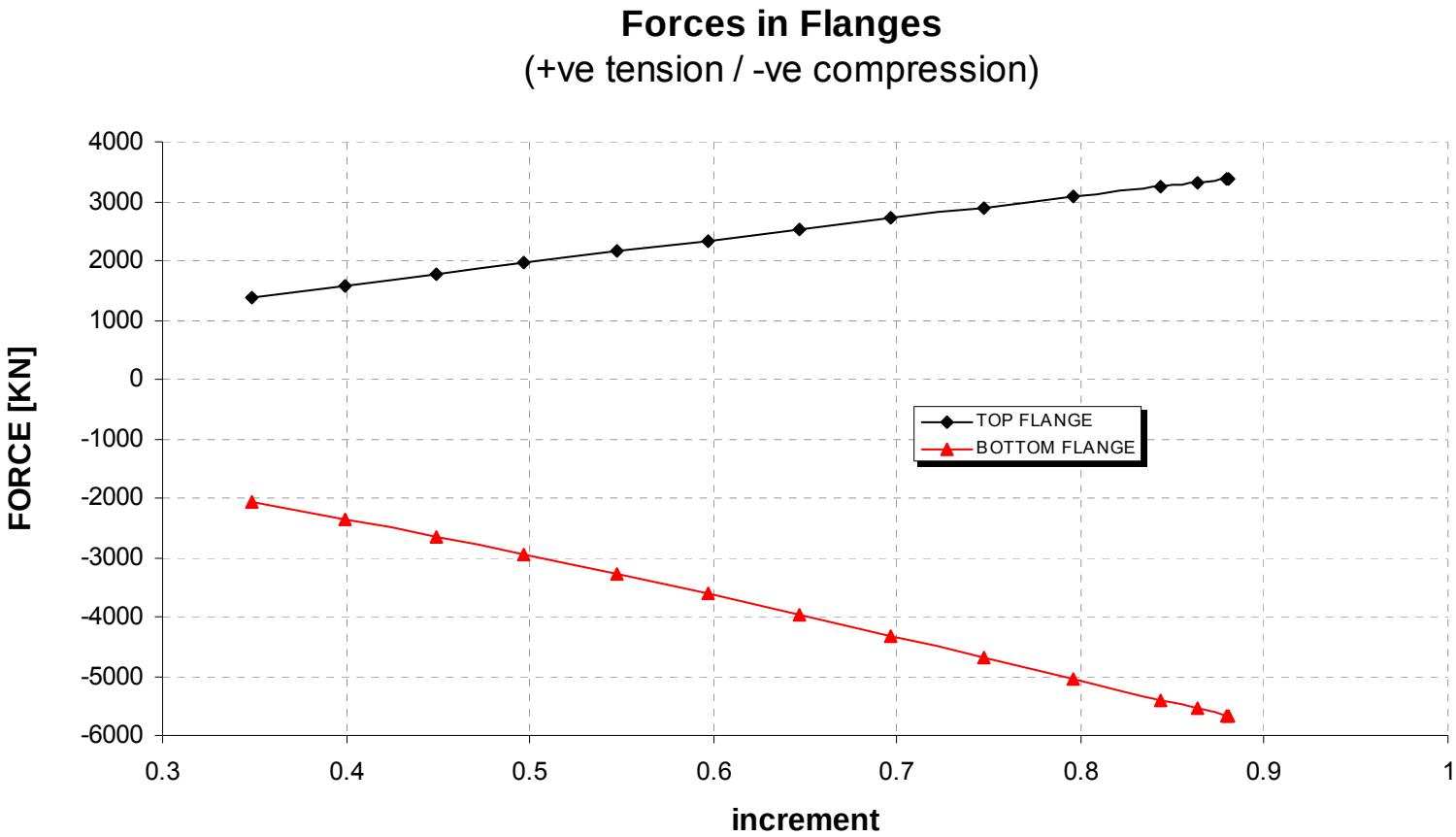

Fig. 4.88 – Section S3 – Longitudinal forces in flanges (refer to Figure 4.82)

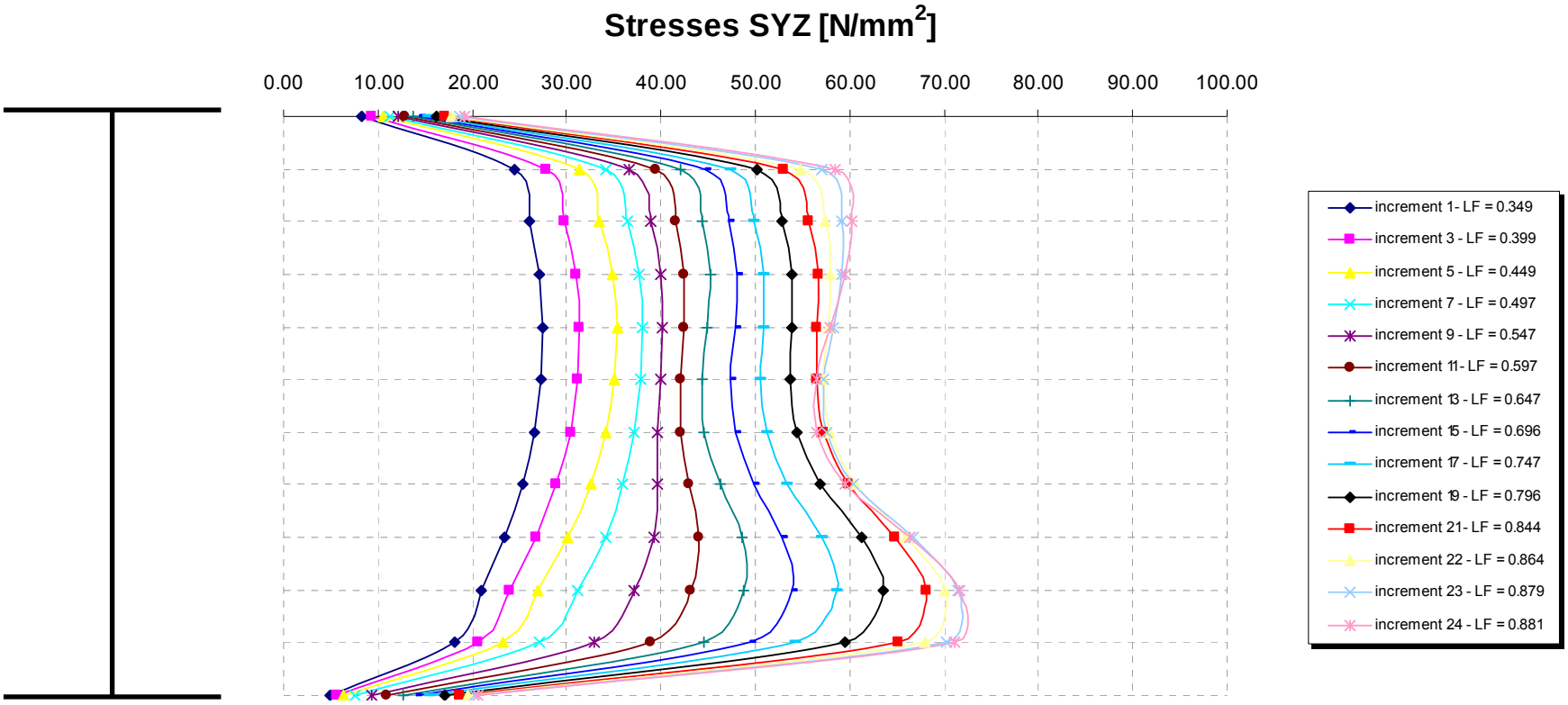

Fig. 4.89 – Section S3 – Shear stresses in web (refer to Figure 4.82)

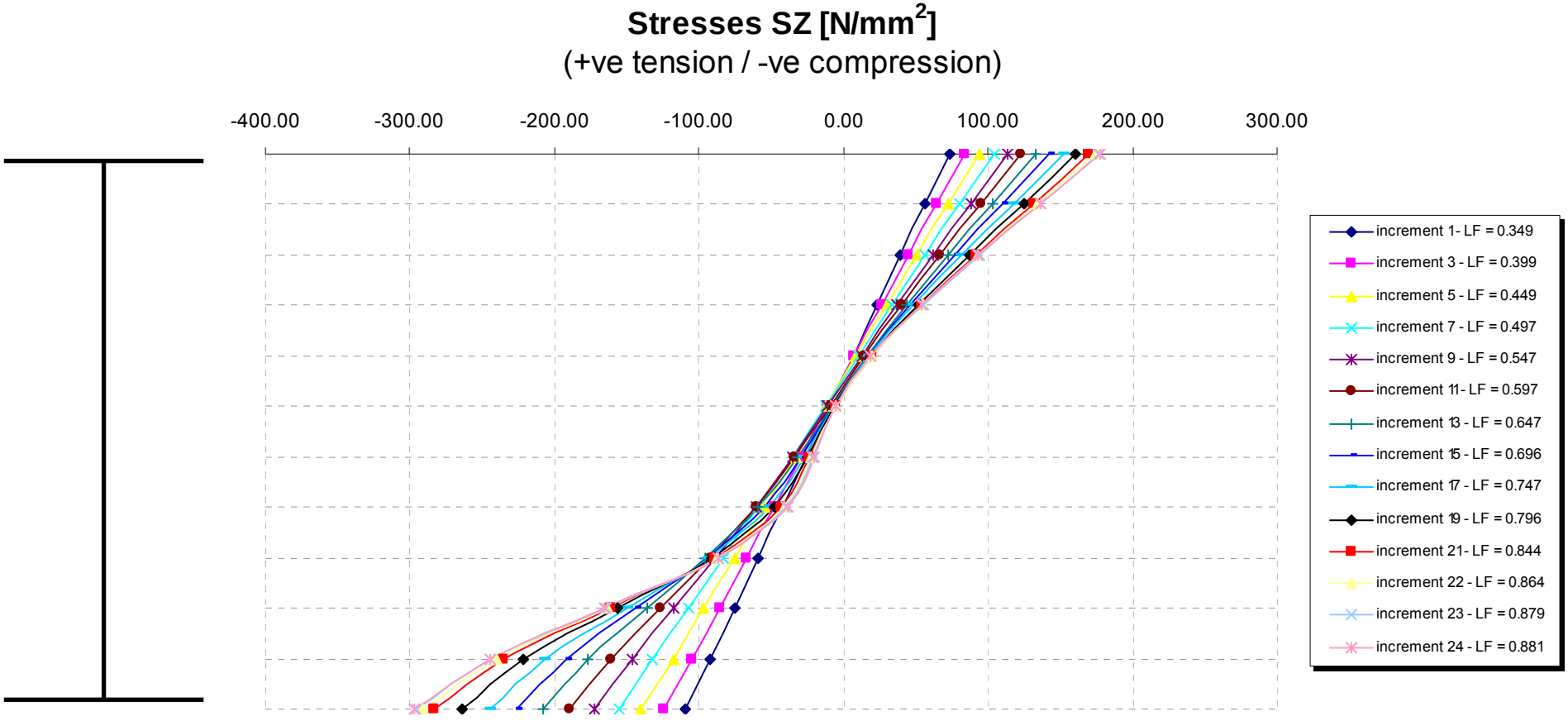

Fig. 4.90 – Section S2 – Longitudinal stresses in web (refer to Figure 4.82)

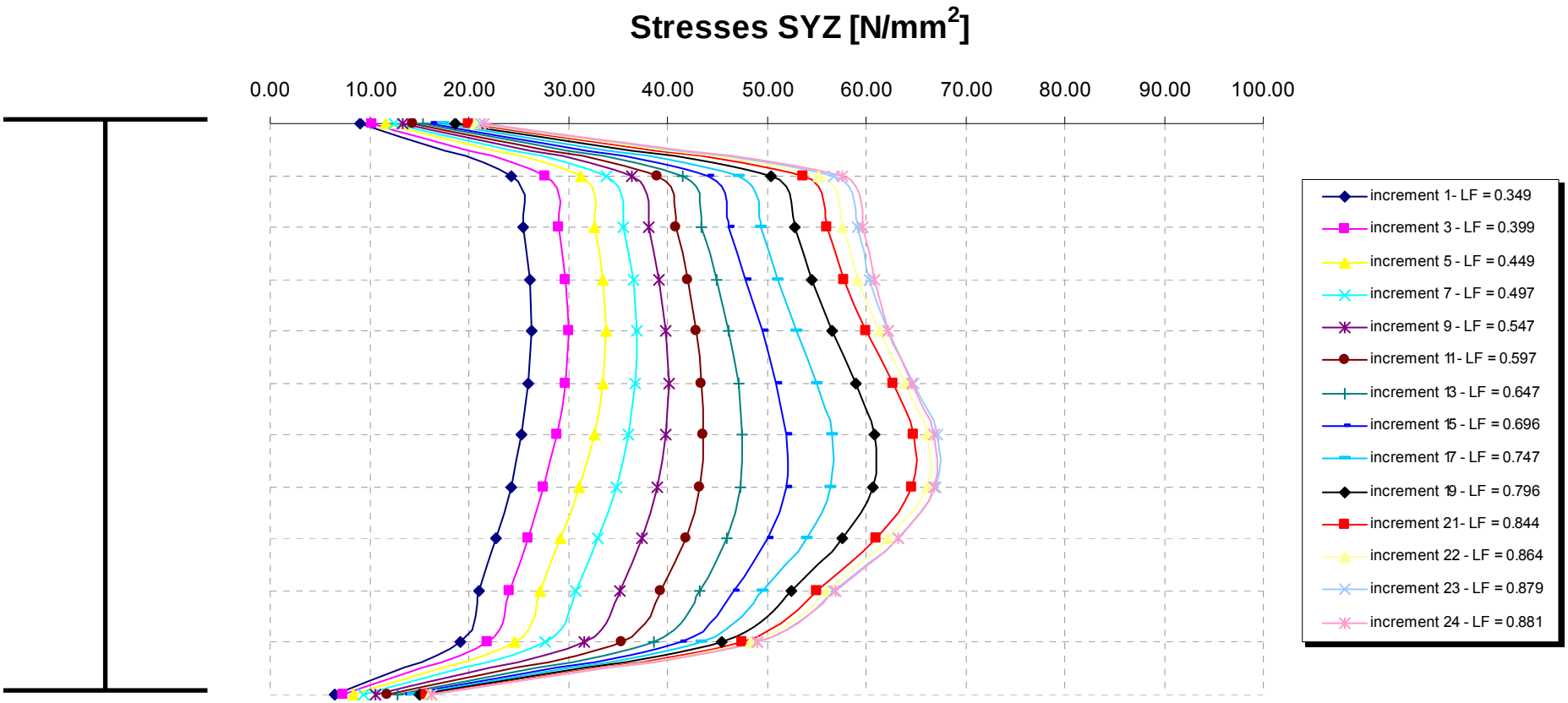

Fig. 4.91 – Section S2 – Shear stresses in web (refer to Figure 4.82)

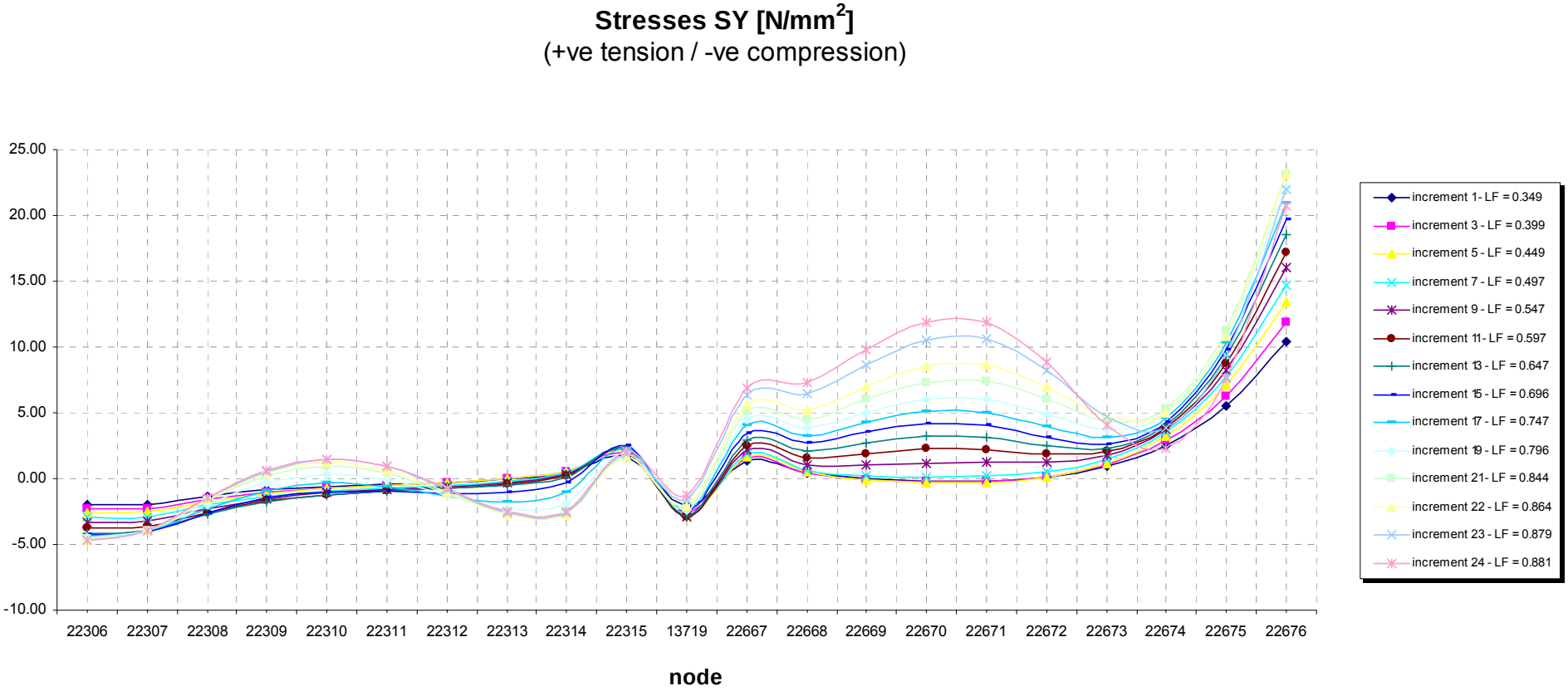

Fig. 4.92 – Section S4 – Vertical stresses in web (refer to Figure 4.82)

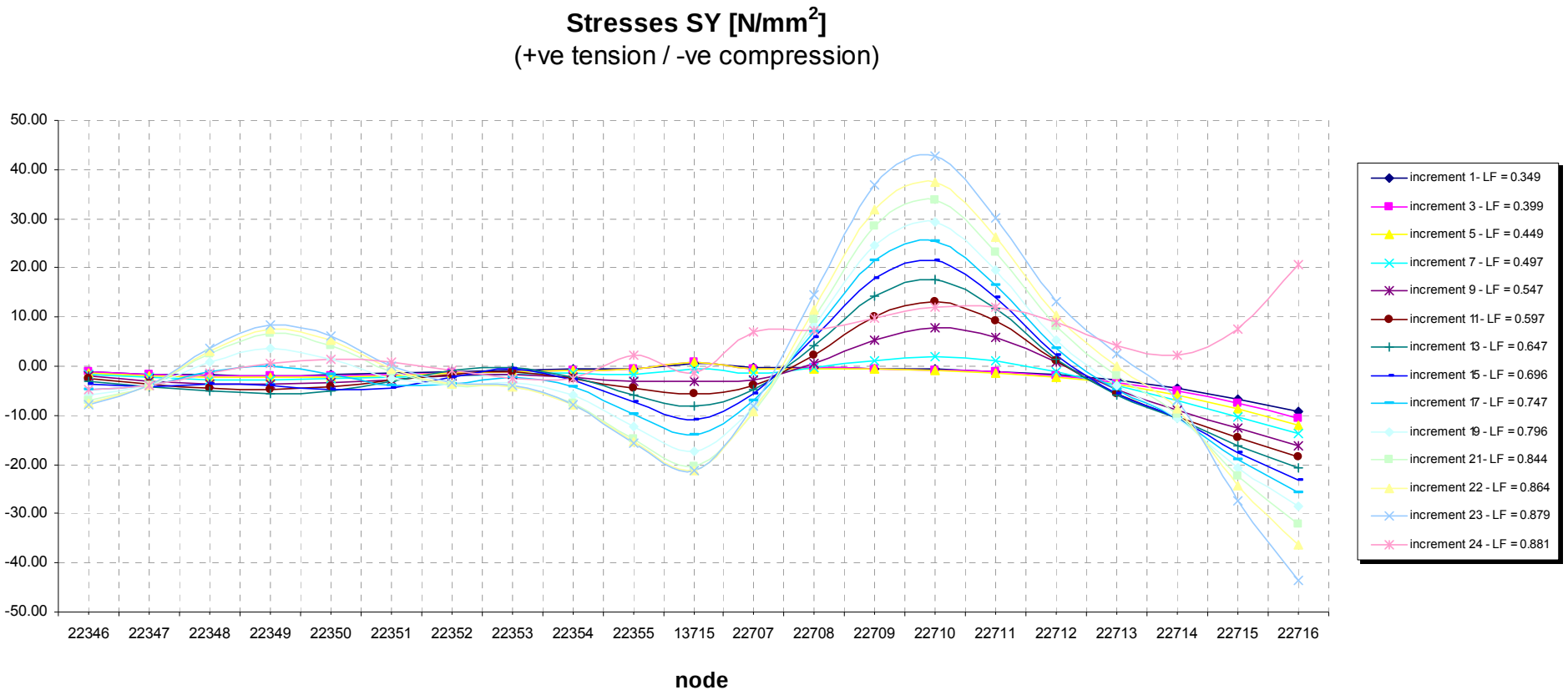

Fig. 4.93 – Section S6 – Vertical stresses in web (refer to Figure 4.82)

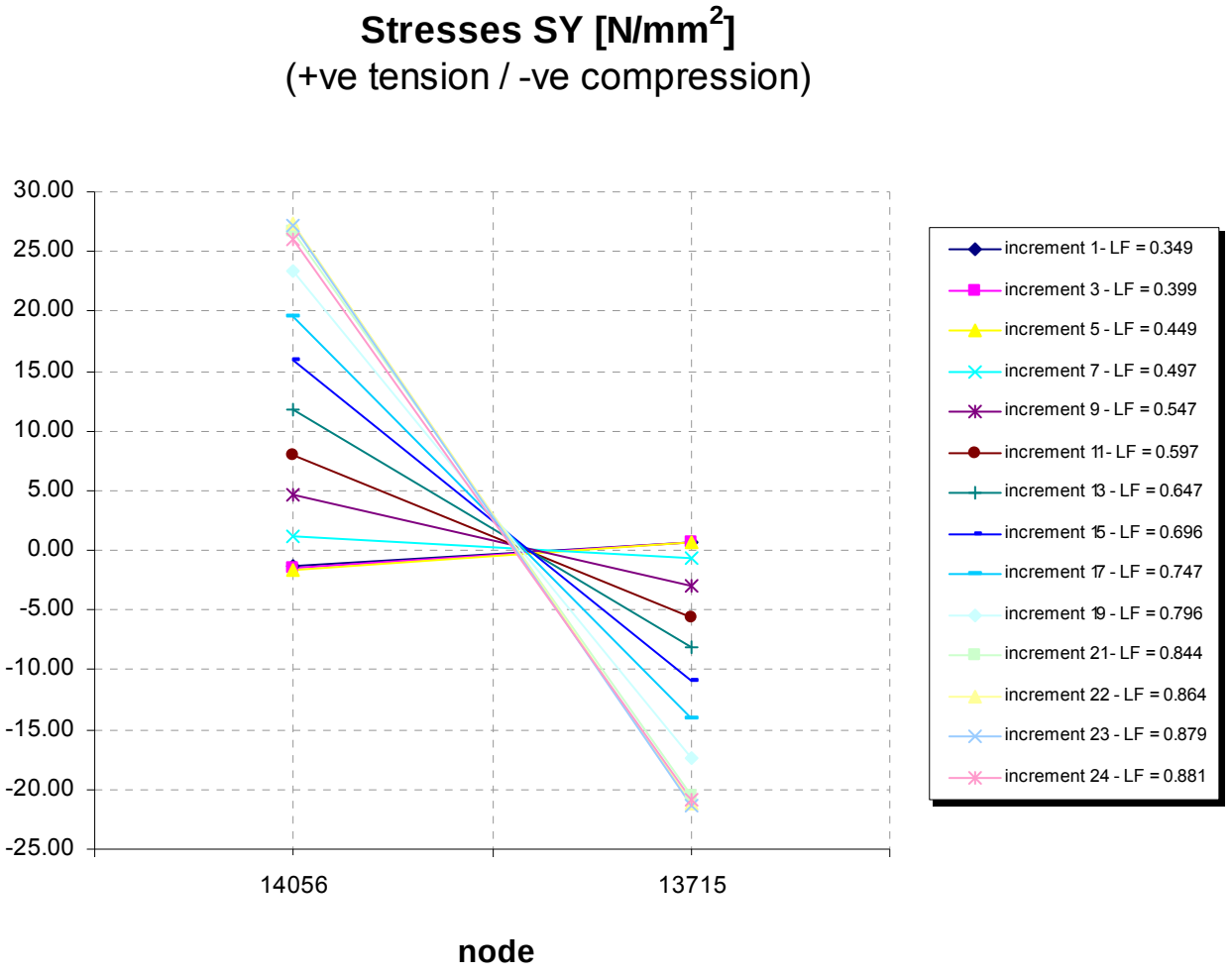

Fig. 4.94 – Section S8 – Vertical stresses in stiffener (refer to Figure 4.82)

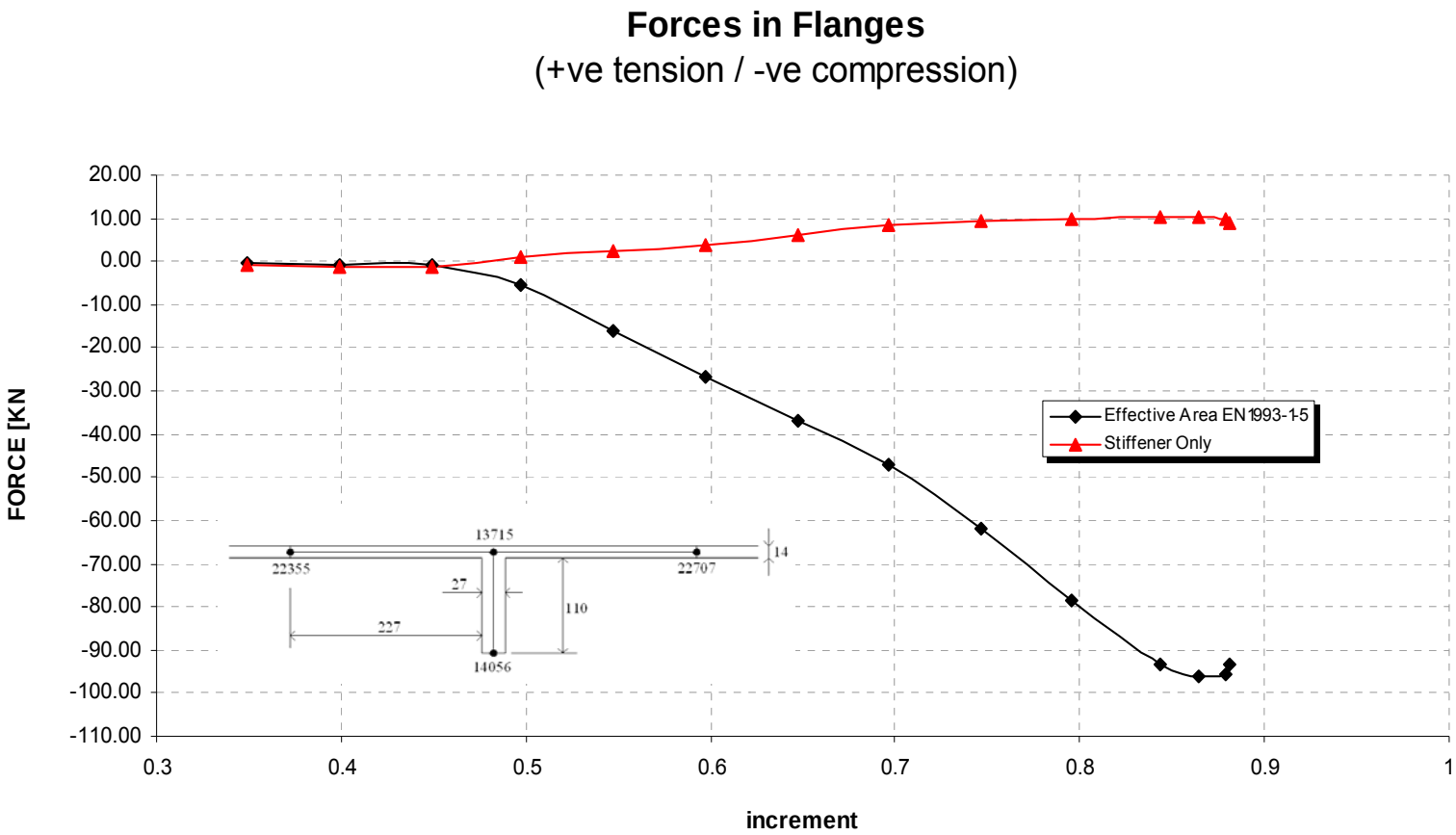

Fig. 4.95 – Section S8 – Vertical forces in stiffener (refer to Figure 4.82)

4.2.3 Case 6

A force F = 7270 KN at midspan, if applied alone would produce the following effects:

M_{max} = F x L / 4 = 7270 x 30 / 4 = 54525 KNm

V = F / 2 = 7270 / 2 = 3635 KN

In order to obtain the required M/V ratio, as shown in figure 4.56, ends moments M_{end} of 48285 KNm have to be applied. The midspan moment is equal to:

$M_{midspan} = M_{max} - M_{end}$ = 54525 – 48285 = 6240 KNm

The non-linear analysis stops when it fails to find an equilibrium beyond a load factor 1.725.

M_{NL} = 1.725 x 6240 = 10764 KNm $\longrightarrow$ $\overline{\eta}_1$ = 0.344

V_{NL} = 1.725 x 3635 = 6270 KN $\longrightarrow$ $\overline{\eta}_3$ = 1.672

The load-deflection curve obtained from the finite element analysis is illustrated in Figure 4.96. The graph shows that up to the increment 55 a downward vertical deflection is developed, due to the big ends moment applied.

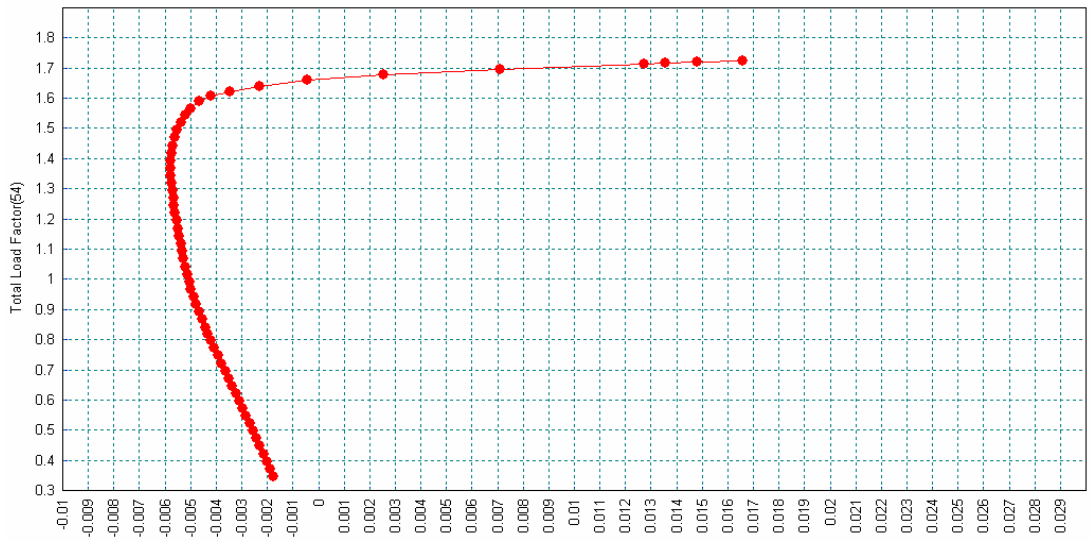

Figure 4.96 – Vertical Displacement vs Total Load Factor

The lateral deflections of the web at this point are illustrated in Figures 4.98 to 4.100. It can be seen that the girder has failed by the web bowing out laterally, while stiffeners remain almost straight. However the failure happens in the second panel away from midspan, which is probably due to the high bending moment in that panel.

The M-V interaction domain from EN 1993-1-5 and the results obtained from the non-linear analysis are illustrated in Figure 4.97. The interaction curve has been built according to EN 1993-1-5 clause 7.1(1). Possible benefits considering clause 7.1(2), regarding performing the interaction at "0.5 h_w" from support or checking at support using $V_{pl,Rd}$, have not been considered.

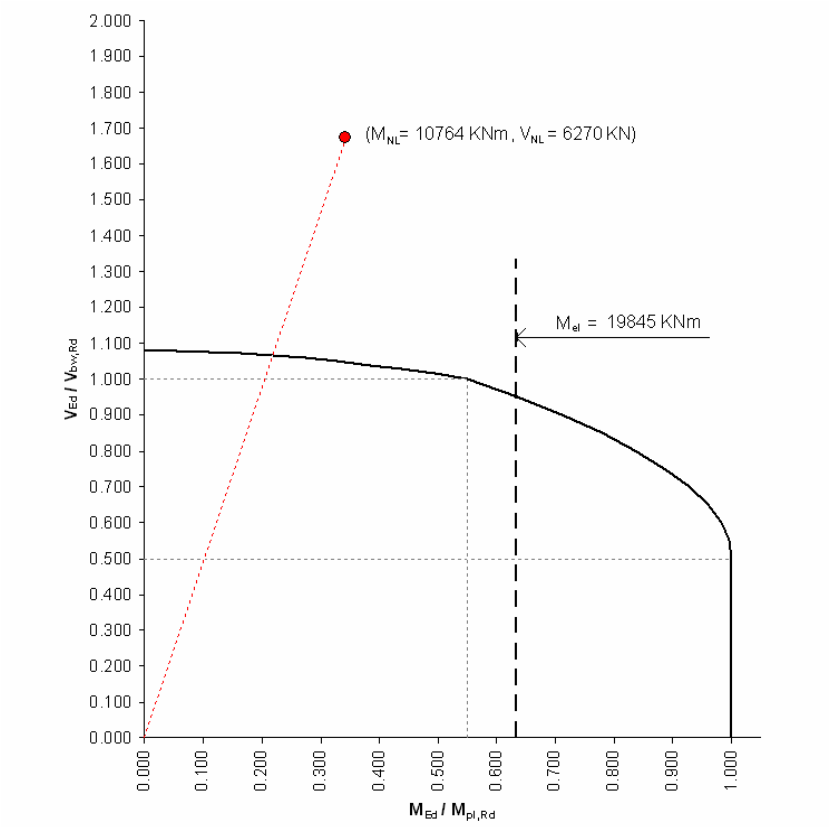

Figure 4.97 – Eurocode M-V interaction domain and result from NL analysis

The sections through the girder at various stages in the analysis to establish the distribution of internal forces are illustrated in Figures 4.101 to 4.114.

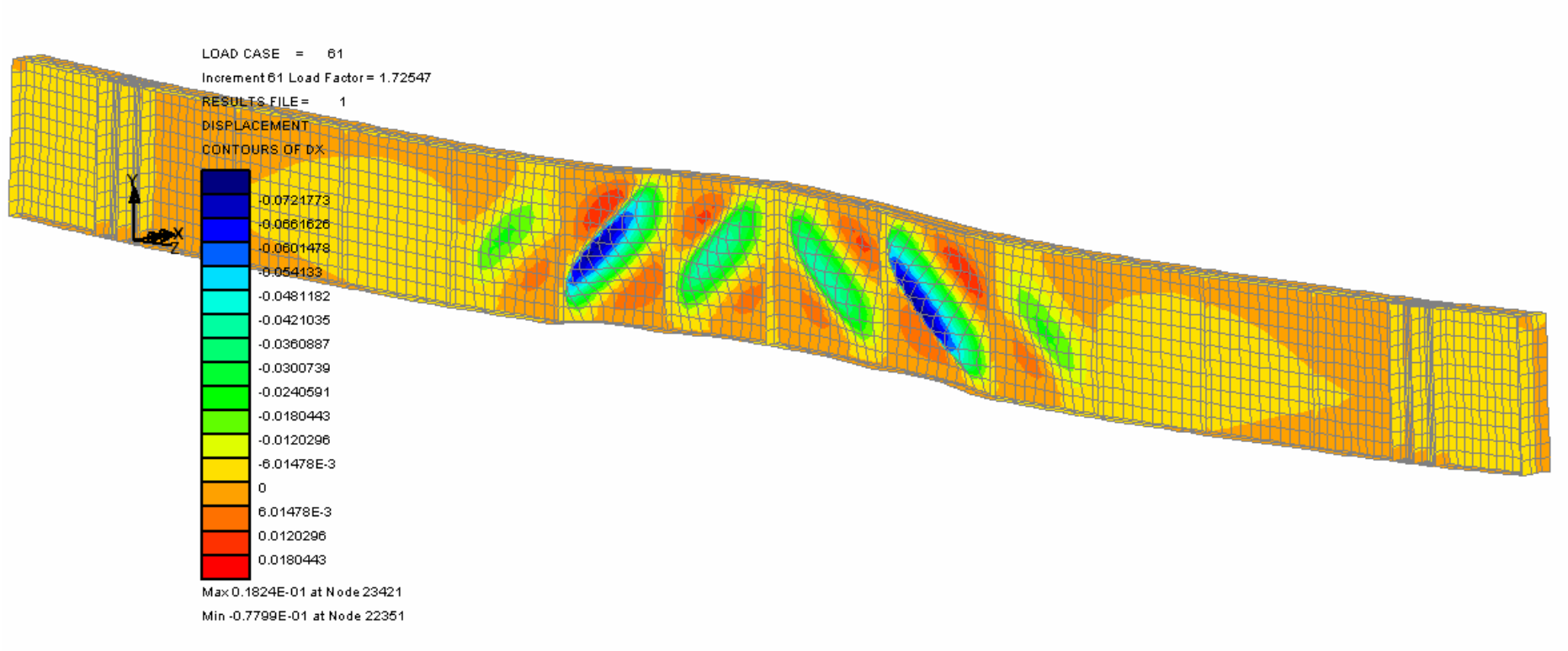

Figure 4.98 – Lateral Displacement Contour (m) at failure

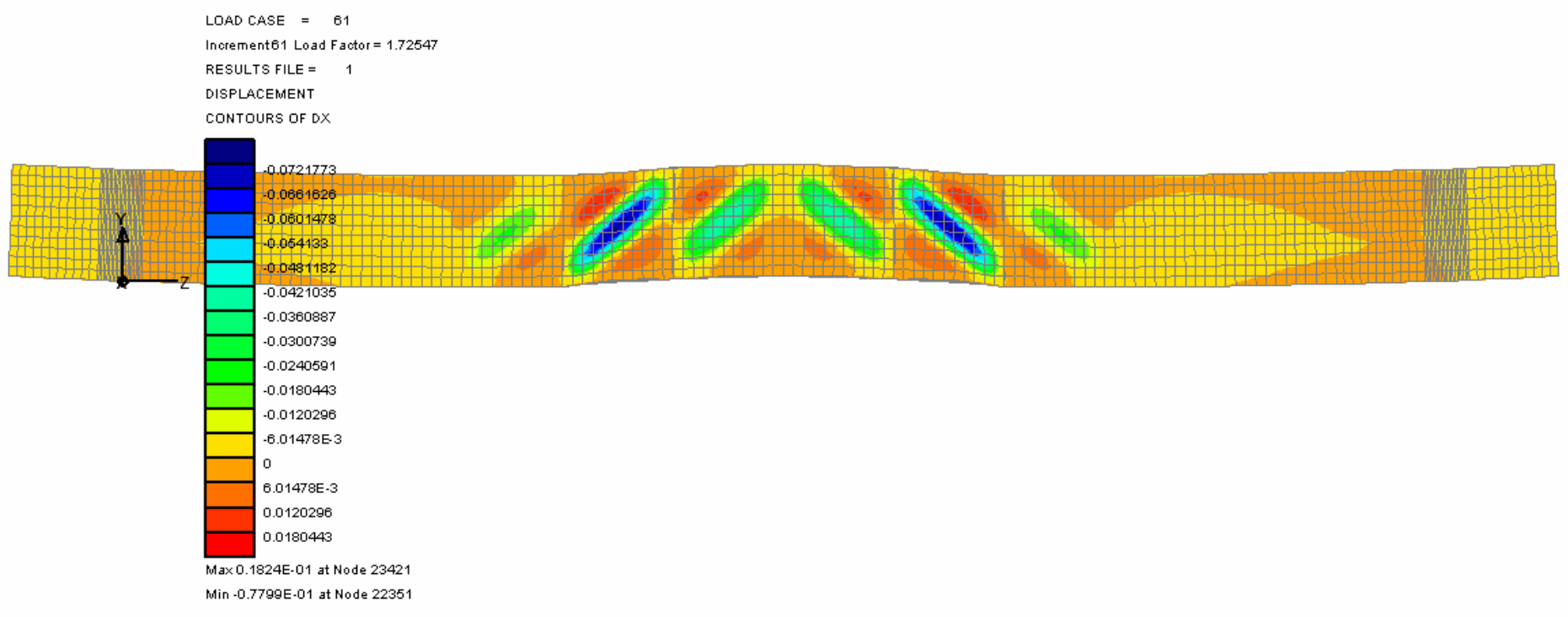

Figure 4.99 – Lateral Displacement Contour (m) at failure

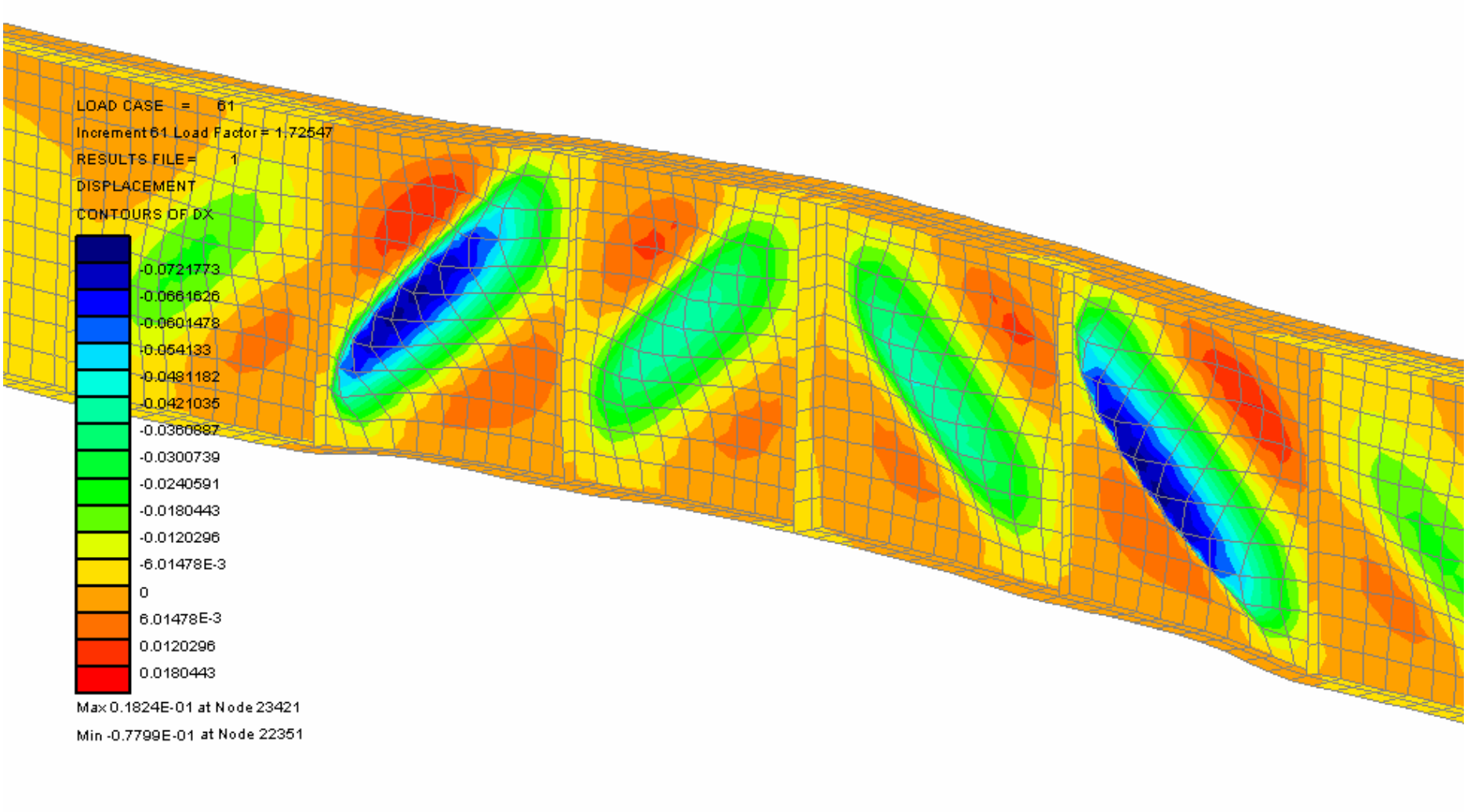

Figure 4.100 – Lateral Displacement Contour (m) at failure

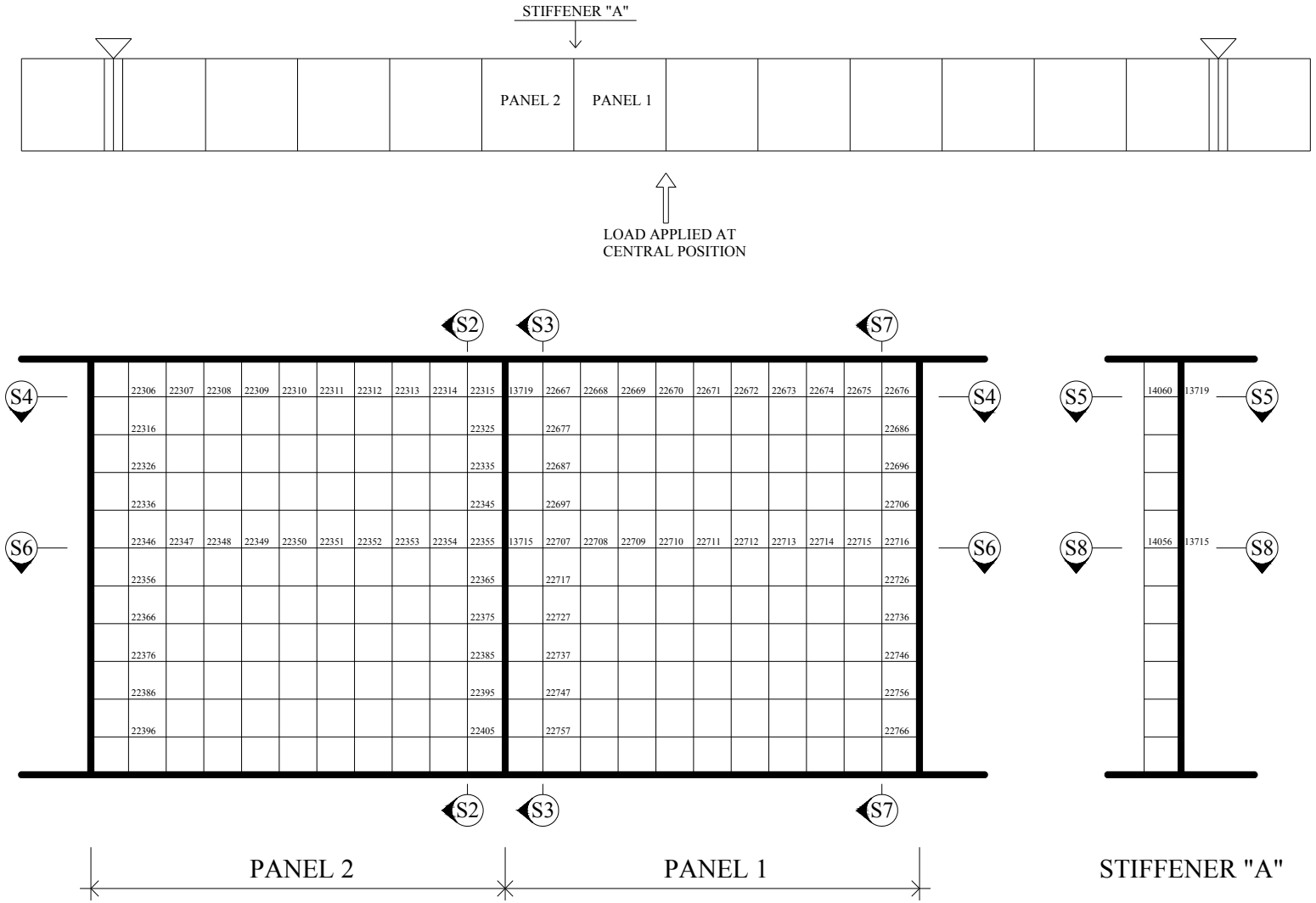

Fig. 4.101 – Investigated area and location of sections

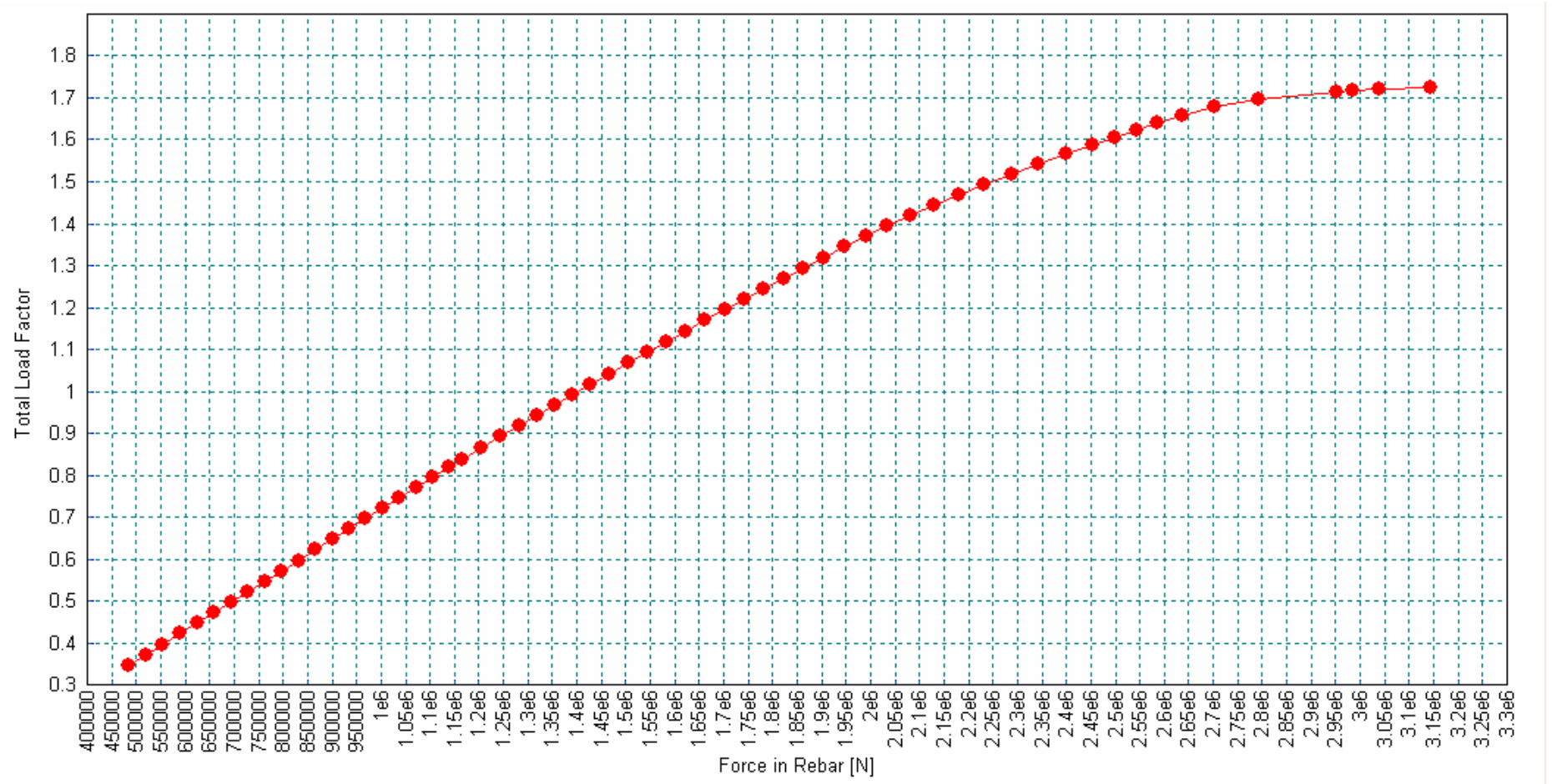

Fig. 4.102 – Section S7 – Force in Rebar [N] (refer to Figure 4.101)

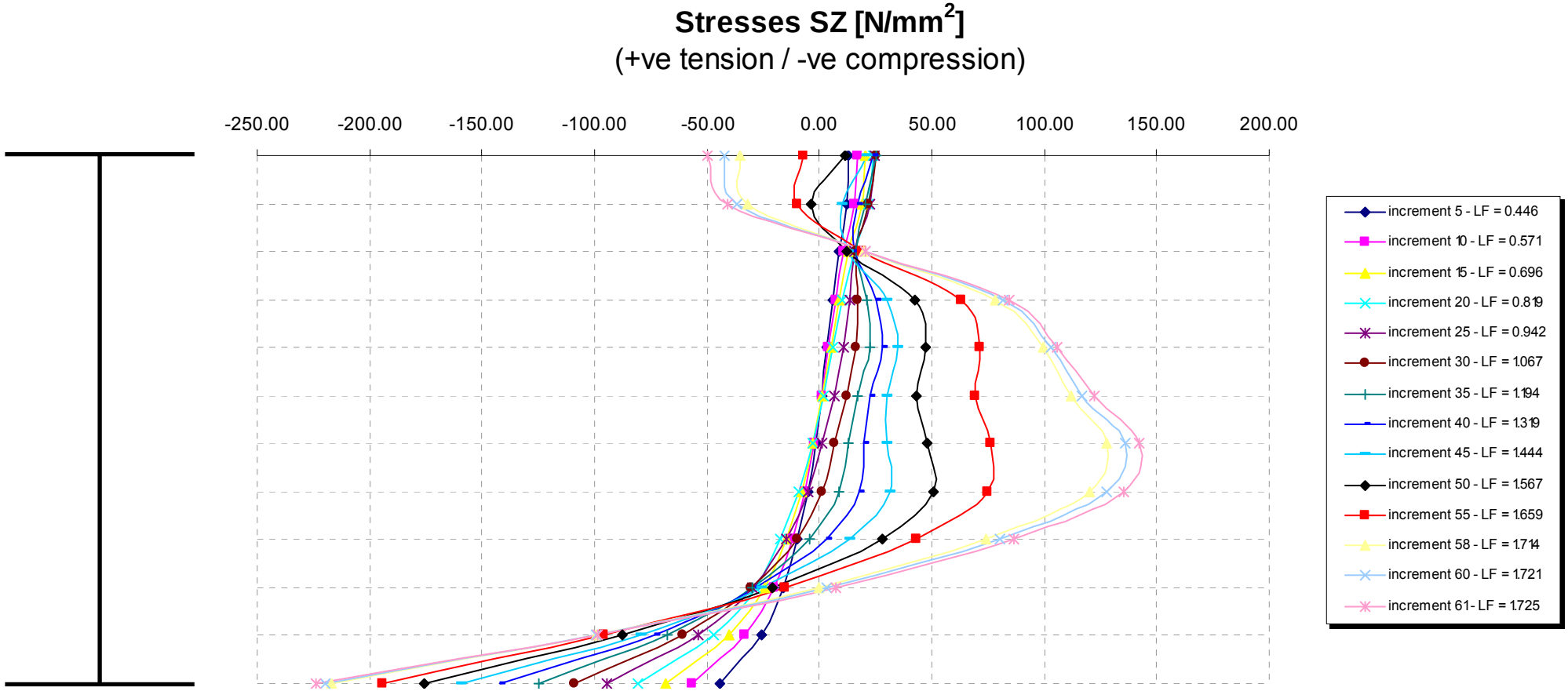

Fig. 4.103 – Section S7 – Longitudinal stresses in web (refer to Figure 4.101)

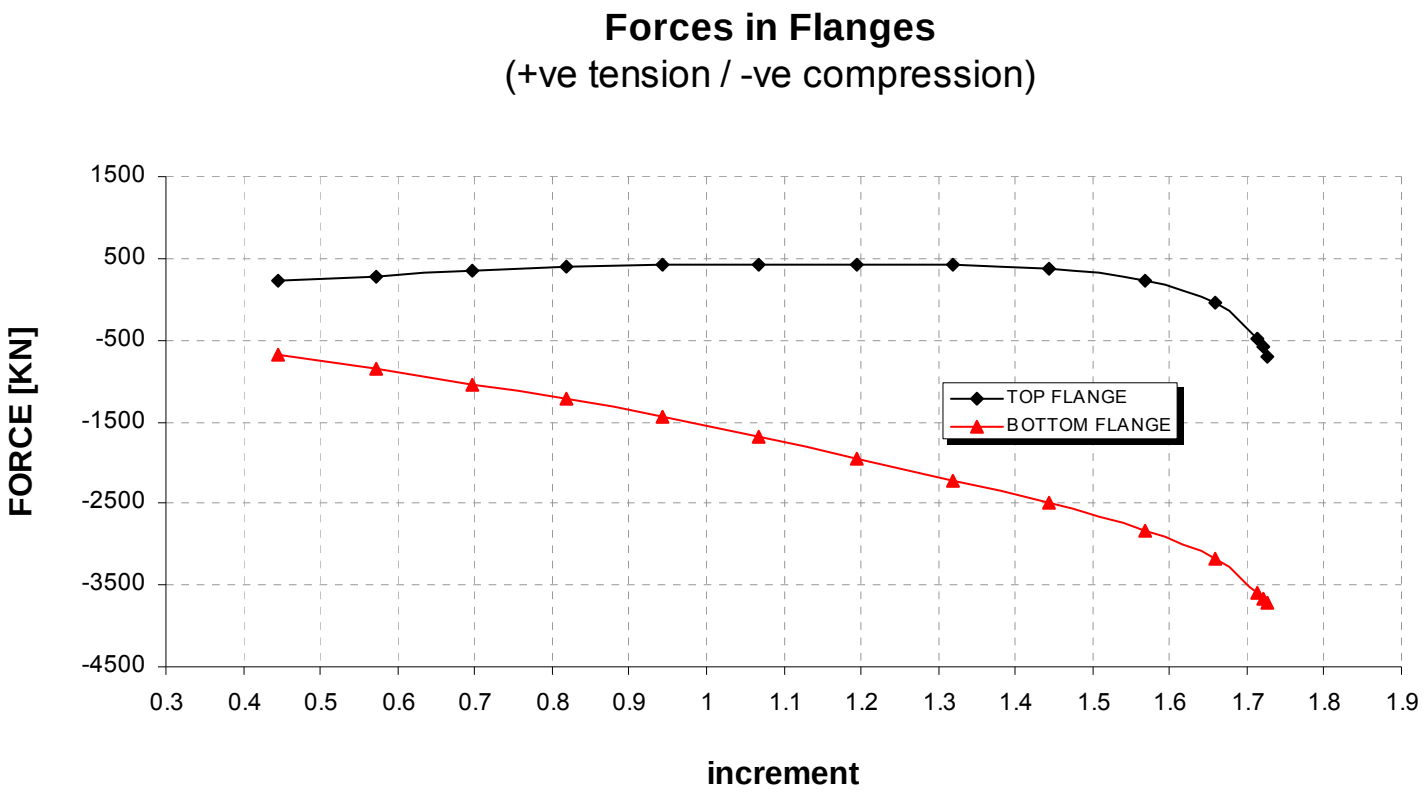

Fig. 4.104 – Section S7 – Longitudinal forces in flanges (refer to Figure 4.101)

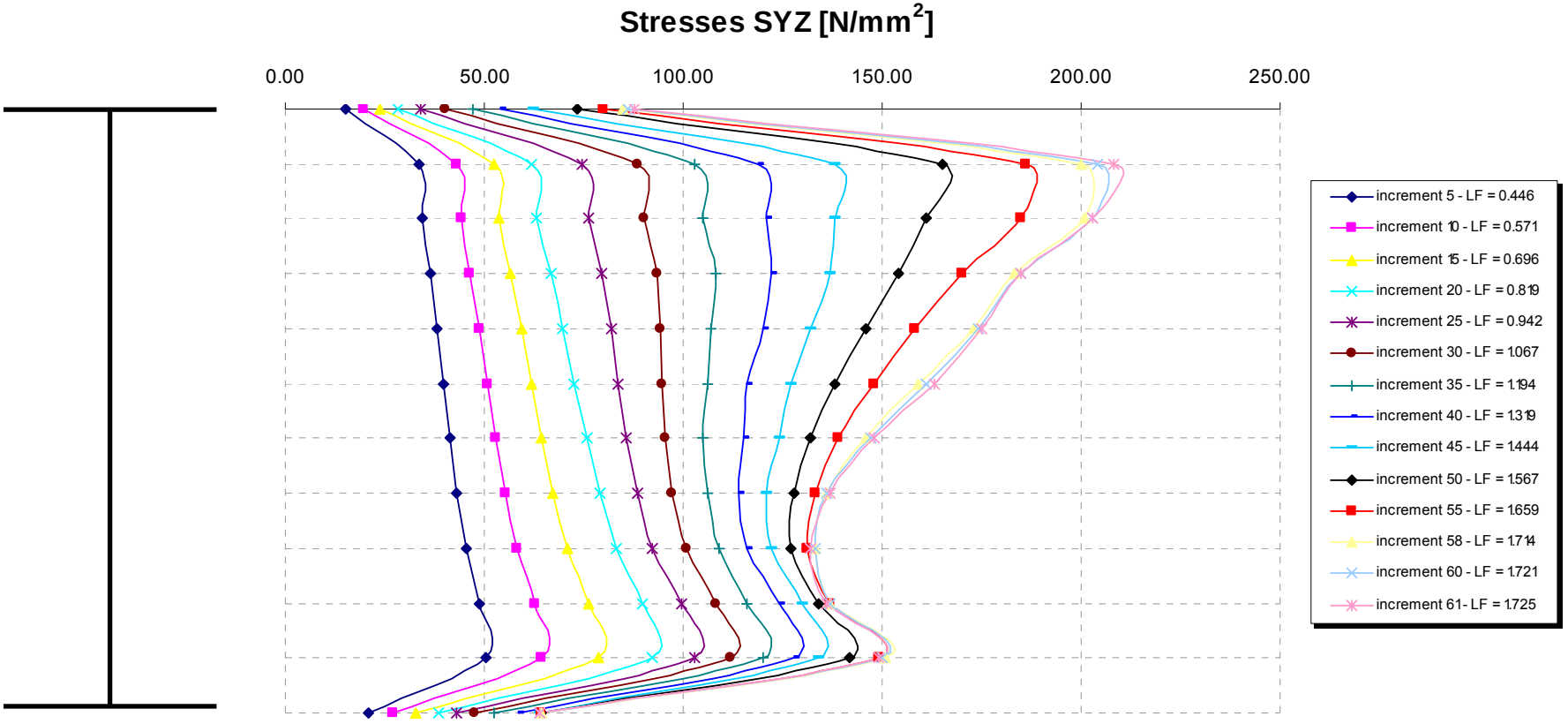

Fig. 4.105 – Section S7 – Shear stresses in web (refer to Figure 4.101)

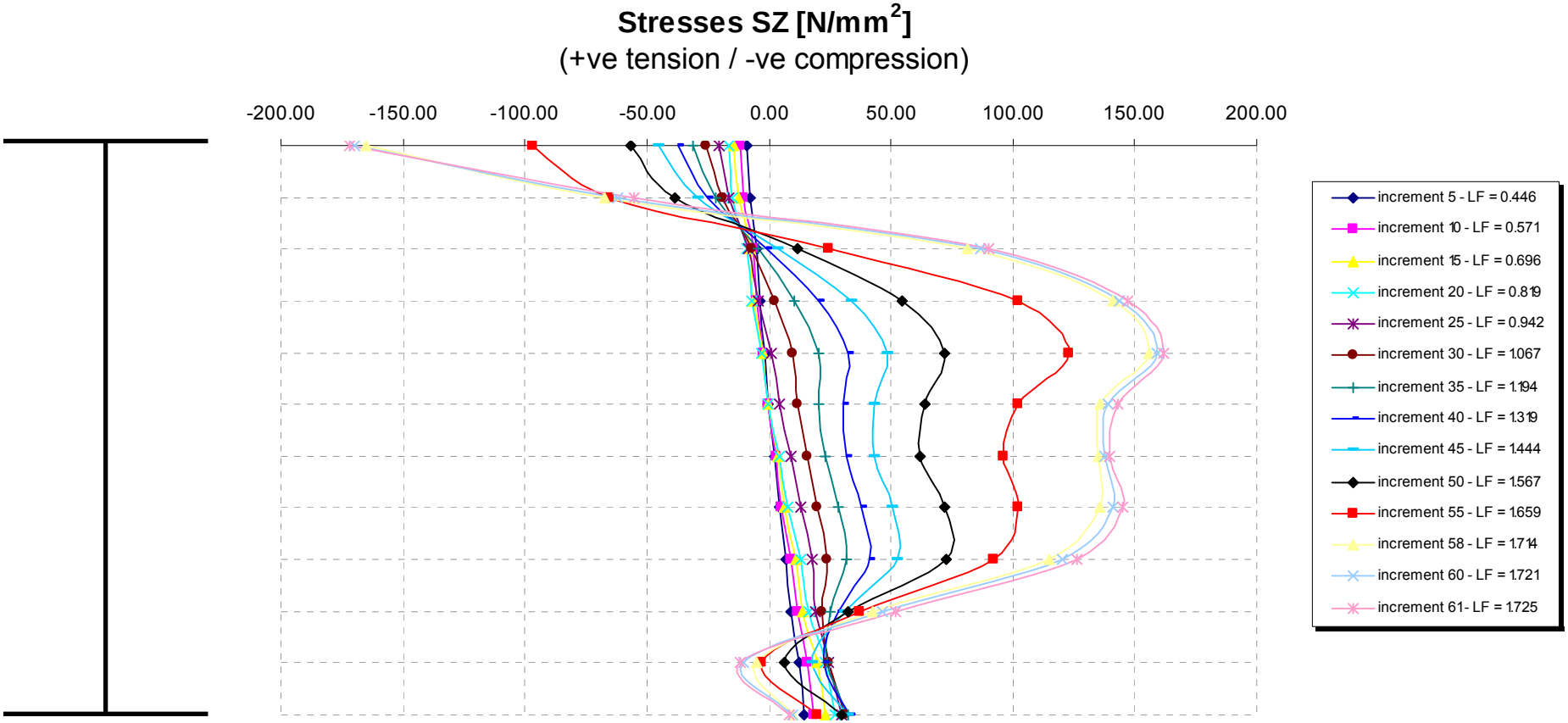

Fig. 4.106 – Section S3 – Longitudinal stresses in web (refer to Figure 4.101)

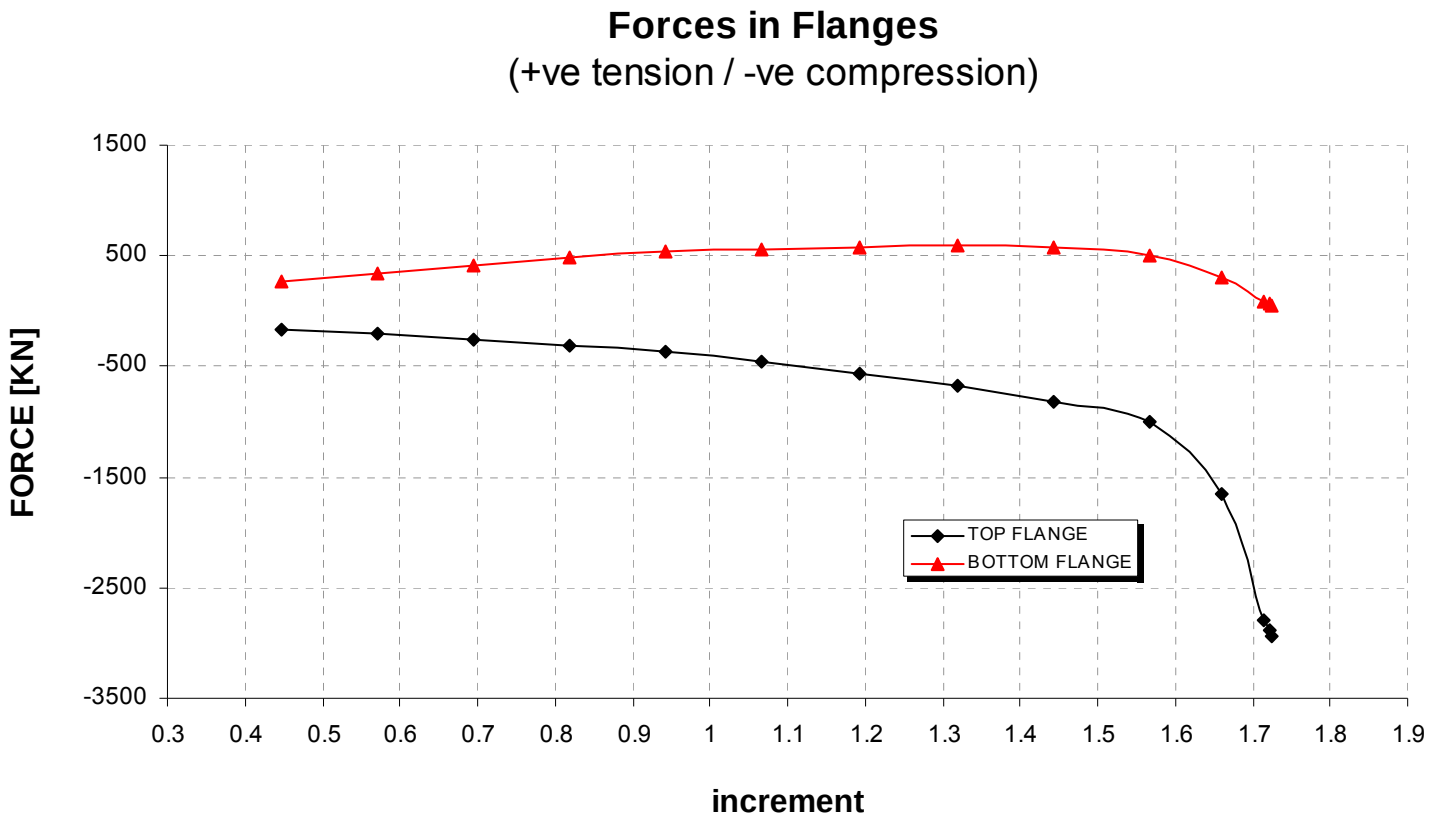

Fig. 4.107 – Section S3 – Longitudinal forces in flanges (refer to Figure 4.101)

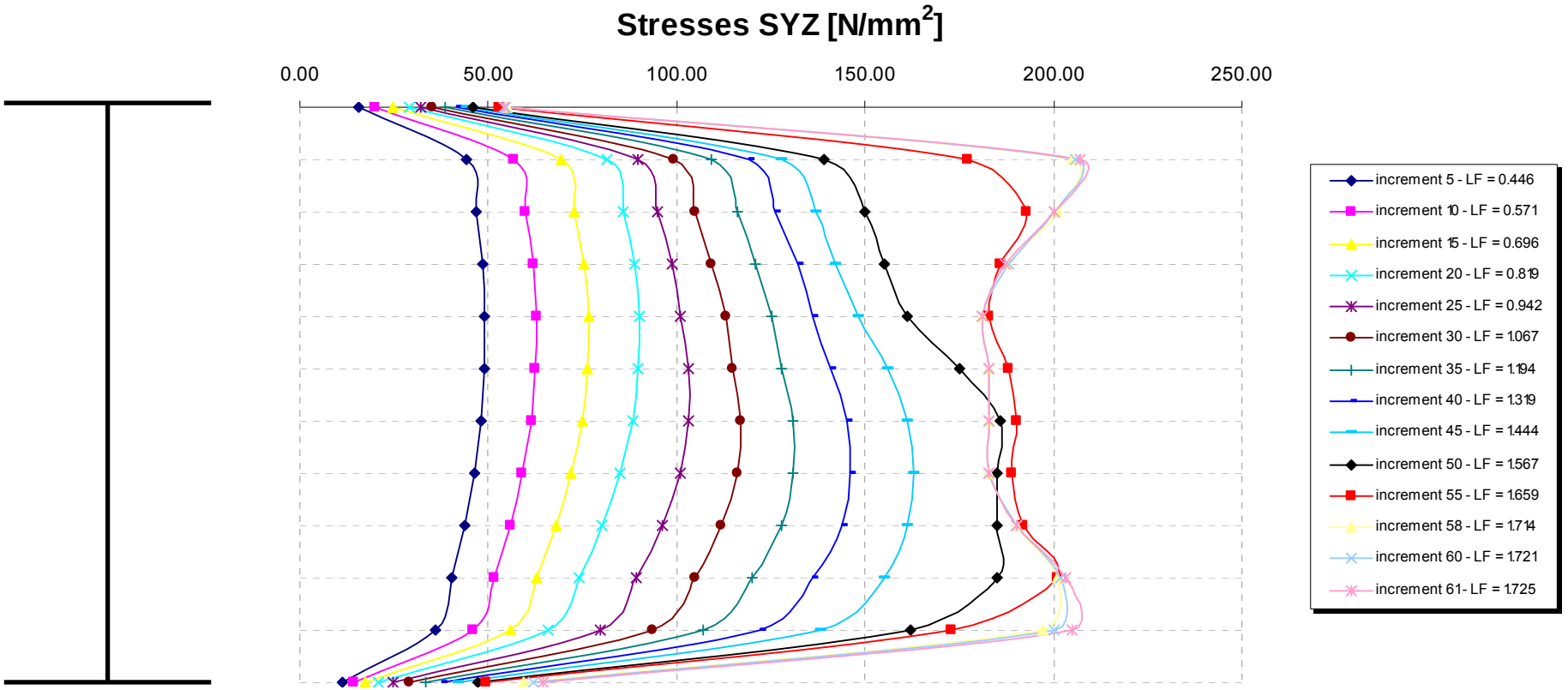

Fig. 4.108 – Section S3 – Shear stresses in web (refer to Figure 4.101)

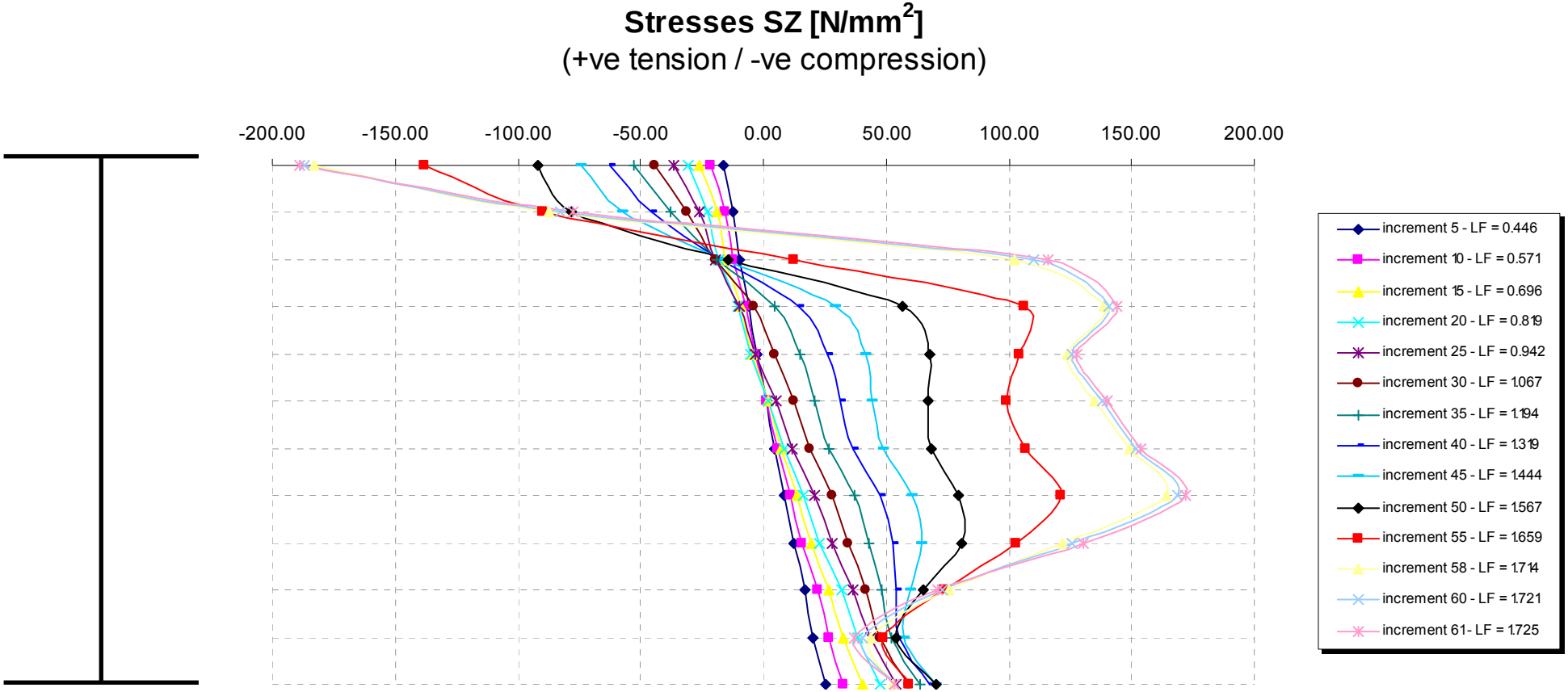

Fig. 4.109 – Section S2 – Longitudinal stresses in web (refer to Figure 4.101)

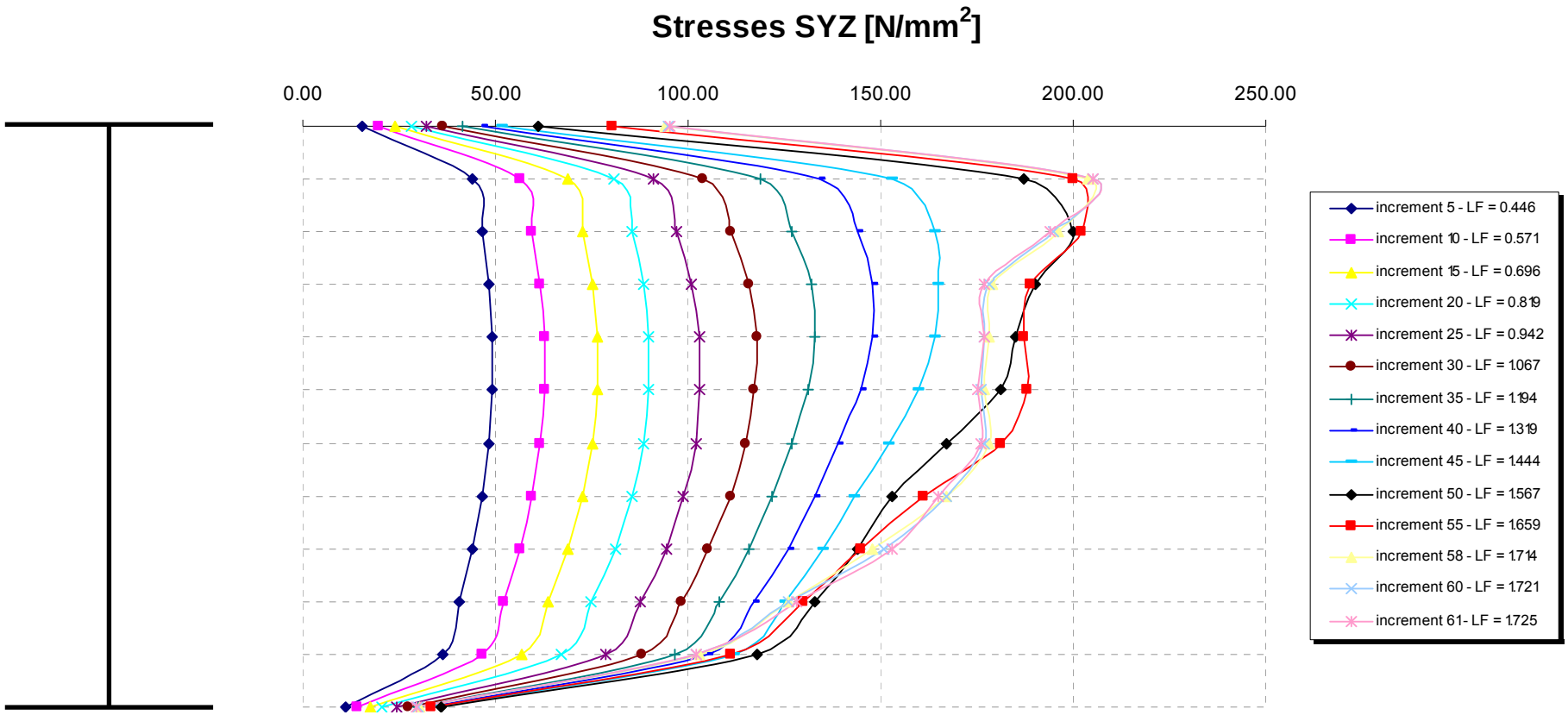

Fig. 4.110 – Section S2 – Shear stresses in web (refer to Figure 4.101)

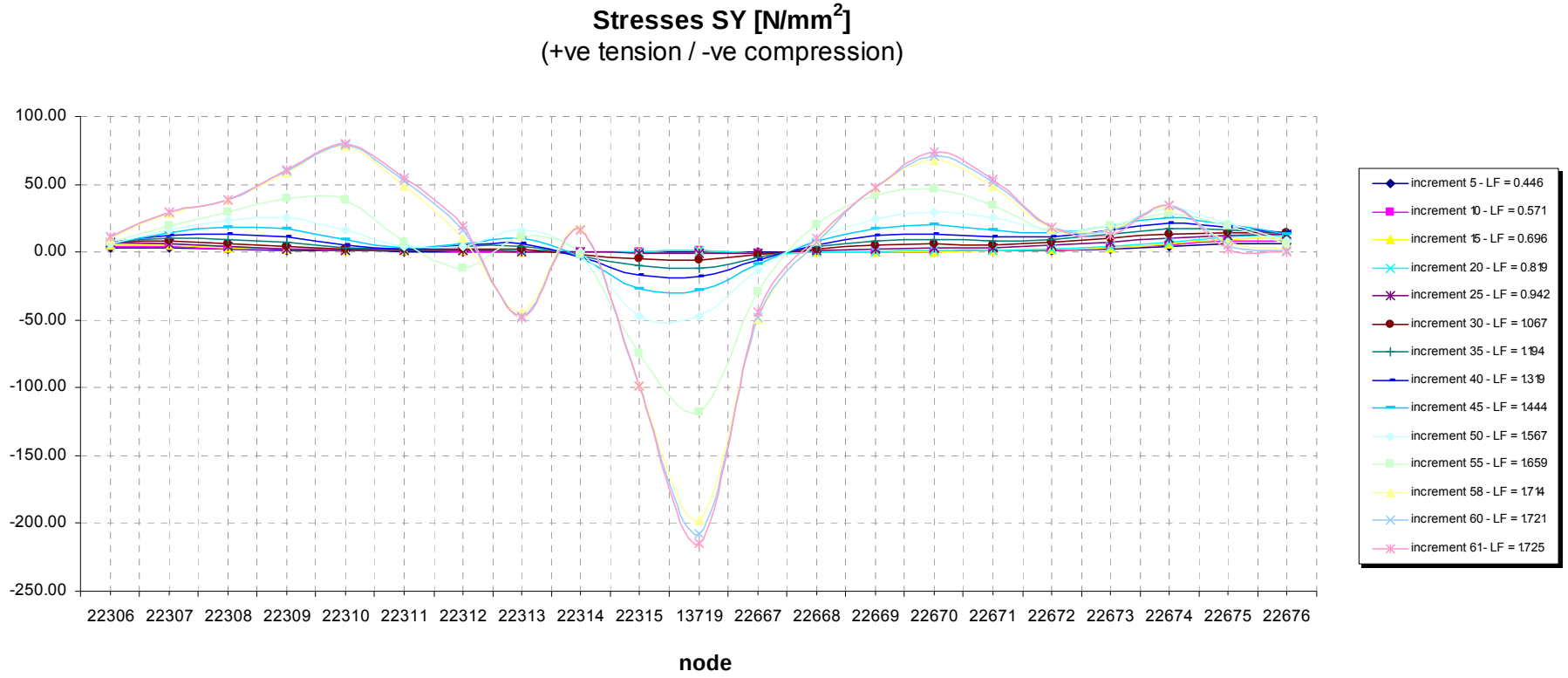

Fig. 4.111 – Section S4 – Vertical stresses in web (refer to Figure 4.101)

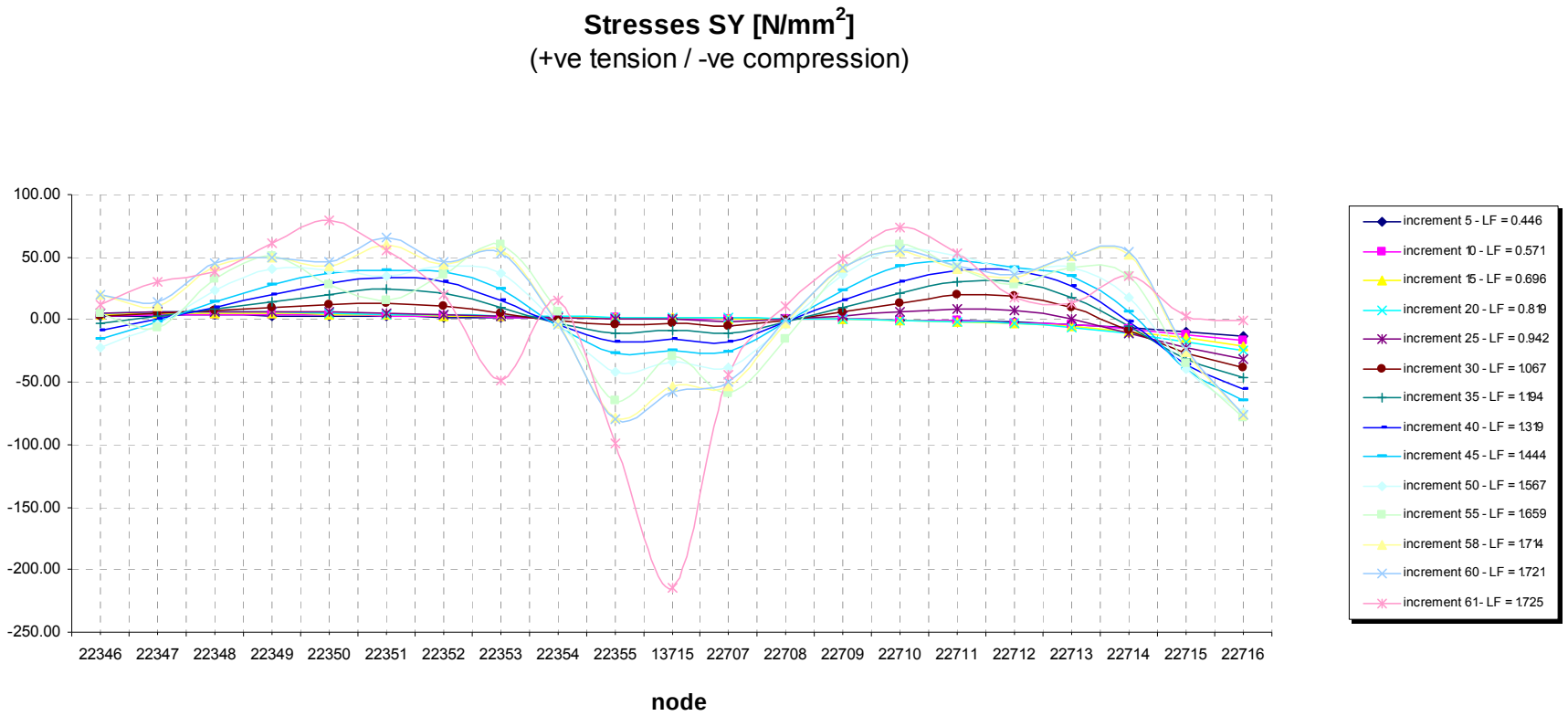

Fig. 4.112 – Section S6 – Vertical stresses in web (refer to Figure 4.101)

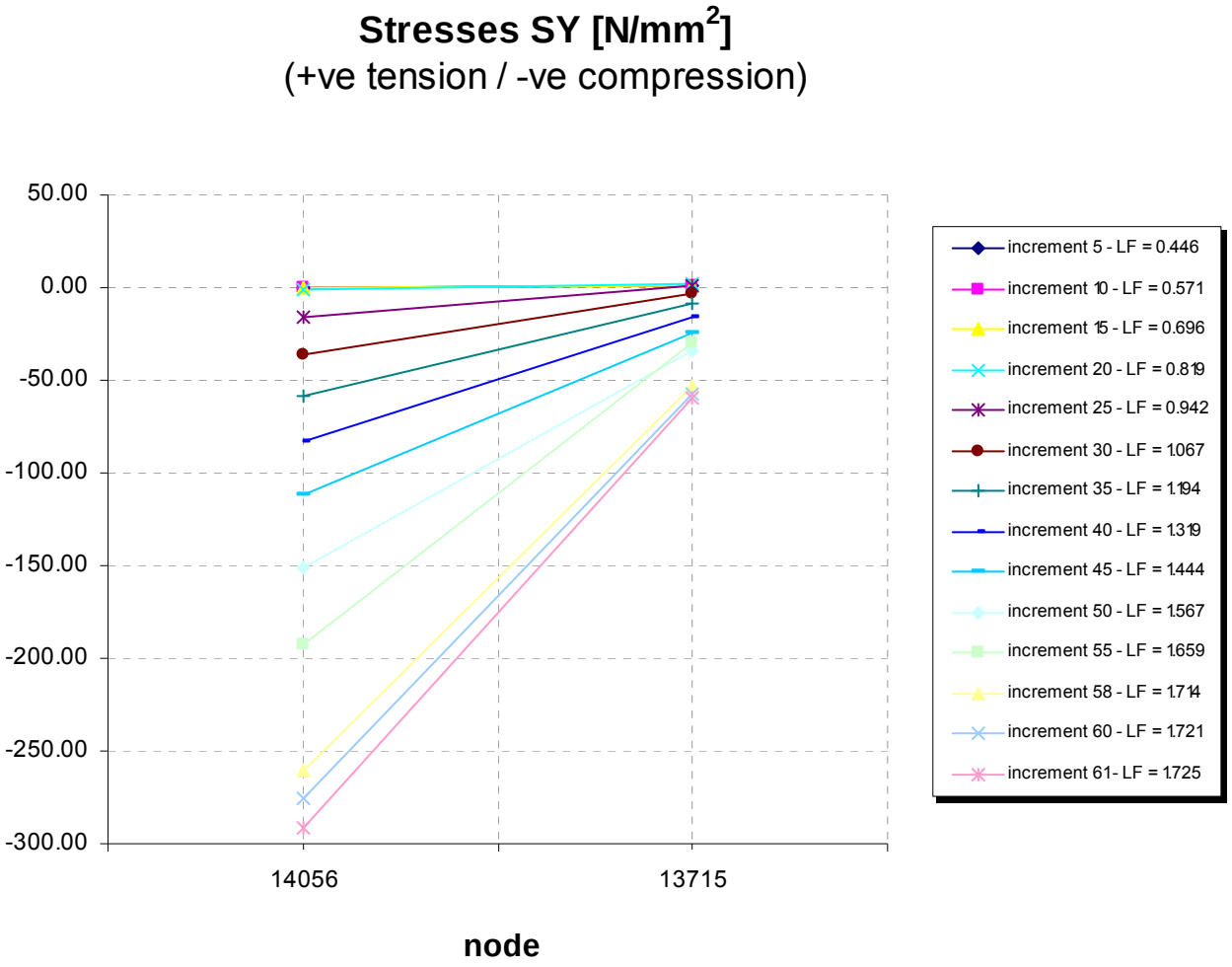

Fig. 4.113 – Section S8 – Vertical stresses in stiffener (refer to Figure 4.101)

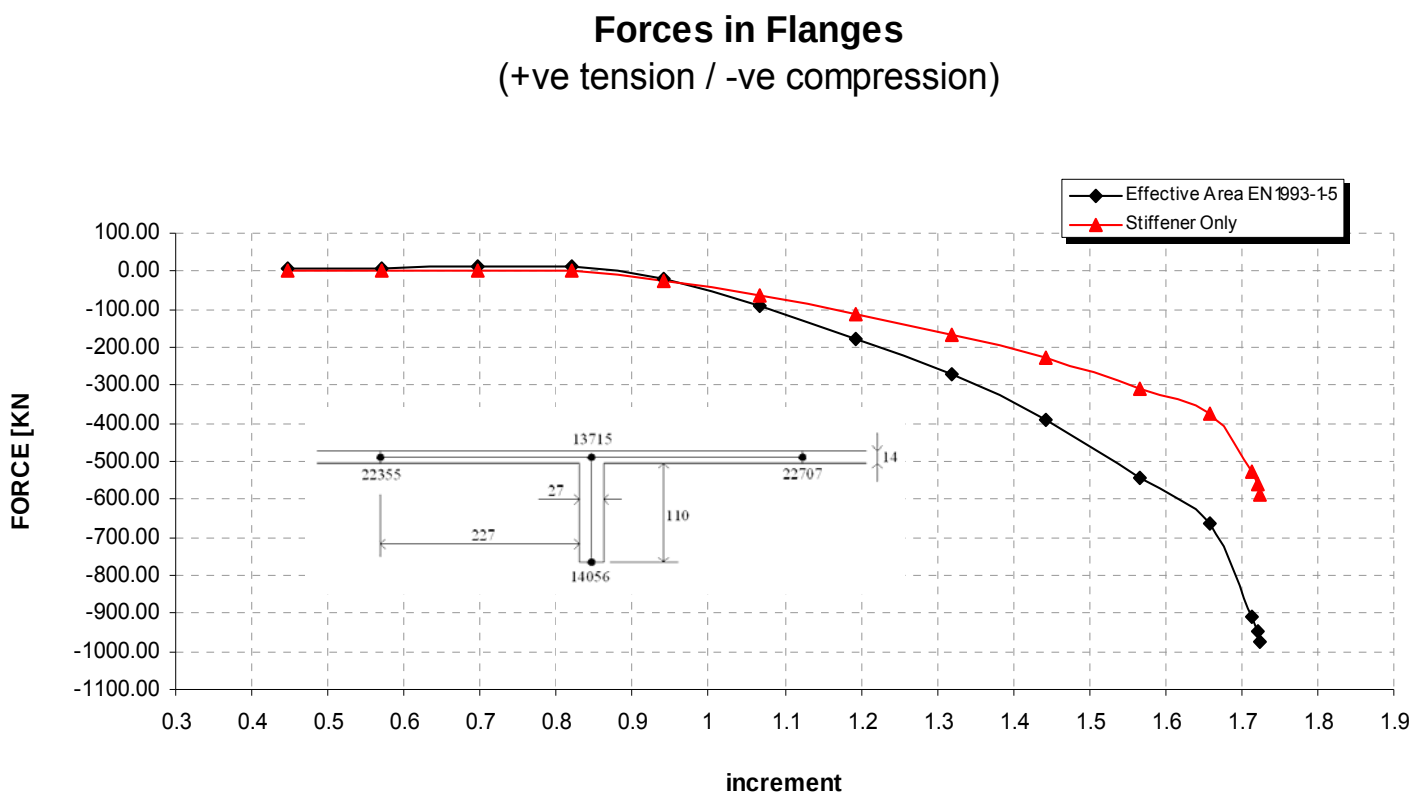

Fig. 4.114 – Section S8 – Vertical forces in stiffener (refer to Figure 4.101)

4.3 Discussion of results

4.3.1 General behaviour of web in bending and shear

When shear and moment is applied to the symmetrical beams in increments, up until a shear stress of around the elastic critical shear stress, a linear distribution of bending stress occurs across the depth of the cross section. Beyond this shear stress, a membrane tension develops which modifies the distribution of direct stress in the girder. This gives rise to a net tension in the web which is balanced by opposing compressive forces in the flanges, adding to the flexural compressive stress in one flange and reducing the flexural tensile stress in the other. This behaviour gives an increase in compressive flange force beyond that predicted from elastic behaviour, but not from that compared with the code M-V interactions. Figure 4.115 illustrates the behaviour as seen in previous paragraphs.

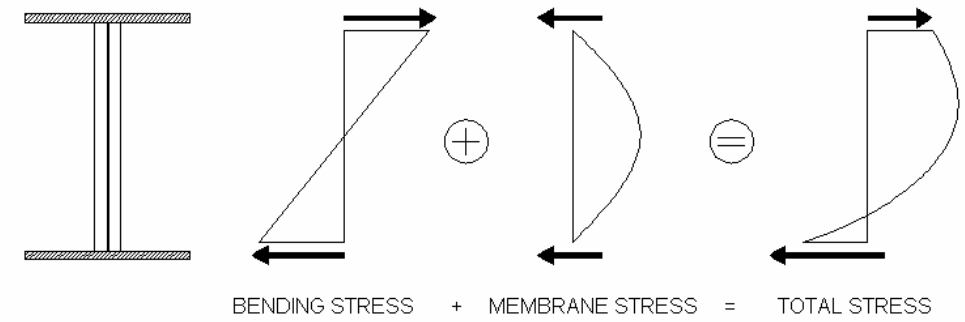

Fig 4.115 – Stress distribution under bending and shear at the ultimate load away from the internal support

Further, adjacent to the internal support, the membrane tension is much less marked and therefore so is the increase in compression flange force. The flange forces are almost equal and opposite as would be the case for bending without shear. This can be seen, for example, in Figures 4.16 and 4.19. This seems to be analogous to the variable angle truss method in Eurocode 2 for concrete, where the truss behaviour increases the flange force along the span from that predicted by bending theory alone, but the force produced nowhere exceeds the flange force at the position of maximum bending moment under bending alone.

4.3.2 Symmetrical steel girder

Behaviour

In all cases there is clear evidence that tension field forces pass through the first stiffener and that they induce much smaller forces in the stiffeners than assumed in the codes.

It is apparent that in each case the elastic critical stresses for the webs corresponded to those with the flange boundaries restrained against out-of-plane rotation. The comparisons of the non-linear results with the interaction curves gives a much closer fit if the value of $V_{bw,Rd}$ is based on restrained boundaries. This is however a function of the large flange size and close stiffener spacing used here.

The shear strengths calculated using BS 5400 Part 3 and EN 1993-1-5, based on restrained boundaries, are not very different from the strengths observed in the non-linear analyses, as shown in Table 4.

Case	V_{ult}	V_{ult}	V_{ult}
	FE Model	BS 5400:3	EN1993-1-5
	[KN]	[KN]	[KN]
1-1	9009	7991	8514
1-2	8811	7991	8514
2-1	6120	6743	5692
2-2	6120	6743	5692
4	8613	7978	8096
11	4653	4880	4406

Table 4 – Shear strengths

Forces in the intermediate stiffeners

Analysis of the stiffener forces has been undertaken on the basis used for BS 5400 Part 3 and EN 1993-1-5 which assume that the forces equate to the observed ultimate shear forces minus the critical shear forces, considered with boundary restraint, as shown in Table 5. These are compared with the forces derived from non-linear analyses results. Also shown in Table 5 are the forces calculated from reference [10] which are based solely on the reactions from the flange contributions to shear resistance.

Case	V_{ult}	V_{crit}	$V_{bw,Rd}$	Stiffener Force			
	FE Model	Restrained Boundaries	EN1993-1-5	$V_{ult} - V_{crit}$	$V_{bf,Rd}$ [10]	$V_{ult} - V_{bw,Rd}$	FE Model
	[KN]	[KN]	[KN]	[KN]	[KN]	[KN]	[KN]
1-1	9009	7590	7286	1419	1228	1723	425
1-2	8811	7590	7286	1221	1228	1525	175
2-1	6120	3010	4378	3110	1314	1742	1030
2-2	6120	3010	4378	3110	1314	1742	1075
4	8613	7590	7303	1023	793	1310	290
11	4653	2660	5103	1993	0	$V_{ult} < V_{bw,Rd}$	130

Table 5 – Forces in stiffeners

It can be seen that the approach used in BS 5400 Part 3 and EN 1993-1-5 gives high value for the forces in the stiffeners when compared to the ones obtained from the non-linear analyses, and it can lead in same cases to very conservative design, as it would be for cases 2-1 and 2-2. In order to get a better correlation with the FE results an alternative criteria is proposed. From the evidence that tension field forces pass through the stiffeners, it appears to be reasonable to base the stiffener forces on the difference between the applied shear force and the shear strength of the web $V_{bw,Rd}$ enhanced by the presence of the stiffeners. The force in the stiffener, applied in the plane of the web, can be expressed as follows:

$$F = V_{Ed} - \alpha V_{bw,Rd} \geq 0$$

which contrasts with EN 1993-1-5 and BS 5400 Part 3 approach $V_{Ed} - V_{crit}$.

The enhancement factor α allows for secondary compatibility stresses that develop in the stiffeners due to their function of keeping the panel straight. For this purpose, it would be expected that α would be less than 1. However all the results indicate $\alpha > 1$ and this can be function of the moment gradient, the shear gradient and the strain hardening.

It appears reasonable to propose a value $\alpha = 1$ when using equation 4.1.

The influence of longitudinal stresses

The results for Case 11 show that Clause 9.13.3.2 in BS 5400 is conservative. The equation for the critical shear stress (τ_0 in BS 5400 Part 3) is:

$$\tau_0 = 3.6E\left\{1+\left(\frac{d}{a}\right)^2\right\}\left(\frac{t}{d}\right)^2\sqrt{1-\frac{\sigma_1}{2.9E}\left(\frac{d}{t}\right)^2}$$

It assumes that when the value of the axial stress applied $\sigma_1 \geq 2.9E\left(\frac{t}{d}\right)^2$, as it is in this case, the critical shear stress is equal to zero and the compressive force applied at the transverse stiffener equals the applied shear force. From the results obtained there is not indication of such behaviour, being the axial force in the stiffener from the finite element model quite smaller than the shear force applied.

Also there are not indications of the destabilising influence of the web on the transverse stiffener due to longitudinal compression. Both EN 1993-1-5 and BS 5400 Part 3 require that, in order to resist buckling of the web plate, the stiffener have to carry an equivalent compressive force. This force is function of σ_1 in BS 5400 Part 3 which can cause again conservative design, because no allowance is made for the buckling capacity of the plate panels. In EN 1993-1-5, where there are no longitudinal stiffeners as in this case, out of plane forces on transverse stiffener caused by direct stresses are generally negligible.

4.3.3 Steel-concrete composite girder

Behaviour

As discussed in section 4.3.2, there is clear evidence that tension field forces pass through the first stiffener and that they induce much smaller forces in the stiffeners than assumed in the codes.

The girder section has dimensions from an existing UK bridge, and flange size is smaller than that used for the steel girder cases. The value of $V_{bw,Rd}$ in the interaction curves is based on simply supported boundaries. In reality a degree of fixity is present but it is not consider in this case. The comparisons of the non-linear results with the interaction curves

would gives, as for the steel girders, a much closer fit if the value of $V_{bw,Rd}$ was based on restrained boundaries.

The shear strengths calculated using BS 5400 Part 3 and EN 1993-1-5, based on simply supported boundaries, are shown in Table 6.

Case	V_{ult}	V_{ult}	V_{ult}
	FE Model	BS 5400:3	EN1993-1-5
	[KN]	[KN]	[KN]
1	5950	3650	3815
3	2200	1950	1800
6	6289	4445	4000

Table 6 – Shear strengths

Forces in the intermediate stiffeners

As for the symmetrical steel girder cases, analysis of the stiffener forces has been undertaken on the basis used for BS 5400 Part 3 and EN 1993-1-5 and compared with the forces derived from non-linear analyses results, as shown in Table 7.

Case	V_{ult}	V_{crit}	$V_{bw,Rd}$	Stiffener Force			
	FE Model	Simply Supported Boundaries	EN1993-1-5	$V_{ult} - V_{crit}$	$V_{bf,Rd}$ [10]	$V_{ult} - V_{bw,Rd}$	FE Model
	[KN]	[KN]	[KN]	[KN]	[KN]	[KN]	[KN]
1	5950	1925	3750	4025	65	2200	430
3	2200	1925	3750	275	0	$V_{ult} < V_{bw,Rd}$	95
6	6289	1925	3750	4364	250	2539	965

Table 7 – Forces in stiffeners

It can be seen that the approach used in BS 5400 Part 3 and EN 1993-1-5 gives high value for the forces in the stiffeners when compared to the ones obtained from the non-linear analyses. It can also be noted that the proposed approach to base the stiffener forces on the difference between the applied shear force and the shear strength of the web gives leads to smaller forces in the stiffeners. Better correlation with finite element model results would be obtained if the $V_{bw,Rd}$ was calculated considering restrained boundaries.

M-V interaction

Figure 4.56 shows the interaction curve for bending and shear according to EN 1993-1-5, and the results from the non-linear analyses for different M-V ratios. It is evident that the rules are conservative for both bending and shear. For low shear the resistance to bending moment is close to prediction. It is interesting to note that the bending resistance increases slightly when a small shear force is added. Similar results have been obtained in [22]. The increase can be attributed to the moment gradient applied. In girder with low shear the moment gradient is small and this lead to lower resistance in bending compared to a steeper moment gradient. For low bending moment the resistance to shear is higher than prediction. This could be attributed to boundary restraints of the panel not considered when in the construction of the interaction domain to EN 1993-1-5. For high value of both shear and bending the resistance seems to have very weak interaction.

4.3.4 Beam with weak stiffener yield strength

In order to investigate the influence of the stiffener strength on the behaviour of the girder, Case 2-1 girder arrangement (Section 4.1.1) has been re-analysed several times, each time reducing the steel yield strength of the first stiffener only. The influence on the non-linear analysis load factor is illustrated in Figure 4.116. It can be seen that for a reduction of the yield strength from 355 N/mm^2 up to 200 N/mm^2 the load factor does not change. After this point the graph shows a gradual reduction of the load factor, but as long as the stiffener is stiff enough according to clause 9.3.3, it provides contribution to the post-buckling resistance of the girder.

It is interesting to note that a substantial reduction in yield strength of the stiffener does not influence the type of failure, which remains a web type of failure with the transverse stiffener remaining intact. When the stiffener yield strength is reduced to about 70 N/mm^2 then the tension field passes through the stiffeners which bow out laterally with the web plate, as shown in Figure 4.118.

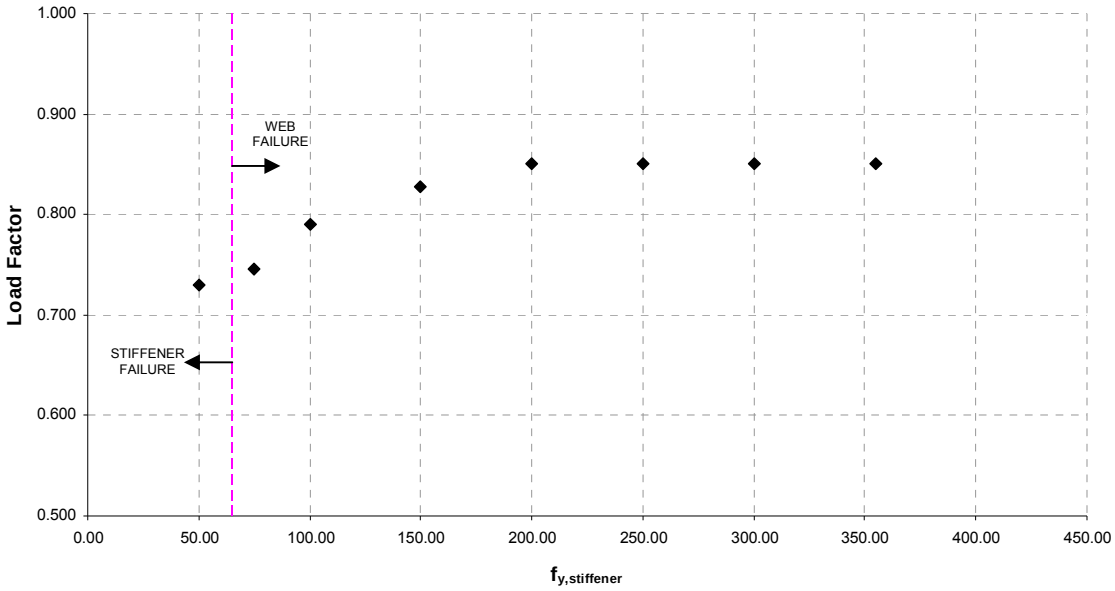

Fig 4.116 – Yield strength of first stiffener vs Total Load Factor for Case 2-1

Figure 4.117 shows the influence of the first stiffener strength on the strength criteria usage factor used in EN 1993-1-5 Clause 9.4. It is evident in this example that the criteria can be very conservative and lead to bigger size stiffeners. For a yield strength of 355 N/mm^2, a usage factor of 3.62 would already predict the stiffener to fail whereas it can be seen that only when the yield strength is about 70 N/mm^2 the stiffener fails. This only happens when the usage factor is equal to 14.

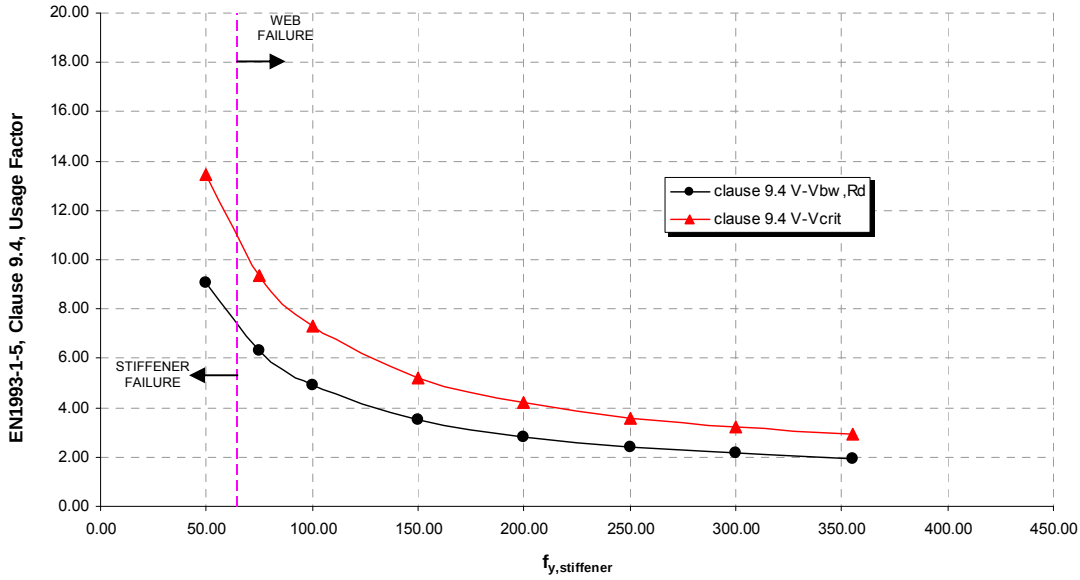

Fig 4.117 – Yield strength of first stiffener vs Strength Criteria Usage Factor

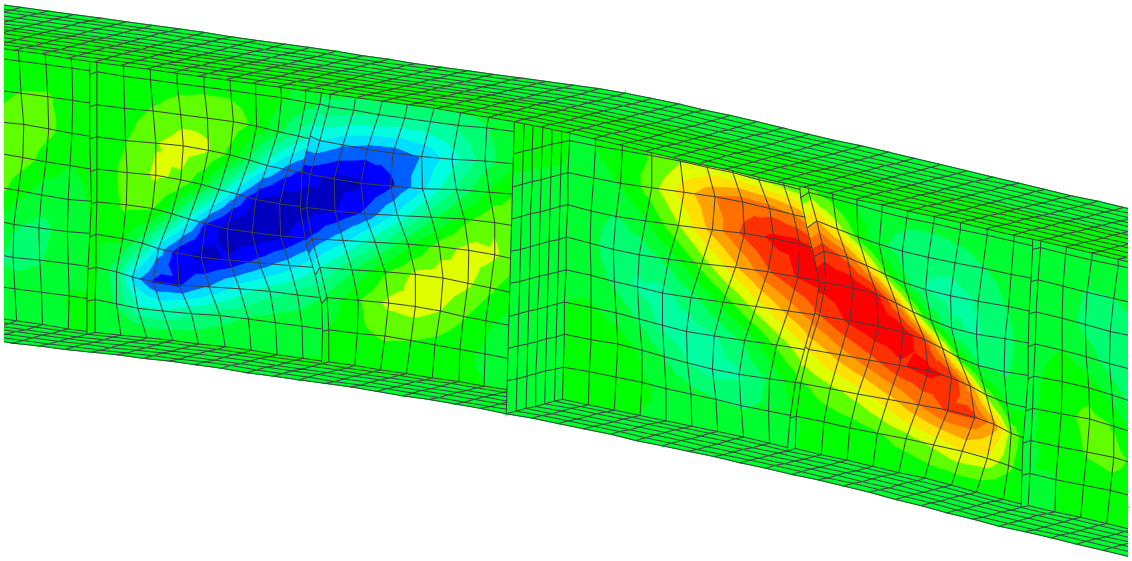

Fig 4.118 – Girder failed by the web plate and intermediate stiffener bowing out laterally

The same exercise can be repeated for the other cases, but the finding for Case 2-1 suggests that the stiffness-only approach is safe. In particular, when designing to stiffness criteria, a simple rule might be proposed, and the stiffness-only approach considered safe when $f_{y,stiffener} \geq f_{y,web}$. This needs further investigation.

An extreme situation has also been investigated. Case 2-1 girder arrangement has been modified, and “Stiffener A” in Figure 4.14 has been removed and replaced with a line support vertically down the web plate at its location, which prevents out of plane movement along the line but allows vertical movement, as shown in Figure 4.119.

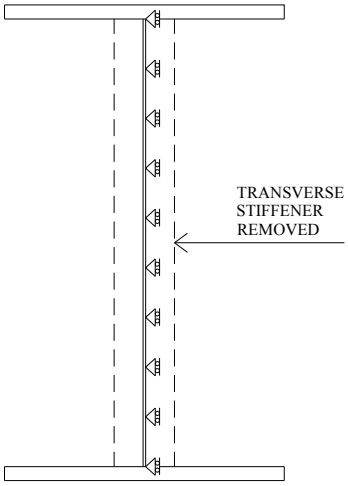

Fig 4.119 – Girder section at stiffener location and line support along web plate

It is interesting to note that the non-linear analysis stops when it fails to find equilibrium beyond a load factor 0.88, which is slightly bigger than load factor obtained in Section 4.1.1 where the transverse stiffener had dimensions 100x12.5 mm. The load factor in that case was 0.85.

This means that the girder still achieves the $V_{bw,Rd}$ without relying to a truss model to increase its shear resistance. It means that the mechanism predicted by Rockey is not actually happening and that the stiffener axial force in a truss behaviour is not necessary for loading beyond V_{crit}.

Conclusions

i) The finite element modelling for both steel and composite girders showed that in no case the failure was due to a stiffener, as long as its stiffness was in accordance with the minimum required by EN 1993-1-5 and its yield strength was the same of the web panel. Failures were located in the web panel and the Eurocode was always safe;

ii) The axial stress, considered in some of the analyses, had an influence on the final load bearing resistance of the girder, but had limited effect on the stiffener forces;

iii) A correction has been proposed for the forces in the stiffeners in order to get a better correlation with the finite element results;

iv) The effects of different M-V ratios have been investigated and compared with the moment-shear interaction diagram by EN 1993-1-5. The non-linear solutions, as seen, have always been found outside the domain, showing EN1993-1-5 to be safe;

v) The girder behaviour under M-V was well described by Höglund theory;

vi) The girders modelled were relatively insensitive to initial imperfections in the stiffeners;

vii) The effects of reducing the yield strength of the stiffener, when designing to stiffness criteria, have been investigated for case 2-1, showing that the stiffness-only approach is safe. A simple rule has been suggested;

viii) Further works would strengthen the conclusion that EN 1993-1-5 is safe for the design of plate girders and transverse stiffeners and could lead to better design rules to be proposed.

Bibliography

[1] K. C. Rockey, *Web buckling and the Design of Webplates*, The Structural Engineer, 1958, February, 45-60

[2] K. Basler, B. T. Yen, J.A. Mueller, B. Thürlimann, *Web Buckling Tests on Welded Plate Girders*, Bulletin No. 64, Welding Research Council, New York, September 1960

[3] K. Basler, *Strength of Plate Girders in Shear*, Journal of the Structural Division Proceedings of the American Society of Civil Engineers, 151-180, October 1961

[4] P. S. Bulson, *The Stability of Flat Plates*, Chatto & Windus, London, 1970

[5] K. C. Rockey, M. Skaloud, *The ultimate load behaviour of plate girders loaded in shear*, The Structural Engineer, 1972, No 1, January, 29-47

[6] M. Mele, *Sul dimensionamento delle nervature di irrigidimento d'anima nelle travi in acciaio*, Costruzioni Metalliche, No. 4 e 5, 1973

[7] G. Ballio, S. Caramelli, F. De Miranda, M. Mele, *Commenti alle nuove istruzioni CNR: nervature di irrigidimento delle anime di travi a parete piena*, Costruzioni Metalliche, No. 5, 1975

[8] D. M. Porter, K. C. Rockey, H. R. Evans, *The collapse behaviour of plate girders loaded in shear*, The Structural Engineer, 1975, No 8, August, 313-325

[9] D. M. Porter, K. C. Rockey, H. R. Evans, *A design method for predicting the collapse behaviour of plate girders*, Proceedings of the Institution of Civil Engineers, Part 2, 1978, 65, March, 85-112

[10] T. Höglund, *Design of thin plate I girders in shear and bending with special reference to web buckling*, Bulletin No. 94, Division of Building Statics and Structural Engineering, Royal Institute of Technology, Stockholm, Sweden, 1973

[11] K. C. Rockey, G. Valtinat, K. H. Tang, *The design of transverse stiffeners on webs loaded in shear - an ultimate load approach*, Proceedings of the Institution of Civil Engineers, Part 2, 1981, 71, December, 1069-1099

[12] H. R. Evans, K. H. Tang, *A Report on Five Tests Carried out on a Large-Scale Transversely Stiffened Plate Girder - TRV3*, Report No. DT/SC/8, Department of Civil and Structural Engineering, University College, Cardiff, December 1981

[13] British Standards Institution, *Code of Practice for Design of Steel Bridges*, BSI, Milton Keynes, 1982, BS5400: Part 3

[14] G. Ballio, F. M. Mazzolani, *Strutture in acciaio*, Hoepli, Milano, 1987

[15] CEN, *Eurocode 3: Design of Steel Structures, Part 1.1: General Rules and Rules for Buildings*, BSI, Milton Keynes, 1992, ENV 1993-1-1

[16] CEN, *Eurocode 3: Design of Steel Structures, Part 1.5: Plated structural elements*, BSI, Milton Keynes, 2004, ENV 1993-1-5

[17] A. W. Davies, D. S. C. Griffith, *Shear strength of steel plate girders*, Proceedings of the Institution of Civil Engineers, 1999, 34, May, 147-157

[18] B. Johansson, R. Maquoi, G. Sedlacek, *New design rules for plated structures in Eurocode 3*, Journal of Constructional Steel Research, 2001, 57, 279-311

[19] J. C. Chapman, M. Xie, *Design of web stiffeners: axial forces*, Journal of Constructional Steel Research, 2003, 59, 1035-1056

[20] C. R. Hendy, C. J. Murphy, *Designers' Guide to EN 1993-2 - Eurocode 3, Design of steel structures. Part 2, Steel bridges*, Thomas Telford, London, 2007

[21] M. R. Horne, B. G. R. Holloway, *Structural action in steel box girders*, CIRIA GUIDE 3, London, April 1977

[22] M. Veljkovic, B. Johansson, *Design for buckling of plates due to direct stress*, Proceedings of the Nordic Steel Construction Conference, Helsinki, 2001

Appendix A

Calculation of critical stresses

The buckling shear stress τ_{cr} is given by:

$$\tau_{cr} = k_b \frac{\pi^2 E}{12\left(1-\upsilon^2\right)}\left(\frac{t}{b}\right)^2$$

where

- k_b is the buckling coefficient;
- E is the modulus of elasticity;
- ν is the Poisson's ratio;
- t is the thickness of the plate
- b is the width of the plate

For a simply supported plate k_b is given by

$$k_b = 5.35 + 4\left(\frac{b}{a}\right)^2 \quad \text{for} \quad a/b \geq 1$$

$$k_b = 5.35\left(\frac{b}{a}\right)^2 + 4 \quad \text{for} \quad a/b < 1$$

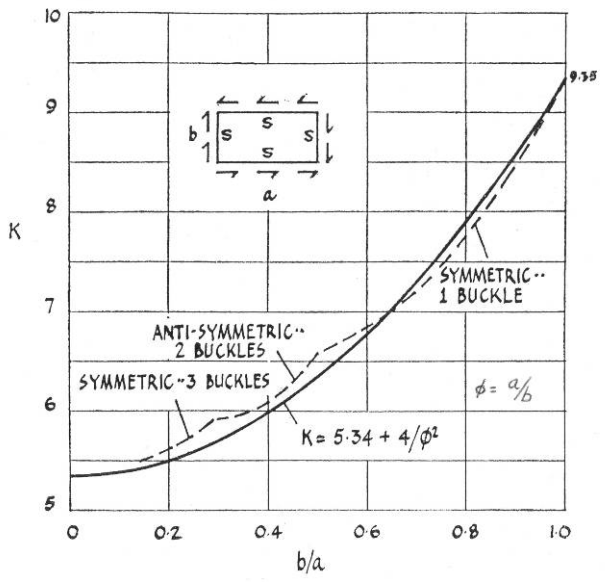

Figure A.1 – Buckling coefficient for simply supported plates in shear (Extract from [4])

For a built-in plate k_b is given by

$$k_b = 8.98 + 5.6\left(\frac{b}{a}\right)^2 \quad \text{for} \quad a/b \geq 1$$

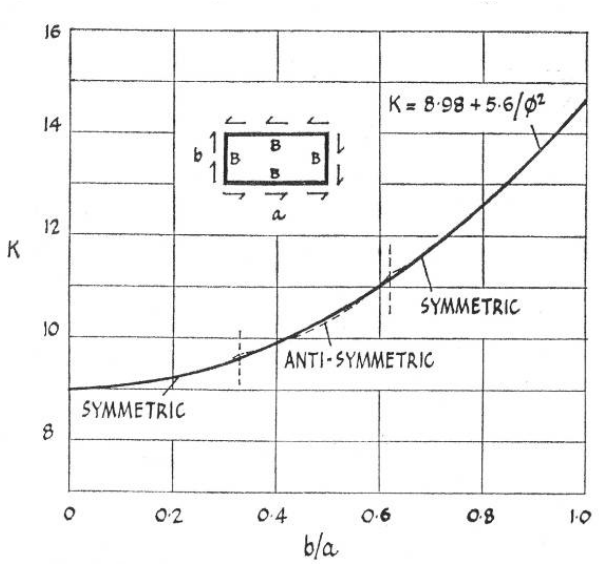

Figure A.2 – Buckling coefficient for built-in plates in shear (Extract from [4])